ABSTRACT

Belz, Robert M. Integrated Modeling Analysis of Glass Furnace Forehearths as Applied to Production Planning Optimization. (Under the direction of Dr. John S. Strenkowski)

A two-dimensional model was developed to investigate thermal variations within a glass furnace forehearth as used in the production of glass fibers. The goal of the simulations was to develop a production planning tool that can be used not only to help establish product changeover guidelines but also to identify undesirable processing conditions. Commercially available software, FLUENT and FIDAP, were utilized as the finite element computational fluid dynamic (CFD) solvers. The models incorporated sufficient detail to investigate primary production control parameters for various types, configurations, and geometries of forehearths as used throughout the industry. The models incorporated various throughput rates as represented by different fiber forming bushings and processing parameters. In addition, the height of the glass surface was computed and integrated into the molten glass flow and heat transfer equations.

Steady-state and transient forehearth simulations were conducted and the results were compared with previously published forehearth experimental operating data. The simulations illustrated that a bushing changeover has a significant impact on the glass temperature and flow in the forehearth, whereas variations of glass height were shown to have a minimal effect. The models developed in this thesis are adaptable to other bushing configurations and the models should provide useful product changeover guidance for the purpose of optimizing production planning.

INTEGRATED MODELING ANALYSIS OF GLASS FURNACE FOREHEARTHS AS APPLIED TO PRODUCTION PLANNING OPTIMIZATION

by

ROBERT MICHAEL BELZ

A thesis submitted to the Graduate Faculty of
North Carolina State University
in partial fulfillment of the
requirements for the Degree of Master of Science

DEPARTMENT OF MECHANICAL AND AEROSPACE ENGINEERING

Raleigh, North Carolina

2004

APPROVED BY:

_____	_____
Dr. James W. Leach	Dr. Jerome J. Cuomo

_____
Dr. John S. Strenkowski
Chair of Advisory Committee

BIOGRAPHY

Robert Michael Belz was born in Buffalo, New York on May 07, 1978. He is the son of Harold and Linda Belz, and he has one brother, Jeffrey Belz, and one sister, Cynthia Belz–Reynolds. He attended Pembroke Junior Senior High School in Corfu, NY where he received Honors and was awarded the Senior Athletic Award for earning major letter awards in the following high school level sports: volleyball, basketball, golf, and baseball. He graduated high school in the spring of 1996 achieving a NYS Regents diploma, and enrolled in the curriculum of Mechanical Engineering at the Rochester Institute of Technology, in Rochester, NY.

There he pursued numerous cooperative education (Co-op) opportunities throughout his undergraduate career, with companies such as New Venture Gear Inc. and Robert Bosch Corporation. In the spring of 2001, he received a Bachelor of Science degree in Mechanical Engineering with an Automotive Option and concentrating in plastics. Immediately following his degree, Robert began working for Robert Bosch Corporation as a Plastics Manufacturing Engineer, in Charleston, SC.

While working for Robert Bosch, Robert was extended an invitation to return to Academia to pursue a Master's of Science in Mechanical Engineering at the North Carolina State University in Raleigh, NC. Working under the direction of Dr. John Strenkowski, research began into analyzing problems associated within the Glass Fiber Manufacturing Industry. More specifically, his researched focused on how advanced forms of thermal CFD analysis could be applied to improve on energy conservation, productivity, and reduction of waste. Upon successful completion of the requirements for

the Degree of Master of Science in Mechanical Engineering, he will begin employment with Northrop Grumman Electronic Systems in Baltimore, MD.

ACKNOWLEDGEMENTS

I would like to sincerely thank my advisor Dr. John S. Strenkowski for his constant encouragement and guidance during my research work. His patience and knowledge during this project were invaluable. I would also like to thank my other faculty members who served on my thesis advisory committee, Dr. Jerome J. Cuomo who helped to focus my desire to continually think "outside of the box" and push every aspect of my technical abilities to their limits, and also to Dr. James W. Leach whose guidance and endless knowledge in the areas of thermal sciences were instrumental to the success of my research.

A special thanks goes to Ashish Kulkarni of the Fluent Inc. Academics Support Team for assisting me with questions regarding FLUENT. I would like to sincerely thank Nilesh Gandhi, also of the Fluent Inc. Academics Support Team, for his patience, knowledge, and assistance in answering questions regarding to and development of the FIDAP simulation code. I would also like to express my appreciation to Jim Koewing and Guosheng Kang especially for their technical support on the project as my industry liaisons.

Finally, I would like to thank my parents, sister, and brother for their continued love, support, and encouragement throughout everything I have ever done. In addition, I would like to Shannon Jackson for her unwavering love and support, without her I could not be the person I have grown to be today and the type of person I aspire to become in the future. I would also like to thank all of my friends for their support and patience.

TABLE OF CONTENTS

LIST OF TABLES

CHAPTER 3

CHAPTER 4

LIST OF FIGURES

CHAPTER 1

CHAPTER 3

CHAPTER 4

1 INTRODUCTION

The formation of glass fibers is a complex thermal process. The quality of the fiber formation process depends on the production system's ability to not only mix and melt the solid raw materials into a homogeneous liquid state, but to also continually supply the down line fiber forming equipment with thermally consistent molten glass. However, the principles that underlie this complex thermal process have not yet been completely understood. As a result, most glass fiber manufacturers rely heavily on the experience of their process control operators to achieve daily production quotas.

In today's glass fiber industry, both glass quality and production yields are being elevated to higher levels. At the same time, the industry is striving to reduce the so-called critical drivers. These critical drivers include the needs to minimize manufacturing costs, achieve current and future environmental goals, develop new products and processes, and comply with the increasing quality requirements of new products. To meet these needs, a more thorough understanding of the thermal process is required, so that the process is not solely dependent on its skilled labor force.

The glass fiber industry is undertaking vast and rapid changes to meet today's needs. In recent years, the industry has begun to utilize advanced numerical simulation tools to optimize the thermal process. This growing interest in numerical simulation is an acknowledgment that modeling can be an effective and efficient method to meet the challenges presented by the critical drivers. In addition, current numerical simulation modeling techniques have achieved a high degree of reliability and applicability for providing new insight into the glass fiber formation process.

1.1 Main Objective

The main objective of this research is to develop a two-dimensional thermal model of a glass furnace forehearth as used in the production of glass fibers. The focus of this model is to develop a production planning tool that can be used not only to help establish product changeover guidelines but also to identify undesirable processing conditions. The key to the model's success is not only to incorporate sufficient detail to investigate the primary production control parameters, but also to minimize the overall computational time of the numerical simulations.

Within this overall objective, several requirements must be met. In order to properly gauge the sensitivities of the numerical simulation and gain confidence in the results, the first aspect is to develop generic and realistic forehearth model geometry and to identify the appropriate processing parameters. The second requirement is to determine the equations describing the molten glass flow and heat transfer. The third requirement is to develop a model that is adaptable to various types, configurations, and geometries of forehearths used throughout the industry, and that allows for variations of throughput rates (represented by different fiber forming bushings) and processing parameters. The final requirement is to empirically validate the model for results that are typically seen in day-to-day production.

1.2 Significance of the Research

Temperature uniformity of the molten glass entering the fiber forming bushings is essential for achieving glass fiber product quality. It is important to realize that the fiber forming process is a combination of extrusion (hydrostatic pressure of the molten glass above) and pultrusion (pull force via winders or traverses[1]), and that the entire process

depends on minimizing temperature variations throughout the molten glass. Temperature non-uniformity causes sudden changes in viscosity and fiber tensile strength, which often leads to fiber breakage during manufacturing. However, it is very difficult to obtain a completely uniform temperature distribution over the entire length of the forehearth in practical processes. To help minimize the temperature variations ahead of the bushing inlets, the temperature of the glass surface is adjusted by means of a series of gas burners and the use of cooling air along the forehearth length.

Until recently, temperature adjustments have been achieved by relying on operator experience. Using computer controls, it is now a possible to automate a manufacturing process close to the optimum operating point. In order to automate the glass fiber manufacturing process, a deeper understanding of the physical phenomena that occurs during real-time production is required to manage the temperature variations within the forehearth.

Numerical simulation of the glass forming process can be used to gain a deeper understanding of the critical parameters associated with the manufacturing process. In many instances, control of the fiber forming process has been left to the experience of the line operators. Numerical simulations can be used to bridge the information gap and provide cost effective solutions. The growing interest in numerical simulations as applied to the glass industry is reflected in the rising number of technical papers being published. These papers document both research and experimental studies of numerous physical aspects of the manufacturing and thermal processing system, from furnace combustion models to the attenuation of the glass fiber itself. Topics that have been covered include molten glass flow and heat transfer and the physical geometry of the processing equipment itself, which will be

discussed further in the literature review. One modeling parameter that is documented throughout all of the papers is the use of a constant throughput or mass flow rate out of each of the fiber forming bushings, irregardless of the number of positions.

Applying constant mass flow rates out of the bushings is important from a mathematical modeling standpoint. Setting the flow rates to be constant allows for a simpler analysis to be conducted while providing a basic understanding of the heat transfer out of the molten glass surface. However, in a day-to-day production environment, customer orders can fluctuate which results in various types of fiber forming bushings running simultaneously on a given manufacturing line. Consequently, maintaining constant mass flow rates out each of the bushing positions in a simulation neglects important manufacturing questions like "How does a specific bushing arrangement of different mass flow rates running simultaneously operate ?," and "Will the interaction change with different bushing arrangements?". In addressing these and similar questions, the research presented in this thesis will focus on the thermal response of a forehearth system to different bushing arrangements.

1.3 Balanced Runner Concept

The glass fiber forming process is similar in concept to the injection molding of plastics[2]. Both processes involve the flow of a highly viscous, temperature-dependent fluid to form a final product. A major difference is that injection molding flow is driven by an external pressure in an enclosed channel and the geometry of the cavities within a mold tool determines the final product dimensions. In contrast, molten glass flow is driven by the force of gravity in an open channel and the geometry of the fiber forming bushing determines the

final fiber diameter. Nonetheless, a mold tool and a forehearth have many fundamental aspects in common as shown in figure 1.1. Both facilitate the delivery of a high temperature fluid to multiple forming positions. It is also important in both processes that the temperature of the molten fluid and its properties remain fairly constant until the product is formed. In the case of multi-cavity mold tools, the cavities are not always the same volume, which results in different filling rates. To compensate for the difference in filling volumes, the runner diameters are varied which alters the flow velocities to each cavity. The fluid flow velocities can also be managed by having individual controllable temperature zones imbedded into specific areas of the mold tool. The overall idea is to achieve a "balanced runner" system, such that all cavities receive homogeneous material at a constant rate. Otherwise, cavities would not fill at the same rate, which would cause some cavities to be partially filled and create so-called "short shots". This is highly undesirable since the unfilled parts are considered production scrap and cannot be reworked, which results in a loss of production and profits.

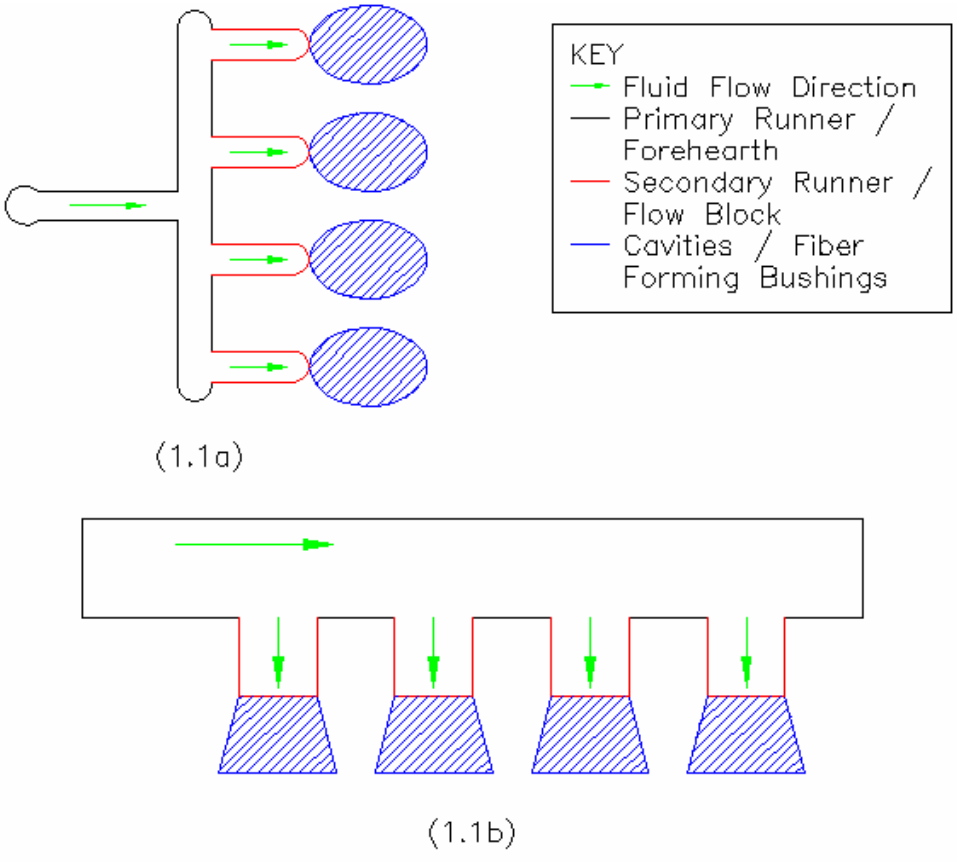

Figure 1.1 – System Comparison Illustrating (1.1a) Injection Molding Mold Tool Runner System and (1.1b) Glass Fiber Forming Delivery System

A similar "balanced runner" approach can be applied to the forehearth and its multiple bushings. It is obvious that a high throughput bushing requires more glass flow than a low throughput one. However, different flow rate bushings running simultaneously cannot be avoided due to fluctuations in customer demands and it is hypothesized that there are certain bushing arrangements that will cause more fiber breakage. In order to create a "balanced runner" system, the process needs to be controlled. Unlike an injection mold tool, the physical geometry of the forehearth cannot be altered. However, the glass surface temperature and specific placement of individual bushings can be controlled. By coupling these elements together, the goal of optimizing production planning can be addressed.

1.4 Thermal Processing System

The manufacturing of glass fiber is a high temperature conversion of various raw materials, commonly referred to as a glass batch, into a homogeneous melt. This is followed by the attenuation of this melt into glass fibers. The conversion takes place in a closed system which, for the purpose of this research, is referred to as the Thermal Processing System (TPS). A simplified layout of a TPS can be seen in figure 1.2. The layout has been simplified because of the numerous manufacturing strategies resulting in a large number of variations used throughout the industry. The TPS itself can be divided into individual thermal components. The following subsections contain brief summaries of each of the components. A more extensive description can be found in Reference [1].

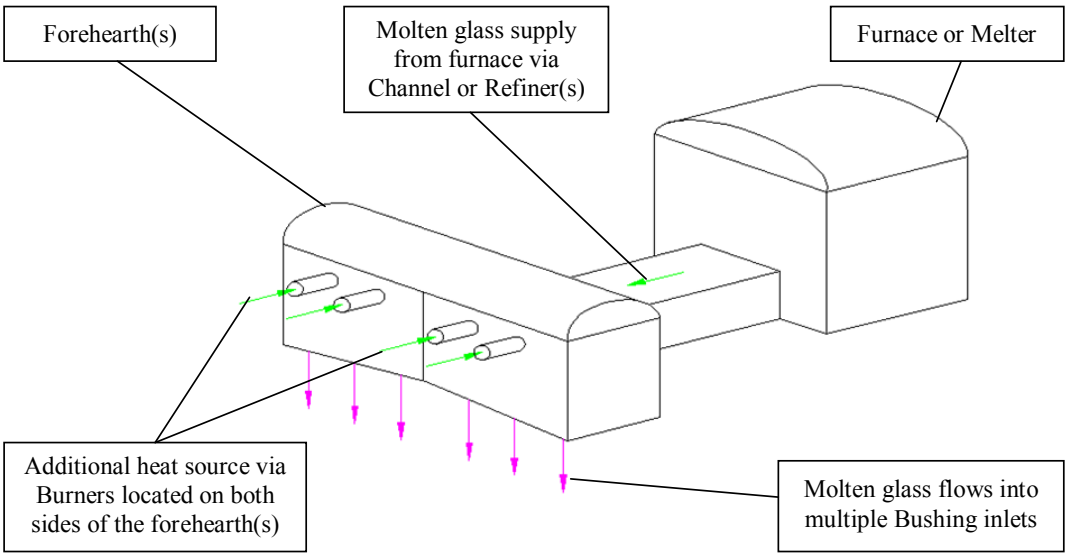

Figure 1.2 – Simplified Layout of a Thermal Processing System Used to Manufacture Glass Fibers

1.4.1 Furnace

The basic function of the furnace or melter, is to convert dry E glass batch into a molten state (temperature>1800°K) which is then fed into the rest of the system. E glass is an alkali–free glass with high electrical resistivity, high strength, and moisture resistant glass composition commonly used in the production of continuous glass fibers[3]. Originally, E glass was developed over 60 years ago for electrical engineering purposes. It is now most commonly used in the textile industry and in the production of composites, where it accounts for nearly 90% of the used reinforcements[4]

A furnace is typically constructed from numerous layers and types of refractory material. Burners positioned above the glass are the primary source for heating (see figures 1.3). The key characteristic of a furnace is to achieve constant operating conditions. This requires that the glass depth and furnace pull (or mass flow rate out), batch quality, and

thermal uniformity all remain constant. Variations in operating conditions can significantly influence the productivity and quality of the produced glass fibers.

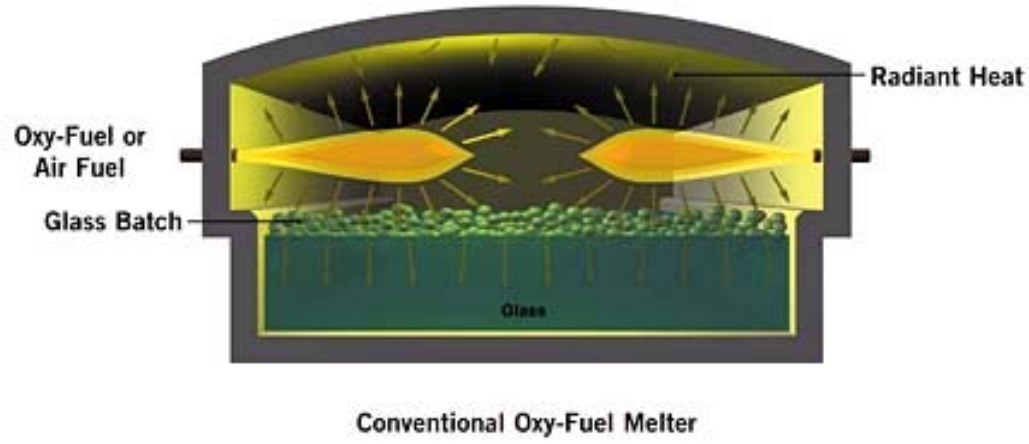

Figure 1.3 – Example of Burner Positions in a Conventional Furnace[5]

1.4.2 Channels or Refiner

The molten glass is transported from the furnace to the forehearth(s) via a network of covered channels[6]. These channels are constructed of several different layers of refractory material, and they also utilize burners to help maintain thermal uniformity.

1.4.3 Forehearth

The forehearth is the distribution channel for all of the fiber forming bushings contained below it. The molten glass is feed from the channel and is delivered to each of the bushing inlets located at the bottom of the forehearth. Coupled with the channels, these two components are often referred to as the molten glass delivery system[7] Size and throughput of the furnace, the E glass batch being processed, and plant layouts are some of the variables that contribute to the layout of the specific design configuration of the channels and forehearths for a plant. Figure 1.4 shows two different typical configurations. The figure on

the left (1.4a) shows a system for low pull, whereas the one on the right (1.4b) depicts a high pull system.

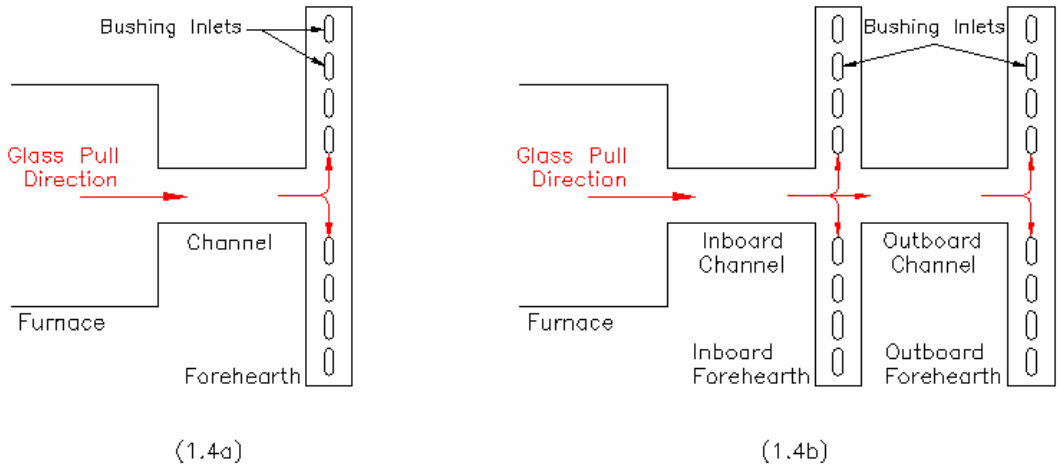

Figure 1.4 – Examples of Typical Molten Glass Delivery Systems Illustrating (1.4a) a Low Furnace Pull System and (1.4b) a High Furnace Pull System

1.4.4 Burners

Burners are used throughout the thermal processing system, either to assist in melting the glass batch or to help control the molten gas temperature within the delivery system. Figure 1.5 depicts an example of a typical oxygen-fuel burner. Burners are typically positioned longitudinally above the glass level and they fire laterally across the glass surface as a non-contact heating source that utilizes oxygen–fuel melting technologies (i.e. a mixture of natural gas and oxygen). Heat transfer is a mix of convection and radiation between the hot combustion gases, the surrounding refractory material, the cooling air, and the molten glass surface.

Figure 1.5 – Example of an Oxygen–Fuel Burner Featuring Flat Flame Geometry[8]

1.4.5 Fiber Forming Bushings

The glass fibers are created in the fiber forming bushings, which cannot be seen in figure 1.2. The molten glass flows from one of the several forehearth outlets, into what are known as bushings, then through one of the hundreds of tiny orifices to form filaments. These filaments are attenuated, cooled and gathered together to form strands as show in figure 1.6.

Figure 1.6 – A Bottom View of a Bushing During Operation[9]

The tiny orifices where the molten glass exits the TPS are often referred to as nozzle tips, and in any given bushing, the number of nozzle tips can vary from 500 to 5000 tips depending on the application as shown in figure 1.7.

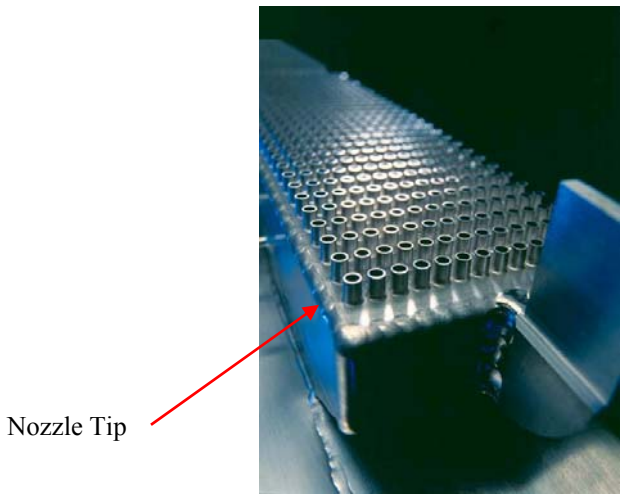

Figure 1.7 – Bottom View of a Typical Glass Fiber Forming Bushing[10]

The two forces associated with the production of glass fibers are developed by means of pultrusion and extrusion (see figure 1.8). "F1" represents a hydrostatic pressure of the molten glass above, which is directly related to the glass depth in the forehearth. In contrast, "F2" represents a tensile force exerted by the take-up winder, which has an associated velocity, V.

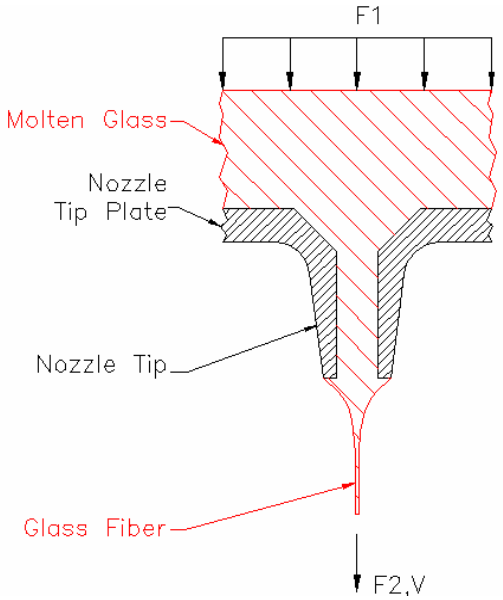

Figure 1.8 – Attenuation of a Single Glass Fiber

1.5 Overview of Thesis

The following chapter presents a literature review of glass furnace forehearth operating parameters and material characteristics of molten E glass used to produce glass fibers. The review also includes past research regarding experimental and analytical analyses of molten glass flow within forehearths. In addition, the use of mathematical models and commercially available computational fluid dynamics software (CFD) for simulating thermal variations in molten glass flow are described. In Chapter 3, an overview of the commercially available thermal CFD software that was used to conduct the numerical simulations is discussed. The development of a generic two-dimensional thermal model of a forehearth and its operating parameters used in the production of glass fibers are described. Various production scenarios are developed for determining the thermal responses of the forehearth system to different bushing arrangements. The effects of glass height variations and bushing

changeovers are also investigated in this chapter. Simulation results and conclusions are given in Chapter 4, accompanied by recommendations for future work.

2 LITERATURE REVIEW

There have been a number of research publications in the open literature in the area of glass furnace forehearth simulation models. Numerical simulations have ranged from simple two-dimensional fluid flow and heat transfer models to fairly complex three-dimensional models involving not only fluid flow and heat transfer, but also glass height variations. Many of these simulation codes were originally developed within universities and then transferred to institutes, supplier companies, and glass manufacturers for further development[11]. Recently the usage of commercially available CFD software has become a justifiable cost for improving the quality and efficiency of glass fiber manufacturing.

In general, previous studies have not accounted for the full-scale details and intricacies of a typical forehearth system. More specifically, only a few studies have included the effects of non-symmetrical glass withdrawal from the delivery channels by adjacent forehearths within a single production line or even the effects of variations in glass height. This is partially due to the fact that including such details significantly complicates the models and increases the simulation time. Nevertheless, over-simplified models do not accurately represent glass fiber formation in a production control sense. A model encompassing these rarely analyzed aspects would be more accurate for production planning purposes.

Carling[12,13,14] developed various mathematical models to calculate glass flow and heat transfer in forehearths. The first model consisted of a simple two-dimensional longitudinal forehearth, whereas the second was of a simple two-dimensional transverse forehearth model. Both models assumed the glass was a homogeneous, incompressible, Newtonian

fluid with temperature-dependent viscosity and thermal conductivity. Based on results computed by the second transverse model, an interesting interaction between the longitudinal flow and the transverse circulation was found. It was shown that in order to capture enough detail to investigate all significant effects in a real production forehearth, an analysis would require a full scale three-dimensional model.

Carling also described a third development, which consisted of two models. One consisted of a three-dimensional but parabolic model and the other was of a fully elliptic three-dimensional model. The main focus of reference [14] was to reevaluate the use of these two models by outlining their advantages and disadvantages and not to concentrate on the details of the analytical and numerical simulations. It was reported that the computed steady-state temperatures obtained using a three-dimensional model correlated well with measurements taken from a full-scale forehearth. Carling also indicated several drawbacks of mathematical modeling that are often overlooked, such as time-dependent behavior. He suggested that future developments should investigate transient versions of the models.

Lin[15] investigated the development of a three-dimensional dynamic computer model of a glass furnace forehearth that could be used as a production tool for determining forehearth performance data necessary to facilitate computer process control. The basis for his work was that previous forehearth models were not sufficiently detailed to realistically describe a production forehearth process. Lin also indicated that there had been no attempts to simultaneously include the effects of natural convection or temperature-dependent glass properties in a single dynamic model. In order to adequately describe the system, his model coupled the fluid flow heat transfer problem within the glass with the heat transfer problem

associated with the surrounding refractory walls. Lin assumed that molten glass was an incompressible, homogeneous, Newtonian fluid with temperature-dependent viscosity and thermal conductivity. The molten glass was also modeled in terms of a simplified steady-state Navier-Stokes equation in the primary flow direction. The secondary flows produced by natural convection in the glass region, along with temperatures of the glass and the surrounding refractory, were analyzed with a three-dimensional transient computer simulation program.

Because of the complexity of Lin's mathematical model, a decoupling approximation was used to simplify the model. The decoupling allowed for simulation of the glass flow with substantial heat transfer due to convection in the primary flow direction. Lin's models were validated by comparing solutions of simplified fluid flow and heat transfer problems with previously published analytical and numerical solutions. Good agreement with the simulation results was found. The forehearth steady-state and transient simulations were also compared with available experimental operating data from a glass forehearth. The forehearth simulation program was shown to be adaptable and useful for providing valuable performance data for the process control of a glass forehearth.

Chengxu and Xiufeng[16] developed a two-dimensional mathematical model of the flow and heat transfer of molten glass along the central longitudinal cross-section of a glass furnace forehearth. The model was created from the basic fundamental governing equations that pertain to molten glass. The molten glass was assumed to be a homogeneous, Newtonian fluid with temperature-dependent viscosity and density. Other assumptions included stable fluid flow and heat transfer and constant fluid height within the forehearth.

The analysis showed that numerical simulations can provide cost saving guidelines in terms of optimizing production planning and forehearth design. For example, an analysis simulated the effect of yield on molten glass flow and temperature. It showed that in order to lower the amount of heat loss throughout the forehearth, the production yields should be increased to the maximum limit where it does not affect the process's stability. The simulation results compared favorably with a physical model of a forehearth that was two and a half times smaller than an actual forehearth.

Three papers published by Choudhary[6,7,17] documented the development of several different types of mathematical models to calculate glass flow and heat transfer in glass furnace channels and forehearths. In the first paper, a three-dimensional computational model of a channel and forehearth system was developed, originating from the furnace outlet and ending at the first bushing position. The entire domain had a rectangular cross section, and it was symmetrical about the central longitudinal plane of the channels. Choudhary assumed the molten glass to be a homogeneous optically thick incompressible Newtonian fluid. The model incorporated temperature-dependent physical glass properties and variations in the cross-sectional geometry of the glass delivery system. The results demonstrated that the presence of natural convection had significant influence on the flow path lines throughout the delivery system, regardless of the fact that throughput average velocities were greater than the natural convection velocities. The results also illustrated glass channel path line distribution variations along the bottom and top surface entering into different forehearth configurations.

In a second paper published by Choudhary, a modeling study of delivery system sensitivities was conducted. Using a similar three-dimensional model from his previous work, two and four forehearth configurations were analyzed. In addition, the velocity, temperature distribution, and flow path lines from the previous work were used to study the effects of glass depth, natural convection, and the non-symmetrical glass withdrawal from opposing forehearth positions. The numerical simulations showed a fairly uniform temperature distribution across the delivery system width with gradients confined to close proximity of the sidewalls. Previous findings were also confirmed that the natural convection has a significant impact on the flow path lines. Simulations of non-symmetrical glass withdrawal from opposing forehearths showed a significant impact on the flow path line distribution in the delivery system, and on the glass flow and temperature variations within a forehearth. However, the glass flow and temperature distribution in the channels remained symmetric even for an exaggerated glass withdrawal with a 70/30 split between opposing forehearths.

In a third paper, Choudhary developed a systematic approach for modeling the free surface flow and heat transfer within a glass furnace forehearth. A three-dimensional four position model was used to calculate non-isothermal, free surface flow in a forehearth. Four positions represented the number of bushing inlets located along the bottom of the forehearth. The model incorporated an equation for calculating glass surface height into the customary equations governing glass flow and heat transfer. These equations have been outlined in Choudhary's previous works[6,7] as well as in the works of Carling[14] and Lin[15]. The commonly used approach in all previous works assumed that the glass surface remains

horizontal and at a constant height. The results showed a gradual decrease in glass surface height along the length of the forehearth, in addition to large temperature gradients along the floor of the forehearth. The velocities of the glass flow exiting through the four positions were observed to be fairly large in magnitude. The temperature of the glass leaving the model domain appeared to be relatively uniform.

Halloin and Boxho[18] experimentally examined the viscous flow of molten glass through a glass furnace forehearth. A room temperature physical model utilizing model fluids was constructed to reproduce the flow and heat transfer similar to those of molten glass in forehearths. Measurement techniques were developed to study the temperature and three-dimensional velocity fields under different experimental conditions. Experimental results showed that velocity profiles in the length direction were not parabolic due to the density gradients and outlet geometry. The velocity profiles were found to have smaller components near the free surface and higher components towards the bottom of the forehearth. It was noted that the decoupling of free and forced convection as originally hypothesized by Carling[14] could not be verified.

A commercially available computer code, FLUENT, was used to develop two- and three-dimensional models in reference [18]. As a result of incorrectly specifying the thermal boundary conditions, invalid results were obtained. By comparing with experimentally obtained temperature gradients, it was found that the thermal boundary condition was poorly defined on the glass surface. Further work was to be continued by the authors.

Recently Robb et al.[19] considered a two-dimensional model of a glass furnace forehearth. The main objective was to determine the amount of draw-down by simulating a

free surface profile of molten glass flowing in a forehearth. Draw-down refers to any change in height of a glass free surface across the length of a forehearth. Robb et al. coupled the effect of surface tension and gravity with the assumption that molten glass was a homogeneous incompressible Newtonian fluid with temperature-dependent viscosity. Commercially available finite element CFD software, FIDAP, was chosen for simulating the glass flow and heat transfer and computing the variations in glass height. This problem is difficult to solve because of the highly non-linear glass properties, the highly coupled governing equations, and the presence of a free surface. In order to achieve numerical stability, the simulation was run in a transient state. This allowed for the free surface shape to be calculated as a function of the channel length. Robb et al. concluded that there were relatively small changes in magnitude of the free surface height over a long forehearth length (Δlength to Δheight ratio $\approx$ 800:1), and that the free surface shape and temperature variations were consistent with actual manufacturing observations

Of the forehearth modeling studies mentioned above, only works reported by Choudhary[6,7,17] and Robb et al.[19] consider either the mass imbalance within the molten glass delivery system or glass surface deformations. There have been no previous attempts to include the effects of bushing interactions within a single glass forehearth. With the exception of the work reported by Robb et al. and Halloin, there have only been minimal attempts to utilize commercially available CFD software to analyze a real production forehearth system.

3 COMPUTER MODEL DESCRIPTIONS AND VALIDATIONS

3.1 Fluent Flow Modeling Software Description

For this work, the commercially available software developed by Fluent Inc. was used. Fluent Inc. is the world's leading provider of CFD software and consulting services. In 1996, Fluent began applying CFD to simulate glass flow in the glass industry. Since then, Fluent has developed integrated modeling capabilities to simulate glass flow in glass furnaces, channels, and forehearths. Fluent has also been used to predict the neck down region and the velocities and temperatures associated with glass fiber drawing[20]. Fluent now offers numerous software packages that can be used to model many production aspects commonly found in the glass fiber industry.

The FLUENT software was chosen for several reasons. The modular nature of the program allows the user to incorporate numerical models that are not included in the standard software libraries. FLUENT is also well-suited for modeling all aspects of the thermal processing system that are temperature–dependent. The primary focus of this research is on the forehearth component of the TPS, but future work could address the entire TPS. Fluent offers the flexibility to couple future component model simulations with an initial analysis.

Another simulation software, FIDAP, can be used to model free surfaces. It has been used to predict the neck down region while accounting for the highly non-linear viscosity temperature relationship, surface tension, and special heat transfer laws[20]. Modeling the neck down region is much more complex problem, which is outside the scope of this work.

Several Fluent integrated modeling software packages were used for the numerical simulation of glass flow in a forehearth. GAMBIT 2.1.6 was selected as the preprocessor

software and PreSTO 1.0 was used as the problem template interface for the FIDAP solver. The CFD simulations were separated into two parts. FLUENT 6.1.22 was selected as the heat and mass transfer solver and FIDAP 8.7.2 was chosen as the free surface CFD solver.

3.2 Gambit Overview

Preprocessing is the first step in developing a fluid flow model. The steps consist of creating the model, applying a meshing technique, and entering outlining information. Fluent offers three separate preprocessing tools, each having its own unique features. GAMBIT was chosen for its fast geometry modeling and high quality meshing capabilities. These aspects are crucial for conducting a successful simulation.

GAMBIT utilizes a single graphical user interface (GUI) for geometry construction and meshing that combines all of Fluent's preprocessing technologies in one environment. Advanced tools (PreSTO) allow for creating a simplified template that guides the user through the problem setup process in a straightforward and efficient manner for the more complex CFD solvers such as FIDAP. Specific information regarding the use of Gambit can be found in Appendix A.

3.2.1 Forehearth Geometry – Glass Domain

A mathematical model was developed to calculate flow, heat transfer, and the draw-down phenomena in a glass furnace forehearth. Following the previous studies published by Choudhary[6,17], and given that there have been no previous attempts to include the effects of bushing interactions within a single forehearth, the geometry had to be extrapolated from available information. Choudhary's most recent work utilized a three-dimensional four

position forehearth model. He reported all parameters in non-dimensional form. Actual dimensions were scaled with respect to the forehearth width because the goal was to apply the simulations as a production planning tool. Therefore, dimensions of the forehearth and bushing were developed for a typical manufacturing operation.

In reference [6], Choudhary developed a three-dimensional model of a channel and forehearth system, which originated from the furnace outlet and extended along the forehearth length to the first bushing position. The entire domain was modeled as a rectangular cross-section, and it was symmetrical about the central longitudinal plane of the channels. Specific parameters reported by Choudhary did not represent any specific glass fiber manufacturer's design or operation of a glass delivery system.

Using data derived from Choudhary, a four position model was used as a guide to develop an eight position three-dimensional forehearth model. The values of the forehearth width and entrance length were known. Using Choudhary's length scale as shown in equation (1), the forehearth dimensions were calculated and tabulated as shown in Table 3.1.

$$x = \frac{\left(w_1 \times C_x\right)}{C_{w1}} \tag{1}$$

In this equation, w_1 is the forehearth length, x is the dimension to be determined, and C_x represents the length scale reference values.

Table 3.1 – Physical Dimensions Used in Simulations

Symbol (1)	Definition	Length Scale Reference Value (Cx)	Value	
			SI	US
w_1	Forehearth Width	1.00	0.2290 m	9.02 in
w_2	Bushing Width	0.17	0.0389 m	1.53 in
w_3	Width From Forehearth Wall to Bushing Edge	0.42	0.0962 m	3.79 in
h_1	Overall Reference Height	$h_1 = \sum h_i$	0.3405 m	13.41 in
h_2	Glass Depth in Forehearth	(2)	0.2000 m	7.87 in
h_{3a}	Flow Block	0.17	0.0389 m	1.53 in
h_{3b}	Bushing Block	(3)	0.1016 m	4.00 in
l_1	Forehearth Section Length	$l_1 = \sum l_i$	3.6797 m	144.88 in
l_2	Forehearth Entrance Length	(4)	0.4600 m	18.11 in
l_3	Bushing Length	0.67	0.1534 m	6.04 in
l_4	Length Between Bushing Inlets	1.16	0.2656 m	10.46 in
l_5	End Length from Last Bushing Position	0.58	0.1328 m	5.23 in

Notes:
(1) – Symbols correspond to Figure 3.3
(2) – Value from the work of Choudhary[6,7] as an initial guess. Final value will be discussed in later sections.

(3) – Value was input as an initial guess and it will be adjusted to allow for the simulation flow to fully develop.

(4) – Value from the work of Choudhary[17].

As shown in figure 3.1 and 3.2, a three-dimensional view was created in the SolidWorks 2003 solids modeling software to better illustrate the values in Table 3.1. The inlets into the flow blocks and bushings are shown in red, whereas the exterior of the bushings are represented by blue.

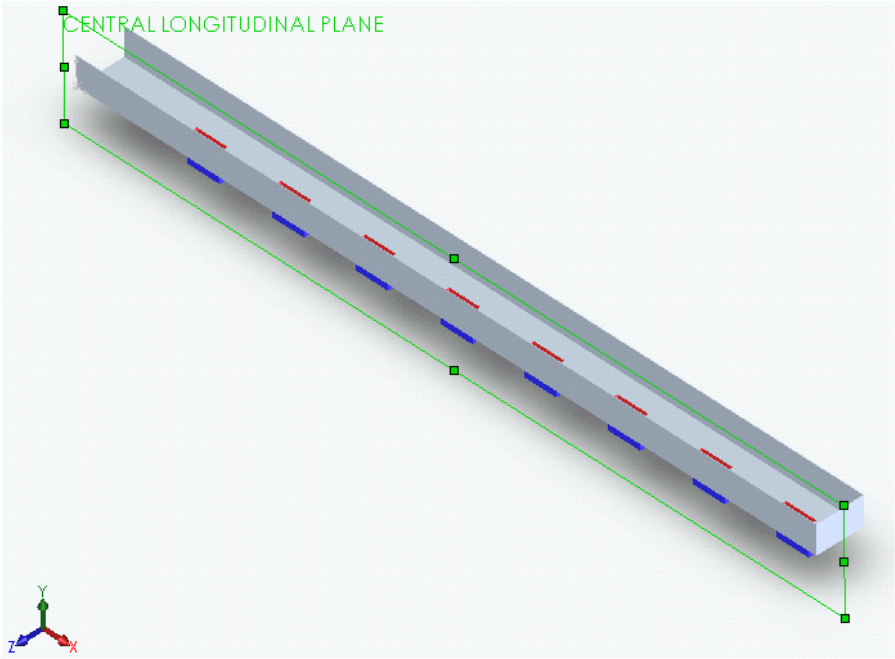

Figure 3.1 – Perspective View 1 of the Forehearth System

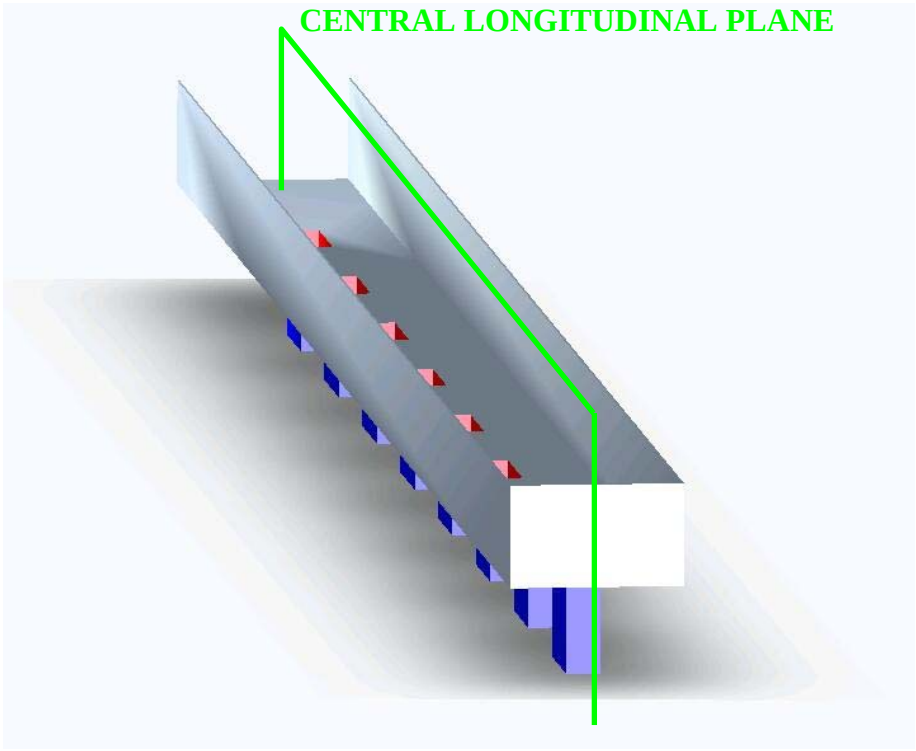

Figure 3.2 – Perspective View 2 of the Forehearth System

The geometry required for the model was the glass domain, which was extracted from the forehearth geometry shown in figure 3.3. To reduce the simulation complexity and save initial computational time, the glass domain was limited to only the central longitudinal plane of the forehearth (at $w_1/2$) as seen in figures 3.1 and 3.4. This was considered to be an acceptable approximation since the three-dimensional cross-sectional shape of the forehearth was assumed to be constant rectangular throughout the calculation domain.

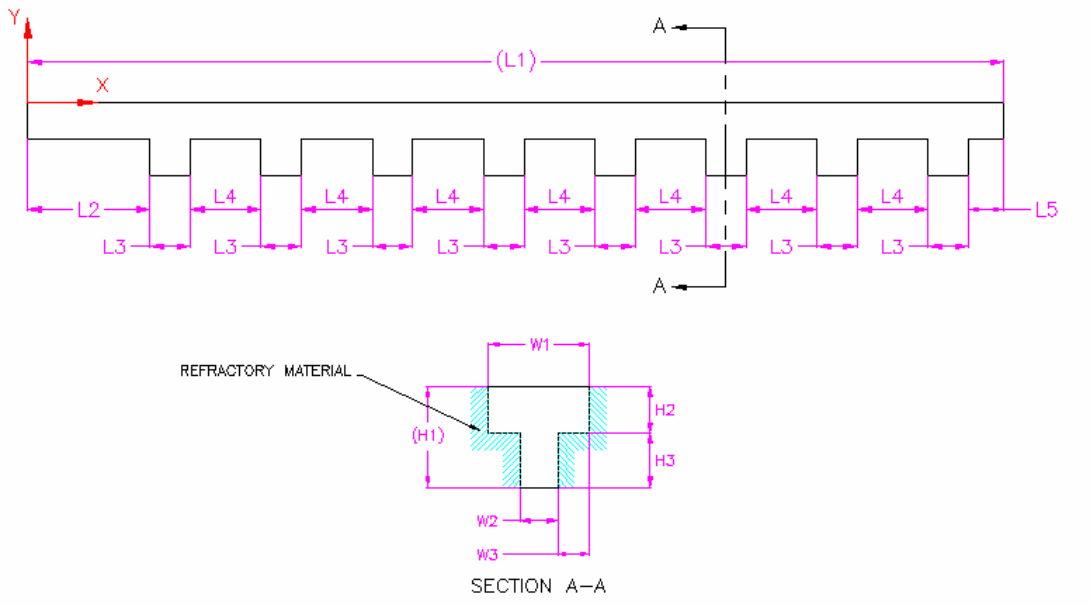

Figure 3.3 – Dimensioned Drawing of the Glass Domain

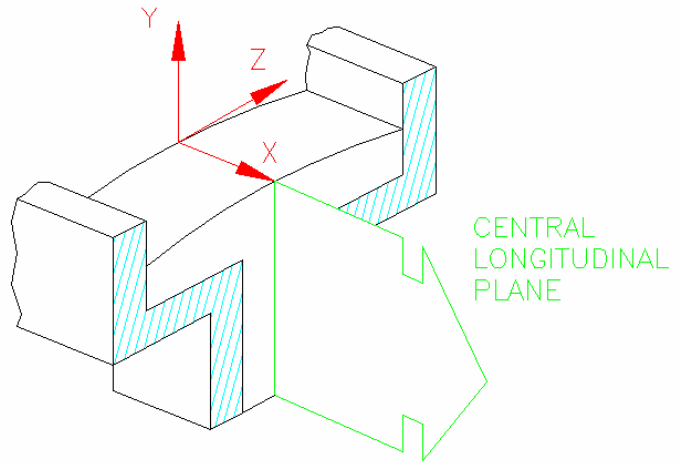

Figure 3.4 – Central Longitudinal Plane of the Model

3.2.2 Mesh Generation

The CFD solvers selected for the research simulations, FLUENT and FIDAP, accept grids comprised of quadrilateral, triangular, or a combination of the two elements for two-dimensional geometries. The choice of the mesh type to apply to a face depends solely on the application. For this research, the set-up time, computational cost, and numerical diffusion were considered. Since the forehearth geometry is relatively simple, there was no clear significant savings in set-up time with any of the three options. From previous work, the flow appears to conform well to the shape of the geometry, so a quadrilateral element was chosen. The quad elements simplify the velocity component calculations, since the components are calculated normal to the elements and the major flow direction is parallel to the global coordinate system in either the X or –Y direction.

Numerical diffusion, or false diffusion, is a dominant source of error in multi-dimensional problems. The term "false diffusion" is used because the diffusion is not a real phenomenon, yet its effect on a flow calculation is analogous to that of increasing the real

diffusion coefficient."[21]. There are three points that can be made about numerical diffusion. The first is that when real diffusion is large or the flow is not convection-dominated, numerical diffusion is least noticeable. The second is that all realistic mathematical models for solving fluid flow problems contain a finite amount of numerical diffusion. This arises from truncation errors that arise as a result of representing the governing flow equations in discrete form. The third point is that numerical diffusion is minimized when the flow is aligned with the mesh. Based on the last point, the most appropriate element choice is the quadrilateral, which will minimize numerical diffusion for the anticipated simple flow fields.

Using quadrilateral elements, the meshing scheme was defined next. A unique feature of GAMBIT is that it will automatically evaluate a specified face with respect to its shape, topological characteristics, and vertex types and recommend a face meshing scheme. From the GAMBIT evaluation and recommendation, a submap meshing scheme was selected. For mesh refinement, originally GAMBIT recommended large uniform interval count spacing on each edge. However, this mesh prevented the solutions to reach the convergence criteria. For the convergence criteria to be achieved, the uniform interval count spacing was refined by doubling the original values prescribed on each edge. The mesh as generated by GAMBIT is shown in figures 3.5 and 3.6.

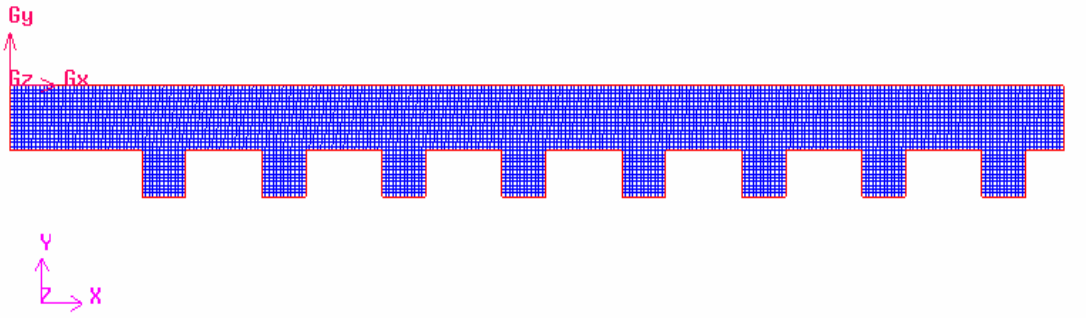

Figure 3.5 – Quadrilateral Submap Meshing Scheme

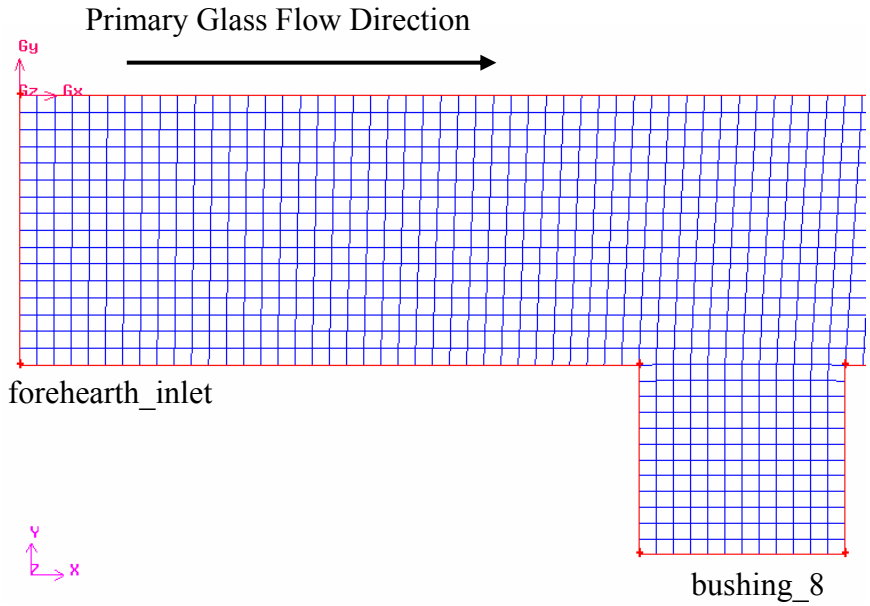

Figure 3.6 – Forehearth Inlet Quad Submap Mesh Close-Up of Bushing Position 8

3.3 FLUENT Overview

The selection of an appropriate CFD solver is an important step in developing and analyzing a fluid flow model. FLUENT was selected as the transport phenomena CFD solver for heat and mass transfer. The commercially available software package was written in the C programming language. This allows for extensive customization by making full use

of the flexibility and power offered by the C programming language. FLUENT provides comprehensive modeling capabilities for a wide range of two and three-dimensional flows. Capabilities include incompressible or compressible fluids, Newtonian or non-Newtonian, viscous or inviscid, and laminar or turbulent flows. Analyses can be performed in either a steady or transient state.

3.3.1 Governing Equations

For all flows, FLUENT can be used to solve the two-dimensional continuity and momentum equations. Equation (2) illustrates the general form of the continuity equation in symbolic notation:

$$\frac{\partial \rho}{\partial t} + \nabla \cdot \left(\rho \vec{\upsilon} \right) = 0 \qquad (2)$$

where:

ρ	=	Mass density (kg/m^3)
t	=	Time (sec)
$\vec{\upsilon}$	=	Overall velocity vector (m/s)

Equation (2) reduces to the form of equation (3) for the special case of incompressible flows:

$$\nabla \cdot \vec{\upsilon} = 0 \qquad (3)$$

The following equation (4) represents the conservation of momentum in an inertial reference frame:

$$\frac{\partial}{\partial t}\left(\rho\vec{\upsilon}\right)+\nabla\cdot\left(\rho\vec{\upsilon}\vec{\upsilon}\right)=-\nabla p+\nabla\cdot\left(\bar{\bar{\tau}}\right)+\rho\vec{g}+\vec{F} \qquad (4)$$

where:

p = Static Pressure (Pa)

$\bar{\bar{\tau}}$ = Viscous stress tensor (Pa)

$\rho\vec{g}$ = Gravitational body force (N)

$\vec{g}$ = Gravitational acceleration (m/s^2); standard value = $9.80665 m/s^2$

$\vec{F}$ = External body force (N)

The viscous stress tensor is given by the following equation (5):

$$\bar{\bar{\tau}}=\mu\left(\nabla\vec{\upsilon}+\nabla\vec{\upsilon}^{T}\right) \qquad (5)$$

where:

μ = Dynamic viscosity (kg/m-s)

In addition, for fluid flows involving heat transfer, the energy equation must be included as:

$$\frac{\partial}{\partial t}(\rho h) + \nabla \cdot \left(\vec{\upsilon} \rho h\right) = k_{eff} \nabla^2 T + 2\mu s : s \qquad (6)$$

where:

h = Sensible enthalpy (J/kg)

k_{eff} = Effective thermal conductivity (W/m-K)

T = Temperature (K)

2μs:s = Viscous Dissipation Term (W/m^3)

The sensible enthalpy is given by equation (7) to be :

$$h = \int_{T_{ref}}^{T} c_p dT \qquad (7)$$

where:

c_p = Specific heat at constant pressure (J/kg-K)

T_{ref} = 298.15°K

3.3.2 Modeling Goals

The FLUENT CFD model was used to determine the sensitivity of the forehearth system to various bushing arrangements. The results can be used as a production planning tool and to identify unfavorable processing conditions. This represents the concept of a

"balanced runner" forehearth. Note that free surface variations cannot be considered in FLUENT, which is a limitation of the solver.

3.3.3 Computational Model

The complete physical forehearth system was isolated to the glass domain, as discussed previously. The computational domain of the model begins at the forehearth inlet and ends at each of the eight bushing inlets, as shown in figure 3.7.

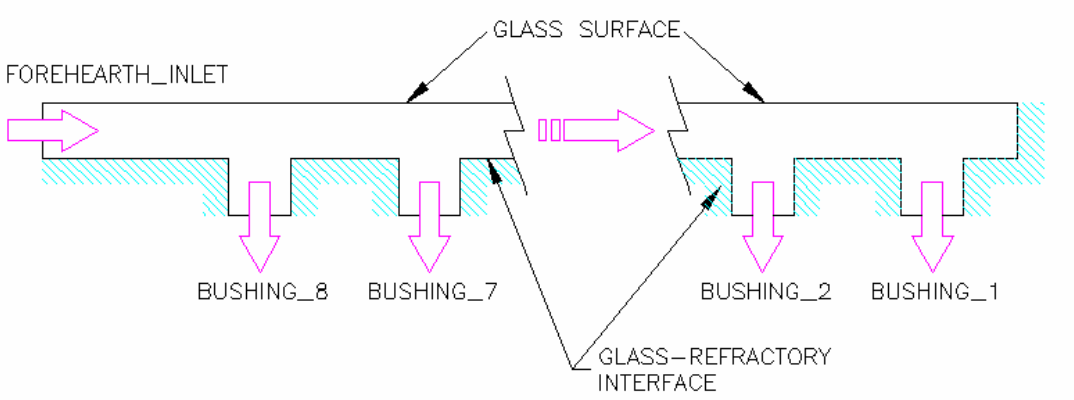

Figure 3.7 – Glass Domain Flow Computational Model

The boundary conditions were defined as shown in figure 3.7. The glass-refractory interfaces were prescribed as solid surfaces (Zone Type: Wall) with normal and tangential velocity components set equal to zero, which implies a no-slip condition. The forehearth inlet and bushing inlet positions were prescribed as the boundary edges for glass flow (Zone Type: Mass Flow Rate). The glass surface was assumed to be a flat, horizontal surface (Zone Type: Wall) with no specified shear, implying a slippery boundary condition. For a detailed list of the FLUENT CFD specified zone-types, see Appendix B.

3.3.4 Physical Model

As mentioned previously, the forehearth dimensions were based on Choudhary's work[6]. The physical properties, boundary conditions, and operating conditions used were also consistent with Choudhary's model.

3.3.4.1 E Glass Physical Properties

It was assumed that the molten glass is an incompressible, homogeneous, Newtonian fluid with temperature–dependent thermal conductivity and viscosity. In previous derivations of the energy equation within molten glass, it was necessary to introduce an effective conductivity that combined the effects of conductive and radiative heat transfer. In order to do this, the molten glass was assumed to be optically thick. The specific physical properties are summarized in table 3.2.

Table 3.2 – Molten E Glass Physical Property Values[6]

E Glass Property	Symbol	Value	Units
Density	ρ	2500.00	kg/m^3
Dynamic Viscosity	μ	$\log \mu = -2.427 + 2952.8 / (T - 810.8)$	kg/(m-s)
Effective Thermal Conductivity	k_{eff}	$1.73 + (4.53 \times 10^{-9})T^3$	W/(m-°K)
Specific Heat	c_p	1401.60	kg-°K

The glass material property definitions were customized to allow for the glass viscosity and thermal conductivity to be temperature-dependent. A User Defined Function (see Appendix C) was written in the C programming language, interpreted, and applied to the glass material properties within FLUENT.

3.3.4.2 Boundary Conditions

To account for the conductive, convective, and radiative heat transfer lost by the refractory walls, an effective heat transfer coefficient (U_{conv}) was derived. To minimize the model complexity, the associated refractory wall thickness was integrated into the conduction term of the coefficient derivation. Three different types of refractory material were chosen to determine the effective heat transfer coefficient. The assigned thermal conductivity values were calculated as an average of published values from various refractory material suppliers, as shown in table 3.3.

Table 3.3 – Refractory Material Parameters

Refractory Parameter	Symbol	Value	Units
Refractory Interface Thermal Conductivity	k_{rg}	4.05	W/(m-°K)
Refractory Interface Thickness	L_1	7.62E-02	m
Refractory Brick Thermal Conductivity	k_{rb}	2.03	W/(m-°K)
Refractory Brick Thickness	L_2	7.62E-02	m
Refractory Insulation Thermal Conductivity	k_{ri}	0.81	W/(m-°K)
Refractory Insulation Thickness	L_2	10.20E-02	m
Refractory Insulation Emissivity	ε_g	0.90	

Carling[14] specified two different refractory layers in his early simulations, each with its own relative thickness. Recent publications have shown that current technologies utilize multiple layers, each with a unique purpose. For this research, three different refractory layers were selected. The work of Carling was utilized as a template in assigning arbitrary thickness values. Note that the assigned values are used to illustrate the modeling approach and they do not pertain to any actual forehearth design. In addition to the refractory

parameters, the data in table 3.1 was used to derive an effective heat transfer coefficient taking into account the three modes of heat transfer. The calculation is described in the following section.

3.3.4.3 Refractory Material Heat Transfer Coefficient (U_{conv}) Calculations

To initiate the calculations, an initial guess of the refractory material exterior surface temperature (T_1) is made. For example, let

$$T_1 = 600^\circ K$$

The effective convection coefficient (h_{eff}) is calculated by equation (8) to be:

$$h_{eff} = h_{rad} + h_{conv} \tag{8}$$

The radiation heat transfer coefficient is first determined. Using the variables shown in table 3.4, the coefficient at the exterior surface of the refractory material is calculated by equation (9)

Table 3.4 – Radiation Heat Transfer Coefficient Variables

Radiation Heat Transfer	Symbol	Value	Units
Dimensions (see figure 3.8)			
Forehearth Unit Depth	X	0.23	m
Flow Block to Bushing Inlet Height	Y	0.14	m
Distance from Flow Block Edge to Workstation Wall ($L_4/2$)	Z	0.13	m
View Factors			
Y / X		0.60	m
Z / X		0.60	m
F_{1-1}		0.28	
F1-3		0.72	
Properties of Air at 310°K[22]			
Coefficient of Volumetric Thermal Expansion	β	3.23E-03	$°K^{-1}$
Kinematic Viscosity	υ	1.67E-05	m^2/s
Thermal Conductivity	k	2.70E-02	W/(m-°K)
Prandtl Number	Pr	0.71	
Thermal Diffusivity (Absorptivity)	α_{air}	2.37E-05	
Transmissivity	τ_{air}	0.00	
Miscellaneous			
Gravitational Acceleration	g	9.81	m/s^2
Stefan-Boltzmann Constant	σ	5.67 x 10-8	$W(/m^2-°K^4)$
Heat Transfer Coefficient at the Forehearth Bottom	h_{bf}	5.10	$W/(m^2-°K)$
Temperature Below Forehearth	T_{sur}	310.00	°K
Reference Molten Glass Temperature	T_{opt}	1561.00	°K

$$h_{rad} = \frac{q''_{rad}}{(T_1 - T_{sur})} \tag{9}$$

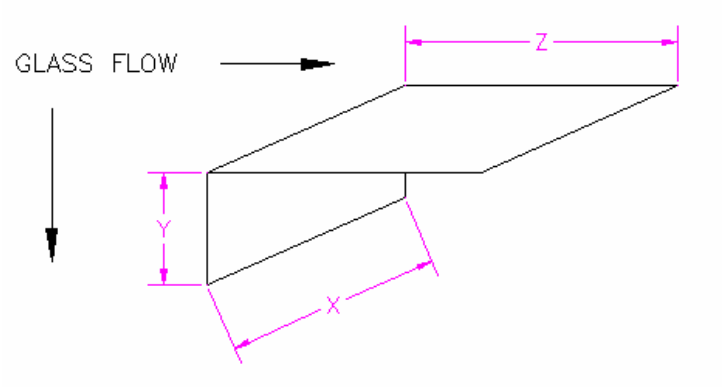

Figure 3.8 – Radiation View Factor Drawing

The heat flux through the refractory is to be determined before a value for the radiation heat transfer coefficient can be computed. This is given by equation (10) to be:

$$q'' = J_1 + G_1 \tag{10}$$

where:

J_1 = Radiosity, "total radiation which leaves a surface per unit time and per unit area"[22] (W/m^2)

G_1 = Irradiation, "total radiation incident upon a surface per unit time and per unit area"[22] (W/m^2)

The radiosity is determined as the sum of the amount of radiation emitted (E_1) plus the amount of radiation reflected (ρG_1) from the refractory surface, as shown in equation (11)

$$J_1 = E_1 + \rho\, G_1 \tag{11}$$

where:

$$G_1 = F_{1\text{-}1}J_1 + F_{1\text{-}3}J_3 \tag{12}$$

To calculate the radiosity (J_1), it is necessary to determine the fraction of radiation that is reflected (ρ_1). The total effects of incident radiation striking a material surface (see figure 3.9) is equal to one, as illustrated by equation (13).

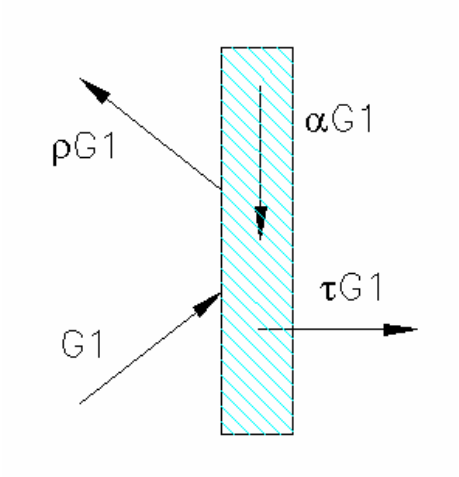

Figure 3.9 – The Resulting Effects of Radiant Energy (G_1) Striking a Material Surface

$$1 = \rho_1 + \alpha_{air} + \tau_{air} \tag{13}$$

where:

ρ_1 = Reflectivity, fraction of incident radiation reflected

α_{air} = Absorptivity, fraction of incident radiation absorbed

τ_{air} = Transmissivity, fraction of incident radiation transmitted

From Kirchhoff's law, it is known that:

$$\varepsilon = \alpha_{air}$$

By substituting the values into equation (12), the fraction of radiation that is reflected (ρ1) is solved for as:

$$\rho_1 = 1 - 0.90 - 0.00 = 0.10$$

In addition the radiosity and irradiation can then be solved for:

$$J_1 = 6844.79 \, W/m^2$$

$$G_1 = 2313.03 \, W/m^2$$

Finally, by substituting the computed values of radiosity and irradiation into equation (10) and then substituting the value of the radiation heat flux out of the refractory surface into equation (9), the radiation heat transfer coefficient is determined to be:

$$q''_{rad} = 6844.79\text{-}2313.03 = 4531.76 \, W/m^2$$

$$h_{rad} = \frac{4531.76}{(600\text{-}310)} = 15.63 \, W/m^2 - {}^\circ K$$

Next the convective heat transfer coefficient (h_{conv}) is determined. The calculation for the convective coefficient assumes that the room air is quiescent and the horizontal portion of the two perpendicular walls is neglected. Using the variables shown in table 3.4, the convection coefficient on the exterior surface of the refractory material is calculated by equation (14) to be,

$$h_{conv} = \frac{\left(Nu_y \times k\right)}{y} \tag{14}$$

In order to compute the convection coefficient using equation (14), the Nusselt number (Nu_y) has to be determined. The Nusselt number is a function of both the Grashof (Gr_y) and Rayleigh (Ra_y) numbers, which are computed by equations (15) and (16) as,

$$Gr_y = \frac{\left[g\beta\ \left(T_1 - T_{sur}\right) y^3\right]}{\upsilon^2} = 9.11\times10^7 \tag{15}$$

$$Ra_y = Gr_y \,\mathrm{Pr} = 6.43\times10^7 \tag{16}$$

Since the Rayleigh number was determined to be less than 10^9, the equation used to calculate the Nusselt number is given by equation (17) to be,

$$Nu_y = 0.68 + \left[\frac{\left(0.67 \times Ra_y^{1/4}\right)}{\left[1 + \left(0.49 \times \Pr\right)^{9/16}\right]^{4/9}} \right] \qquad (17)$$

$$Nu_y = 57.27$$

Therefore, the convective heat transfer coefficient is determined as to be:

$$h_{conv} = 10.05 \, W/m^2 - °K$$

Finally, an effective heat transfer coefficient is computed as:

$$h_{eff} = 25.67 \, W/m^2 - °K$$

As shown in figure 3.10, the conduction through the refractory material layers (k_1, k_2, k_3) and the convection coefficient at the refractory–glass interface (h_{bf}) are incorporated into the final equation (18) to determine a refractory material heat transfer coefficient (U_{conv}). Equation (18) represents a summation of all the refractory thermal resistances.

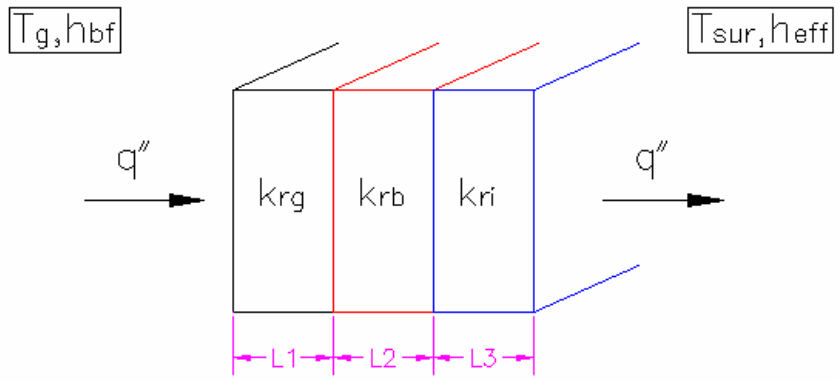

Figure 3.10 – Summation of All Refractory Thermal Resistances

$$U_{conv} = \frac{1}{\left[\left(1/h_{bf}\right) + \left(L_1/k_1\right) + \left(L_2/k_2\right) + \left(L_3/k_3\right) + \left(1/h_{eff}\right)\right]} \qquad (18)$$

Using the variables shown in table 3.3, the initial refractory material heat transfer coefficient through the refractory material is calculated to be:

$$U_{conv} = 2.40 \, W/m^2 - °K$$

The initial guess for the refractory surface temperature (T_1) is then evaluated. This is achieved by substituting the determined internal thermal resistance variables into equation (19). Equation (19) is then rewritten to solve for the surface temperature, as given by equation (20). The newly determined surface temperature is compared to that of the initial guess. In the event that the two surface temperatures differ by more than 1.0 x 10^{-2} °K, a new guess is entered and the entire process is repeated.

$$\frac{\left(T_g - T_s\right)}{\left[\left(1/h_{bf}\right) + \left(L_1/k_1\right) + \left(L_2/k_2\right) + \left(L_3/k_3\right)\right]} = \frac{\left(T_g - T_{sur}\right)}{\left[\left(1/h_{bf}\right) + \left(L_1/k_1\right) + \left(L_2/k_2\right) + \left(L_3/k_3\right) + \left(1/h_{eff}\right)\right]} \qquad (19)$$

$$T_s = \frac{\left[T_g \left(1/h_{eff} \right) + T_{sur} \left(\left(1/h_{bf} \right) + \left(L_1/k_1 \right) + \left(L_2/k_2 \right) + \left(L_3/k_3 \right) \right) \right]}{\left[\left(1/h_{bf} \right) + \left(L_1/k_1 \right) + \left(L_2/k_2 \right) + \left(L_3/k_3 \right) + \left(1/h_{eff} \right) \right]} \qquad (20)$$

This iterative process was repeated ten times before the computed surface temperature met the convergence criteria as shown in table 3.5.

Table 3.5 – Refractory Material Exterior Surface Temperature Evaluation

Convergence Criteria, ±0.01°K

Iterations	$T_{1,\,guess}$ (K)	$T_{1,\,check}$ (K)	U_{conv} (W/m^2-K)
1	600.00	426.90	2.40
2	500.00	458.77	2.33
3	475.00	468.42	2.31
4	472.00	469.64	2.31
5	471.00	470.05	2.31
6	470.50	470.25	2.31
7	470.35	470.31	2.31
8	470.33	470.32	2.31
9	470.33	470.32	2.31
10	470.32	470.32	2.31
11	470.32	470.32	2.31

A summary of the parameters used in the FLUENT simulations is shown in table 3.6. Note that the burners were represented by a constant temperature (T_s) of 1589°K on the glass surface. The specific temperature value was taken to be the same value assumed at the forehearth inlet (T_i) of 1589°K.

Table 3.6 – FLUENT Glass Domain Boundary Conditions

Physical Property / Parameter	Symbol	Value	Units
Glass Temperatures[6]			
Temperature Below Forehearth	T_{sur}	310.00	K
Glass Surface Temperature	T_s	1589.00	K
Inlet Temperature	T_i	1589.00	K
Initial Conditions			
Gravitational Acceleration	g	9.81	m/s^2
Atmospheric Pressure	P_{atm}	101.33	kPa
Effective Heat Transfer Coefficient for the Refractory Walls	U_{conv}	2.31	$W/(m^2\text{-}K)$

3.3.4.4 Operating Conditions

At the entrance to the glass domain, the flow was assumed to only have a longitudinal velocity component and it was represented as a fully developed profile. Since the simulation deals with low Reynolds number flow wherein the boundary layer develops within a short distance of the entrance, it was assumed that the resulting molten glass flow front would have a fully developed velocity profile. To confirm this assumption, the flow was specified as a constant mass flow rate at the inlet, and a simulation was run to calculate the appropriate velocity profile. The total inlet mass flow rate ($\dot{m}_{i,1}$) specified for the analyses conducted by Choudhary[6,7] was applied to the three-dimensional glass domain flow computational model. For two-dimensional models, a unit depth of one meter is assumed by FLUENT. The glass domain has a unit depth of 22.90 x 10^{-2} meters within the forehearth area, and a unit depth of 3.89 x 10^{-2} meters within the flow block/bushing inlet area. The calculations are shown in

table 3.7. In order to apply an equivalent inlet mass flow rate ($\dot{m}_{i,2}$), a correction factor equation (21) based on a ratio of the areas was developed.

$$\dot{m}_2 = \left(\frac{A_2}{A_1} \right) \dot{m}_1 \tag{21}$$

To account for the fact that the flow block/bushing inlet unit depth is smaller than the unit depth of the forehearth area, and additional area ratio term (A_1'/A_1) was introduced as shown in equation (22).

$$\dot{m}_2 = \left(\frac{A_2 / A_1}{A_1' / A_1} \right) \dot{m}_1 \tag{22}$$

where:

A_1 = Actual flow block/bushing inlet area (m^2)

A_1' = Flow block/bushing inlet area determined with actual glass domain unit depth (m^2)

A_2 = Flow block/bushing inlet area determined with unit depth of 1 meter as assumed by FLUENT (m^2)

Three different types of bushing throughput rates were used in various arrangements. The first bushing throughput rate was determined by dividing the $\dot{m}_{i,2}$ by the eight bushing positions in the forehearth model ($\dot{m}_B$). This represented the constant throughput rate

system, which provided the benchmark for comparison with all other simulations. The additional bushing throughput rates were determined by increasing two times ($\dot{m}_C$) and reducing by half ($\dot{m}_A$), the calculated constant throughput rate as shown in table 3.7. A summary of the specific mass flow rate values are shown in table 3.8.

Table 3.7 - Mass Flow Rate 3D to 2D Correction Factor Calculations

FOREHEARTH INLET	BUSHINGS
A_1 = 9.02in x 5.37in	A_1 = 1.53in x 6.04in
A_1 = 48.44 in^2	A_1 = 9.24 in^2
	A_1' = 9.02in x 6.04in
	A_1' = 54.4808 in^2
A_2 = (1m / 0.0254m/in) x 5.37in	A_2 = (1m / 0.0254m/in) x 6.04in
A_2 = 211.42 in^2	A_2 = 237.80 in^2
$MFR_{i,1}$ = GIVEN	$MFR_{b,1}$ = (1 / 8) x $MFR_{i,1}$
$MFR_{i,1}$ = 0.1250 kg/s	$MFR_{b,1}$ = 0.0156 kg/s
$MFR_{i,2}$ = (A_2 / A_1) x $MFR_{i,1}$	$MFR_{b,2}$ = [(A_2 / A_1) / (A_1' / A_1)] x $MFR_{b,1}$
$MFR_{i,2}$ = 0.5456 kg/s	$MFR_{b,2}$ = 0.0682 kg/s
Inlet Velocity	High Mass Flow Rate ($\dot{m}_C$)
V_{inlet} =	2 x $MFR_{b,2}$ = 0.1364 kg/s
($MFR_{i,2}$ / ρ_T) / (1m x (5.37in * 0.0254m/in))	Low Mass Flow Rate ($\dot{m}_A$)
V_{inlet} = 0.0016 m/s (+X)	0.5 x $MFR_{b,2}$ = 0.0341 kg/s

Table 3.8 – Corrected Two-Dimensional Mass Flow Rates

Mass Flow Rates	Symbol	Value	Units
Constant Inlet Mass Flow Rate	$\dot{m}_{i,2}$	0.55	kg/s
Low Throughput Bushing	$\dot{m}_A$	3.41E-02	kg/s
Constant Throughput Bushing	$\dot{m}_B$	6.82E-02	kg/s
High Throughput Bushing	$\dot{m}_C$	0.14	kg/s

Ten generic production cases were developed to evaluate the response of the forehearth system. A significant effect that was included in some of the cases was the introduction of a fiber forming bushing changeover. Although bushing changes occur regularly in production, there have been no published studies of the effect of a bushing changeover on subsequent bushing positions. During a bushing changeover, glass flow is restricted by cooling the molten glass so that it solidifies as shown in figure 3.11. Once the glass has solidified, the bushing is removed and replaced by another type of bushing.

Figure 3.11 – A View of Solidified Glass during a Bushing Changeover[10]

Solidification of the glass represents a large disturbance in the thermal homogeneity of the molten glass being supplied to each bushing position. Within the FLUENT simulations, a bushing changeover was represented by converting the prescribed Mass Flow

Inlet boundary condition on a bushing outlet to a no-slip Wall condition. Since the bushing is still attached as the glass is cooled, the nozzle tip plate was approximated as an isothermal heated horizontal plate facing downward, with both natural convective and radiative heat transfer. It was assumed that the surrounding air flow was stagnant, which resulted in radiation becoming the dominate form of heat transfer. To represent the radiation heat transfer out of the glass domain, an external radiation emissivity value was assigned on the changeover bushing positions.

The appropriate external emissivity value was determined by examining the nozzle tip plate surface in greater detail. Throughout the glass industry, nozzle tip plates are primarily composed of a platinum-rhodium materials, with an effective emissivity value, ε_{pr}, of approximately 0.16[10]. However, this value assumes that the metallic surface is perfectly clean, which in a production environment is only true for a short period of time. As a result, the initial guess for the effective emissivity value was increased by a factor of two (see table 3.9). This accounted for the decrease in ability to emit as much radiation at a given wavelength and temperature as a blackbody. The purpose was to achieve simulation results for glass temperatures at the wall.

Table 3.9 – Bushing Changeover Parameters

Changeover Parameters	Symbol	Value	Units
FLUENT Boundary Zone Type	– –	WALL	
External Radiation Temperature	T_{sur}	310.00	°K
Pt–Rh Emissivity	ε	0.32	

3.3.5 Determination of the Solution Procedure

The Segregated solver was chosen as the numerical solution method in FLUENT. This approach segregates the governing equations and solves them sequentially. In addition, the governing equations are non-linear and tightly coupled, which requires several iterations of the solution loop to be performed. Inherently, iterative solution methods require that a convergence criteria be met, which determines when the iterations can be terminated. The solution iterations follow the steps outlined in Figure 3.12.

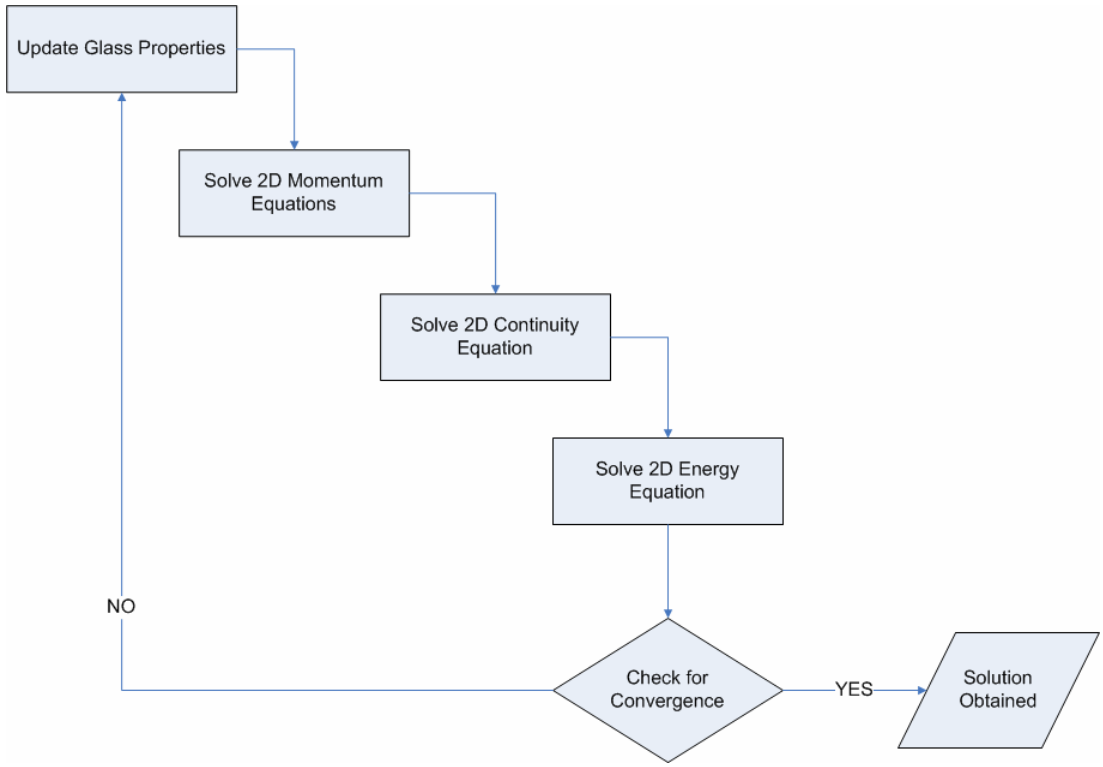

Figure 3.12 – FLUENT Segregated Solution Method Overview

From the glass property assumptions, the solver flow regime was selected as Incompressible. The solver flow type was set as laminar, as prescribed in the literature. Since there were no time-dependent terms, the simulation type was chosen as steady-state.

Two-dimensional single-precision calculations were determined to be inadequate to represent the node coordinates since the forehearth geometry has features of very unequal length scales, i.e. a very long, thin channel. Therefore the solver was set to perform two-dimensional double-precision calculations.

The residuals in a numerically stable solver must reach the convergence criteria, such that the error is acceptable to the user. Determination of the unconditional numerical stability and convergence (or error estimation) is an important topic in the fundamental numerical solution of partial differential equations (PDEs). Typically, a convergence criterion value of 1.00E-03 is a nominal value that is often suggested for incompressible, laminar flow calculations[21]. This was determined to be acceptable for the residual sum which is computed after each iteration of the momentum equation. Note that it is sometimes necessary to solve a pressure correction equation to obtain correction factors to apply to the velocity fields within the momentum equation. These solutions may not have initially satisfied the continuity equation. This In turn increases the difficulty in reaching smaller convergence criterion values. The residual sums computed for the continuity and energy equations do not entail such correction factors. Therefore the convergence criterion was increased to a value of 1.00E-06.

3.4 FIDAP Overview

FIDAP was selected as the transport free surface CFD solver. The commercially available software package was written in FORTRAN programming language. This allows for extensive customization capabilities, making full use of the flexibility and power offered by this programming language. FIDAP provides extensive modeling capabilities for the

simulation of two and three-dimensional flows involving free surfaces and/or moving boundaries. It utilizes a deforming mesh (Arbitrary Lagrangian–Eulerian, ALE) approach to capture the position and shape of the fluid free surface. Typical modeling capabilities include the selections of incompressible or compressible, Newtonian or non-Newtonian, viscous or inviscid, and laminar or turbulent flows. Analyses can be performed in either a steady-state or transient state.

3.4.1 Governing Equations

FIDAP treats the same equations as those solved by the FLUENT software. . Conservation of mass is represented by equation (3), conservation of momentum is governed by equation (4), and energy conservation is represented by equation (6). In addition, a governing equation is introduced to determine the free surface deformation of the fluid. FIDAP assumes that the free surface of the fluid satisfies a kinematic condition, which implies that the liquid–vapor interface remains constant without any mass transfer across the interface. In other words, the assumed kinematic condition is a statement that the portion of fluid on the surface remains on the surface at all times. For two-dimensional incompressible fluid flow, the impermeability of the free surface is expressed by equation (23) as,

$$\frac{\partial S}{\partial t} + \vec{\upsilon} \cdot \nabla S = 0 \qquad (23)$$

where:

S = height of the fluid (m)

3.4.2 Modeling Goals

The FIDAP CFD model was used to determine the sensitivity of the forehearth system to bushing changeovers and to predict glass depth variations. The FIDAP results

complement the findings from the FLUENT simulations for creating a production planning tool and identifying unfavorable processing conditions. Note that bushing array variations cannot be considered in the FIDAP models due to restrictions in the solver capabilities.

3.4.3 Computational Models

The two-dimensional glass domain flow model used for the FLUENT simulations was transferred directly to the FIDAP models. As stated previously, the computational domain of the model begins at the forehearth inlet and ends at each of the eight bushing positions, as shown in figure 3.5.

Boundary conditions were applied to the FIDAP models. Referring to figure 3.5, the glass-refractory interfaces were prescribed as solid convective surfaces (Zone Type: Convection) with normal and tangential velocity components set equal to zero, which implies a no-slip condition. The forehearth inlet and bushing positions were prescribed as boundary edges for glass flow (Zone Type: Plot). Initially the glass surface was assumed to be a flat, horizontal surface (Zone Type: Slip) with no specified shear, which implies a slippery boundary condition. In addition, the glass surface was also assumed to be a free surface (Zone Type: Surface), which allows for deformation to be predicted. For a detailed list of the FIDAP CFD zone-types that were specified see Appendix B.

3.4.4 Physical Models

To maintain consistency between the FLUENT and FIDAP models, the same physical properties, boundary, and operating conditions were used. In addition, the same assumptions were applied to both the FIDAP and FLUENT models. Any differences in the assumptions used in the FIDAP and FLUENT models are stated at the appropriate places.

3.4.4.1 E Glass Physical Properties

Recall that the general assumptions for the FLUENT models were that the molten glass is an incompressible, homogeneous, optically thick, Newtonian fluid. Due to the complexity of the FIDAP solver, the viscosity and thermal conductivity were specified as constant and not temperature-dependent. Using the previously prescribed temperature-dependent equations, the constant values for viscosity and thermal conductivity were calculated from the average of the molten glass temperature range solved by FLUENT for the constant bushing throughput case. The new physical properties are summarized in table 3.10.

Table 3.10 – Modified E Glass Physical Properties for FIDAP Simulations

Glass Property	Symbol	Value	Units
Temperature Range Obtained with Results Generated by FLUENT	- -	1540 - 1600	°K
Average Dynamic Viscosity	μ_{avg}	30.26	kg/(m-s)
Average Effective Thermal Conductivity	k_{avg}	19.27	W/(m-°K)

3.4.4.2 Boundary Conditions

The boundary conditions have been described previously in great detail within the FLUENT overview. For the FIDAP simulations, an additional boundary condition must be applied to the free glass surface. In FIDAP, a free surface problem refers to four different types of problems. The four different types have one common characteristic, which is a moving boundary that can be interior or exterior to the fluid domain. According to the types of free surface analyses outlined by FIDAP, this research is classified as a free-surface

boundary problem. This is because the simulation of the molten glass flow in an open channel is essentially a liquid-vapor interface problem. In this case the interface between a liquid phase and a gas phase is an unknown moving boundary and must be solved as part of the fluid and heat flow solution. The gas phase is essentially ignored, restricting the computational domain to only the liquid phase. Unless indicated otherwise, the stresses generated by the gas phase are then set equal to zero.

In determining a free-surface problem solution, both the nodes on the free surface and below are allowed to move. FIDAP provides a number of different options as to how the movements are specified. The specifications entail how the nodes on the free-surface are allowed to move, the number of nodes below the free surface that are allowed to displace, and also how these subsurface nodes are repositioned. The specification technique selected was the method of Spines. Spines are theoretical curves (usually straight lines) that begin at a point on the free surface and extend a prescribed length below surface. They prescribe the allowable movement of free-surface nodes and how the nodes below move with respect to the free-surface nodes. For the glass domain, the number of interior nodes specified was set to a value of 5 or half the glass depth within the forehearth. This determines the spine length or number of nodes that are allowed to move. Straight is specified as the controlling option for the movement of the free surface, which is the preferred option for the method of spines. To properly constrain the free surface, the first node (Node 1) is fixed, representing the constant glass height supplied by the furnace. The last nodal position on the free surface (Node 486) is defined with a constant value for the contact angle equal to zero. The free surface specifications that were applied are summarized in table 3.11.

Table 3.11 – FIDAP Free Surface Modeling Specifications

Free Surface Parameter	Symbol	Value	Units
Free Surface Type	- -	External	
Surface Tension Coefficient of E Glass[23]	γ	0.30	N/m
Reference Pressure	P_{ref}	0.00	kPa
Movement of Interior Nodes and Free Surface	- -	Spines - Straight	
Number of Interior Nodes (Depth)	- -	5.00	
Contact Angle	- -	0.00	

3.4.4.3 Operating Conditions

Similarly for the Fluent simulations, the inlet glass flow was assumed to only have longitudinal velocity components and it was defined by a fully developed profile. However, an inlet mass flow rate cannot be specified within FIDAP. Therefore to overcome apparent inlet classification restrictions, a simulation restart was incorporated. Briefly, a simulation restart allows for FIDAP to run two simulations in series. The first simulation utilizes a prescribed constant inlet velocity and temperature to determine good initial guesses of the overall velocity and temperature fields. The calculated guesses are then input directly into the second simulation as a set of initial conditions. A detailed discussion of the FIDAP solution strategy will be reviewed in a later section.

The constant inlet velocity (V_{inlet}) was obtained by solving equation (24), which is obtained from the conservation of mass principle as,

$$V_{inlet} = \frac{\dot{m}}{(\rho A_n)} \tag{24}$$

Where:

ρ = Density of E glass (kg/m^3)

$\dot{m}$ = $\dot{m}_{i,2}$ (kg/s)

A_n = Cross-sectional area normal to the glass flow direction (m^2)

A unit depth correction factor was not applied, since it was already incorporated in the inlet mass flow rate, $\dot{m}_{i,2}$. Since a mass flow rate could not be applied as a boundary condition, the outlet positions were left as unprescribed.

Similar to the bushing changeover analyses performed with FLUENT, three specific cases were duplicated within FIDAP. Each of these cases had only one bushing changeover position (bushing_8, _5, and _2). The only difference was in the method chosen to prescribe the boundary conditions in FIDAP. Due to the increased simulation capabilities of FIDAP, applying radiation to the frozen-off bushing position was far more complex and it significantly increased the computational time. To help minimize the computational time, a heat flux was calculated from the results obtained from the FLUENT simulations. The temperature distributions across the three sealed bushing outlets were averaged ($T_{i,avg}$) and substituted into equation (25) to determine the heat flux for each case (q_i") as follows

$$q_i'' = \sigma \, \varepsilon \, \left(T_{i,avg}^4 - T_{sur}^4\right) \tag{25}$$

each bushing changeover position was analyzed individually in FLUENT with all other simulation parameters held constant, as shown in table 3.12.

Table 3.12 – FIDAP Bushing Changeover Heat Flux Calculations

σ =	5.67E-08	W(/m^2-K^4)
ε_g =	0.32	
T_{sur} =	310.00	°K

	bushing_8	bushing_5	bushing_2	
(+ X) ↓	1194.70	1179.44	1149.03	
	1196.59	1181.37	1151.10	
	1197.71	1182.56	1152.47	
	1198.17	1183.10	1153.25	
	1198.04	1183.07	1153.51	
	1197.41	1182.54	1153.31	
	1196.34	1181.60	1152.70	
	1194.92	1180.30	1151.72	
	1193.21	1178.70	1150.40	
	1191.25	1176.82	1148.75	
	1189.06	1174.68	1146.76	
	1186.61	1172.24	1144.36	
T_{avg} =	1194.50	1179.70	1150.61	°K
q" =	37099.57	35302.93	31963.65	W/m^2

The highest heat flux value calculated (q_{max}") was chosen to ensure for all cases that the molten glass solidified (T < 1200°K), and was applied to all three FIDAP simulations. A summary of the FIDAP operating conditions are presented in table 3.13. Refer to table 3.4 for all other shared operating conditions.

Table 3.13 – FIDAP Specific Operating Conditions

Physical Property / Parameter	Symbol	Value	Units
Cross-Sectional Area Normal to the Inlet Glass Flow Direction	A_n	0.14	m^2
Inlet Velocity	V_{inlet}	1.60E-03	m/s
Heat Flux, Maximum	q_{avg}''	3.71E+04	W/m^2

3.4.5 Determination of the Solution Procedures

A two-dimensional, incompressible, laminar, Newtonian fluid was defined in the FIDAP models. To include the convective terms in the momentum and energy equations, the problem was defined as nonlinear. Both steady state and transient analyses were conducted. This was accomplished by computing two separate simulations in series, a common technique known as a Restart. The first simulation was solved as a steady-state, fixed surface type problem by defining the glass free surface as a SLIP entity (no shear stress) and setting the normal velocity at the glass surface to zero. The second simulation, essentially a restart, was computed as a transient, free surface type problem with the glass free surface unconstrained. The key to the Restart technique is that the first simulation is used to provide good initial values for the velocity and temperature fields, which are then used for the second actual simulation. This was chosen as a way to increase the solution and convergence stability, as well as decreasing the computational time.

The method used for solving the nonlinear system of equations was the segregated solution algorithm. The convergence criterion was similar to the criteria used for the FLUENT simulations. In addition, criteria were developed for the free surface determination. A majority of the default values were used, but because the glass surface

tension was approximately zero, the maximum number of kinematic free surface updates was significantly increased from the default value of five. This was recommended in the FIDAP user manuals[24]. The convergence criterion is summarized in table 3.14.

Table 3.14 – FIDAP Solution Parameters

Solution Command Definitions	Symbol	Steady State	Transient
Segregated Solution Algorithm	SEGRE	500	500
Velocity Convergence Tolerance	VELCONV	0.001	0.001
Free Surface Convergence Tolerance	SURF	- -	0.01
Default Percentage Change in Solution Magnitude	SCHANGE	0	0
Kinematic Iteration for Free Surface Update	KINE	- -	30

When using the segregated method, the use of relaxation factors is very important for convergence of the free surface analysis. There are two ways to specify relaxation factors in FIDAP. A constant global relaxation factor can be applied to all degrees of freedom (DOF) or individual relaxation factors can be specified for each DOF (u_x, u_y, u_z, p, T, s, k, ε, and c_n). Specification of individual relaxation factors was selected. The explicit Hybrid relaxation strategy for specifying individual relaxation factors is the default method for the segregated solution algorithm. The relaxation factors for each DOF for both the steady-state and transient analyses are shown in table 3.15. These values were obtained in consultation with the FLUENT Inc. academic technical support group.

Table 3.15 – FIDAP Explicit Hybrid Relaxation Factors

Degree of Freedom Description	Symbol	Steady State	Transient
X Component of Velocity	u_x	0.3	0.1
Y Component of Velocity	u_y	0.3	0.1
Pressure	p	0.5	0.5
Temperature	T	0.5	0.5
Surface Position	s	0.7	0.9

For the transient analysis, an implicit time integration method was selected. All parameters were developed using a trial and error method. The final transient parameters included a small fixed time step for the first ten time steps and then used a variable time step algorithm. This was used to minimize potential time step reductions when the truncation error criterion was not satisfied. The keyword "NOFIXED" was used to control when the time step algorithm was initiated. The transient parameters are summarized in table 3.16. For a detailed example of the FIDAP solver formulation code, see Appendix D.

Table 3.16 – FIDAP Implicit Time Integration Parameters

Transient Parameter	Symbol	Value
Number of Time Steps To Be Computed	NSTEP	200.00
Time at Start of Solution	TSTART	0.00
Time Step Increment	DT	0.01
Maximum Increase in Time Increment per Time Step	INCMAX	1.20
Maximum Value of Time Step Increment	DTMAX	0.10
Number of Fixed Increment Backward Euler Steps	NOFIXED	10.00

4 RESULTS AND CONCLUSIONS

4.1 FLUENT Results

A benchmark simulation was developed for comparison with other simulations. The benchmark analysis represented the ideal production scenario. The ideal scenario fixed the sum of the outlet mass flow rates to equal the constant prescribed inlet mass flow rate. Therefore, the change in mass is zero. For the purpose of this research, the ideal scenario was identified as the Balanced Mass Flow Rate System. The sign conventions used in calculations of the mass flow rate imbalances are that mass flow rates into the system are denoted by positive integers, whereas the mass flow rates out of the system are denoted by negative integers.

The first simulation (FL–1) was computed with the mass flow rate conditions shown table 4.1. Figures 4.1 through 4.9 illustrate the FLUENT solutions for FL–1. All FLUENT simulations were based on a revised molten glass depth of 0.14 meters.

Table 4.1 – FLUENT Trial FL–1: The Balanced Mass Flow Rate System

Position	$\dot{m}$ (kg/s)
forehearth_inlet	0.5456
bushing_8	-0.0682
bushing_7	-0.0682
bushing_6	-0.0682
bushing_5	-0.0682
bushing_4	-0.0682
bushing_3	-0.0682
bushing_2	-0.0682
bushing_1	-0.0682

$\Delta\dot{m}$ =	0.0000

Figures 4.1 through 4.3 show the temperature variations along the length of the forehearth for the benchmark trial, FL–1. The temperature variations shown in figure 4.1 ranged from 1559°K to 1589°K. This is slightly less compared to what has been previously published. This is due mainly to the boundary condition assumption that the surface of the glass had a constant temperature of 1589°K. Previous studies focused on the effects of convection and radiation heat transfer at the glass surface. Since the purpose of this research was to evaluate the influence of different bushing arrangements, the assumption of a constant temperature on the glass surface was considered acceptable. Note that FLUENT can be used in future investigations to incorporate other forms of heat transfer at the glass surface.

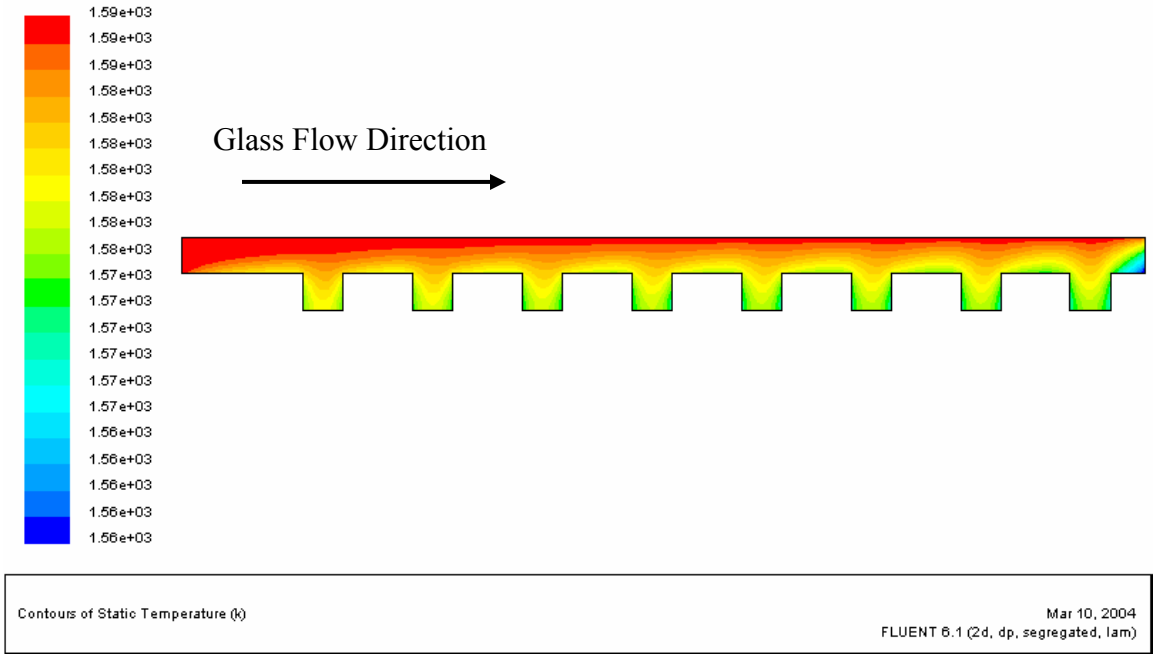

Figure 4.1 – Balanced Mass Flow Rate System Glass Temperature Contours (°K)

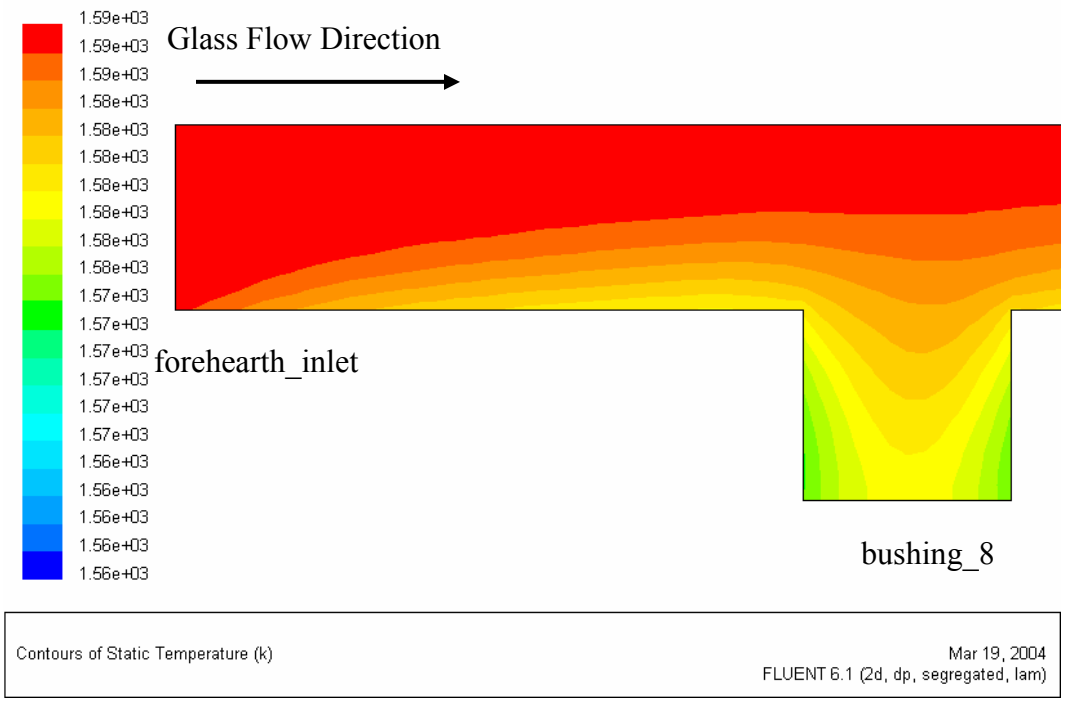

Figure 4.2 – Balanced Mass Flow Rate System Glass Temperature Close-Up of Bushing 8 Inlet (°K)

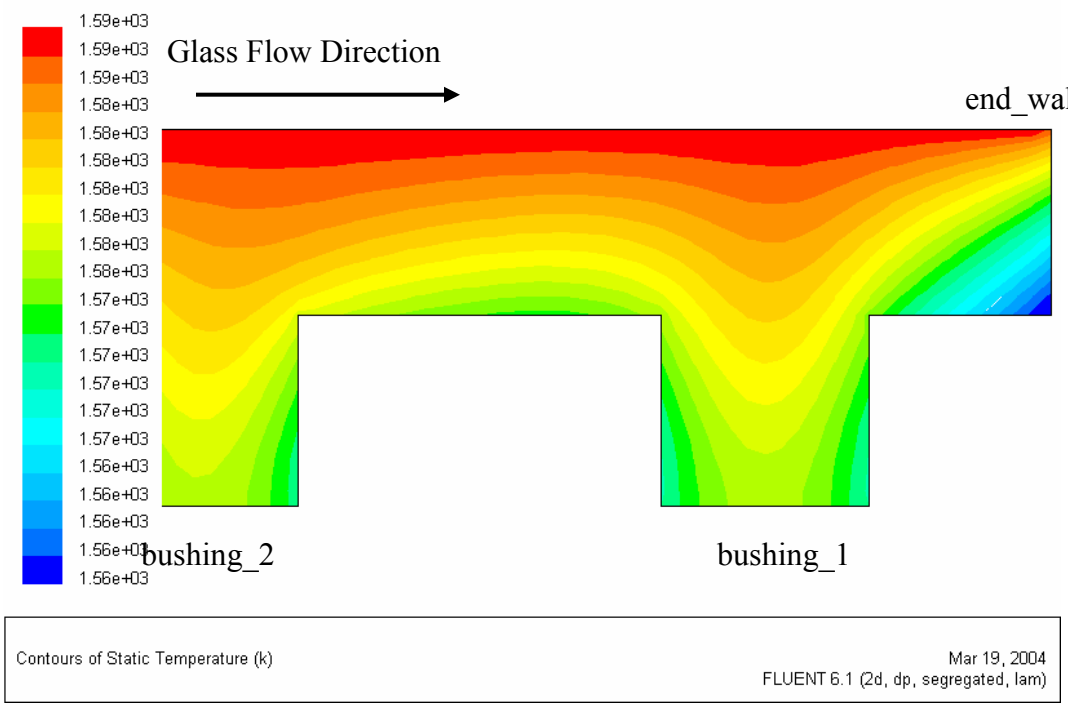

Figure 4.3 – Balanced Mass Flow Rate System Glass Temperature Close-Up of Bushing 1 and 2 Inlets (°K)

More importantly are the variations of glass temperature at the nozzle tip plate, which can significantly influence fiber breakage. Figure 4.4 shows the computed parabolic temperature profile at each of the tip plates. The glass temperatures at the walls are lower than at the center of the outlet. This is a result of prescribing an effective heat transfer coefficient boundary condition on all refractory walls. The average temperature variation from the center maximum to the wall minimum at all eight positions was about 5°K. Note that as expected, bushing_8 has the highest temperature profile since it is the nearest to the inlet. In contrast, bushing_1, which is the farthest from the inlet, has the lowest temperature distribution. The difference between the average outlet temperatures of bushing_8 and bushing_1 is approximately 3.3°K. The difference calculated between the average outlet temperatures of bushing_8 and bushing_1 is approximately 3.3°K. This is an important result because even under this ideal scenario, temperature variations occur throughout the glass domain. The introduction of other bushings and arrangements would increase the temperature variations and increase the need for better understanding of the bushing interactions for production planning purposes.

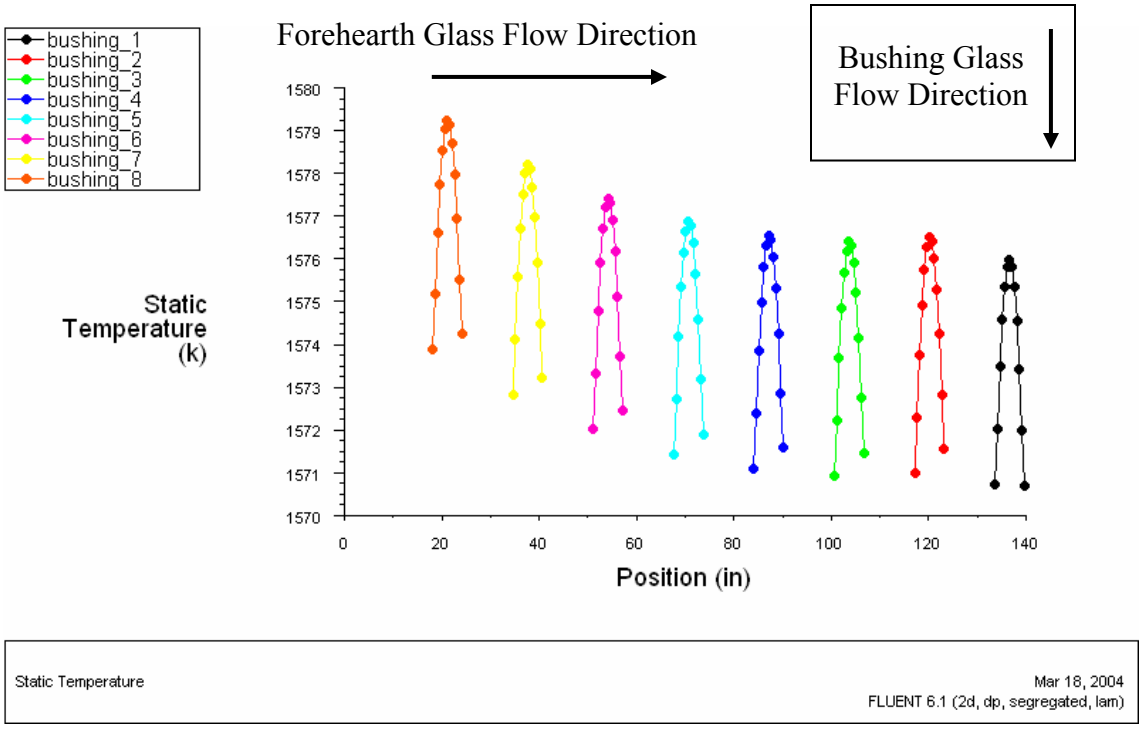

Figure 4.4 – FLUENT TRIAL 1: Bushing Inlet Temperatures (°K)

The resultant velocity magnitudes can be used to confirm the coupled temperature-dependent viscosity with the no slip boundary conditions prescribed along all refractory-glass interface surfaces. Figures 4.5 through 4.7 demonstrate the fundamental physics that the highest velocity magnitudes occur in the regions of higher glass temperature, which is on the glass surface and in the center of each of the bushing inlet positions. The velocity vectors shown in figures 4.8 through 4.10 are aligned parallel to the glass surface, which is consistent with the assumed slippery boundary condition. The velocity distribution at the nozzle tip plates shown in figure 4.11 was used as a reference value for comparison with all other simulations. The actual velocity distribution at the nozzle tip plate is determined by the geometry of nozzle tip plate and the down-line processing equipment (i.e. winders), which is a complex function of the simultaneous pultrusion and extrusion process. Note that the

actual outlet area is approximately 5% of the area depicted in the glass domain model. In addition, the length of the flow block and bushing inlet were treated as arbitrary to obtain a fully developed flow at the outlets and for the FLUENT solution to converge.

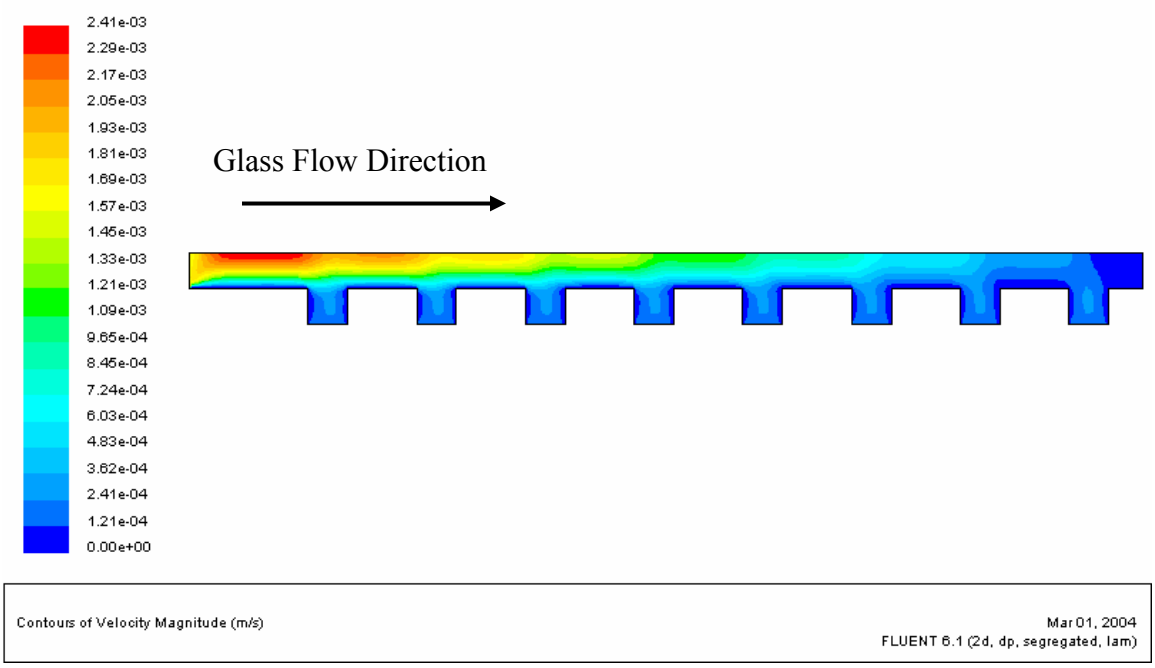

Figure 4.5 - Balanced Mass Flow Rate System Velocity Magnitudes (m/s)

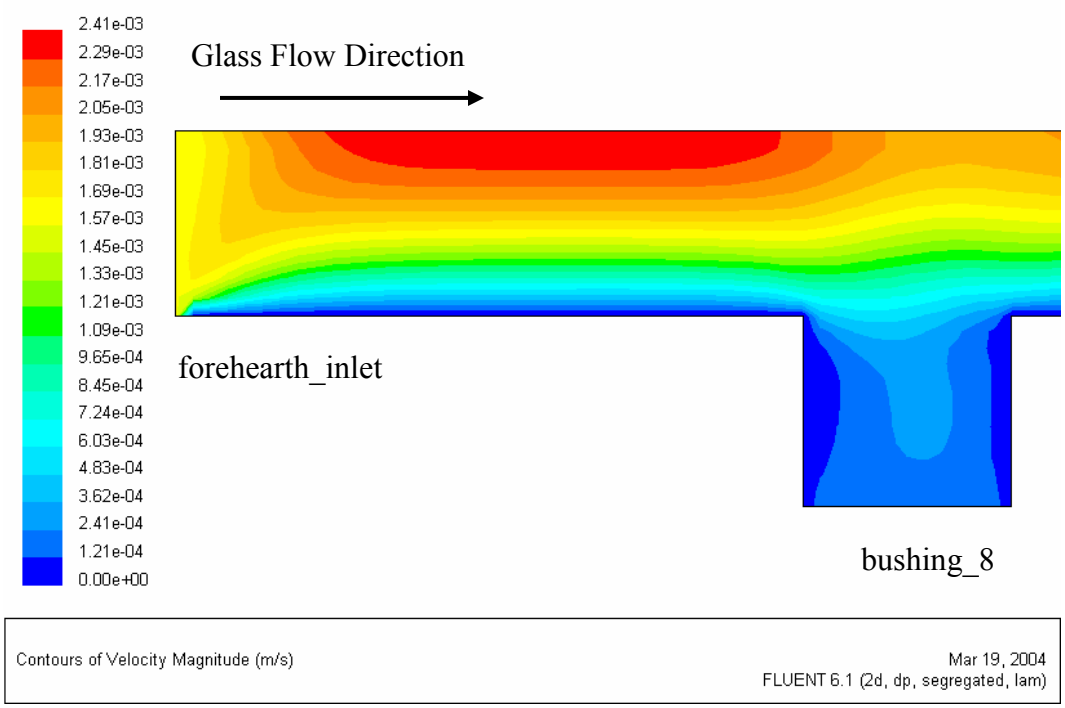

Figure 4.6 – Balanced Mass Flow Rate System Velocity Magnitudes Close-Up of Bushing 8 Inlet (m/s)

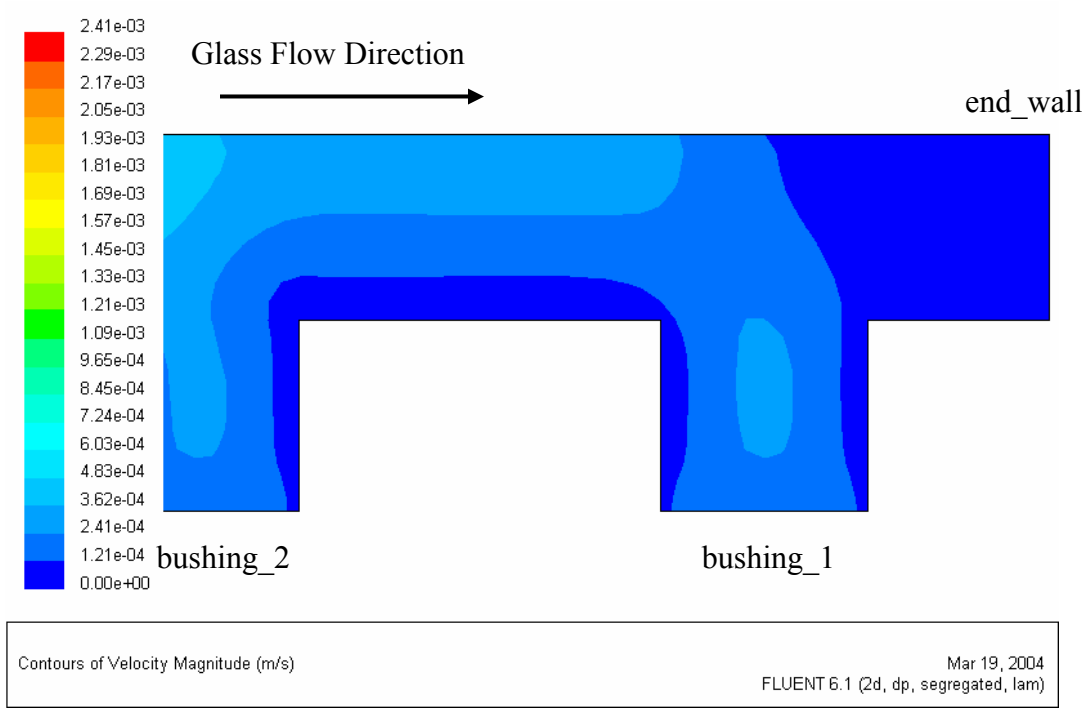

Figure 4.7 – Balanced Mass Flow Rate System Velocity Magnitudes Close-Up of Bushing 1 and 2 Inlet (m/s)

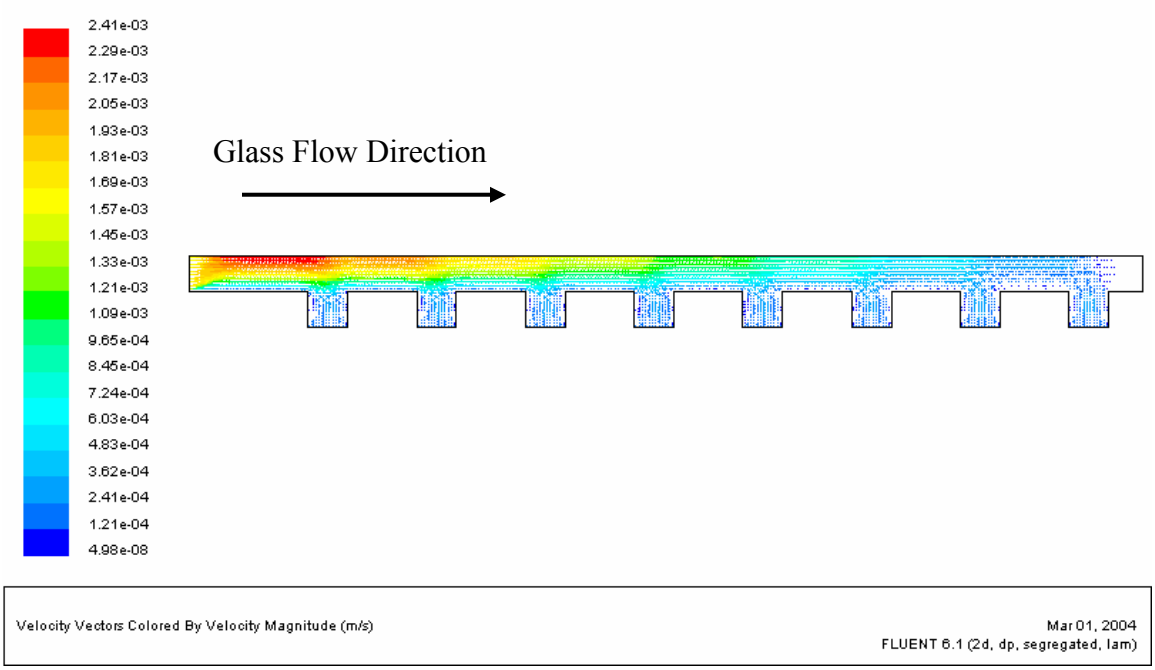

Figure 4.8 - Balanced Mass Flow Rate System Velocity Vectors (m/s)

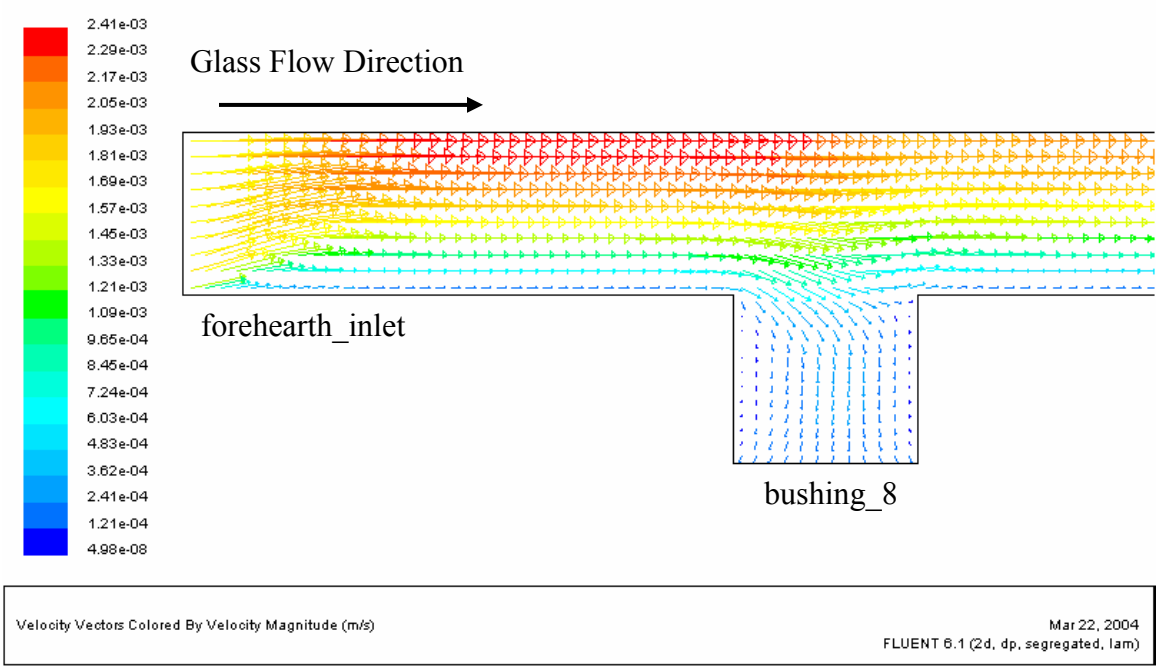

Figure 4.9 – Balanced Mass Flow Rate System Velocity Vectors Close-up 1, Scale 1:2 (m/s)

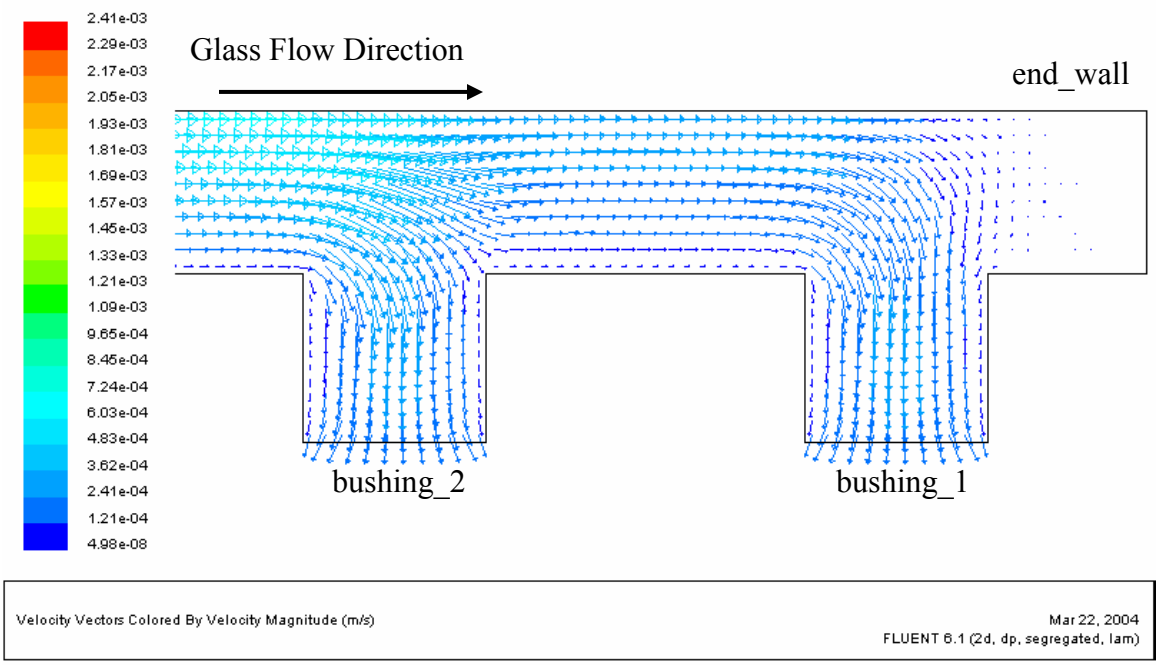

Figure 4.10 – Balanced Mass Flow Rate System Velocity Vectors Close-up 2, Scale 1:8 (m/s)

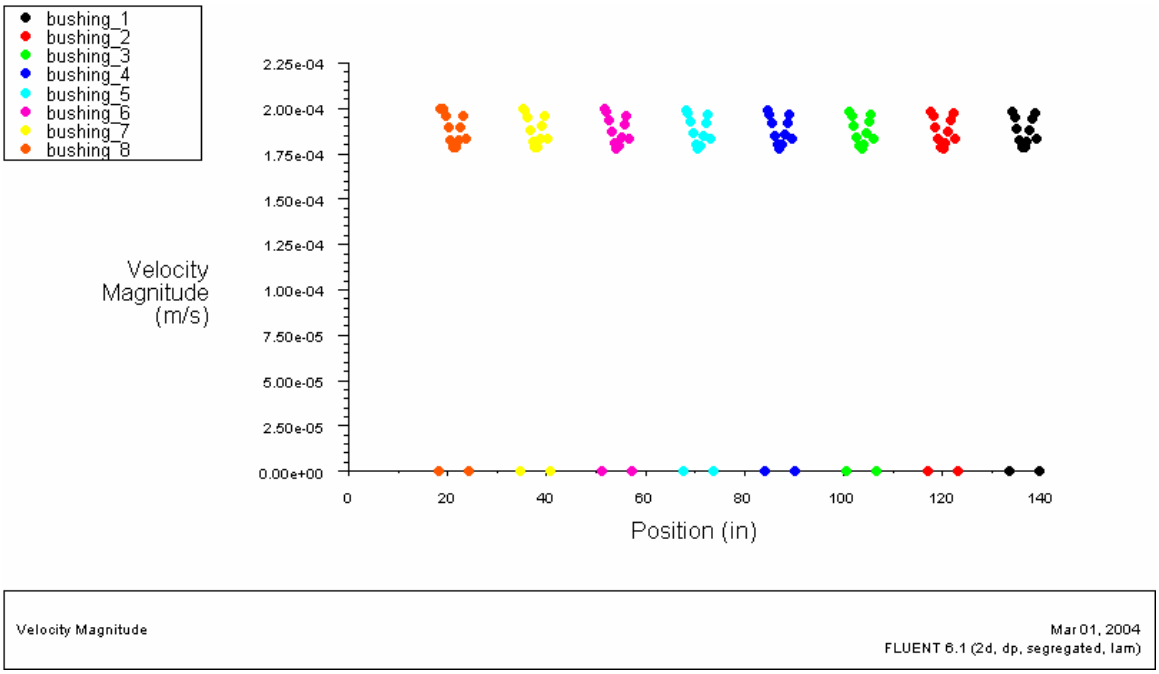

Figure 4.11 – FLUENT Trial 1: Bushing Outlet Velocity Magnitudes (m/s)

Nine other production cases were developed in order to determine the influence that various bushing arrangements have on the temperature uniformity throughout the forehearth. The specific mass flow rates for the FLUENT trials are shown in table 4.2. Trial FL–2 represents a case in which the initial bushing positions have high throughput and the last position is a low throughput bushing. This situation is reversed in trial FL–3 by placing a single high throughput bushing in the last position and multiple low throughput bushings near the entrance. Trials FL–4 through FL–6 maintains constant mass flow rates with the introduction of a single bushing changeover position. The changeover position is prescribed individually in each trial first at the position nearest to the inlet, then at the middle, and finally at the second to the last position. Trials FL–7 through FL–10 are a mixture of all previous simulation parameters, each one developed randomly in an attempt to identify a potential undesirable bushing arrangement.

Table 4.2 – FLUENT Trials: Specified Mass Flow Rates

FL–2	
Position	$\dot{m}$ (kg/s)
forehearth_inlet	0.5456
bushing_8	-0.1364
bushing_7	-0.1364
bushing_6	-0.1364
bushing_5	-0.1364
bushing_4	-0.0682
bushing_3	-0.0682
bushing_2	-0.0682
bushing_1	-0.0341

FL–3	
Position	$\dot{m}$ (kg/s)
forehearth_inlet	0.5456
bushing_8	-0.0341
bushing_7	-0.0341
bushing_6	-0.0341
bushing_5	-0.0341
bushing_4	-0.0682
bushing_3	-0.0682
bushing_2	-0.0682
bushing_1	-0.1364

FL–4	
Position	$\dot{m}$ (kg/s)
forehearth_inlet	0.5456
bushing_8	0.0000
bushing_7	-0.0682
bushing_6	-0.0682
bushing_5	-0.0682
bushing_4	-0.0682
bushing_3	-0.0682
bushing_2	-0.0682
bushing_1	-0.0682

FL–5	
Position	$\dot{m}$ (kg/s)
forehearth_inlet	0.5456
bushing_8	-0.0682
bushing_7	-0.0682
bushing_6	-0.0682
bushing_5	0.0000
bushing_4	-0.0682
bushing_3	-0.0682
bushing_2	-0.0682
bushing_1	-0.0682

FL–6	
Position	$\dot{m}$ (kg/s)
forehearth_inlet	0.5456
bushing_8	-0.0682
bushing_7	-0.0682
bushing_6	-0.0682
bushing_5	-0.0682
bushing_4	-0.0682
bushing_3	-0.0682
bushing_2	0.0000
bushing_1	-0.0682

FL–7	
Position	$\dot{m}$ (kg/s)
forehearth_inlet	0.5456
bushing_8	-0.1364
bushing_7	-0.1364
bushing_6	-0.1364
bushing_5	0.0000
bushing_4	-0.0682
bushing_3	-0.0682
bushing_2	-0.0682
bushing_1	-0.0341

FL–8	
Position	$\dot{m}$ (kg/s)
forehearth_inlet	0.5456
bushing_8	-0.0341
bushing_7	0.0000
bushing_6	-0.0341
bushing_5	-0.0341
bushing_4	-0.1364
bushing_3	-0.1364
bushing_2	-0.1364
bushing_1	-0.1364

FL–9	
Position	$\dot{m}$ (kg/s)
forehearth_inlet	0.5456
bushing_8	-0.0341
bushing_7	0.0000
bushing_6	-0.0341
bushing_5	-0.0682
bushing_4	-0.0682
bushing_3	-0.0682
bushing_2	-0.0682
bushing_1	-0.1364

FL–10	
Position	$\dot{m}$ (kg/s)
forehearth_inlet	0.5456
bushing_8	-0.0341
bushing_7	0.0000
bushing_6	-0.0341
bushing_5	-0.0682
bushing_4	-0.0682
bushing_3	-0.0682
bushing_2	-0.0682
bushing_1	-0.0341

Prior to simulation of the additional trials, the differences between the inlet and total outlet mass flow rates were calculated. The intent was to determine if a correlation might appear between a mass flow rate differential and any FLUENT simulation results. For all initially proposed trials, the inlet mass flow rate was held as a constant = 0.55 kg/s. A summary of the calculated mass flow rate differentials are shown in table 4.3. In an initial review of the imbalances calculated, trial FL–2 showed the highest imbalance requiring a larger mass flow rate than what was prescribed and trial FL–10 required less than the prescribed inlet mass flow rate.

Table 4.3 – FLUENT Trials: Mass Flow Rate Differentials

	FL–1	FL–2	FL–3	FL–4	FL–5	FL–6	FL–7	FL–8	FL–9	FL–10
$\Delta \dot{m}$ (kg/s)	0.00	-0.24	0.07	0.07	0.07	0.07	-0.10	-0.10	0.07	0.17

Full simulation results for each of the nine proposed trials can be seen in Appendix E. To quantify the simulation results, each trial was compared to the ideal case (FL–1). Figure 4.12 shows a comparison between the average temperatures across each bushing position for the individual trials. From an initial interpretation of the figure, there appears to be no definite trends or patterns. Further examination of the raw data shows that trials FL–8 and FL–10 have the greatest decrease in average temperature across all outlets as compared to the prescribed constant inlet temperature. This was assumed to be a result of the mass flow rate imbalance calculated within the FLUENT model domain. The average outlet temperature values in both trials were calculated to be approximately two-percent (or 32°K) less than the inlet temperature. This is a significant finding. As discussed in the literature, small

temperature variations can promote fiber breakage during manufacturing. The highest value of standard deviation (STDEV) of temperature across all positions (STDEV > 10) was found in trials FL–7 and FL–8.

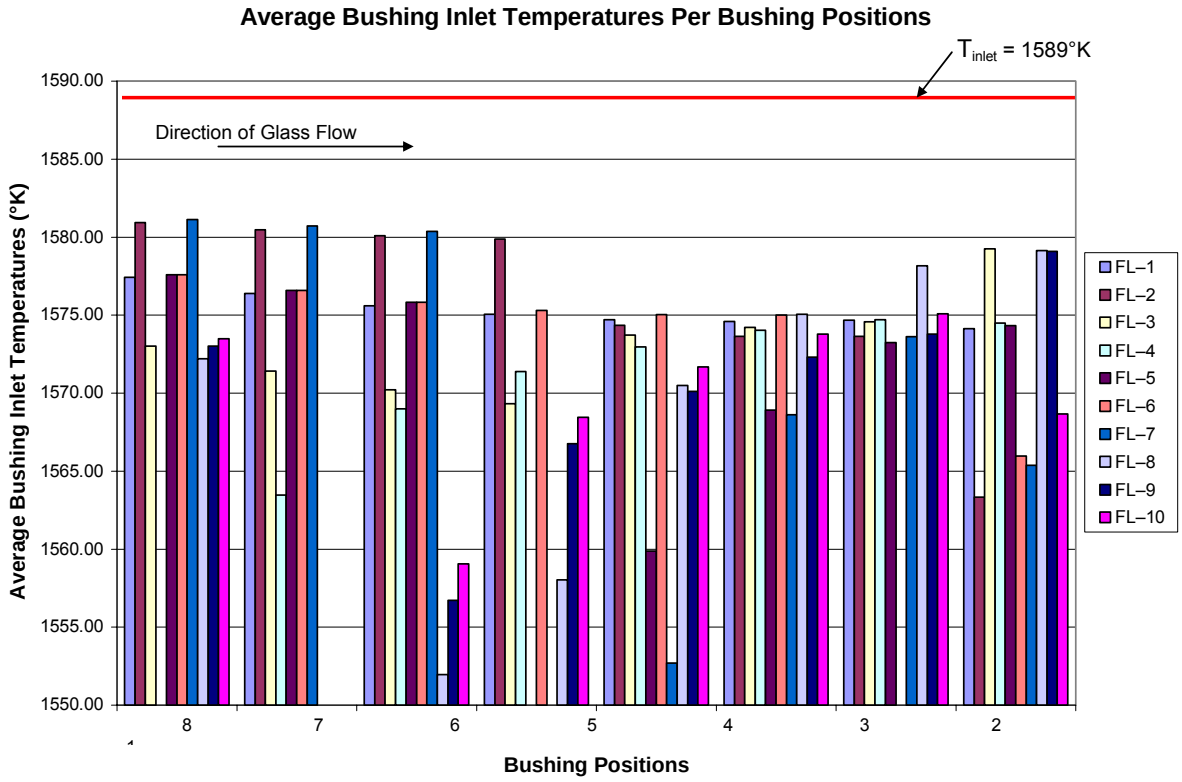

Figure 4.12 – FLUENT Simulation Results: Average Bushing Inlet Temperatures per Bushing Positions

It was initially assumed that a correlation could be made between the imbalance of mass flow rates and bushing temperatures. This means that the largest temperature variations as compared to the prescribed inlet temperature would be seen in simulations that have a mass flow rate differential greater than 18%. To verify this assumption, a pseudo-steady state analysis was performed in which the constant inlet mass flow rates were adjusted to match the total outlet mass flow rates. This would represent adjustments made by operators

on a production line. The concept of a pseudo-steady state analysis was applied to trials FL–2, FL–7, FL–8, and FL–10, all which had mass flow rate differentials greater than 18%.

The correlation proved valid for three of the four trials, in which the pseudo-steady state trials (FL–2a, FL–7a, FL–8a, and FL–10a) showed an increase of approximately 2°K in the average temperatures across all bushing positions, as shown in figure 4.13. However, trial FL–10 showed a decrease of approximately 2°K in the average temperatures across all bushing inlet positions. This is probably due to the fact that trial FL–10a had a lower constant prescribed inlet mass flow rate than prescribed for trial FL–10. In addition, trials FL–2a, FL–7a, and FL–8a all had larger constant prescribed inlet mass flow rates than for the original cases. Therefore, it can be concluded that the correlation is correct only if a bushing changeover didn't occur. Discontinuities in the lines connecting the average outlet temperatures represent a bushing changeover position where the average outlet temperature was excluded because its value was less than 1200°K.

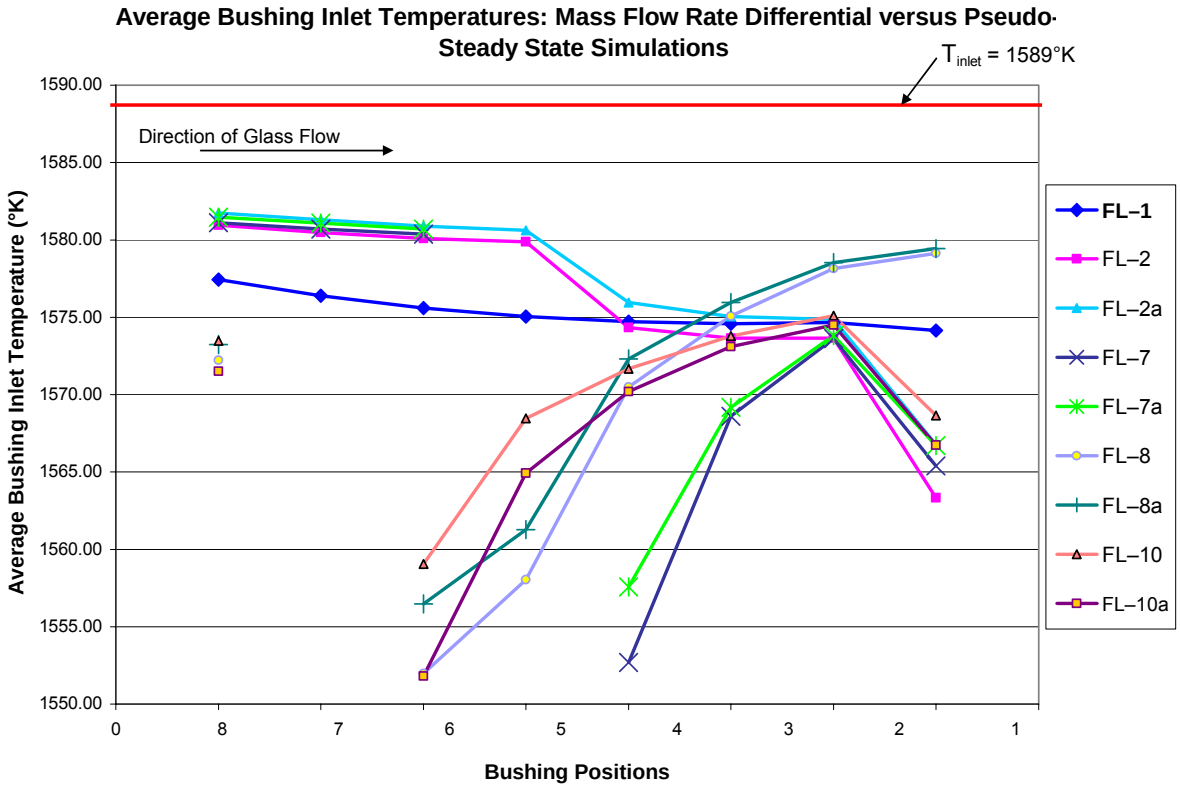

Figure 4.13 – Average Bushing Inlet Temperatures: Mass Flow Rate Differential versus Pseudo-Steady State Trials

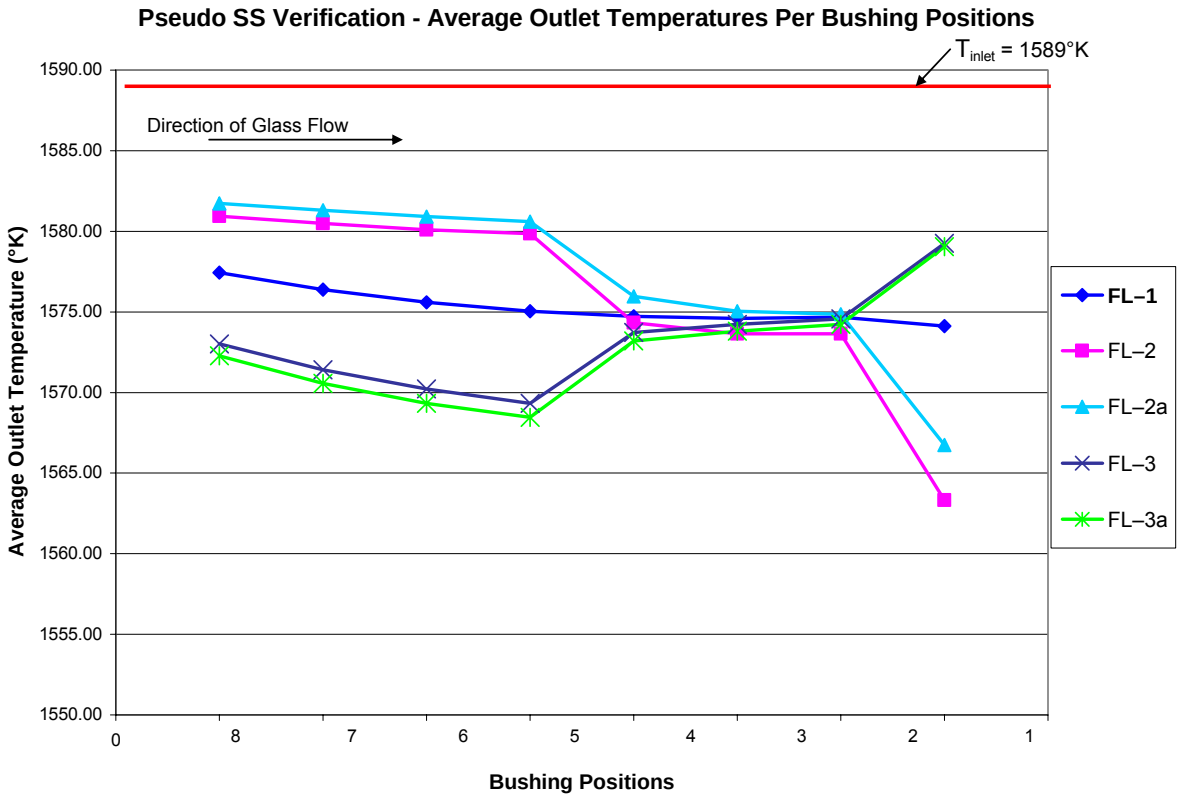

Figure 4.14 – Temperature Verification of Pseudo-Steady State Trials

In an attempt to verify the conclusion, a pseudo-steady state analysis was performed on the original trial FL–3. Trial FL–3 was similar to FL–2 in that it also did not incorporate a bushing changeover, but the bushing arrangements were different. The results shown in figure 4.14 matched the findings observed between FL–10 and FL–10a. A general conclusion can be made that if thermal variations are to be minimized, then the amount of glass flowing into the forehearth must be equal to or greater than the total throughput of all bushing positions.

Two additional findings can be observed with the FLUENT solutions with regards to a bushing changeover position. The first finding is that the closer the bushing changeover

occurs to the inlet, the greater the temperature variations that occur throughout the forehearth. More importantly, the second finding is that the closer the bushing changeover occurs to the inlet, the more the average outlet temperatures vary as compared to the average outlet temperatures of the ideal production scenario (FL–1). This is clearly evident in trials FL–4 through FL–6 as shown in figure 4.15. The temperatures of the changeover positions have been clipped in order to exemplify the variations compared to the benchmark simulation. In addition, variations of throughput only decrease the thermal homogeneity.

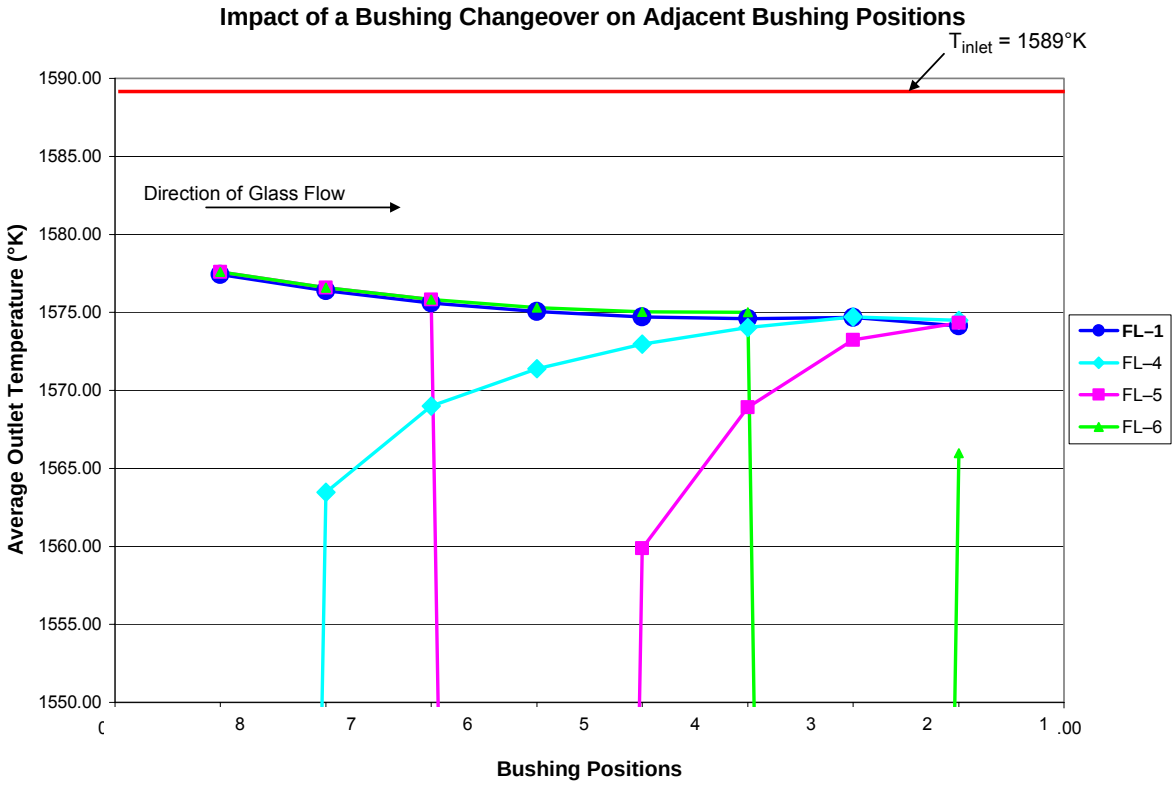

Figure 4.15 – Impact of a Bushing Changeover on Adjacent Bushing Positions

4.2 FIDAP Results

Similar to the FLUENT simulations, a FIDAP simulation benchmark (FD–1) was developed for comparison with other FIDAP simulations. The same ideal production scenario model was used as in the FLUENT benchmark, FL–1, with the exception that 0.20 meters was prescribed as the glass depth. This value was chosen because it was the original physical dimension used in the previous work of Choudhary[6]. The advantage of utilizing FIDAP over FLUENT is that FIDAP allows for the final glass free surface height to be predicted.

The trial FD–1 simulation results showed that the free surface height decreased relatively quickly near the entrance and had a slight decreasing taper for the duration of the forehearth length, as shown in figures 4.16 and 4.17. Note that figure 4.16 shows an exaggerated view of the predicted glass surface, whereas figure 4.17 shows the exact height variations with respect to the originally assumed glass height.

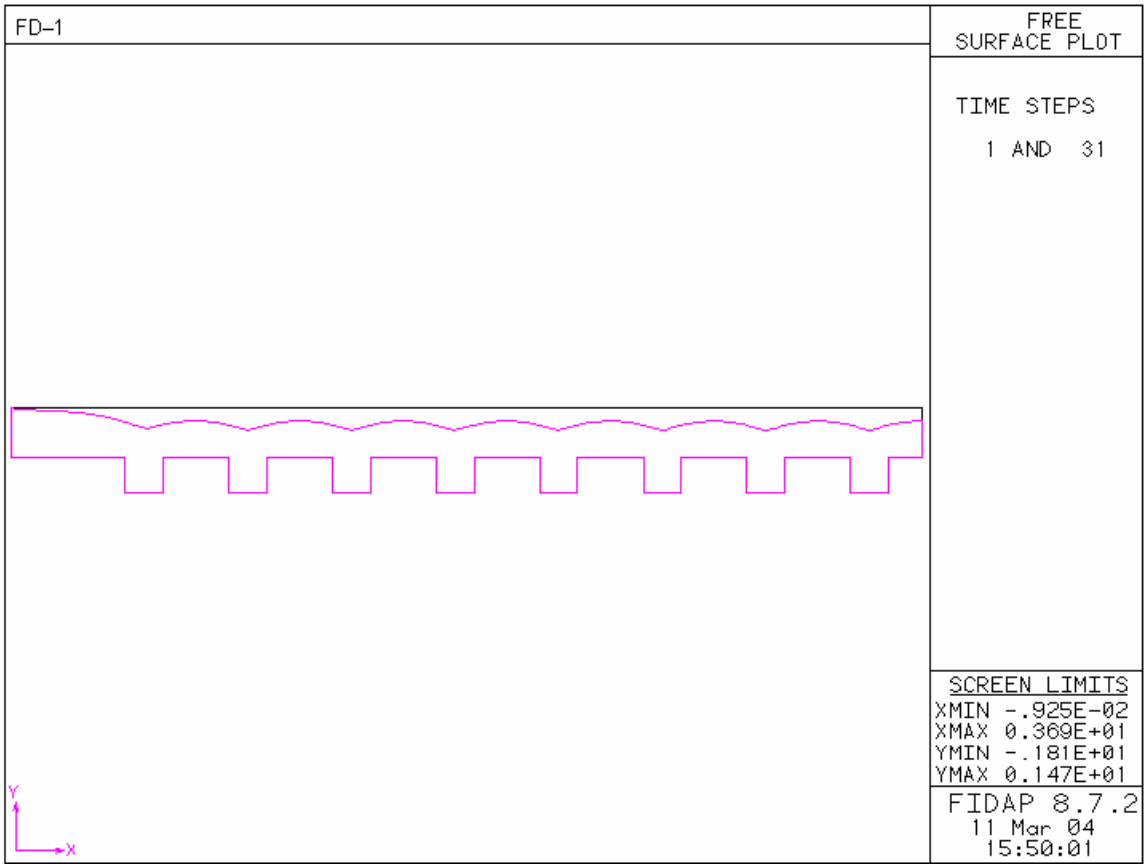

Figure 4.16 – FIDAP Simulation Results: Free Surface Variations from Original 0.20m Glass Height (Exaggerated Scale Factor)

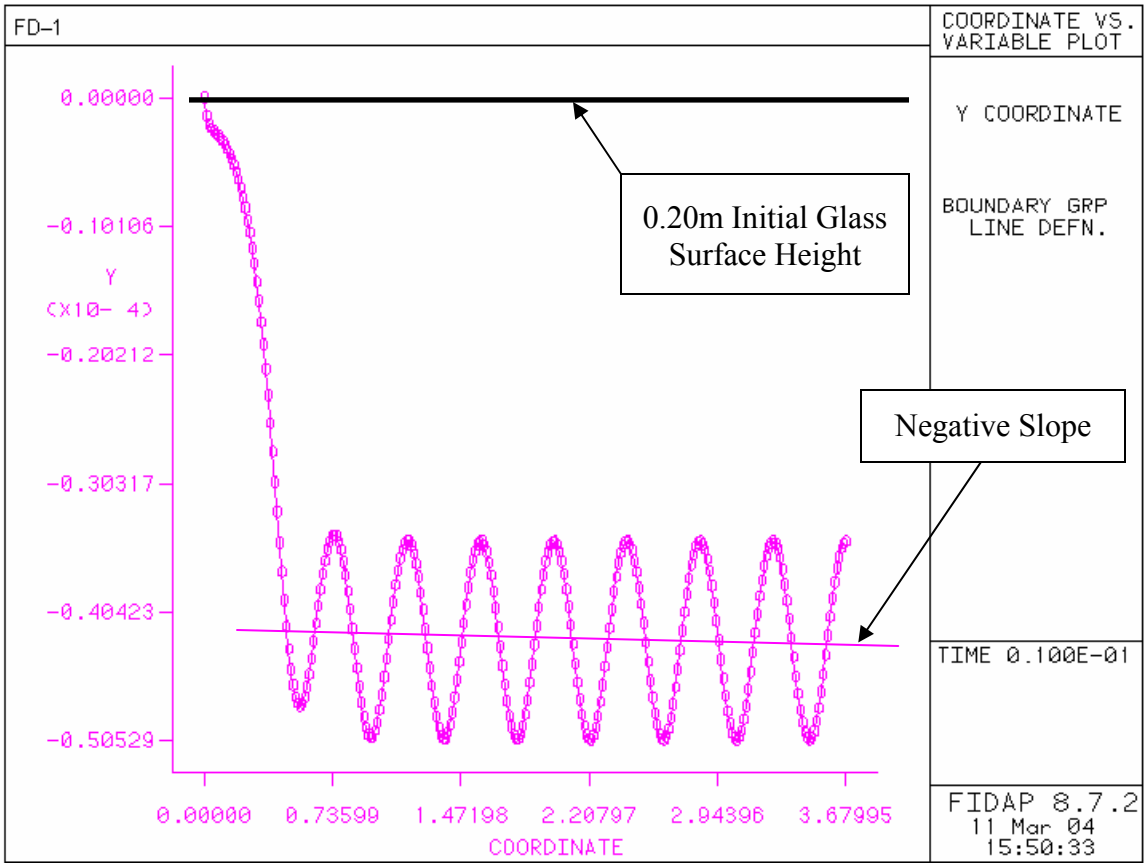

Figure 4.17 – FIDAP Simulation Results: Top Free Surface from Original 0.20m Glass Height (m)

Intuitively, the small negative slope shown in Figure 4.17 makes sense in that a decrease in height would be expected along the length of the forehearth with constant outflows along the bottom. This finding is also consistent with the most recent work published by Choudhary[17]. As compared to Choudhary's work, another similarity is the relatively quick decrease in glass height near the entrance. This implies that the initial prescribed glass height is too great and it needs to be reduced. To confirm this assumption, a new model was constructed with two-thirds of the original glass height and it was re-simulated as trial FD–1a. All other production parameters were held constant.

The Trial FD–1a results show less change in magnitude of height from the original glass surface, as shown in figures 4.18 and 4.19. Therefore the glass height, H_2, was set equal to 0.14 meters and it was updated for all simulations in both FIDAP and FLUENT.

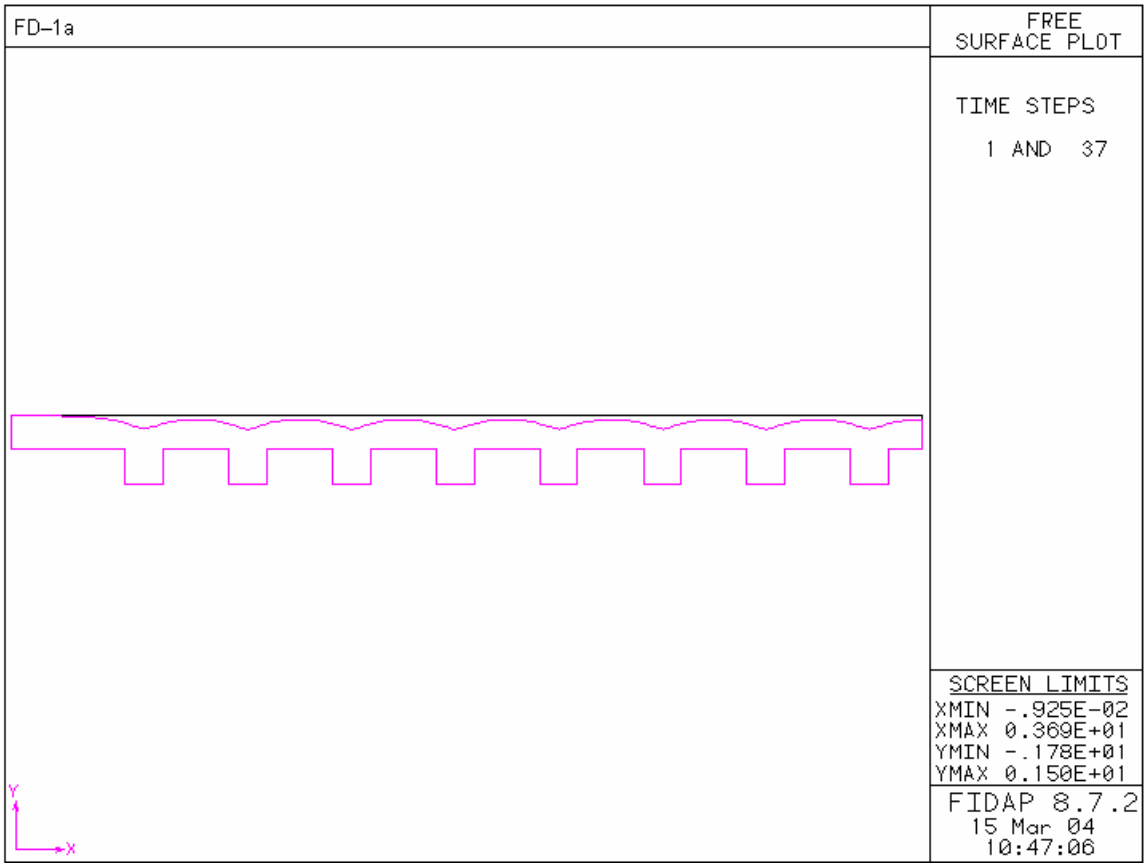

Figure 4.18 – FIDAP Simulation Results: Free Surface Variations from Revised 0.14m Glass Height (Exaggerated Scale Factor)

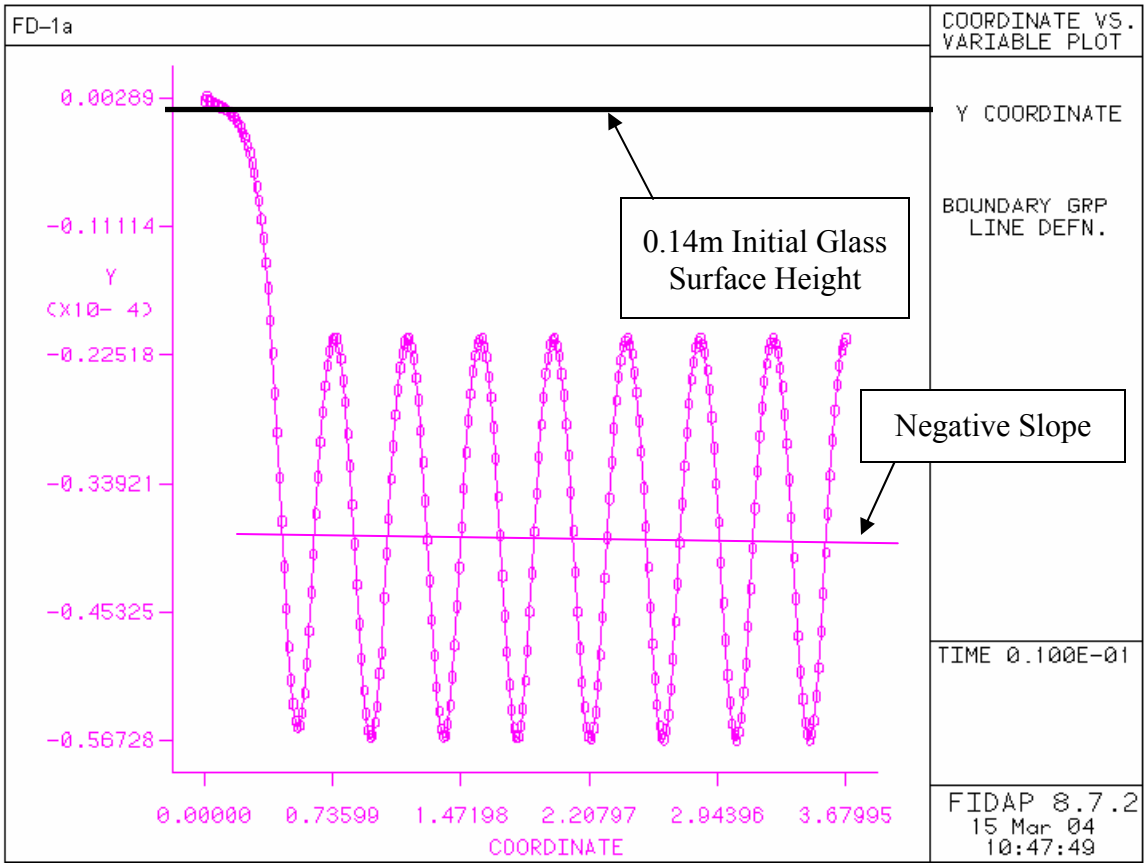

Figure 4.19 – FIDAP Simulation Results: Top Free Surface from Revised 0.14m Glass Height (m)

The primary intent of the FIDAP simulations was to confirm the simulation results from FLUENT. Further investigation of the software capabilities yielded the fact that FIDAP is a CFD code and as such, it does not compute mass flow rates. It was found that if the incoming flow is lower than the total outflow, then the free surface will steadily decrease, which will eventually result in mesh distortion. The same holds true if more mass is flowing into the system than leaving. The result in this case would be that the free surface would continually increase, which would prevent the solution from converging. Therefore the

simulation scope was reduced to three specific trials that included a single bushing changeover position.

Trials FD–2, FD–3, and FD–4 were identical in operating parameters as the FLUENT trials FD–4 through FD–6, in that they all contained constant bushing throughputs with the inclusion of a single changeover position. In trial FD–2 bushing_8 was the changeover position, in trial FD–3 bushing_5 was the changeover position, and in trial FD–4 bushing_2 was the changeover position. The specific simulation parameters and solutions for trials FD–2 through FD–4 can be found in Appendix F. The observed predicted glass height over each changeover position was found to increase slightly as compared to the minimal decrease in elevation across the forehearth. The resulting isotherms computed in the additional FIDAP simulations were found to be fairly consistent with the FLUENT simulations. Note that there was a significant difference in the relative velocity vectors of the two software simulations. This dissimilarity initially raised concern. However, when the FIDAP simulation results were compared to the results published by Choudhary[17], the relative velocity vectors as well as other predicted results (i.e. temperature isotherms and free surface deformation) were similar in magnitude. In a brief summary of all FIDAP results, the ALE free surface model predicted only very small changes to the glass height over the extent of the forehearth length. It can be concluded that for small scale forehearths such as presented in this research, the variation in glass depth can be neglected. It is uncertain as to the effect of glass depth variations across a large scale forehearth, which could include five times the number of bushing positions as were simulated in this research. It can also be concluded that in addition to the negligible glass height variations, the current limitations of the CFD solver to handle

imbalances of mass flow rates makes the FIDAP software inadequate to determine the thermal response of the forehearth system to different bushing arrangements.

4.3 Validation of the CFD Solutions

Validation of the numerical results presented in this thesis was achieved by comparing the ideal production scenario trial with previously published experimental and numerical results. Excellent agreement was found for this case. Since FLUENT and FIDAP are commercially available software, it was concluded that the other trials could be similarly validated. Note that comparisons of the empirical validations of the simulations with typical day-to-day production environments were limited. Minimal published information was found pertaining to the sensitivities of a forehearth system for different bushing arrangements and changeovers in a production environment. Nonetheless the validation of the accuracy and precision of the ideal production scenario provided the confidence to conclude that other trial simulations would provide similar sound predictions of the glass processing environment.

4.4 Production Planning Optimization

The numerical simulations developed in this thesis have confirmed that there are many intricacies in the manufacturing of glass fibers, and the simulations can provide important processing information and guidelines. Processing variations exist not only from the macro-view of a manufacturing plant, but also from a micro-view of each bushing position. Numerical modeling can provide new understanding of manufacturing operations and in particular, provide new insight into persistent problems in a production environment.

For example, it was found from the ten trials examined with FLUENT that the third bushing from the forehearth inlet (bushing_6) consistently had the lowest average outlet temperatures and the largest standard deviation as compared with any other position for all ten trials, as shown in table 4.3. Since all ten generic production trials represented random operating parameters, no correlations can be drawn to support these findings. This demonstrates that there are troublesome positions that are more prone to processing problems. Using more detailed numerical simulations, future modeling efforts can focus on specific positions to resolve these problems.

It was also evident that the temperature uniformity of molten glass arriving at each bushing position is a function of several factors. These include the distance from the forehearth inlet, the surrounding bushing types (variations of throughput rates), and most importantly whether or not there are any bushing changeovers. All these factors combine to identify undesirable production scenarios. By quantifying these types of variations for a specific manufacturing line with numerical models, the development of production guidelines becomes feasible. This research has demonstrated that this can lead to a more systematic approach for production planning.

Table 4.4 – Comparison of FLUENT Simulation Results for All Trials

Glass Flow Direction →

	bushing_8 T (°K)	bushing_7 T (°K)	bushing_6 T (°K)	bushing_5 T (°K)	bushing_4 T (°K)	bushing_3 T (°K)	bushing_2 T (°K)	bushing_1 T (°K)
Trial 1	1577.43	1576.40	1575.60	1575.05	1574.72	1574.59	1574.67	1574.13
Trial 2	1580.95	1580.49	1580.10	1579.87	1574.34	1573.64	1573.64	1563.33
Trial 3	1573.03	1571.41	1570.21	1569.32	1573.72	1574.23	1574.58	1579.25
Trial 4	1194.50	1563.46	1569.01	1571.39	1572.95	1574.01	1574.72	1574.48
Trial 5	1577.60	1576.59	1575.83	1179.70	1559.89	1568.92	1573.25	1574.33
Trial 6	1577.60	1576.59	1575.83	1575.31	1575.03	1575.00	1150.61	1565.98
Trial 7	1581.12	1580.71	1580.36	1127.79	1552.69	1568.61	1573.62	1565.39
Trial 8	1572.21	1162.22	1551.97	1558.04	1570.48	1575.07	1578.15	1579.13
Trial 9	1573.02	1191.42	1556.71	1566.75	1570.11	1572.33	1573.78	1579.09
Trial 10	1573.48	1206.81	1559.06	1568.45	1571.68	1573.78	1575.10	1568.66
Avg Temp	1576.27	1575.09	1569.47	1570.52	1569.56	1573.02	1574.61	1572.38
Std Dev	3.46	5.99	10.16	6.63	7.39	2.37	1.47	6.10

- Signifies bushing changeover positions

This research has shown that with simple two-dimensional forehearth models, undesirable processing conditions can be predicted. Particular bushing arrangements that cause large bushing inlet temperature variations can be identified. More importantly, the impact of bushing changeovers can be evaluated with different bushing arrangements. A good example can be seen with trial FL–8. In this case, four low throughput bushings occur near the entrance, followed by four positions with a high throughput rate. Because a changeover takes place at the second position from the inlet, the following two bushing positions see a large variation in glass temperature, as shown in figure 4.20.

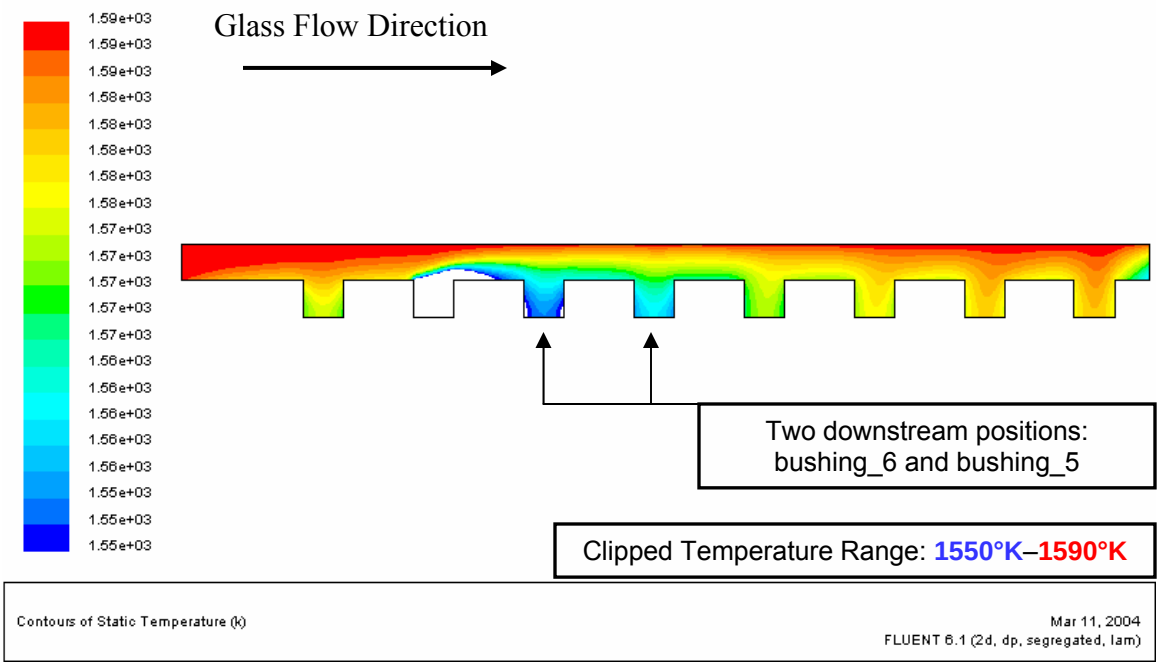

Figure 4.20 – FLUENT Trial FL–8a: Temperature Contours of Molten Glass (°K)

The average temperature at these two downstream positions are 20°K and 15°K degrees less than the bushing position prior to the changeover. This is due to that fact that the glass velocity decreases above the changeover position. As a result, a severe decrease in the molten glass temperatures occurs for the flows into the two downstream positions. In addition, the final four positions have a higher throughput rate, which tends to pull the higher temperature glass over and past the two downstream positions. Using these models to predict such outcomes can lead to the development of specific production planning guidelines that identify undesirable bushing arrangements before they are implemented in a production line. The models can also help guide an operator as to where a bushing changeover should occur. Ultimately, this approach can be used to optimize production planning strategies.

4.5 Recommendations for Future Work

Future work needs to be performed in several key areas. The continued development and simulation of production scenarios to achieve optimal production planning strategies needs to be investigated. The extension of the two-dimensional model to include a significant increase in the number of bushing positions should be conducted. In addition, a three-dimensional forehearth model should be investigated that more realistically treats the actual forehearth. A more detailed investigation of the effective heat transfer coefficient and the refractory material surrounding the molten glass domain should also be conducted, as well as the heat transfer at the glass surface. An investigation should also be conducted of the effect of a horizontal declination angle at the bottom of the forehearth geometry on the mass and heat transfer of the molten glass in the forehearth.

5 REFERENCES

[1] Loewenstein, K.L., *The Manufacturing Technology of Continuous Glass Fibers*, Second Edition, Elservier, New York, 1983

[2] Strong, A.B., *Plastics – Materials and Processing*, Second Edition, Prentice-Hall, inc., NJ, 2000

[3] Rawson, H., *Glasses and Their Applications*, The Institute of Metals, VT, 1991

[4] Kolesov, Y.I., Kudryavtsev, M.Y., Mikhailenko, N.Y., "Types and Compositions of Glass for Production of Continuous Glass Fiber (Review)", *Glass and Ceramics*, Vol. 58, No. 5-6, pp. 197-202, 2001

[5] Glass Furnace Information and Images
http://www.boc.com

[6] Choudhary, M.K., "Mathematical Modeling of Flow and Heat Transfer Phenomena in Glass Furnace Channels and Forehearths", *Journal of the American Ceramic Society*, Vol. 74, No. 12, pp. 3091-3099, 1991

[7] Choudhary, M.K., "A Modeling Study of Flow and Heat Transfer in Channels and Forehearths of Glass Furnaces", *Advances in Fusion and Processing of Glass*, *Ceramic Transactions*, Vol. 29, pp.605-618, American Ceramic Society, Ohio, 1993

[8] Primefire® 400 Oxy-Fuel Burner
http://www.comustiontec.com

[9] PPG Fiber Glass – Images reproduced with the permission of PPG Industries, Inc.
http://www.ppg.com/fgs_main/default.htm

[10] Platinum Alloy Products – Applications in the Glass Industry
http://www.noble.matthey.com/

[11] Muysenberg, Erik, Chmelar, Josef, "Validation of Glass Furnace Models: Believe It or Not", *Ceramic Engineering and Science Proceedings*, Vol. 22, No. 1, pp.1-19, 2001

[12] Carling, J.C., "Two- and Three-Dimensional Mathematical Models of the Flow and Heat Transfer in Forehearths", *Glastrechnische Berichte*, Vol. 49, No. 12, pp. 269-277, 1976

[13] Carling, J.C., "A Note on the Mathematical Modeling of Forehearths", *Glass (International)*, March, pp. 9, 1982

[14] Carling, J.C., "A Reappraisal of the Mathematical Modeling of Flow and Heat Transfer in Glass Tank Forehearths", *Glass Technology*, Vol. 23, pp.201-222, 1982

[15] Lin, Y.S., "Numerical Simulation of Unsteady, Three-Dimensional Fluid Flow and Heat Transfer Occurring in Open Channel Forehearths", PhD Thesis, University of Toledo, Ohio, 1985

[16] Chengxu, Sun, Xiufeng, Tang, "Numerical Simulation of the Flow and Heat Transfer of Molten Glass in the Forehearth for Direct-Melt Spinning Glass Fiber", *Journal of East China Institute of Chemical Technology*, Vol. 16, No. 15, pp. 560-566, 1990

[17] Choudhary, M.K., "Modeling of Free Surface Flow in Glass Furnace Forehearths", *Proceedings of International Congress of Glass, 18th, American Ceramic Society*, pp.721-728, 1998

[18] Halloin, V., Boxho, B., "Experimental Study of Viscous Flow in a Forehearth Model", *Glass Technology*, Vol. 34, pp. 249-255, 1993

[19] Robb, K., Kulkarni, J., Kumar, A., Dutta, A., Grald, E., "Numerical Simulation of the Drawn Down Phenomenon in Glass Furnace Forehearths", *FIDAP/POLYFLOW UGM*, 2001

[20] Fluent Inc. CFD Flow Modeling Software and Services
http://www.fluent.com/index.htm

[21] Fluent Inc. CFD Flow Modeling Software and Services
FLUENT 6.1 Documentation

[22] Holman, J.P., *Heat Transfer*, Eighth Edition, McGraw–Hill Companies, Inc., New York, 1997

[23] Clare, A.G., Wing, D., Jones, L.E., Kucuk, A., "Density an Surface Tension of Borate Containing Silicate Glass Melts", Glass Technology, Vol. 44, No. 2, pp. 59-62. 2003

[24] Fluent Inc. CFD Flow Modeling Software and Services
FIDAP 8.7 Documentation

6 APPENDICES

6.1 Appendix A – GAMBIT Geometry and Mesh Generation

Table 6.1 – GAMBIT Vertice Coordinates

VERTICE LABEL	CARTESIAN COORDINATES			VERTICE LABEL	CARTESIAN COORDINATES	
	X	Y			X	Y
A	0	0		*S*	84.11	-5.37
B	0	-5.37		*T*	84.11	-10.91
C	18.11	-5.37		*U*	90.15	-10.91
D	18.11	-10.91		*V*	90.15	-5.37
E	24.15	-10.91		*W*	100.61	-5.37
F	24.15	-5.37		*X*	100.61	-10.91
G	34.61	-5.37		*Y*	106.65	-10.91
H	34.61	-10.91		*Z*	106.65	-5.37
I	40.65	-10.91		*AA*	117.11	-5.37
J	40.65	-5.37		*BB*	117.11	-10.91
K	51.11	-5.37		*CC*	123.15	-10.91
L	51.11	-10.91		*DD*	123.15	-5.37
M	57.15	-10.91		*EE*	133.61	-5.37
N	57.15	-5.37		*FF*	133.61	-10.91
O	67.61	-5.37		*GG*	139.65	-10.91
P	67.61	-10.91		*HH*	139.65	-5.37
Q	73.65	-10.91		*II*	144.88	-5.37
R	73.65	-5.37		*JJ*	144.88	0

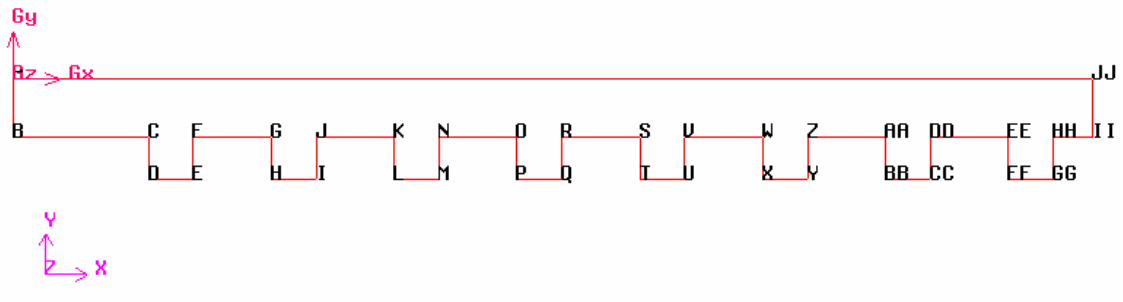

Figure 6.1 – GAMBIT 2–Dimensional Geometry

Table 6.2 – GAMBIT Successive Ratios – Nonsymmetrical Grading Scheme

ENTITY	R_1 (1)	n (2)		ENTITY	R_1 (1)	n (2)
edge.1	1.00	10		*edge.19*	1.00	12
edge.2	1.00	36		*edge.20*	1.00	12
edge.3	1.00	12		*edge.21*	1.00	12
edge.4	1.00	12		*edge.22*	1.00	20
edge.5	1.00	12		*edge.23*	1.00	12
edge.6	1.00	20		*edge.24*	1.00	12
edge.7	1.00	12		*edge.25*	1.00	12
edge.8	1.00	12		*edge.26*	1.00	20
edge.9	1.00	12		*edge.27*	1.00	12
edge.10	1.00	20		*edge.28*	1.00	12
edge.11	1.00	12		*edge.29*	1.00	12
edge.12	1.00	12		*edge.30*	1.00	20
edge.13	1.00	12		*edge.31*	1.00	12
edge.14	1.00	20		*edge.32*	1.00	12
edge.15	1.00	12		*edge.33*	1.00	12
edge.16	1.00	12		*edge.34*	1.00	10
edge.17	1.00	12		*edge.35*	1.00	10
edge.18	1.00	20		*edge.36*	1.00	282

Notes:

(1) R_1 refers to the interval length ratio on an edge

(2) n refers to the interval count on an edge

6.2 Appendix B – CFD Zone–Type Specifications

Table 6.3 – FLUENT Zone–Type Specifications

ENTITY	NAME	ZONE	ZONE TYPE
edge.1	forehearth_inlet	Boundary	Mass Flow Inlet
edge.2	wall_bc		Wall
edge.3	wall_cd		Wall
edge.4	bushing_8		Mass Flow Inlet
edge.5	wall_ef		Wall
edge.6	wall_fg		Wall
edge.7	wall_gh		Wall
edge.8	bushing_7		Mass Flow Inlet
edge.9	wall_ij		Wall
edge.10	wall_jk		Wall
edge.11	wall_kl		Wall
edge.12	bushing_6		Mass Flow Inlet
edge.13	wall_mn		Wall
edge.14	wall_no		Wall
edge.15	wall_op		Wall
edge.16	bushing_5		Mass Flow Inlet
edge.17	wall_qr		Wall
edge.18	wall_rs		Wall
edge.19	wall_st		Wall
edge.20	bushing_4		Mass Flow Inlet
edge.21	wall_uv		Wall
edge.22	wall_vw		Wall
edge.23	wall_wx		Wall
edge.24	bushing_3		Mass Flow Inlet
edge.25	wall_yz		Wall
edge.26	wall_zaa		Wall
edge.27	wall_aabb		Wall
edge.28	bushing_2		Mass Flow Inlet
edge.29	wall_ccdd		Wall
edge.30	wall_ddee		Wall
edge.31	wall_eeff		Wall
edge.32	bushing_1		Mass Flow Inlet
edge.33	wall_gghh		Wall
edge.34	wall_hhii		Wall
edge.35	end_iijj		Wall
edge.36	top_jja		Wall
face.1	eglass	Continuum	Fluid

Table 6.4 – FIDAP Zone–Type Specifications for FIDAP

Edge	Name	ZONE	ZONE TYPE
edge.1	forehearth_inlet	Boundary	Plot
edge.2	wall_bc		Convection
edge.3	wall_cd		Convection
edge.4	bushing_8		Plot
edge.5	wall_ef		Convection
edge.6	wall_fg		Convection
edge.7	wall_gh		Convection
edge.8	bushing_7		Plot
edge.9	wall_ij		Convection
edge.10	wall_jk		Convection
edge.11	wall_kl		Convection
edge.12	bushing_6		Plot
edge.13	wall_mn		Convection
edge.14	wall_no		Convection
edge.15	wall_op		Convection
edge.16	bushing_5		Plot
edge.17	wall_qr		Convection
edge.18	wall_rs		Convection
edge.19	wall_st		Convection
edge.20	bushing_4		Plot
edge.21	wall_uv		Convection
edge.22	wall_vw		Convection
edge.23	wall_wx		Convection
edge.24	bushing_3		Plot
edge.25	wall_yz		Convection
edge.26	wall_zaa		Convection
edge.27	wall_aabb		Convection
edge.28	bushing_2		Plot
edge.29	wall_ccdd		Convection
edge.30	wall_ddee		Convection
edge.31	wall_eeff		Convection
edge.32	bushing_1		Plot
edge.33	wall_gghh		Convection
edge.34	wall_hhii		Convection
edge.35	end_iijj		Convection
edge.36	top_jja		Slip / Surface
face.1	eglass	Continuum	Fluid

6.3 Appendix C – FLUENT User Defined Function (UDF)

A User Defined Function, or UDF, is a function that the user programs that can be dynamically loaded into FLUENT to enhance the standard features of the CFD simulation. UDFs allow the user to customize FLUENT to fit specific modeling requirements. UDFs can be used for a variety of applications, such as the customization of boundary conditions and material property definitions. The functions are written in C programming language using any text editor and the source file is saved with a `.c` file extension. The source files can either contain a single UDF or they can contain several coupled functions. The source files are then either interpreted or compiled into FLUENT.

For the purpose of the research the following UDF was written to customize the E glass material properties. This was necessary because the thermal conductivity and dynamic viscosity are temperature dependent and with each iteration the calculated temperature for individual elements is updated. The specific solution procedure for the Segregated Solver used within FLUENT can be seen in figure 6.3, followed by the C code written for this research.

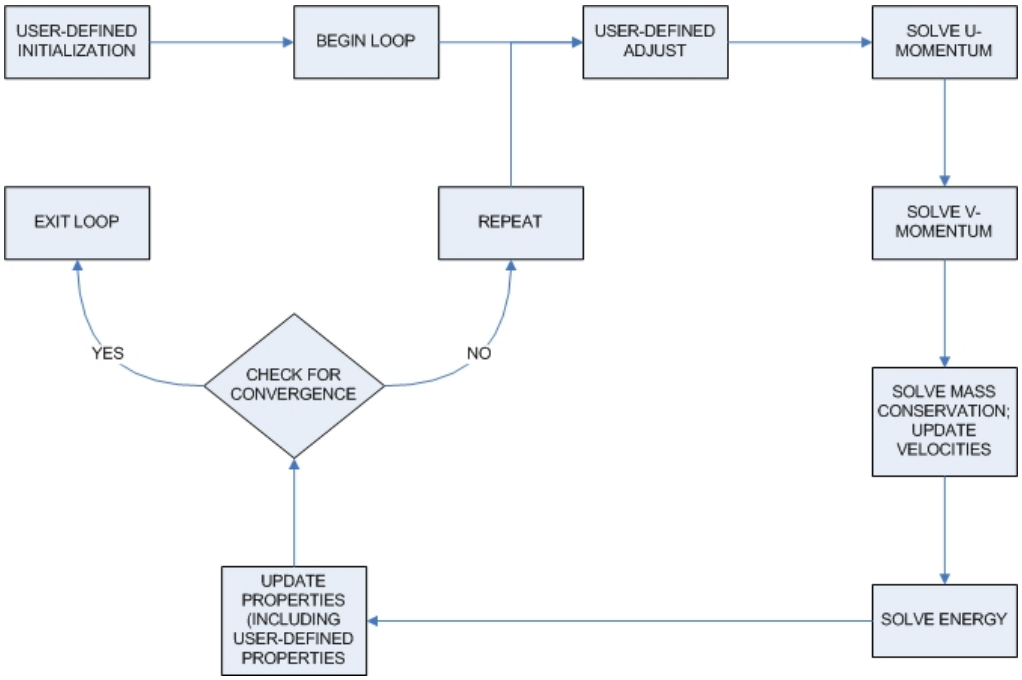

Figure 6.3 – Solution Procedure for the Fluent Segregated Solver

UDF C Code written for the FLUENT simulations:

Filename: **`NCSU_Thesis_1.c`**

Code:

```
/************************************************************/
/*                                                          */
/*  INTEGRATED MODELING ANALYSIS OF GLASS FOREHEARTHS AS    */
/*  APPLIED TO PRODUCTION PLANNING OPTIMIZATION             */
/*                                                          */
/* User-Defined Functions: Temperature-Dependent Equations of */
/*                         State for Molten Glass Modeling  */
/*                                                          */
/*   Author: Robert M. Belz                                 */
/*     Date: February 13, 2004                              */
/* Revision: 1.0                                            */
/*                                                          */
/************************************************************/


#include "udf.h"
#include "sg.h"
#include "prop.h"
```

```
/* constants */

#define C1 1.73
#define C2 0.00
#define C3 0.00
#define C4 0.00000000453
#define CA 2.427
#define CB 2952.8
#define CC 810.8


/*  Thermal Conductivity ; [W/m-K]  */

/* functions */

DEFINE_PROPERTY(thermal_cond, cell, thread)
{
    real cond_glass,T_K;
    {
    if (C_T(cell,thread)<1100.0)
      T_K=1100.0;
    else if (C_T(cell,thread)>2000.0)
      T_K=2000.0;
    else
      T_K=C_T(cell,thread);
    cond_glass=C1+C2*T_K+C3*pow(T_K,2)+C4*pow(T_K,3);
    }
  return cond_glass;
}


/*  Dynamic Viscosity ; [kg/m-s]  */

/* functions */

DEFINE_PROPERTY(dynamic_visc, cell, thread)
{
  real mu_glass,T_K,expo;
    {
    if (C_T(cell,thread)<1100.0)
       T_K = 1100.0;
    else
       T_K = C_T(cell, thread);
    expo = -CA + CB/(T_K-CC);
    mu_glass = pow(10.0, expo);
    }
  return mu_glass;
}
```

6.4 Appendix D – FIDAP Solver Formulation Code Example

Detailed in this section are the two codes used to run the FIDAP simulation for the case of constant inlet flow with eight constant outflows.

FIDAP Simulation Program 1

```
/*************************************************************
/DISCLAIMER: This file has been created by GAMBIT based on the data
/entered in PreSTO.  Please note that not all the capabilities of FIDAP
/are present in the PreSTO template. However, you can add the desired
/capabilities by editing this file with a text editor. You will then
/have to run FIDAP outside the GAMBIT (PreSTO) environment.
/Please send bug reports and/or enhancement requests to:
/ashwini.kumar@fluent.com or marc.horner@fluent.com
/*************************************************************

FICONV( NEUTRAL, INPUT, FDMESH )
INPUT( FILE="fh_new.FDNEUT" )
OUTPUT( DELETE )
END

TITLE
fh_new

FIPREP

EXECUTION (NEWJOB)
PRINT (NONE)
DATA (CONTROL)

PROBLEM(2-d, Energy, Laminar,  NONLINEAR, NEWTONIAN, INCOMPRESSIBLE)
SCALE ( VALUE = 0.0254 )
SOLUTION (SEGRE=500, VELCONV =0.001, SURF =0.01, SCHANGE =0)
RELAXATION(HYBRID)
0.3 0.3 0.3 0.5 0.5 0.7 0.3 0.3
OPTION (SIDES )
EXTRAPOLATE(ON, NOFREE)
PRESSURE ( MIXED = 1e-12, DISCONTINUOUS )
TIME (NSTEP = 200, TSTART = 0, DT = 0.01, INCMAX = 1.2, DTMAX = 0.1,
NOFIXED = 10)

ENTITY( NAME = "eglass", FLUID, PROPERTY = "default" )
DENSITY( SET = "default", CONSTANT = 2500 )
VISCOSITY( SET = "default", CONSTANT= 30.2587 )
CONDUCTIVITY( SET = "default", CONST =19.2713 )
SPECIFICHEAT( SET = "default", CONSTANT = 1401.6 )

ENTITY ( NAME = "forehearth_inlet", PLOT )
BCNODE ( TEMPERATURE, CONSTANT = 1589, ENTITY = "forehearth_inlet" )
BCNODE ( UX, CONSTANT = 0.0016, ENTITY = "forehearth_inlet" )
```

```
BCNODE ( UY, CONSTANT = 0.0, ENTITY = "forehearth_inlet" )

ENTITY ( NAME = "wall_bc", CONVECTION, MCNV = "wall_bc" )
BCNODE ( UX, CONSTANT = 0, ENTITY = "wall_bc" )
BCNODE ( UY, CONSTANT = 0, ENTITY = "wall_bc" )
HTRANSFER ( SET = "wall_bc", CONSTANT = 2.31, REFTEMP = 310 )

ENTITY ( NAME = "wall_cd", CONVECTION, MCNV = "wall_cd" )
BCNODE ( UX, CONSTANT = 0, ENTITY = "wall_cd" )
BCNODE ( UY, CONSTANT = 0, ENTITY = "wall_cd" )
HTRANSFER ( SET = "wall_cd", CONSTANT = 2.31, REFTEMP = 310 )

ENTITY ( NAME = "wall_ef", CONVECTION, MCNV = "wall_ef" )
BCNODE ( UX, CONSTANT = 0, ENTITY = "wall_ef" )
BCNODE ( UY, CONSTANT = 0, ENTITY = "wall_ef" )
HTRANSFER ( SET = "wall_ef", CONSTANT = 2.31, REFTEMP = 310 )

ENTITY ( NAME = "wall_fg", CONVECTION, MCNV = "wall_fg" )
BCNODE ( UX, CONSTANT = 0, ENTITY = "wall_fg" )
BCNODE ( UY, CONSTANT = 0, ENTITY = "wall_fg" )
HTRANSFER ( SET = "wall_fg", CONSTANT = 2.31, REFTEMP = 310 )

ENTITY ( NAME = "wall_gh", CONVECTION, MCNV = "wall_gh" )
BCNODE ( UX, CONSTANT = 0, ENTITY = "wall_gh" )
BCNODE ( UY, CONSTANT = 0, ENTITY = "wall_gh" )
HTRANSFER ( SET = "wall_gh", CONSTANT = 2.31, REFTEMP = 310 )

ENTITY ( NAME = "wall_ij", CONVECTION, MCNV = "wall_ij" )
BCNODE ( UX, CONSTANT = 0, ENTITY = "wall_ij" )
BCNODE ( UY, CONSTANT = 0, ENTITY = "wall_ij" )
HTRANSFER ( SET = "wall_ij", CONSTANT = 2.31, REFTEMP = 310 )

ENTITY ( NAME = "wall_jk", CONVECTION, MCNV = "wall_jk" )
BCNODE ( UX, CONSTANT = 0, ENTITY = "wall_jk" )
BCNODE ( UY, CONSTANT = 0, ENTITY = "wall_jk" )
HTRANSFER ( SET = "wall_jk", CONSTANT = 2.31, REFTEMP = 310 )

ENTITY ( NAME = "wall_kl", CONVECTION, MCNV = "wall_kl" )
BCNODE ( UX, CONSTANT = 0, ENTITY = "wall_kl" )
BCNODE ( UY, CONSTANT = 0, ENTITY = "wall_kl" )
HTRANSFER ( SET = "wall_kl", CONSTANT = 2.31, REFTEMP = 310 )

ENTITY ( NAME = "wall_mn", CONVECTION, MCNV = "wall_mn" )
BCNODE ( UX, CONSTANT = 0, ENTITY = "wall_mn" )
BCNODE ( UY, CONSTANT = 0, ENTITY = "wall_mn" )
HTRANSFER ( SET = "wall_mn", CONSTANT = 2.31, REFTEMP = 310 )

ENTITY ( NAME = "wall_no", CONVECTION, MCNV = "wall_no" )
BCNODE ( UX, CONSTANT = 0, ENTITY = "wall_no" )
BCNODE ( UY, CONSTANT = 0, ENTITY = "wall_no" )
HTRANSFER ( SET = "wall_no", CONSTANT = 2.31, REFTEMP = 310 )

ENTITY ( NAME = "wall_op", CONVECTION, MCNV = "wall_op" )
BCNODE ( UX, CONSTANT = 0, ENTITY = "wall_op" )
```

```
BCNODE ( UY, CONSTANT = 0, ENTITY = "wall_op" )
HTRANSFER ( SET = "wall_op", CONSTANT = 2.31, REFTEMP = 310 )

ENTITY ( NAME = "wall_qr", CONVECTION, MCNV = "wall_qr" )
BCNODE ( UX, CONSTANT = 0, ENTITY = "wall_qr" )
BCNODE ( UY, CONSTANT = 0, ENTITY = "wall_qr" )
HTRANSFER ( SET = "wall_qr", CONSTANT = 2.31, REFTEMP = 310 )

ENTITY ( NAME = "wall_rs", CONVECTION, MCNV = "wall_rs" )
BCNODE ( UX, CONSTANT = 0, ENTITY = "wall_rs" )
BCNODE ( UY, CONSTANT = 0, ENTITY = "wall_rs" )
HTRANSFER ( SET = "wall_rs", CONSTANT = 2.31, REFTEMP = 310 )

ENTITY ( NAME = "wall_st", CONVECTION, MCNV = "wall_st" )
BCNODE ( UX, CONSTANT = 0, ENTITY = "wall_st" )
BCNODE ( UY, CONSTANT = 0, ENTITY = "wall_st" )
HTRANSFER ( SET = "wall_st", CONSTANT = 2.31, REFTEMP = 310 )

ENTITY ( NAME = "wall_uv", CONVECTION, MCNV = "wall_uv" )
BCNODE ( UX, CONSTANT = 0, ENTITY = "wall_uv" )
BCNODE ( UY, CONSTANT = 0, ENTITY = "wall_uv" )
HTRANSFER ( SET = "wall_uv", CONSTANT = 2.31, REFTEMP = 310 )

ENTITY ( NAME = "wall_vw", CONVECTION, MCNV = "wall_vw" )
BCNODE ( UX, CONSTANT = 0, ENTITY = "wall_vw" )
BCNODE ( UY, CONSTANT = 0, ENTITY = "wall_vw" )
HTRANSFER ( SET = "wall_vw", CONSTANT = 2.31, REFTEMP = 310 )

ENTITY ( NAME = "wall_wx", CONVECTION, MCNV = "wall_wx" )
BCNODE ( UX, CONSTANT = 0, ENTITY = "wall_wx" )
BCNODE ( UY, CONSTANT = 0, ENTITY = "wall_wx" )
HTRANSFER ( SET = "wall_wx", CONSTANT = 2.31, REFTEMP = 310 )

ENTITY ( NAME = "wall_yz", CONVECTION, MCNV = "wall_yz" )
BCNODE ( UX, CONSTANT = 0, ENTITY = "wall_yz" )
BCNODE ( UY, CONSTANT = 0, ENTITY = "wall_yz" )
HTRANSFER ( SET = "wall_yz", CONSTANT = 2.31, REFTEMP = 310 )

ENTITY ( NAME = "wall_zaa", CONVECTION, MCNV = "wall_zaa" )
BCNODE ( UX, CONSTANT = 0, ENTITY = "wall_zaa" )
BCNODE ( UY, CONSTANT = 0, ENTITY = "wall_zaa" )
HTRANSFER ( SET = "wall_zaa", CONSTANT = 2.31, REFTEMP = 310 )

ENTITY ( NAME = "wall_aabb", CONVECTION, MCNV = "wall_aabb" )
BCNODE ( UX, CONSTANT = 0, ENTITY = "wall_aabb" )
BCNODE ( UY, CONSTANT = 0, ENTITY = "wall_aabb" )
HTRANSFER ( SET = "wall_aabb", CONSTANT = 2.31, REFTEMP = 310 )

ENTITY ( NAME = "wall_ccdd", CONVECTION, MCNV = "wall_ccdd" )
BCNODE ( UX, CONSTANT = 0, ENTITY = "wall_ccdd" )
BCNODE ( UY, CONSTANT = 0, ENTITY = "wall_ccdd" )
HTRANSFER ( SET = "wall_ccdd", CONSTANT = 2.31, REFTEMP = 310 )

ENTITY ( NAME = "wall_ddee", CONVECTION, MCNV = "wall_ddee" )
```

```
BCNODE ( UX, CONSTANT = 0, ENTITY = "wall_ddee" )
BCNODE ( UY, CONSTANT = 0, ENTITY = "wall_ddee" )
HTRANSFER ( SET = "wall_ddee", CONSTANT = 2.31, REFTEMP = 310 )

ENTITY ( NAME = "wall_eeff", CONVECTION, MCNV = "wall_eeff" )
BCNODE ( UX, CONSTANT = 0, ENTITY = "wall_eeff" )
BCNODE ( UY, CONSTANT = 0, ENTITY = "wall_eeff" )
HTRANSFER ( SET = "wall_eeff", CONSTANT = 2.31, REFTEMP = 310 )

ENTITY ( NAME = "wall_gghh", CONVECTION, MCNV = "wall_gghh" )
BCNODE ( UX, CONSTANT = 0, ENTITY = "wall_gghh" )
BCNODE ( UY, CONSTANT = 0, ENTITY = "wall_gghh" )
HTRANSFER ( SET = "wall_gghh", CONSTANT = 2.31, REFTEMP = 310 )

ENTITY ( NAME = "wall_hhii", CONVECTION, MCNV = "wall_hhii" )
BCNODE ( UX, CONSTANT = 0, ENTITY = "wall_hhii" )
BCNODE ( UY, CONSTANT = 0, ENTITY = "wall_hhii" )
HTRANSFER ( SET = "wall_hhii", CONSTANT = 2.31, REFTEMP = 310 )

ENTITY ( NAME = "end_iijj", CONVECTION, MCNV = "end_iijj" )
BCNODE ( UX, CONSTANT = 0, ENTITY = "end_iijj" )
BCNODE ( UY, CONSTANT = 0, ENTITY = "end_iijj" )
HTRANSFER ( SET = "end_iijj", CONSTANT = 2.31, REFTEMP = 310 )

ENTITY ( NAME = "top_jja", SLIP)
BCNODE ( TEMPERATURE, CONSTANT = 1589, ENTITY = "top_jja" )
BCNODE ( UY, CONSTANT = 0, ENTITY = "top_jja" )

ENTITY ( NAME = "bushing_8", PLOT )
BCNODE ( UX, CONSTANT = 0, ENTITY = "bushing_8" )

ENTITY ( NAME = "bushing_7", PLOT )
BCNODE ( UX, CONSTANT = 0, ENTITY = "bushing_7" )

ENTITY ( NAME = "bushing_6", PLOT )
BCNODE ( UX, CONSTANT = 0, ENTITY = "bushing_6" )

ENTITY ( NAME = "bushing_5", PLOT )
BCNODE ( UX, CONSTANT = 0, ENTITY = "bushing_5")

ENTITY ( NAME = "bushing_4", PLOT )
BCNODE ( UX, CONSTANT = 0, ENTITY = "bushing_4" )

ENTITY ( NAME = "bushing_3", PLOT )
BCNODE ( UX, CONSTANT = 0, ENTITY = "bushing_3" )

ENTITY ( NAME = "bushing_2", PLOT )
BCNODE ( UX, CONSTANT = 0, ENTITY = "bushing_2" )

ENTITY ( NAME = "bushing_1", PLOT )
BCNODE ( UX, CONSTANT = 0, ENTITY = "bushing_1" )

BCNODE ( SURFACE, CONSTANT = 0, NODE )
1 1 1
```

```
BCNODE ( CONTACTANGLE, CONSTANT = 0, NODE = 486 )

BODYFORCE ( ENTITY = "eglass", FX = 0, FY = -9.80665 )

END

CREATE (FIPREP, DELETE)
CREATE (FISOLV)
PARA(LIST)
```

FIDAP Simulation Program 2

```
/*************************************************************
/DISCLAIMER: This file has been created by GAMBIT based on the data
/entered in PreSTO.  Please note that not all the capabilities of FIDAP
/are present in the PreSTO template. However, you can add the desired
/capabilities by editing this file with a text editor. You will then
/have to run FIDAP outside the GAMBIT (PreSTO) environment.
/Please send bug reports and/or enhancement requests to:
/ashwini.kumar@fluent.com or marc.horner@fluent.com
/*************************************************************

FICONV( NEUTRAL, INPUT, FDMESH )
INPUT( FILE="fh_new.FDNEUT" )
OUTPUT( DELETE )
END

TITLE
fh_new

FIPREP

EXECUTION (NEWJOB)
PRINT (NONE)
DATA (CONTROL)

PROBLEM(2-d, Energy, Laminar, Transient, NONLINEAR, FREE, NEWTONIAN,
INCOMPRESSIBLE)
SCALE ( VALUE = 0.0254 )
SOLUTION (SEGRE=500, VELCONV =0.001, SURF =0.01, SCHANGE =0, KINE = 30)
RELAXATION(HYBRID)
0.1 0.1 0.1 0.5 0.5 0.9 0.0 0.0
OPTION (SIDES , UPWIN)
UPWIN (STREAM)
EXTRAPOLATE(ON, NOFREE)
PRESSURE ( MIXED = 1e-12, DISCONTINUOUS )
TIME (NSTEP = 200, TSTART = 0, DT = 0.01, INCMAX = 1.2, DTMAX = 0.1,
NOFIXED = 10)

ENTITY( NAME = "eglass", FLUID, PROPERTY = "default" )
DENSITY( SET = "default", CONSTANT = 2500 )
```

```
VISCOSITY( SET = "default", CONSTANT= 30.2587 )
CONDUCTIVITY( SET = "default", CONST =19.2713 )
SPECIFICHEAT( SET = "default", CONSTANT = 1401.6 )

ENTITY ( NAME = "forehearth_inlet", PLOT )
BCNODE ( TEMPERATURE, CONSTANT = 1589, ENTITY = "forehearth_inlet" )
BCNODE ( UX, CONSTANT = 0.0016, ENTITY = "forehearth_inlet" )
BCNODE ( UY, CONSTANT = 0.0, ENTITY = "forehearth_inlet" )

ENTITY ( NAME = "wall_bc", CONVECTION, MCNV = "wall_bc" )
BCNODE ( UX, CONSTANT = 0, ENTITY = "wall_bc" )
BCNODE ( UY, CONSTANT = 0, ENTITY = "wall_bc" )
HTRANSFER ( SET = "wall_bc", CONSTANT = 2.31, REFTEMP = 310 )

ENTITY ( NAME = "wall_cd", CONVECTION, MCNV = "wall_cd" )
BCNODE ( UX, CONSTANT = 0, ENTITY = "wall_cd" )
BCNODE ( UY, CONSTANT = 0, ENTITY = "wall_cd" )
HTRANSFER ( SET = "wall_cd", CONSTANT = 2.31, REFTEMP = 310 )

ENTITY ( NAME = "wall_ef", CONVECTION, MCNV = "wall_ef" )
BCNODE ( UX, CONSTANT = 0, ENTITY = "wall_ef" )
BCNODE ( UY, CONSTANT = 0, ENTITY = "wall_ef" )
HTRANSFER ( SET = "wall_ef", CONSTANT = 2.31, REFTEMP = 310 )

ENTITY ( NAME = "wall_fg", CONVECTION, MCNV = "wall_fg" )
BCNODE ( UX, CONSTANT = 0, ENTITY = "wall_fg" )
BCNODE ( UY, CONSTANT = 0, ENTITY = "wall_fg" )
HTRANSFER ( SET = "wall_fg", CONSTANT = 2.31, REFTEMP = 310 )

ENTITY ( NAME = "wall_gh", CONVECTION, MCNV = "wall_gh" )
BCNODE ( UX, CONSTANT = 0, ENTITY = "wall_gh" )
BCNODE ( UY, CONSTANT = 0, ENTITY = "wall_gh" )
HTRANSFER ( SET = "wall_gh", CONSTANT = 2.31, REFTEMP = 310 )

ENTITY ( NAME = "wall_ij", CONVECTION, MCNV = "wall_ij" )
BCNODE ( UX, CONSTANT = 0, ENTITY = "wall_ij" )
BCNODE ( UY, CONSTANT = 0, ENTITY = "wall_ij" )
HTRANSFER ( SET = "wall_ij", CONSTANT = 2.31, REFTEMP = 310 )

ENTITY ( NAME = "wall_jk", CONVECTION, MCNV = "wall_jk" )
BCNODE ( UX, CONSTANT = 0, ENTITY = "wall_jk" )
BCNODE ( UY, CONSTANT = 0, ENTITY = "wall_jk" )
HTRANSFER ( SET = "wall_jk", CONSTANT = 2.31, REFTEMP = 310 )

ENTITY ( NAME = "wall_kl", CONVECTION, MCNV = "wall_kl" )
BCNODE ( UX, CONSTANT = 0, ENTITY = "wall_kl" )
BCNODE ( UY, CONSTANT = 0, ENTITY = "wall_kl" )
HTRANSFER ( SET = "wall_kl", CONSTANT = 2.31, REFTEMP = 310 )

ENTITY ( NAME = "wall_mn", CONVECTION, MCNV = "wall_mn" )
BCNODE ( UX, CONSTANT = 0, ENTITY = "wall_mn" )
BCNODE ( UY, CONSTANT = 0, ENTITY = "wall_mn" )
HTRANSFER ( SET = "wall_mn", CONSTANT = 2.31, REFTEMP = 310 )
```

```
ENTITY ( NAME = "wall_no", CONVECTION, MCNV = "wall_no" )
BCNODE ( UX, CONSTANT = 0, ENTITY = "wall_no" )
BCNODE ( UY, CONSTANT = 0, ENTITY = "wall_no" )
HTRANSFER ( SET = "wall_no", CONSTANT = 2.31, REFTEMP = 310 )

ENTITY ( NAME = "wall_op", CONVECTION, MCNV = "wall_op" )
BCNODE ( UX, CONSTANT = 0, ENTITY = "wall_op" )
BCNODE ( UY, CONSTANT = 0, ENTITY = "wall_op" )
HTRANSFER ( SET = "wall_op", CONSTANT = 2.31, REFTEMP = 310 )

ENTITY ( NAME = "wall_qr", CONVECTION, MCNV = "wall_qr" )
BCNODE ( UX, CONSTANT = 0, ENTITY = "wall_qr" )
BCNODE ( UY, CONSTANT = 0, ENTITY = "wall_qr" )
HTRANSFER ( SET = "wall_qr", CONSTANT = 2.31, REFTEMP = 310 )

ENTITY ( NAME = "wall_rs", CONVECTION, MCNV = "wall_rs" )
BCNODE ( UX, CONSTANT = 0, ENTITY = "wall_rs" )
BCNODE ( UY, CONSTANT = 0, ENTITY = "wall_rs" )
HTRANSFER ( SET = "wall_rs", CONSTANT = 2.31, REFTEMP = 310 )

ENTITY ( NAME = "wall_st", CONVECTION, MCNV = "wall_st" )
BCNODE ( UX, CONSTANT = 0, ENTITY = "wall_st" )
BCNODE ( UY, CONSTANT = 0, ENTITY = "wall_st" )
HTRANSFER ( SET = "wall_st", CONSTANT = 2.31, REFTEMP = 310 )

ENTITY ( NAME = "wall_uv", CONVECTION, MCNV = "wall_uv" )
BCNODE ( UX, CONSTANT = 0, ENTITY = "wall_uv" )
BCNODE ( UY, CONSTANT = 0, ENTITY = "wall_uv" )
HTRANSFER ( SET = "wall_uv", CONSTANT = 2.31, REFTEMP = 310 )

ENTITY ( NAME = "wall_vw", CONVECTION, MCNV = "wall_vw" )
BCNODE ( UX, CONSTANT = 0, ENTITY = "wall_vw" )
BCNODE ( UY, CONSTANT = 0, ENTITY = "wall_vw" )
HTRANSFER ( SET = "wall_vw", CONSTANT = 2.31, REFTEMP = 310 )

ENTITY ( NAME = "wall_wx", CONVECTION, MCNV = "wall_wx" )
BCNODE ( UX, CONSTANT = 0, ENTITY = "wall_wx" )
BCNODE ( UY, CONSTANT = 0, ENTITY = "wall_wx" )
HTRANSFER ( SET = "wall_wx", CONSTANT = 2.31, REFTEMP = 310 )

ENTITY ( NAME = "wall_yz", CONVECTION, MCNV = "wall_yz" )
BCNODE ( UX, CONSTANT = 0, ENTITY = "wall_yz" )
BCNODE ( UY, CONSTANT = 0, ENTITY = "wall_yz" )
HTRANSFER ( SET = "wall_yz", CONSTANT = 2.31, REFTEMP = 310 )

ENTITY ( NAME = "wall_zaa", CONVECTION, MCNV = "wall_zaa" )
BCNODE ( UX, CONSTANT = 0, ENTITY = "wall_zaa" )
BCNODE ( UY, CONSTANT = 0, ENTITY = "wall_zaa" )
HTRANSFER ( SET = "wall_zaa", CONSTANT = 2.31, REFTEMP = 310 )

ENTITY ( NAME = "wall_aabb", CONVECTION, MCNV = "wall_aabb" )
BCNODE ( UX, CONSTANT = 0, ENTITY = "wall_aabb" )
BCNODE ( UY, CONSTANT = 0, ENTITY = "wall_aabb" )
HTRANSFER ( SET = "wall_aabb", CONSTANT = 2.31, REFTEMP = 310 )
```

```
ENTITY ( NAME = "wall_ccdd", CONVECTION, MCNV = "wall_ccdd" )
BCNODE ( UX, CONSTANT = 0, ENTITY = "wall_ccdd" )
BCNODE ( UY, CONSTANT = 0, ENTITY = "wall_ccdd" )
HTRANSFER ( SET = "wall_ccdd", CONSTANT = 2.31, REFTEMP = 310 )

ENTITY ( NAME = "wall_ddee", CONVECTION, MCNV = "wall_ddee" )
BCNODE ( UX, CONSTANT = 0, ENTITY = "wall_ddee" )
BCNODE ( UY, CONSTANT = 0, ENTITY = "wall_ddee" )
HTRANSFER ( SET = "wall_ddee", CONSTANT = 2.31, REFTEMP = 310 )

ENTITY ( NAME = "wall_eeff", CONVECTION, MCNV = "wall_eeff" )
BCNODE ( UX, CONSTANT = 0, ENTITY = "wall_eeff" )
BCNODE ( UY, CONSTANT = 0, ENTITY = "wall_eeff" )
HTRANSFER ( SET = "wall_eeff", CONSTANT = 2.31, REFTEMP = 310 )

ENTITY ( NAME = "wall_gghh", CONVECTION, MCNV = "wall_gghh" )
BCNODE ( UX, CONSTANT = 0, ENTITY = "wall_gghh" )
BCNODE ( UY, CONSTANT = 0, ENTITY = "wall_gghh" )
HTRANSFER ( SET = "wall_gghh", CONSTANT = 2.31, REFTEMP = 310 )

ENTITY ( NAME = "wall_hhii", CONVECTION, MCNV = "wall_hhii" )
BCNODE ( UX, CONSTANT = 0, ENTITY = "wall_hhii" )
BCNODE ( UY, CONSTANT = 0, ENTITY = "wall_hhii" )
HTRANSFER ( SET = "wall_hhii", CONSTANT = 2.31, REFTEMP = 310 )

ENTITY ( NAME = "end_iijj", CONVECTION, MCNV = "end_iijj" )
BCNODE ( UX, CONSTANT = 0, ENTITY = "end_iijj" )
BCNODE ( UY, CONSTANT = 0, ENTITY = "end_iijj" )
HTRANSFER ( SET = "end_iijj", CONSTANT = 2.31, REFTEMP = 310 )

ENTITY ( NAME = "top_jja", SLIP)
BCNODE ( TEMPERATURE, CONSTANT = 1589, ENTITY = "top_jja" )
BCNODE ( UY, CONSTANT = 0, ENTITY = "top_jja" )

ENTITY ( NAME = "bushing_8", PLOT )
BCNODE ( UX, CONSTANT = 0, ENTITY = "bushing_8" )

ENTITY ( NAME = "bushing_7", PLOT )
BCNODE ( UX, CONSTANT = 0, ENTITY = "bushing_7" )

ENTITY ( NAME = "bushing_6", PLOT )
BCNODE ( UX, CONSTANT = 0, ENTITY = "bushing_6" )

ENTITY ( NAME = "bushing_5", PLOT )
BCNODE ( UX, CONSTANT = 0, ENTITY = "bushing_5")

ENTITY ( NAME = "bushing_4", PLOT )
BCNODE ( UX, CONSTANT = 0, ENTITY = "bushing_4" )

ENTITY ( NAME = "bushing_3", PLOT )
BCNODE ( UX, CONSTANT = 0, ENTITY = "bushing_3" )
```

```
ENTITY ( NAME = "bushing_2", PLOT )
BCNODE ( UX, CONSTANT = 0, ENTITY = "bushing_2" )

ENTITY ( NAME = "bushing_1", PLOT )
BCNODE ( UX, CONSTANT = 0, ENTITY = "bushing_1" )

BCNODE ( SURFACE, CONSTANT = 0, NODE )
1 1 1
BCNODE ( CONTACTANGLE, CONSTANT = 0, NODE = 486 )

BODYFORCE ( ENTITY = "eglass", FX = 0, FY = -9.80665 )

ICNO (VELO, READ, ALL)
ICNO (TEMP, READ, ALL)

END

CREATE (FIPREP, DELETE)
CREATE (FISOLV)
PARA(LIST)
```

Additional Code for a Bushing Changeover

To account for a bushing changeover, the following generic lines of code are added:

```
/X - represents the actual bushing position frozen off

/ORIGINAL CODE
ENTITY ( NAME = "bushing_X", PLOT )
BCNODE ( UX, CONSTANT = 0, ENTITY = "bushing_X" )

/ADDITIONAL CODE
BCNODE ( UY, CONSTANT = 0, ENTITY = "bushing_X" )
BCFLUX ( HEAT, CONSTANT = -337099.5656, ENTITY = "bushing_X" )
```

6.5 Appendix E – FLUENT Simulation Results

Trial FL–2

Position	MFR (kg/s)
forehearth_inlet	0.5456
bushing_8	-0.1364
bushing_7	-0.1364
bushing_6	-0.1364
bushing_5	-0.1364
bushing_4	-0.0682
bushing_3	-0.0682
bushing_2	-0.0682
bushing_1	-0.0341

ΔMFR =	-0.2387

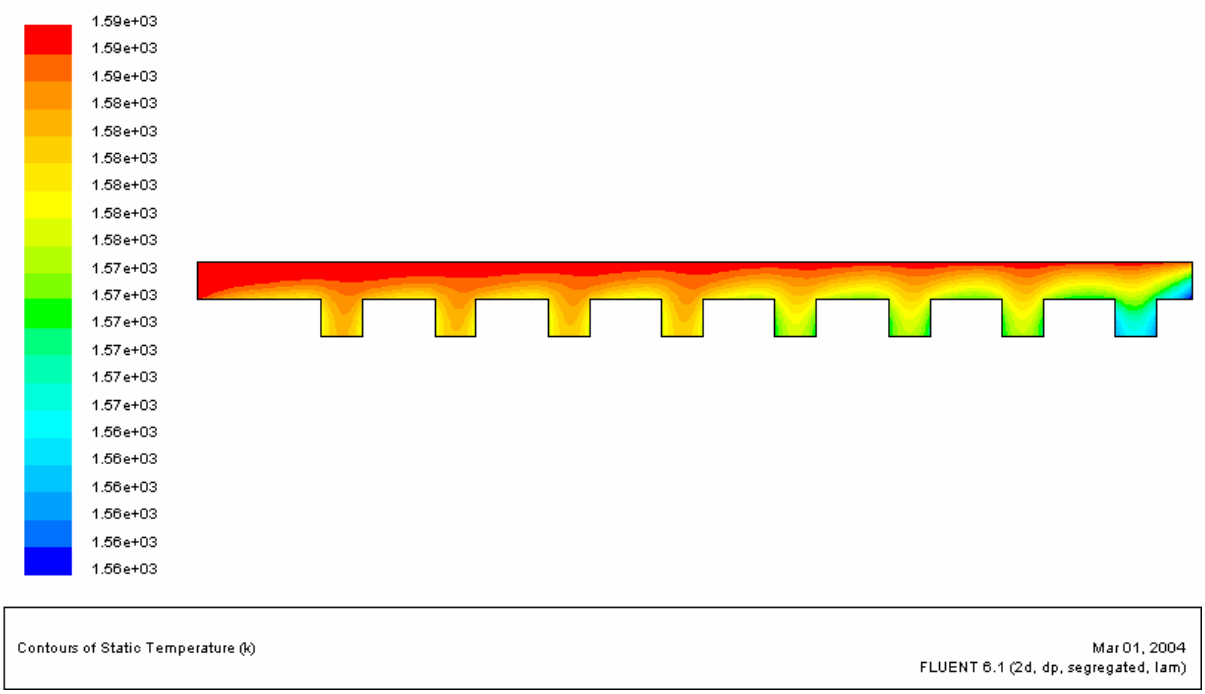

Figure 6.2 – FLUENT Trial FL–2: Temperature Contours of Molten Glass (°K)

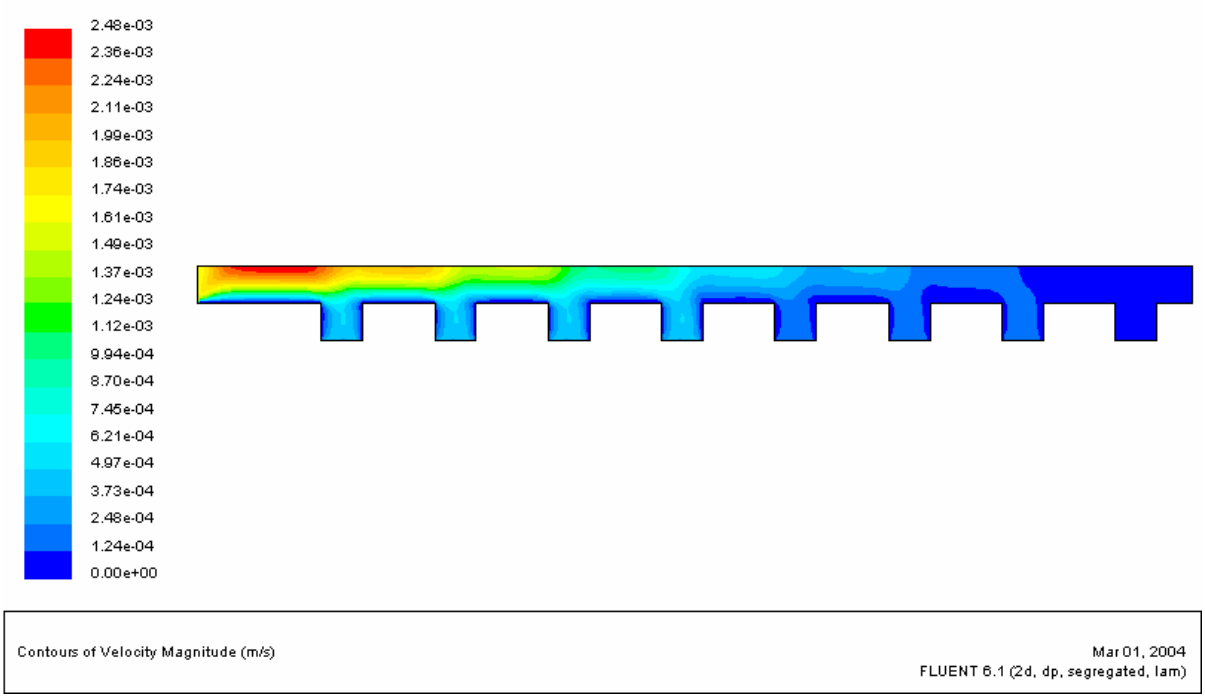

Figure 6.3 – FLUENT Trial FL–2: Velocity Magnitudes (m/s)

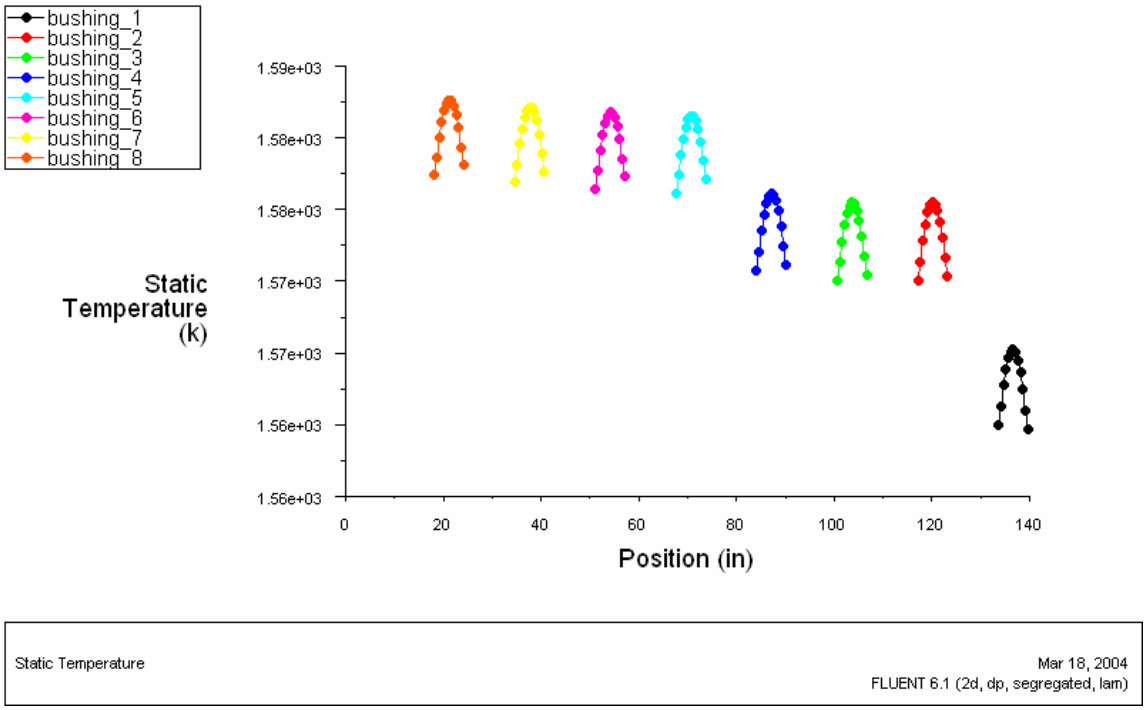

Figure 6.4 – FLUENT Trial FL–2: Bushing Outlet Temperatures (°K)

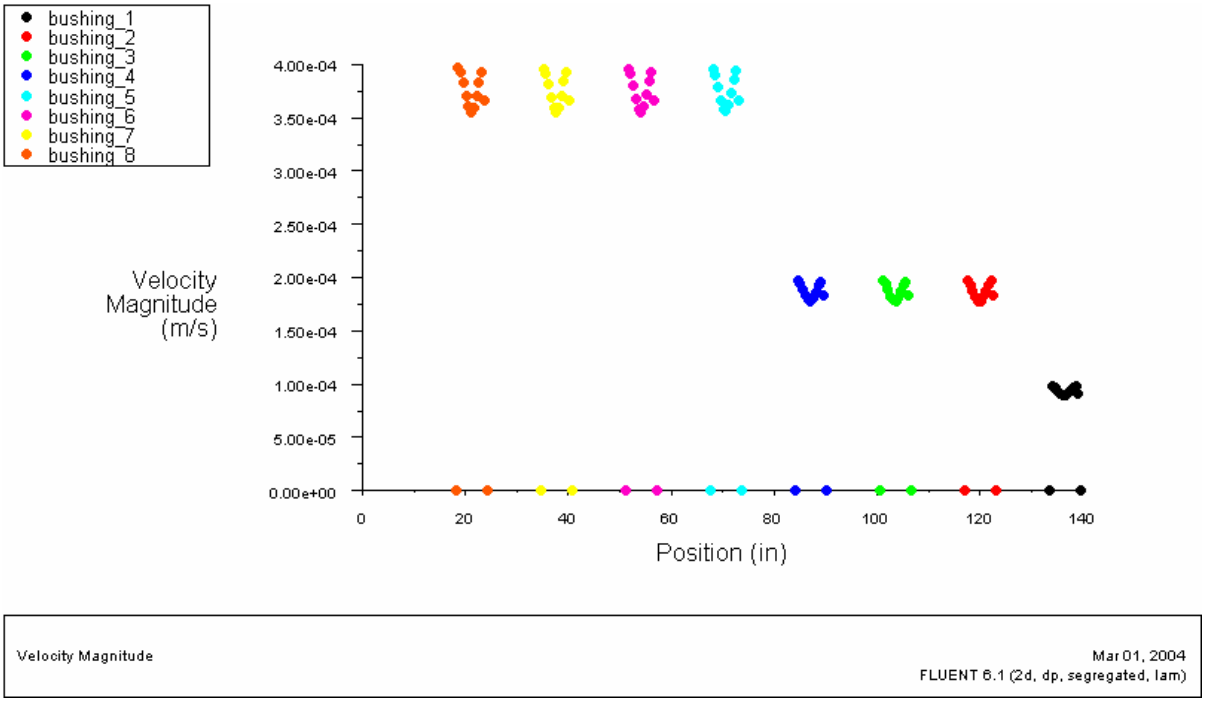

Figure 6.5 – FLUENT Trial FL–2: Bushing Outlet Velocity Magnitudes (m/s)

Trial FL–2a

Position	MFR (kg/s)
forehearth_inlet	0.7843
bushing_8	-0.1364
bushing_7	-0.1364
bushing_6	-0.1364
bushing_5	-0.1364
bushing_4	-0.0682
bushing_3	-0.0682
bushing_2	-0.0682
bushing_1	-0.0341

ΔMFR =	0.0000

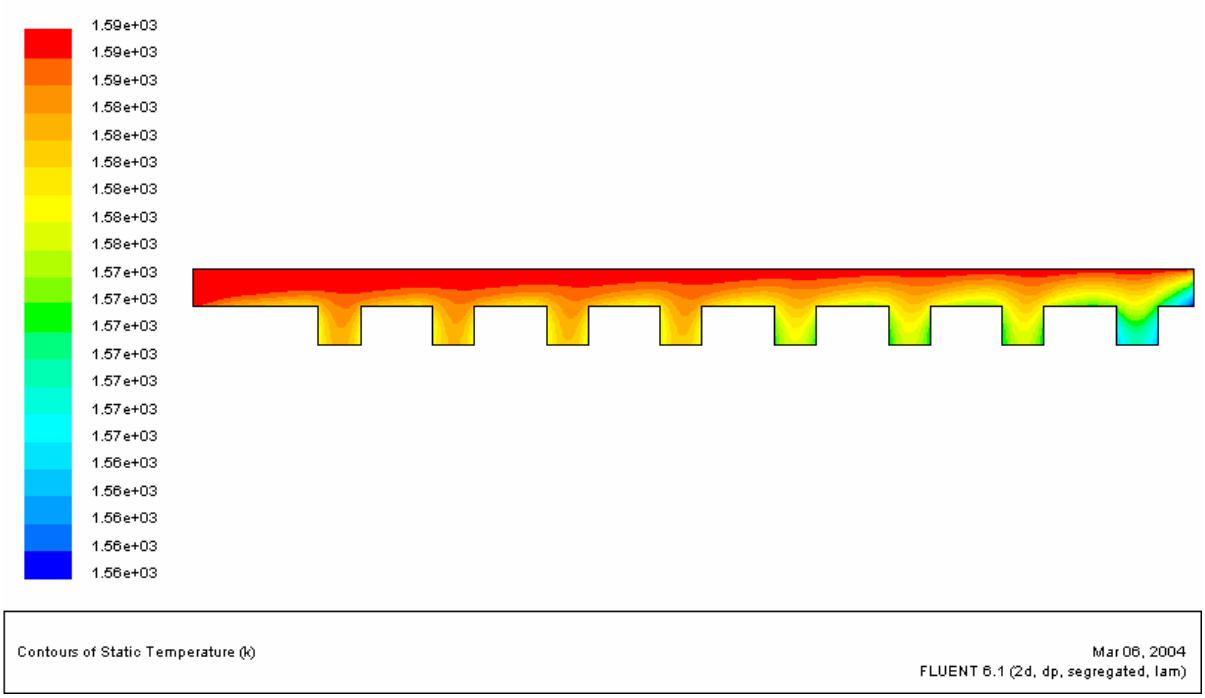

Figure 6.6 – FLUENT Trial FL–2a: Temperature Contours of Molten Glass (°K)

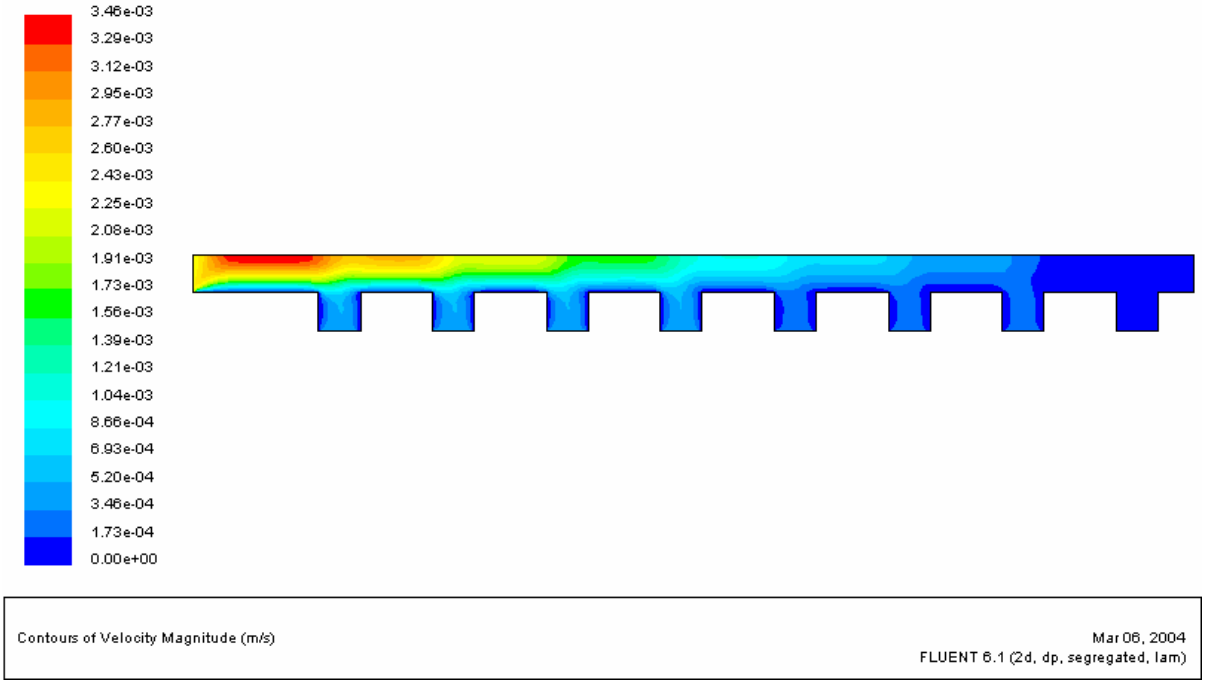

Figure 6.7 – FLUENT Trial FL–2a: Velocity Magnitudes (m/s)

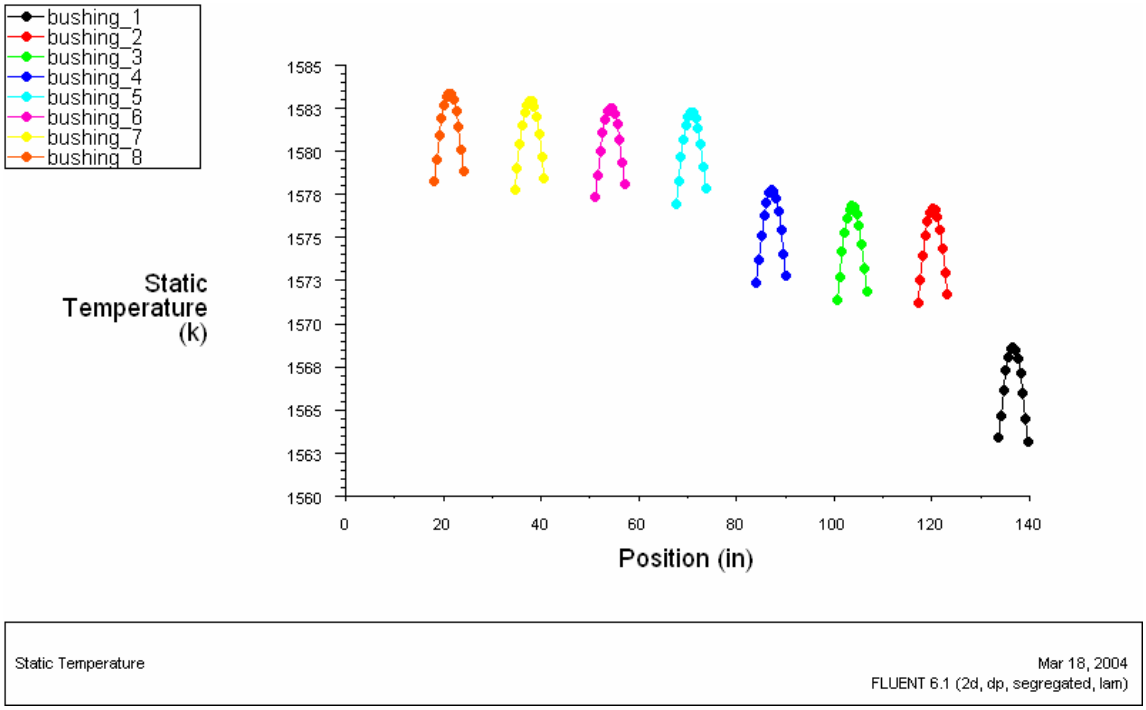

Figure 6.8 – FLUENT Trial FL–2a: Bushing Outlet Temperatures (°K)

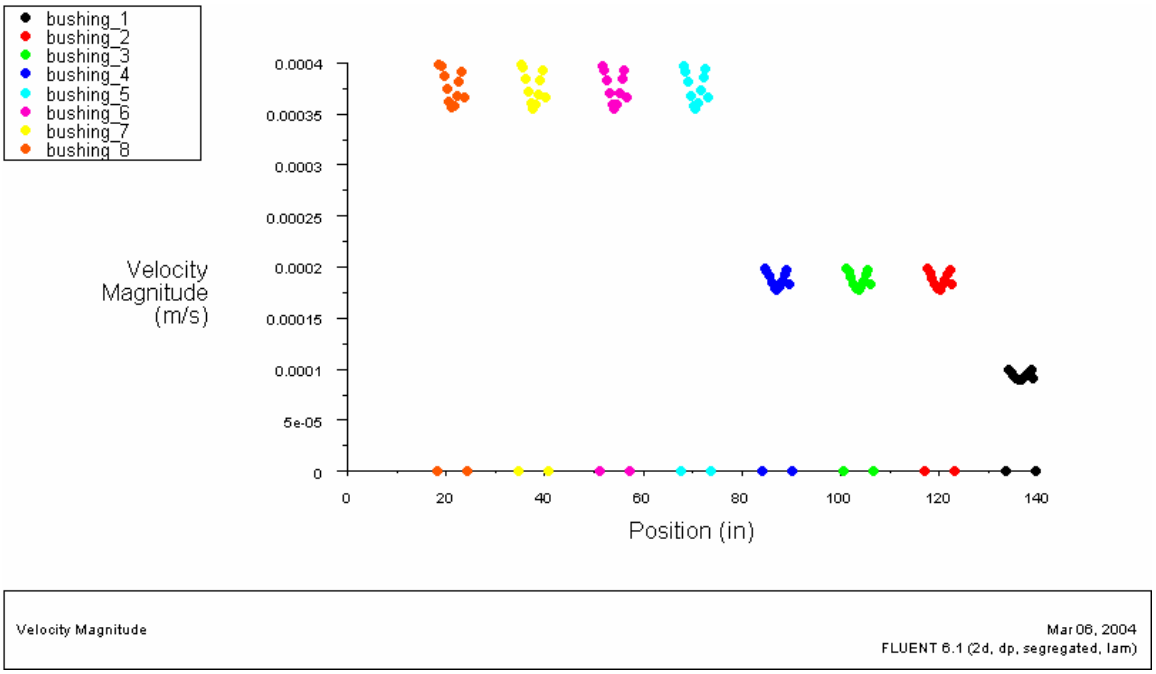

Figure 6.9 – FLUENT Trial FL–2a: Bushing Outlet Velocity Magnitudes (m/s)

Trial FL–3

Position	MFR (kg/s)
forehearth_inlet	0.5456
bushing_8	-0.0341
bushing_7	-0.0341
bushing_6	-0.0341
bushing_5	-0.0341
bushing_4	-0.0682
bushing_3	-0.0682
bushing_2	-0.0682
bushing_1	-0.1364

ΔMFR =	0.0682

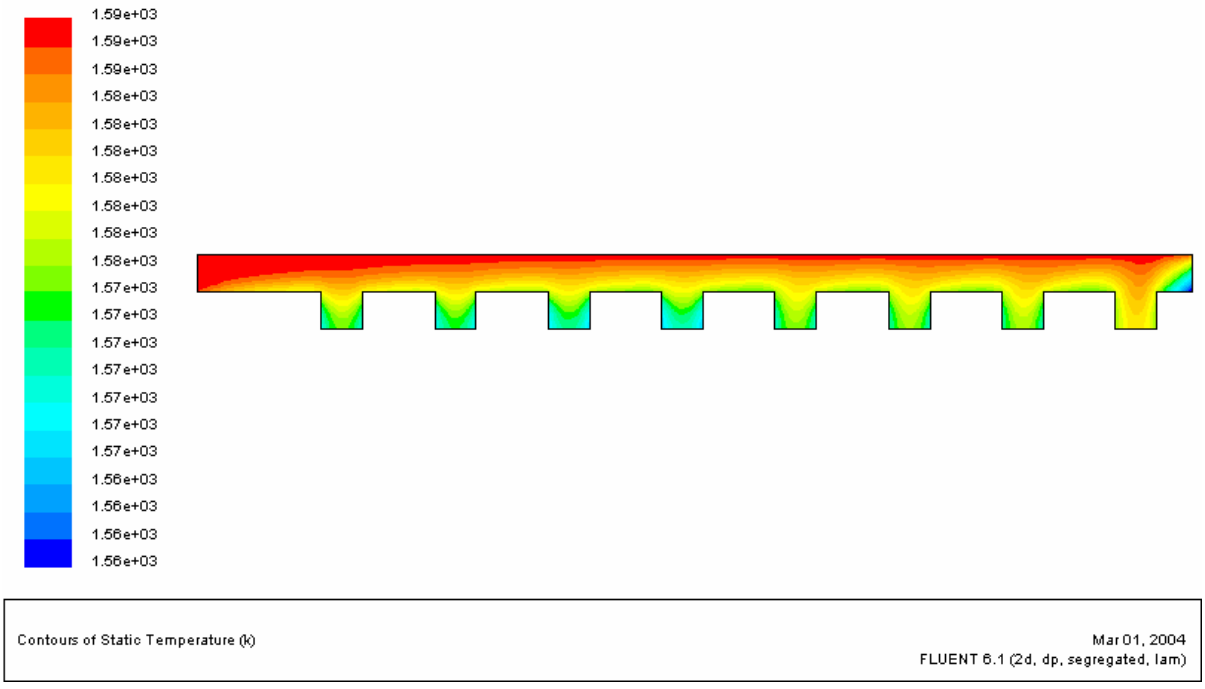

Figure 6.10 – FLUENT Trial FL–3: Temperature Contours of Molten Glass (°K)

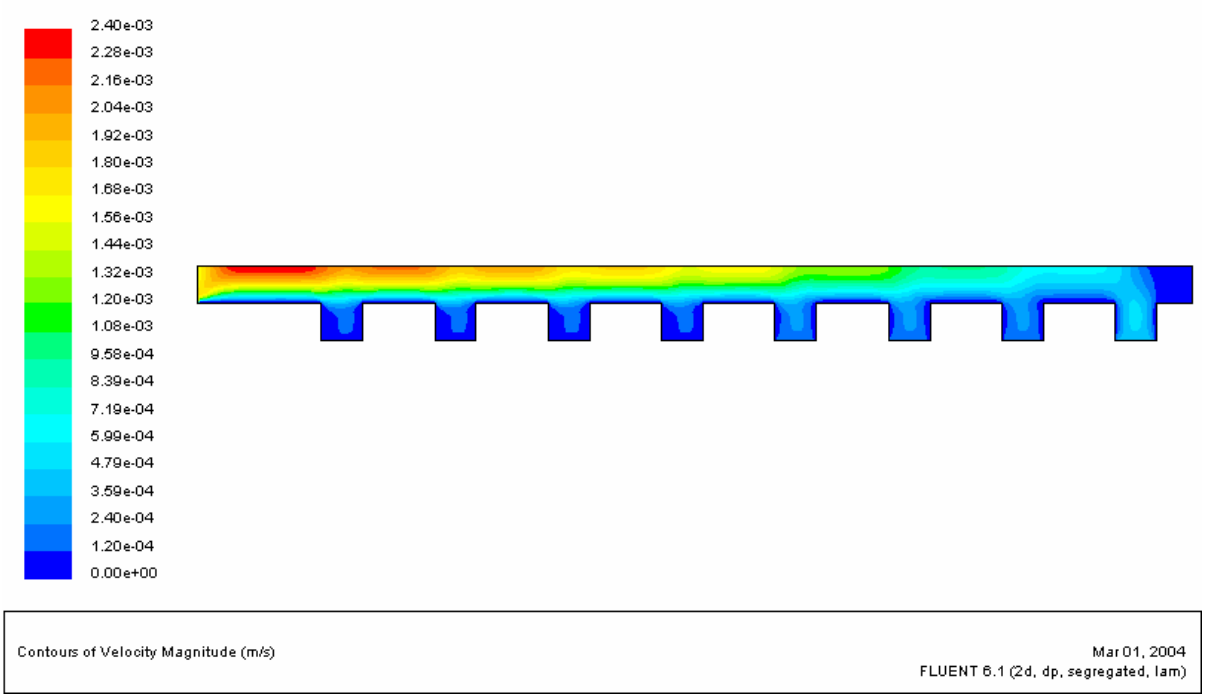

Figure 6.11 – FLUENT Trial FL–3: Velocity Magnitudes (m/s)

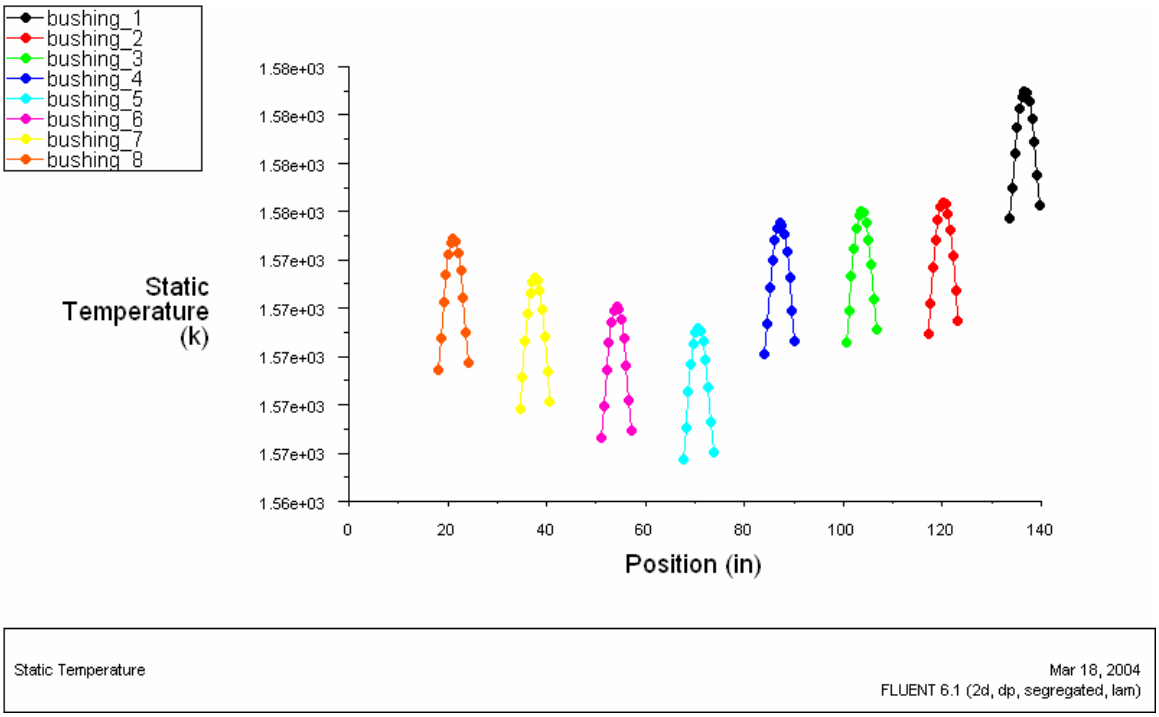

Figure 6.12 – FLUENT Trial FL–3: Bushing Outlet Temperatures (°K)

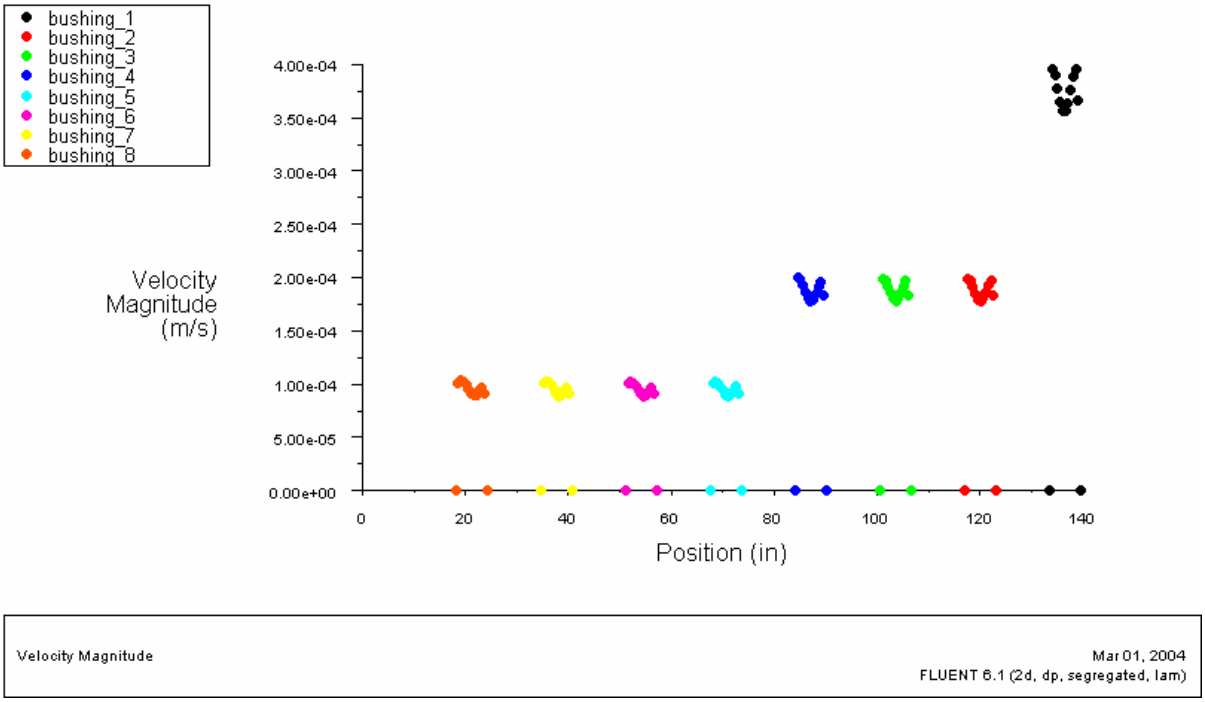

Figure 6.13 – FLUENT Trial FL–3: Bushing Outlet Velocity Magnitudes (m/s)

Trial FL–3a

Position	MFR (kg/s)
forehearth_inlet	0.4774
bushing_8	-0.0341
bushing_7	-0.0341
bushing_6	-0.0341
bushing_5	-0.0341
bushing_4	-0.0682
bushing_3	-0.0682
bushing_2	-0.0682
bushing_1	-0.1364

ΔMFR =	0.0000

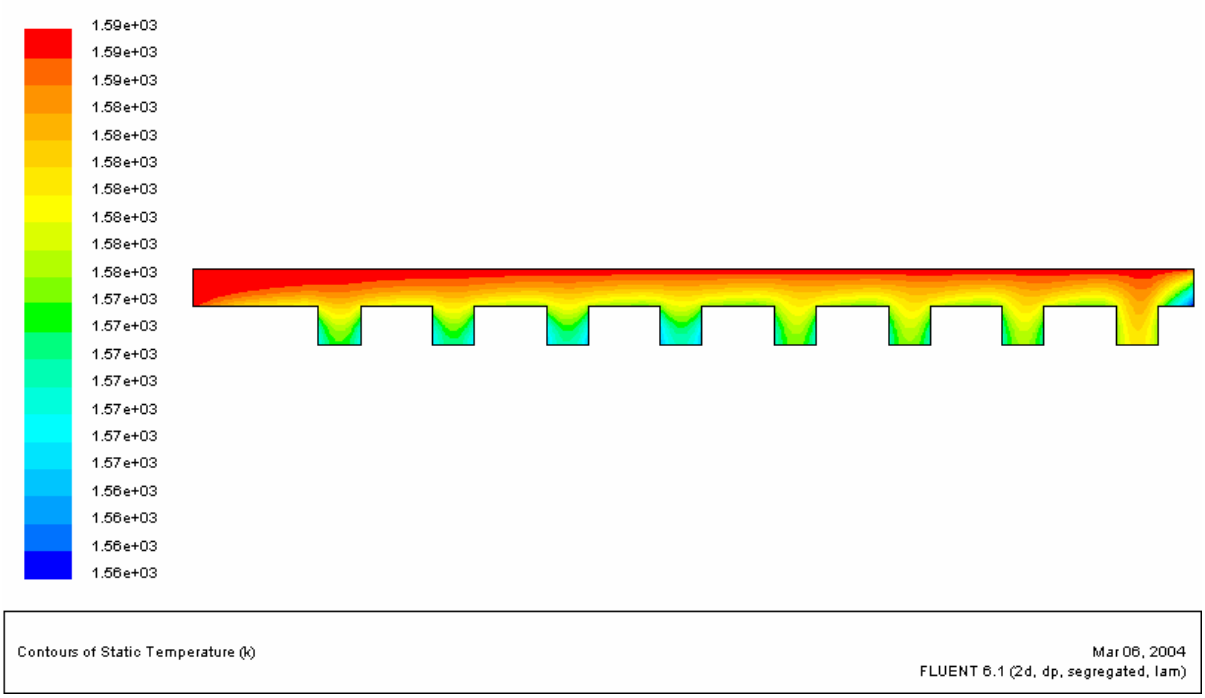

Figure 6.14 – FLUENT Trial FL–3a: Temperature Contours of Molten Glass (°K)

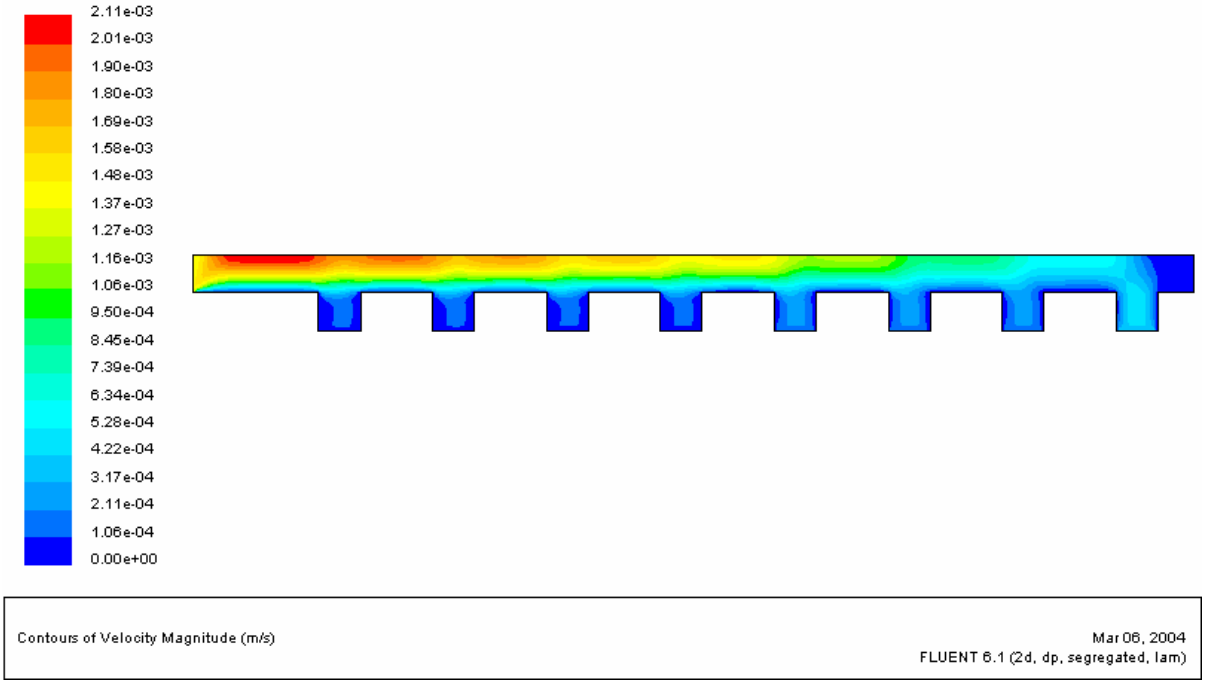

Figure 6.15 – FLUENT Trial FL–3a: Velocity Magnitudes (m/s)

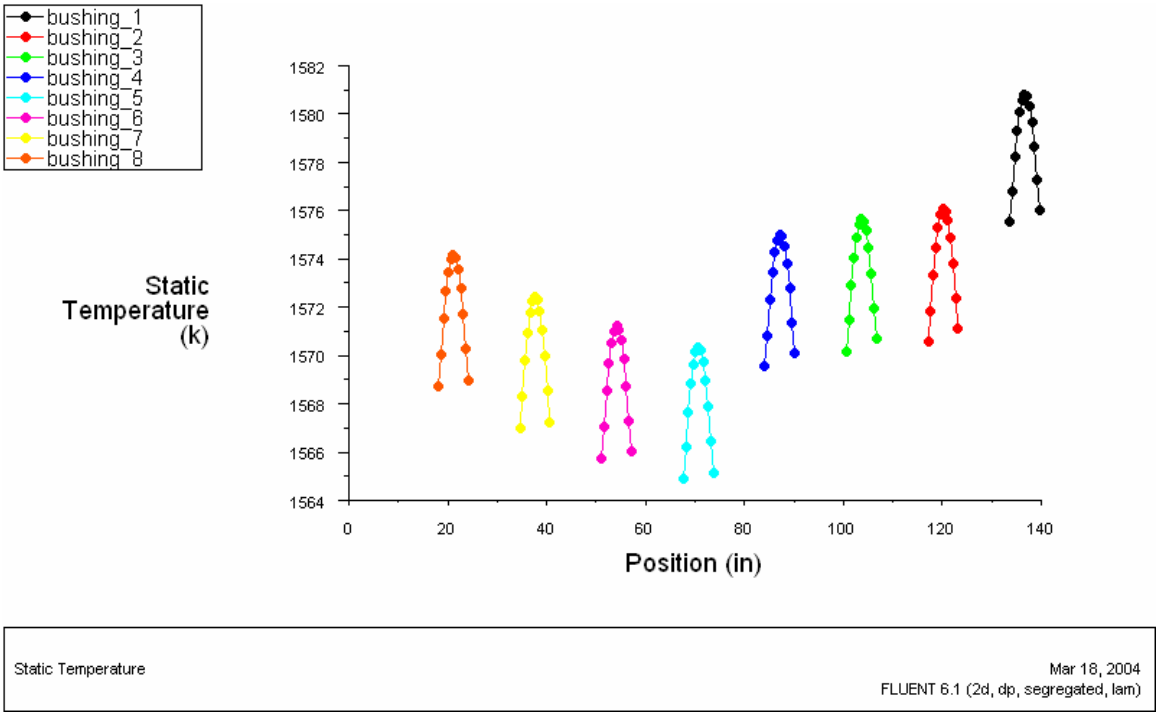

Figure 6.16 – FLUENT Trial FL–3a: Bushing Outlet Temperatures (°K)

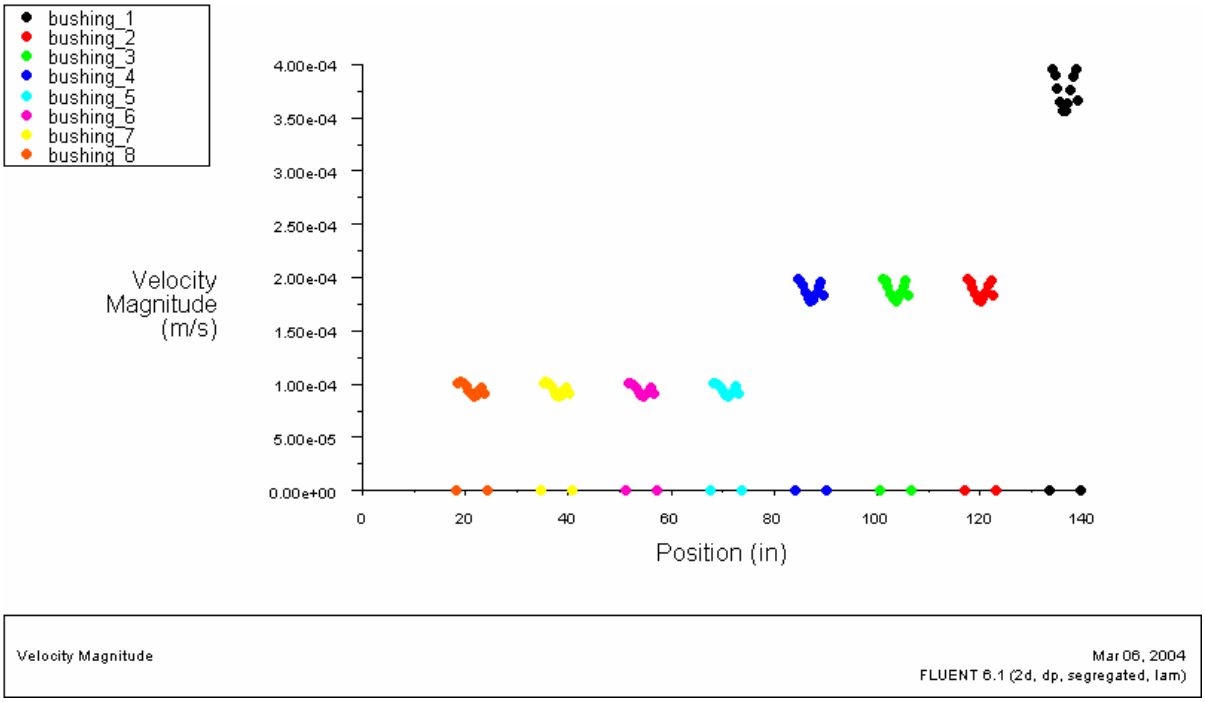

Figure 6.17 – FLUENT Trial FL–3a: Bushing Outlet Velocity Magnitudes (m/s)

Trial FL–4

Position	MFR (kg/s)
forehearth_inlet	0.5456
bushing_8	0.0000
bushing_7	-0.0682
bushing_6	-0.0682
bushing_5	-0.0682
bushing_4	-0.0682
bushing_3	-0.0682
bushing_2	-0.0682
bushing_1	-0.0682

ΔMFR =	0.0682

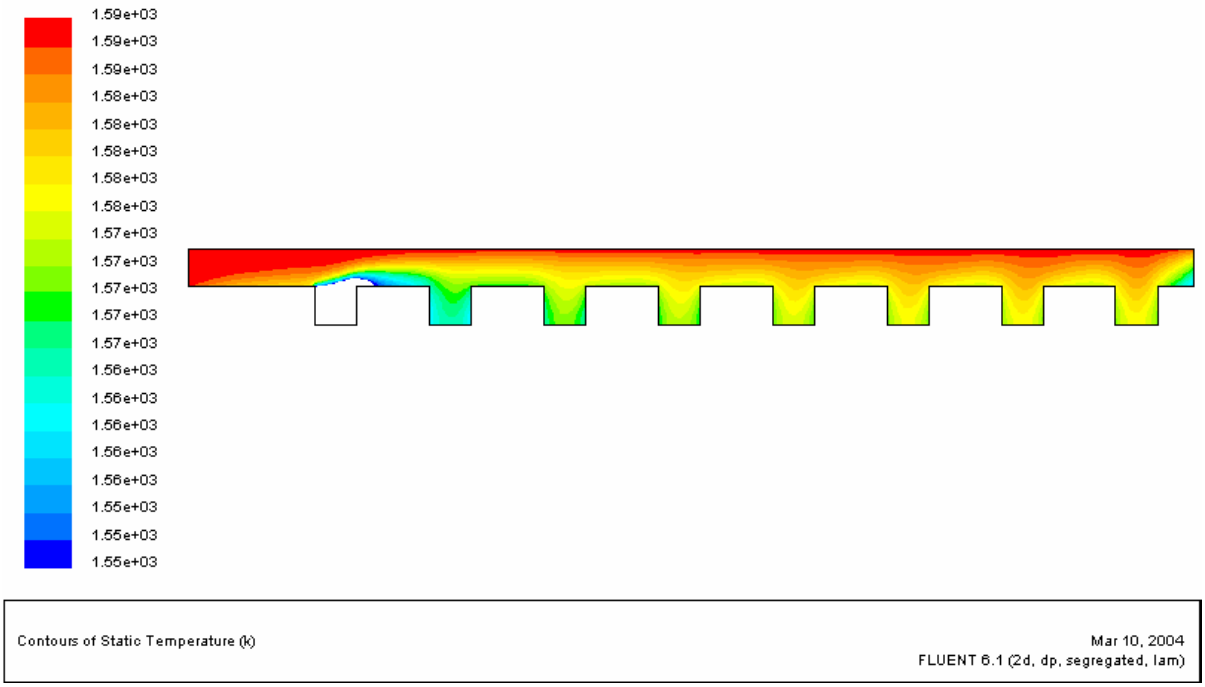

Figure 6.18 – FLUENT Trial FL–4: Temperature Contours of Molten Glass (°K)

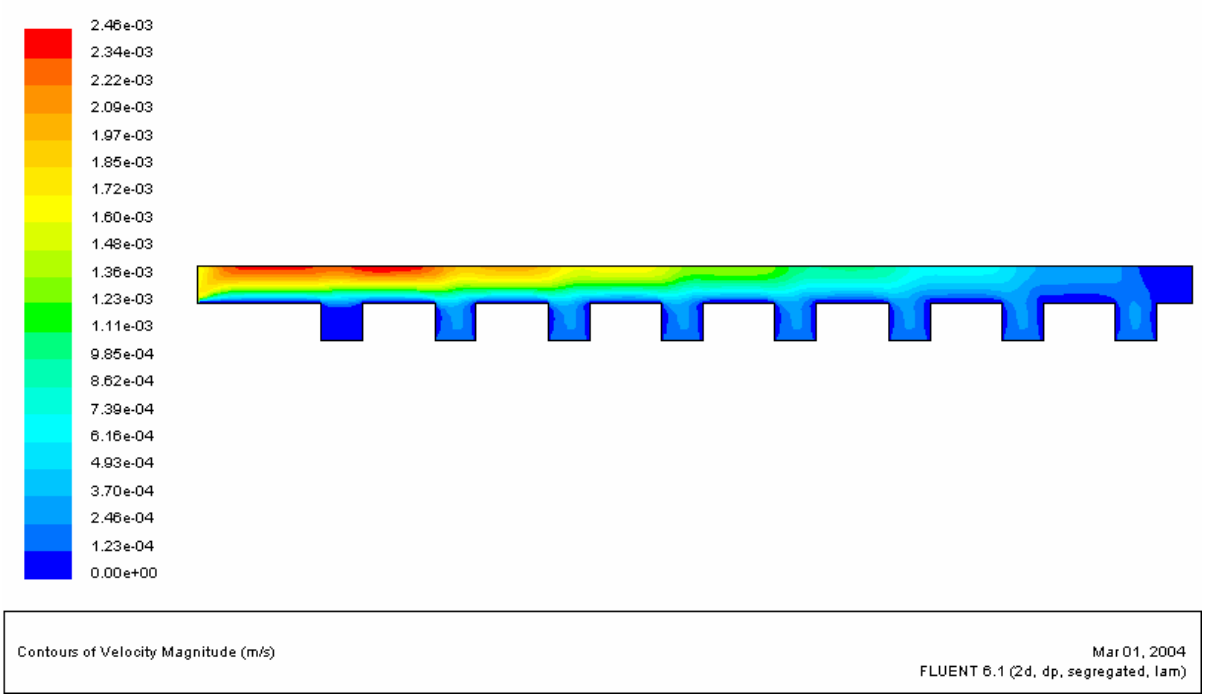

Figure 6.19 – FLUENT Trial FL–4: Velocity Magnitudes (m/s)

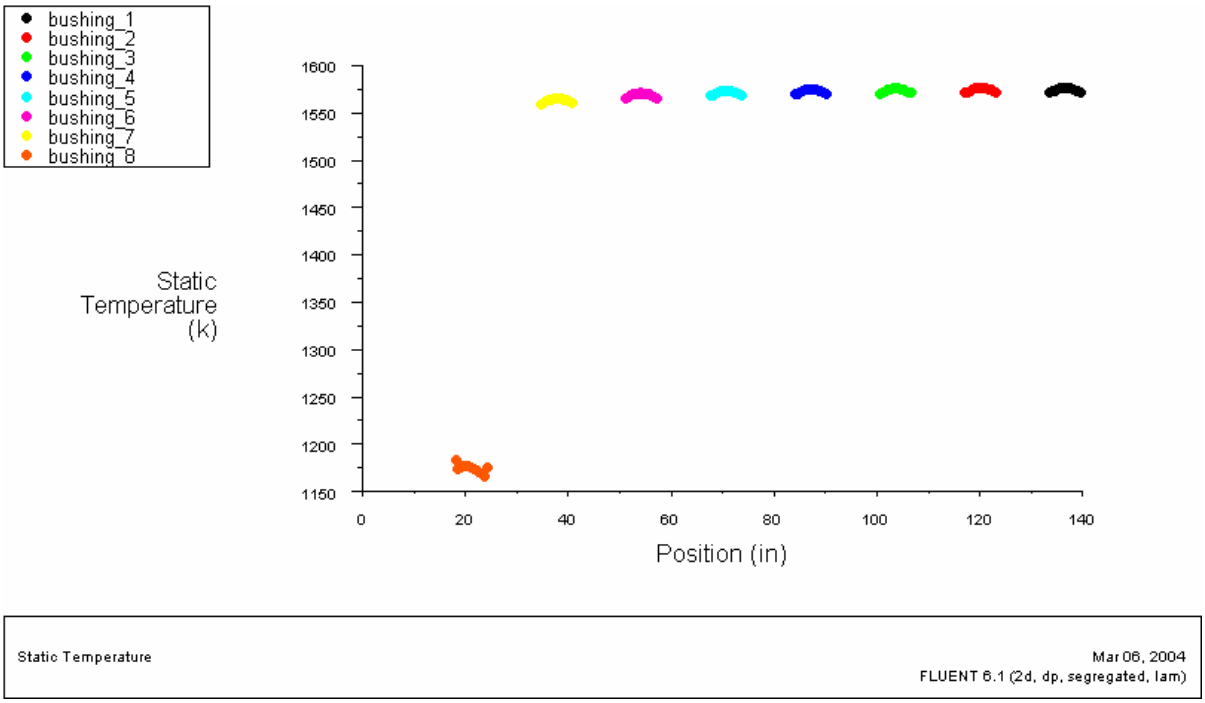

Figure 6.20 – FLUENT Trial FL–4: Bushing Outlet Temperatures 1 (°K)

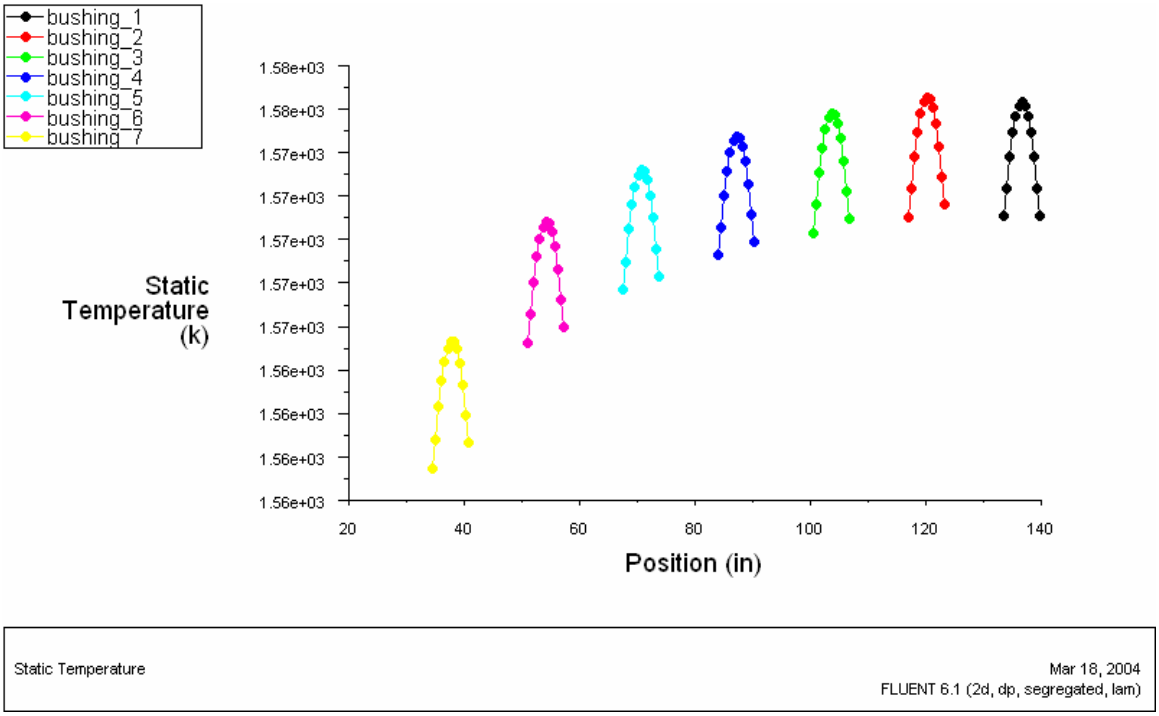

Figure 6.21 – FLUENT Trial FL–4: Bushing Outlet Temperatures 2 (°K)

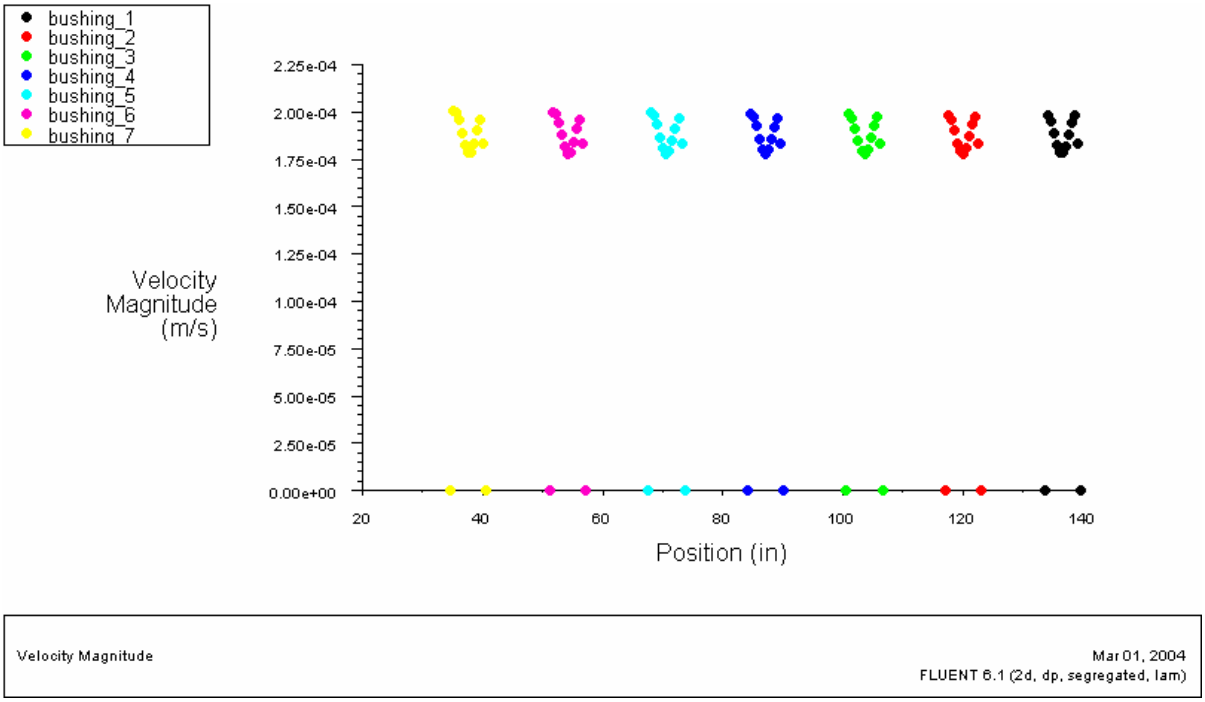

Figure 6.22 – FLUENT Trial FL–4: Bushing Outlet Velocity Magnitudes (m/s)

Trial FL–5

Position	MFR (kg/s)
forehearth_inlet	0.5456
bushing_8	-0.0682
bushing_7	-0.0682
bushing_6	-0.0682
bushing_5	0.0000
bushing_4	-0.0682
bushing_3	-0.0682
bushing_2	-0.0682
bushing_1	-0.0682

ΔMFR =	0.0682

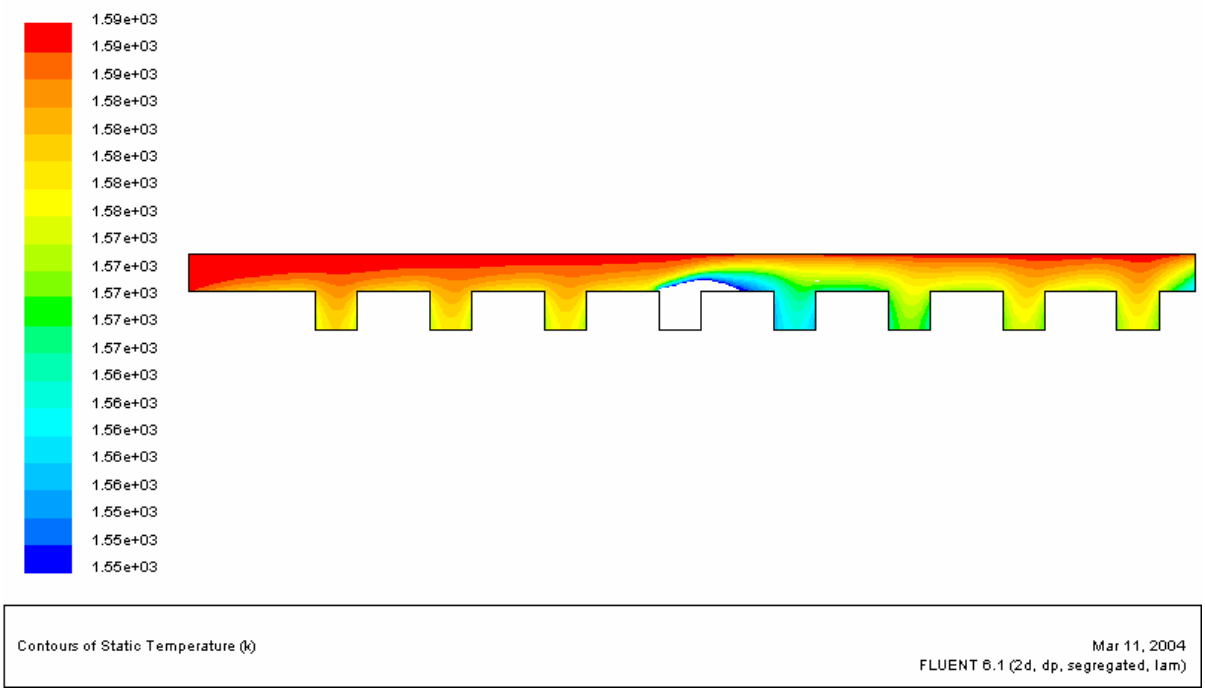

Figure 6.23 – FLUENT Trial FL–5: Temperature Contours of Molten Glass (°K)

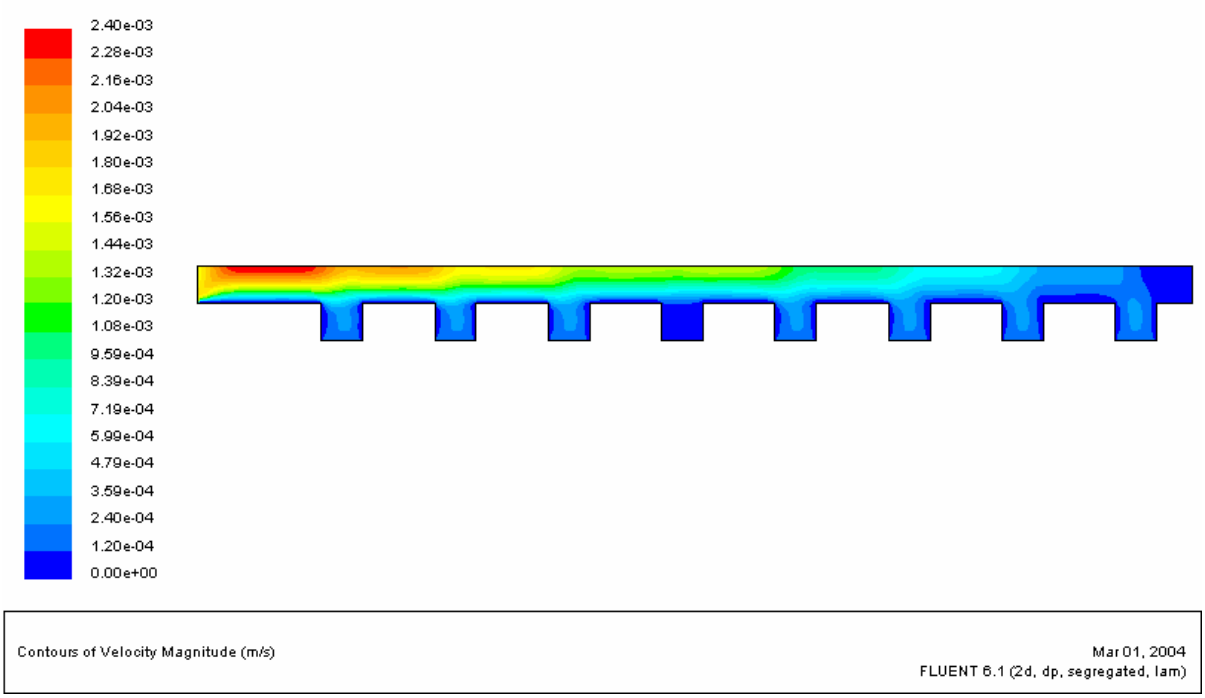

Figure 6.24 – FLUENT Trial FL–5: Velocity Magnitudes (m/s)

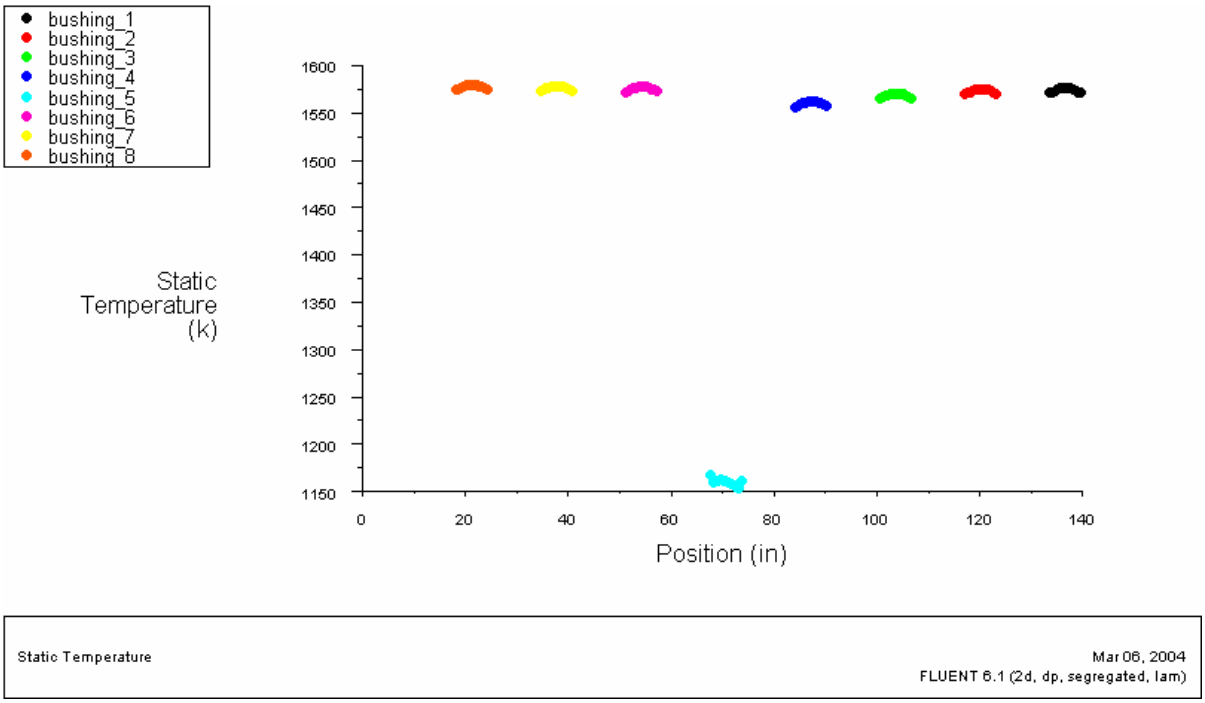

Figure 6.25 – FLUENT Trial FL–5: Bushing Outlet Temperatures 1 (°K)

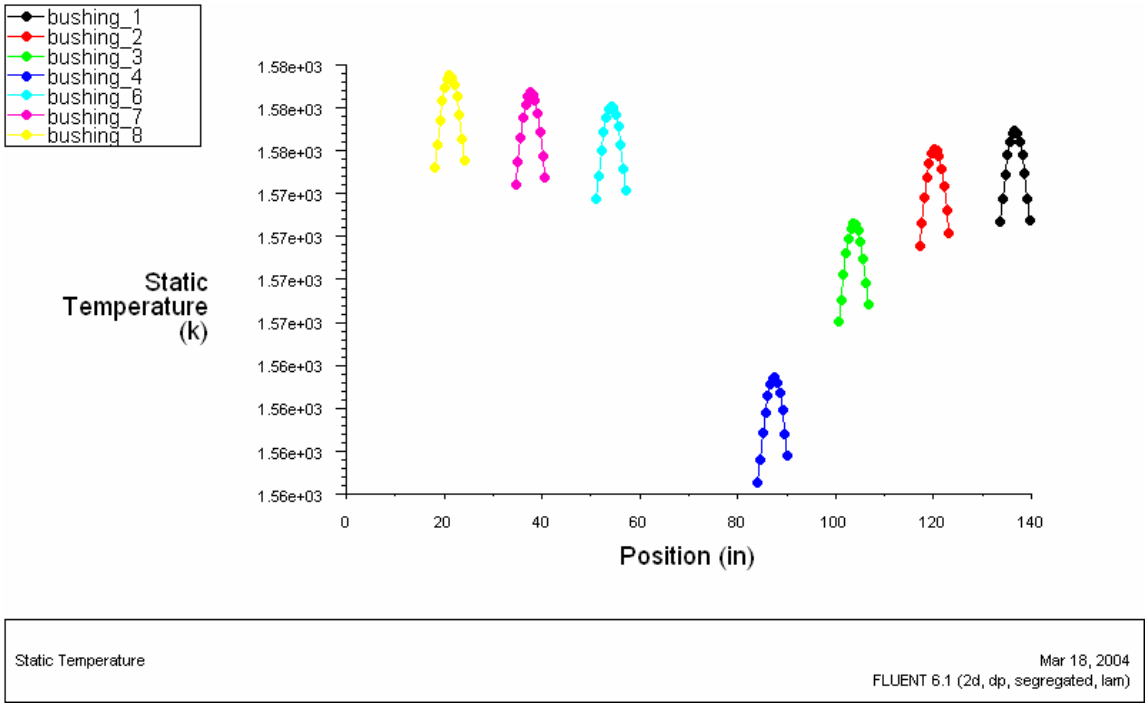

Figure 6.26 – FLUENT Trial FL–5: Bushing Outlet Temperatures 2 (°K)

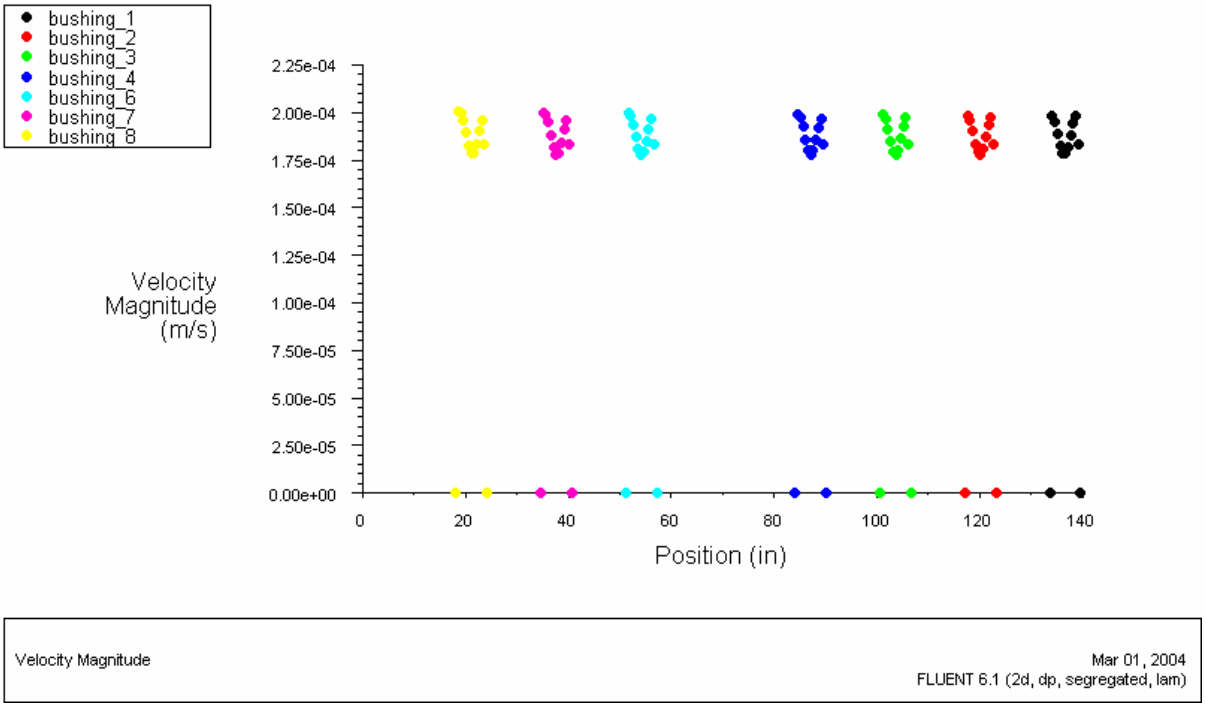

Figure 6.27 – FLUENT Trial FL–5: Bushing Outlet Velocity Magnitudes (m/s)

Trial FL–6

Position	MFR (kg/s)
forehearth_inlet	0.5456
bushing_8	-0.0682
bushing_7	-0.0682
bushing_6	-0.0682
bushing_5	-0.0682
bushing_4	-0.0682
bushing_3	-0.0682
bushing_2	0.0000
bushing_1	-0.0682

ΔMFR =	0.0682

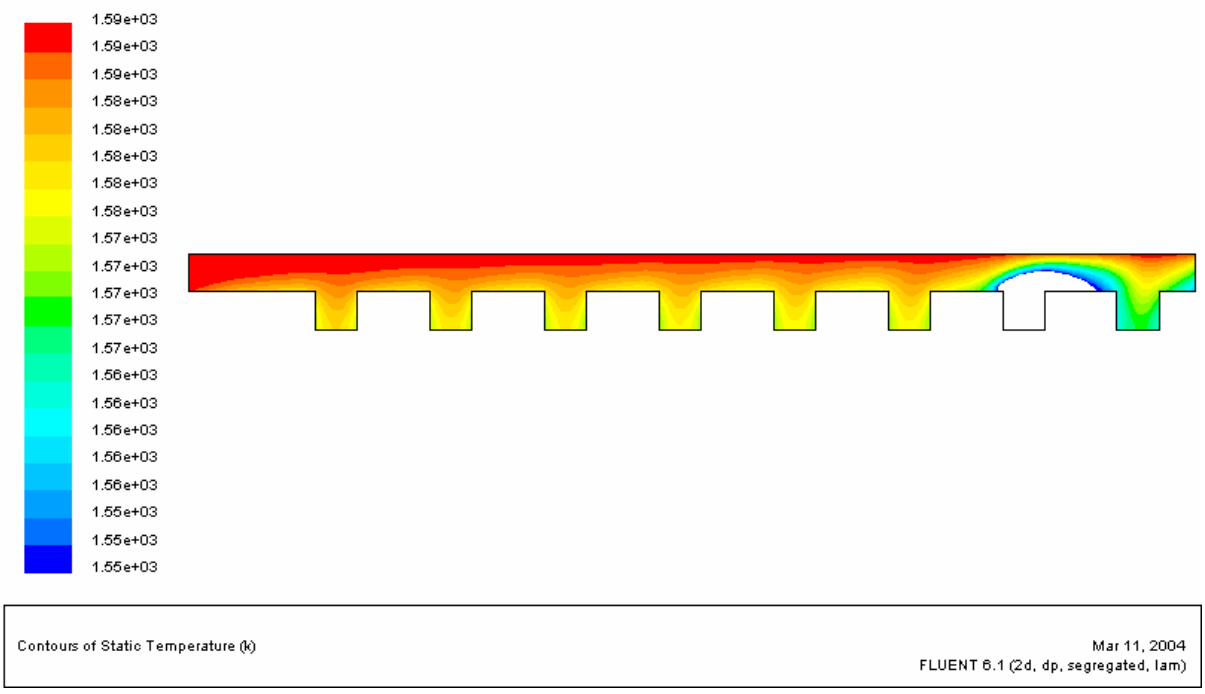

Figure 6.28 – FLUENT Trial FL–6: Temperature Contours of Molten Glass (°K)

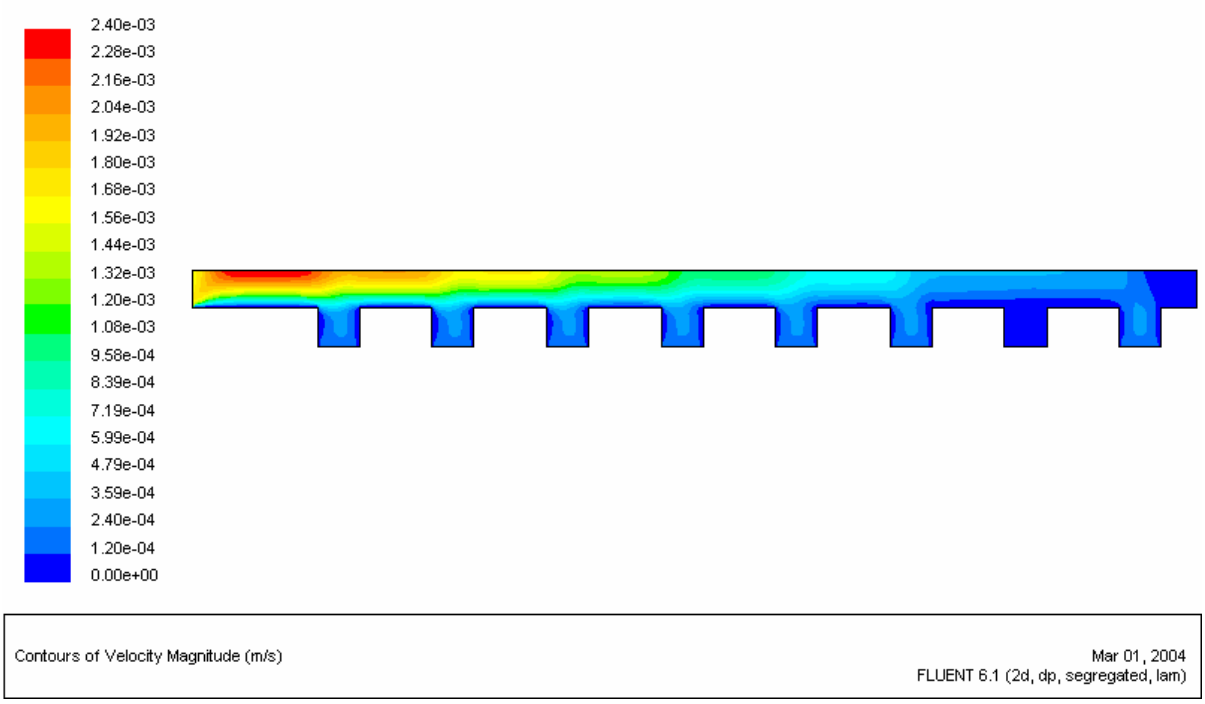

Figure 6.29 – FLUENT Trial FL–6: Velocity Magnitudes (m/s)

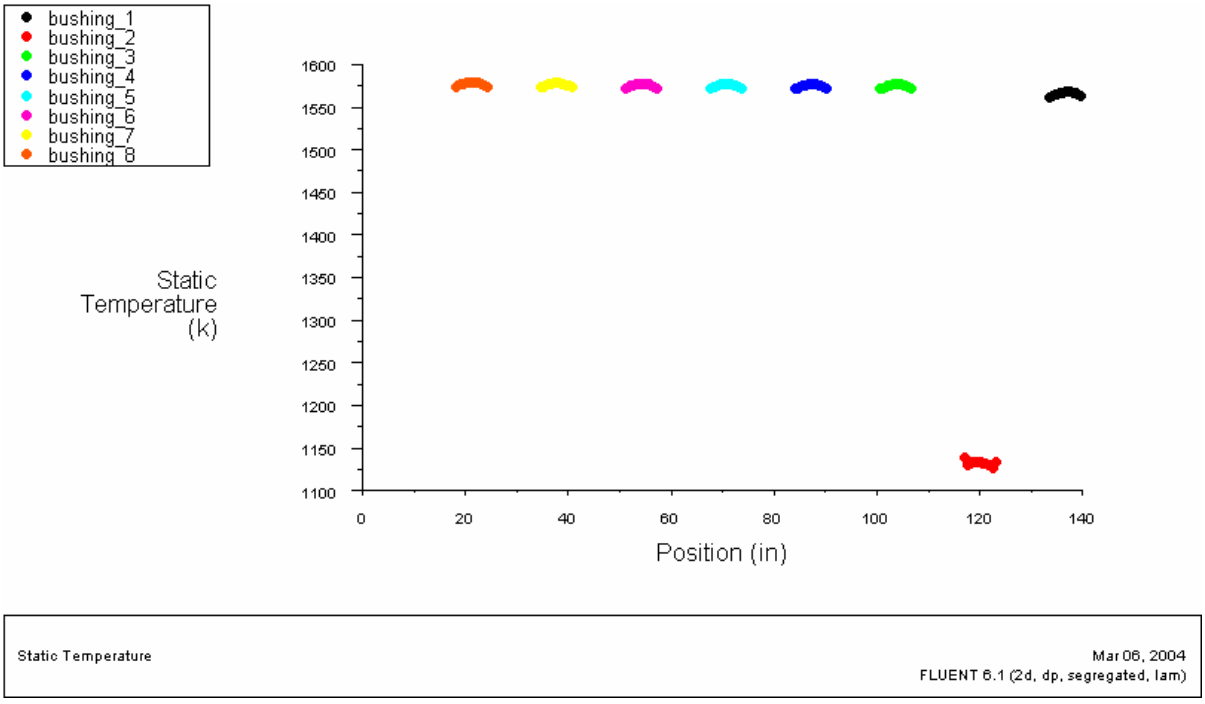

Figure 6.30 – FLUENT Trial FL–6: Bushing Outlet Temperatures 1 (°K)

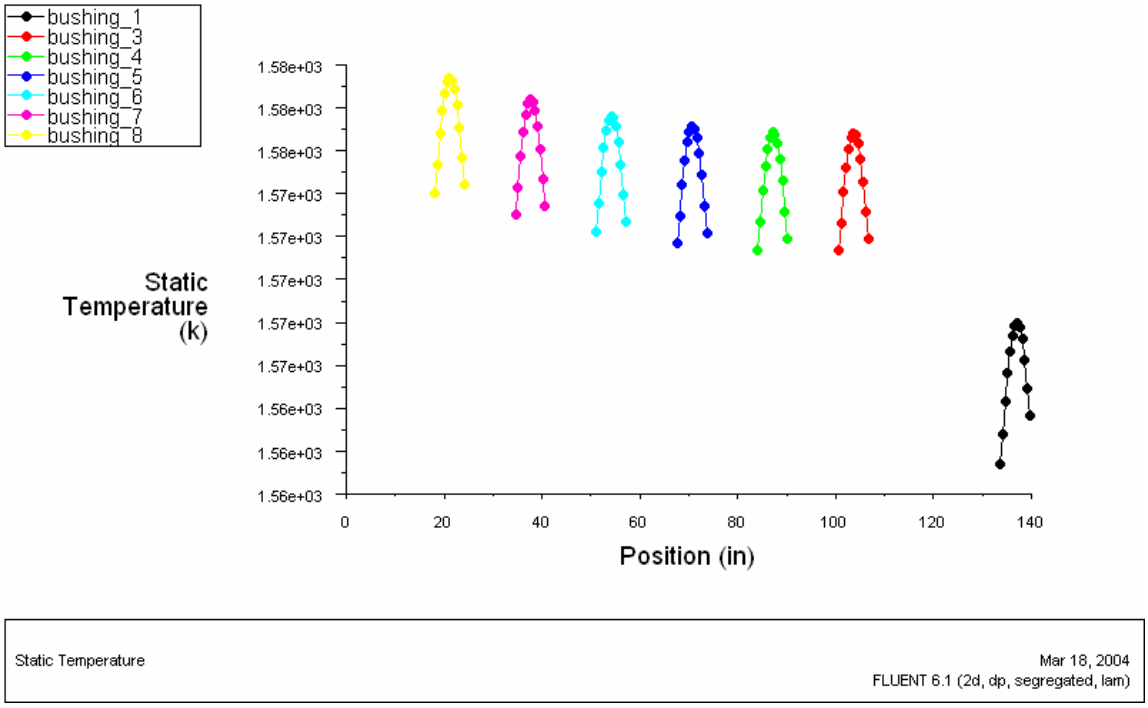

Figure 6.31 – FLUENT Trial FL–6: Bushing Outlet Temperatures 2 (°K)

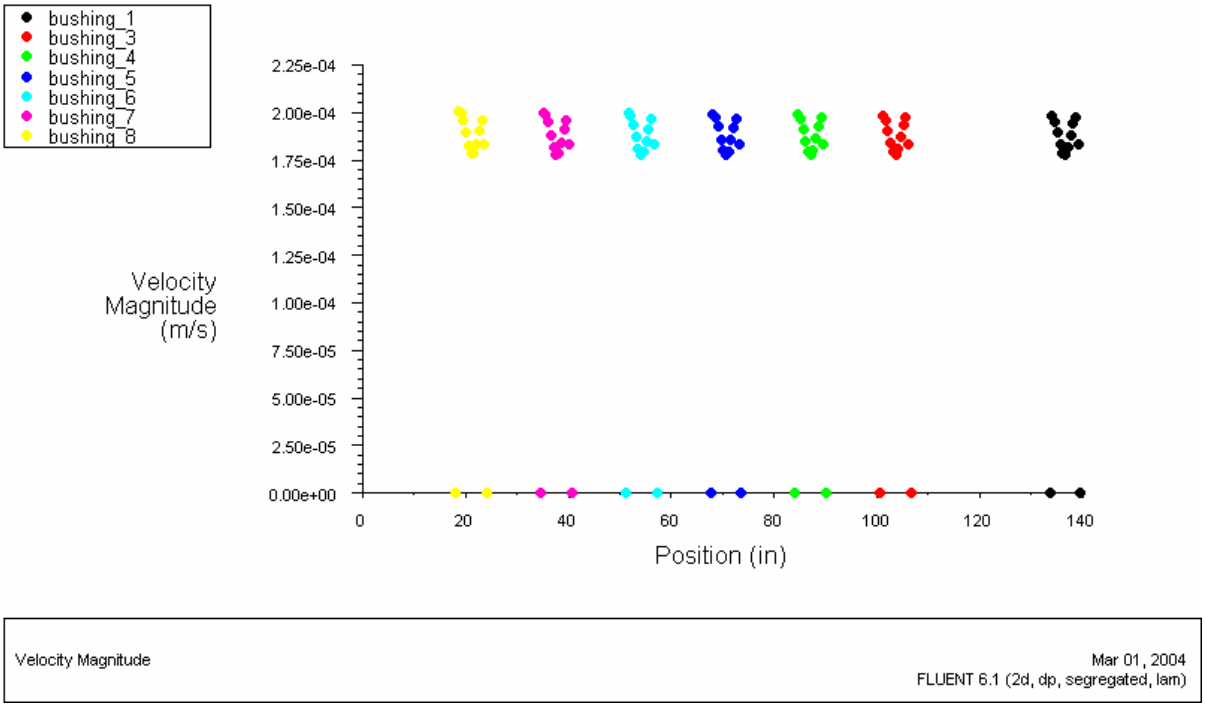

Figure 6.32 – FLUENT Trial FL–6: Bushing Outlet Velocity Magnitudes (m/s)

Trial FL–7

Position	MFR (kg/s)
forehearth_inlet	0.5456
bushing_8	-0.1364
bushing_7	-0.1364
bushing_6	-0.1364
bushing_5	0.0000
bushing_4	-0.0682
bushing_3	-0.0682
bushing_2	-0.0682
bushing_1	-0.0341

ΔMFR =	-0.1023

Figure 6.33 – FLUENT Trial FL–7: Temperature Contours of Molten Glass (°K)

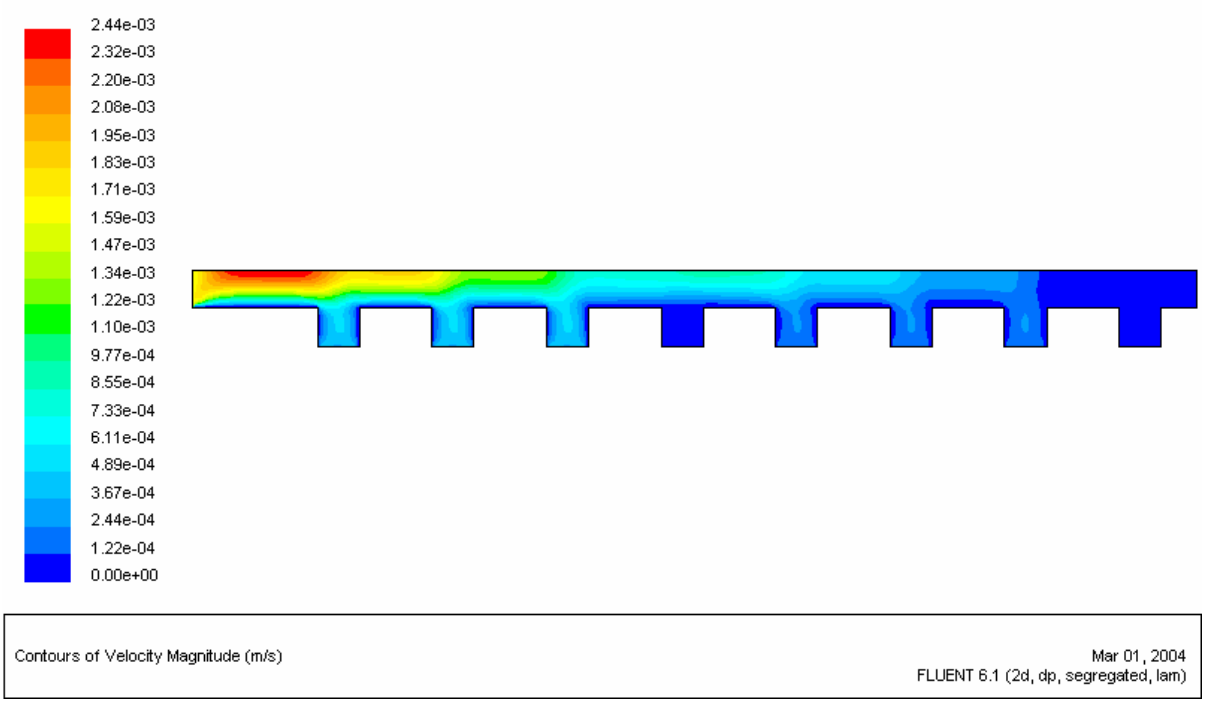

Figure 6.34 – FLUENT Trial FL–7: Velocity Magnitudes (m/s)

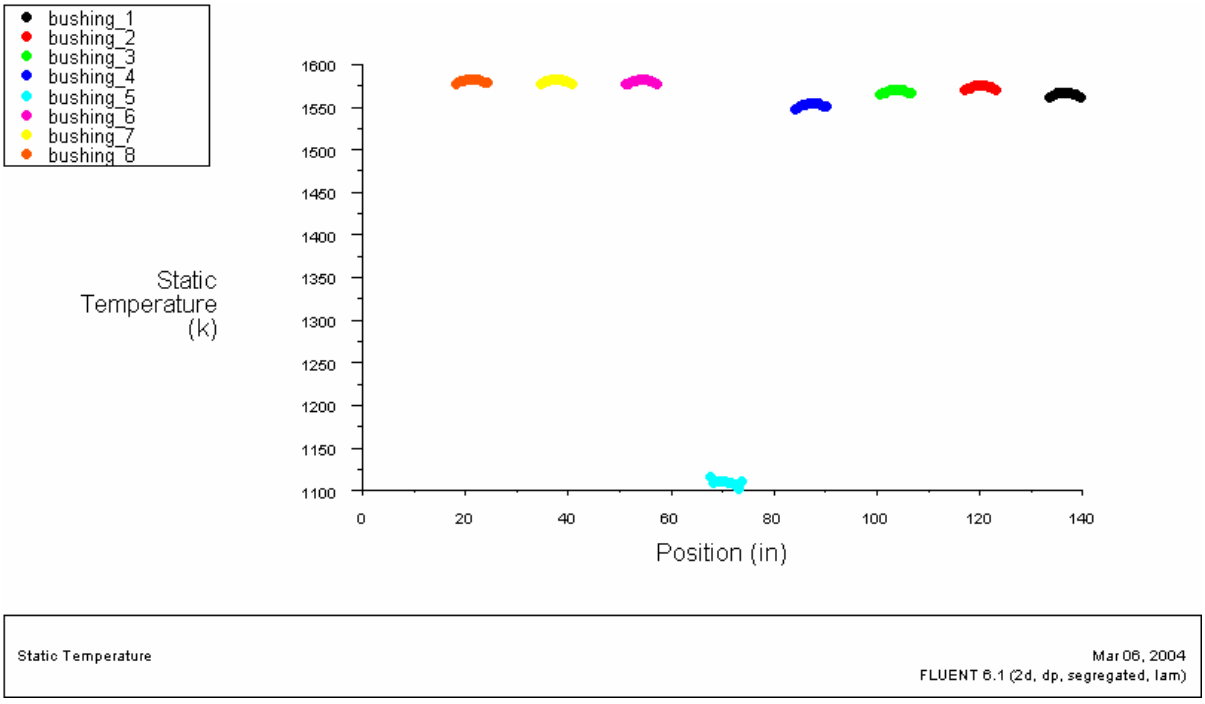

Figure 6.35 – FLUENT Trial FL–7: Bushing Outlet Temperatures 1 (°K)

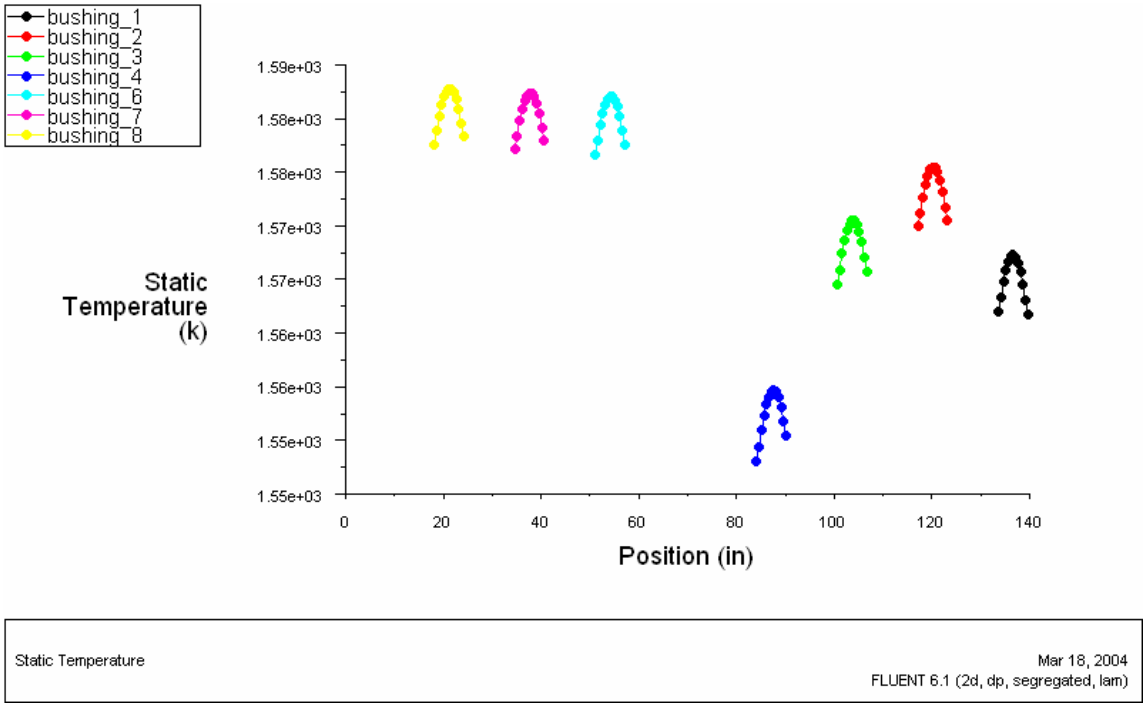

Figure 6.36 – FLUENT Trial FL–7: Bushing Outlet Temperatures 2 (°K)

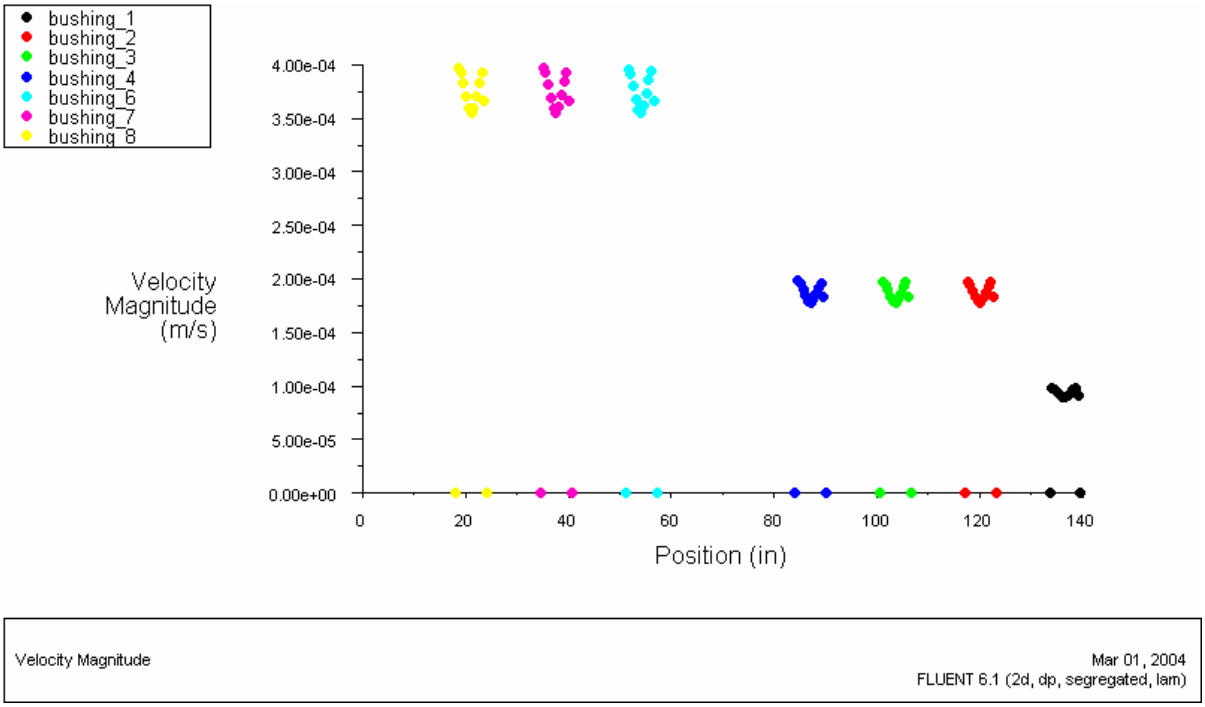

Figure 6.37 – FLUENT Trial FL–7: Bushing Outlet Velocity Magnitudes (°K)

Trial FL–7a

Position	MFR (kg/s)
forehearth_inlet	0.6479
bushing_8	-0.1364
bushing_7	-0.1364
bushing_6	-0.1364
bushing_5	0.0000
bushing_4	-0.0682
bushing_3	-0.0682
bushing_2	-0.0682
bushing_1	-0.0341

ΔMFR =	0.0000

Figure 6.38 – FLUENT Trial FL–7a: Temperature Contours of Molten Glass (°K)

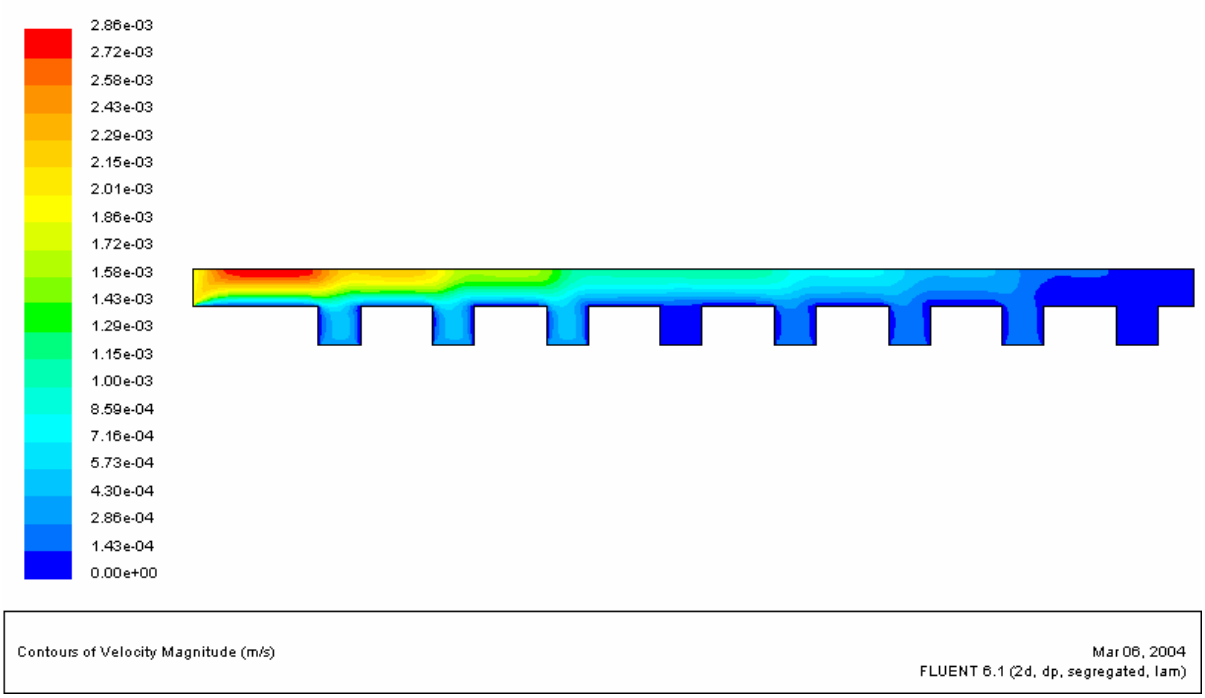

Figure 6.39 – FLUENT Trial FL–7a: Velocity Magnitudes (m/s)

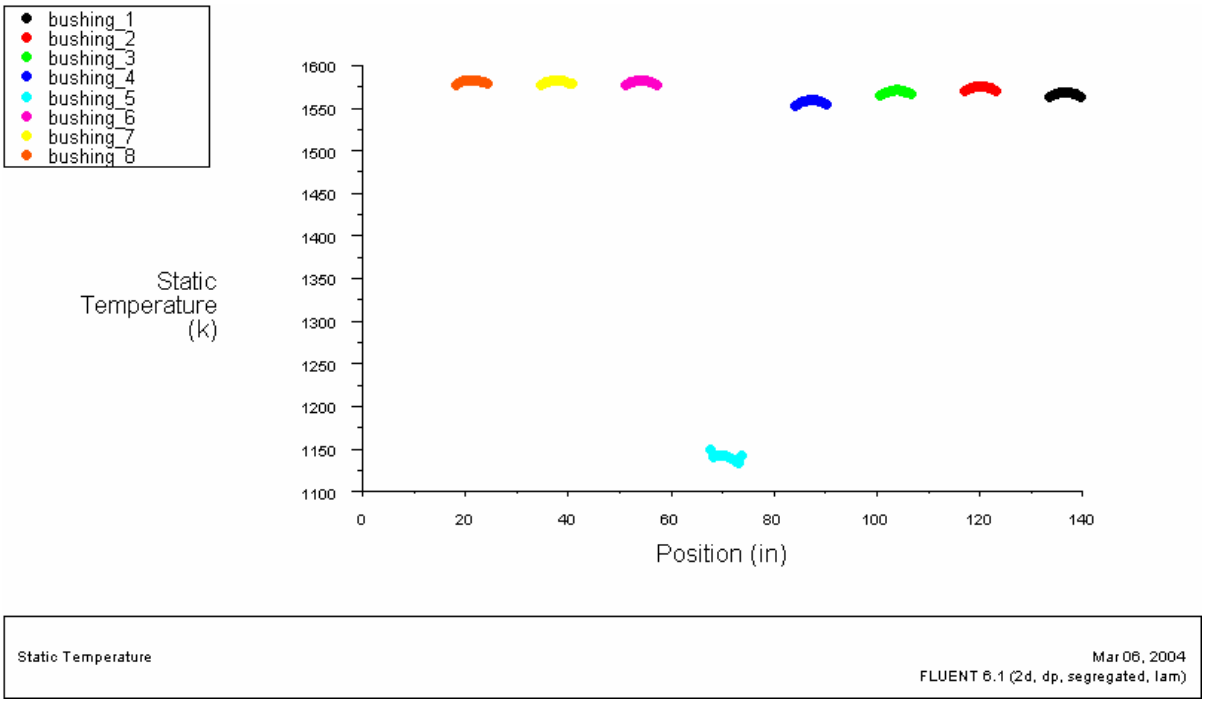

Figure 6.40 – FLUENT Trial FL–7a: Bushing Outlet Temperatures 1 (°K)

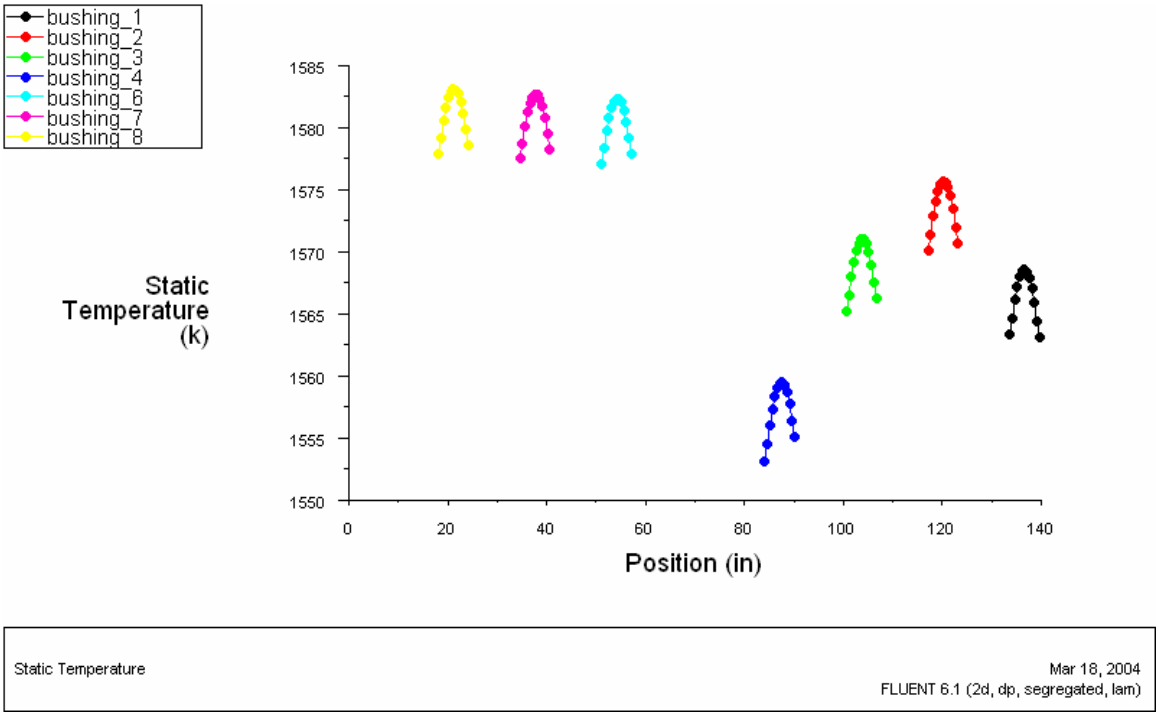

Figure 6.41 – FLUENT Trial FL–7a: Bushing Outlet Temperatures 2 (°K)

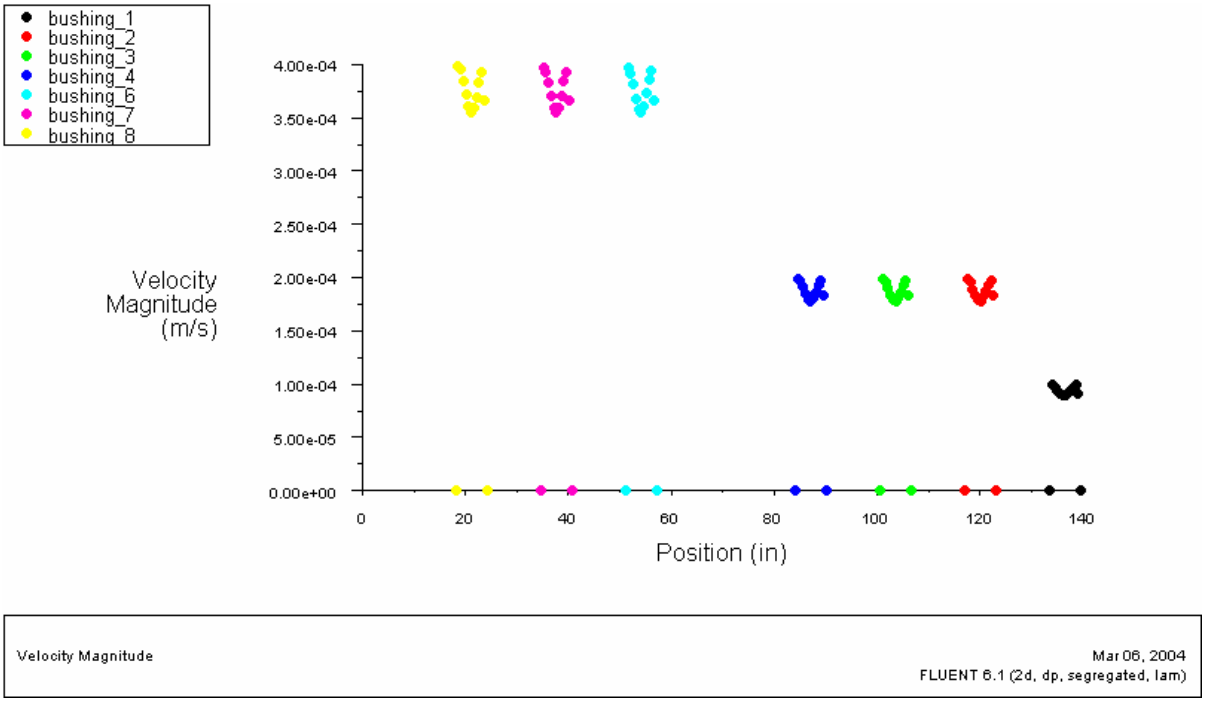

Figure 6.42 – FLUENT Trial FL–7a: Bushing Outlet Velocity Magnitudes (m/s)

Trial FL–8

Position	MFR (kg/s)
forehearth_inlet	0.5456
bushing_8	-0.0341
bushing_7	0.0000
bushing_6	-0.0341
bushing_5	-0.0341
bushing_4	-0.1364
bushing_3	-0.1364
bushing_2	-0.1364
bushing_1	-0.1364

ΔMFR =	0.0682

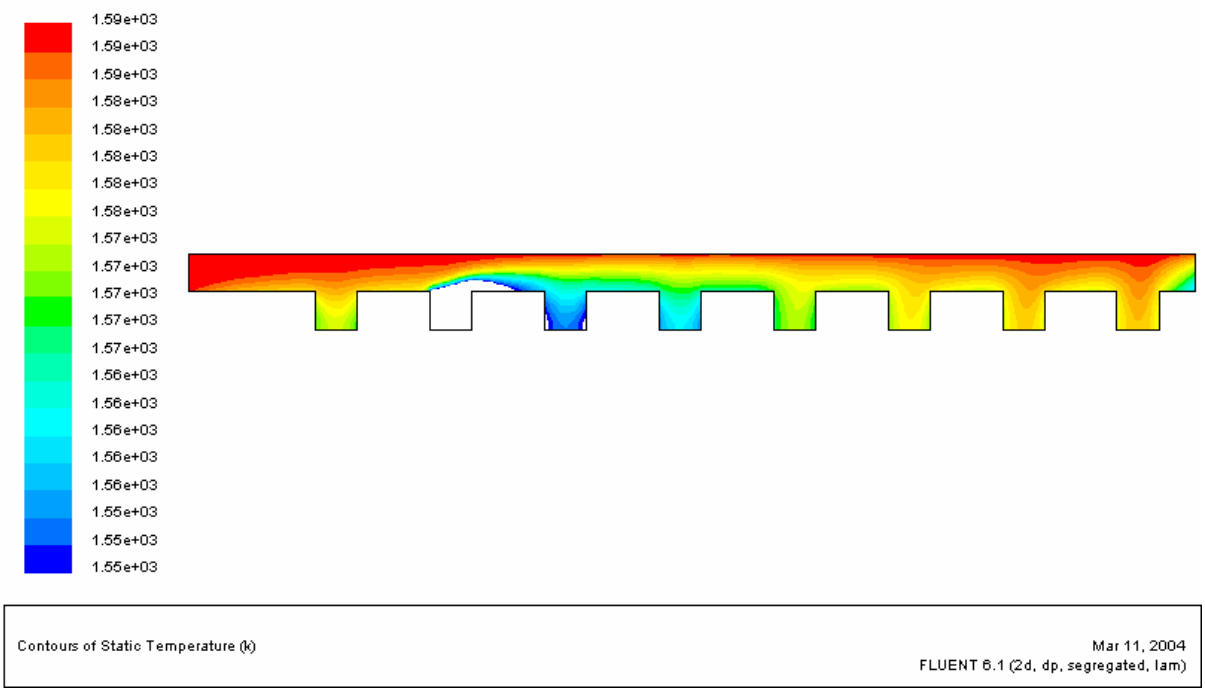

Figure 6.43 – FLUENT Trial FL–8: Temperature Contours of Molten Glass (°K)

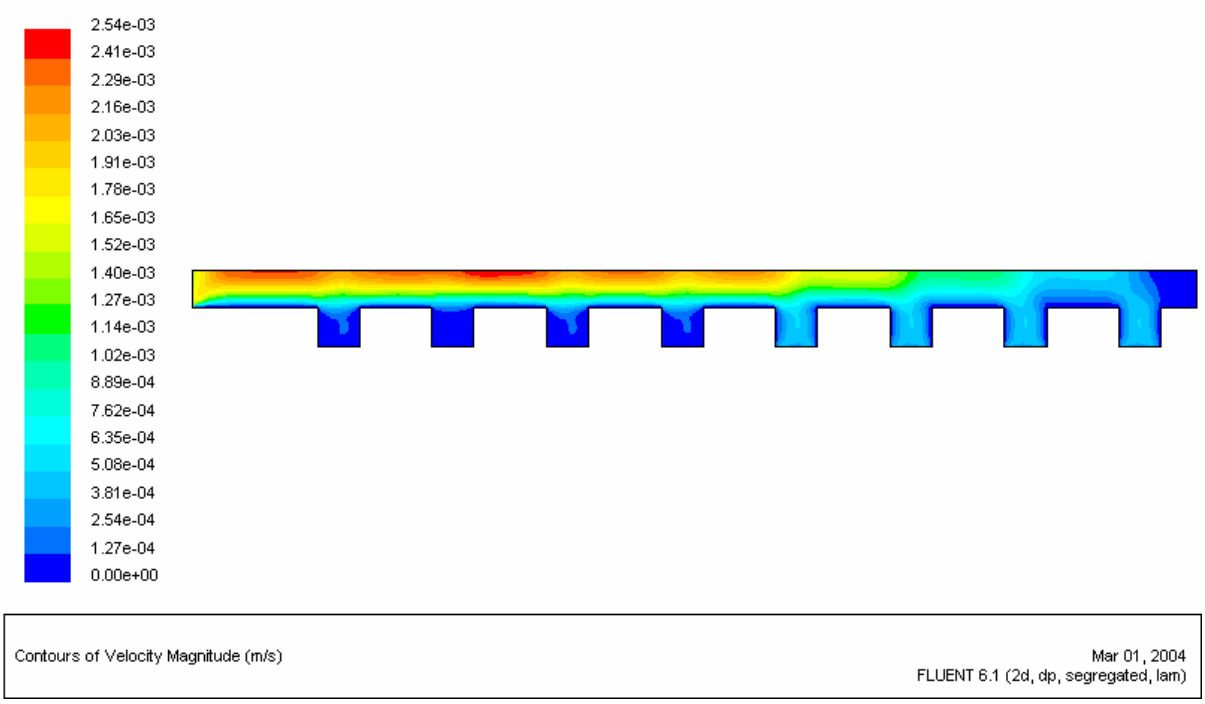

Figure 6.44 – FLUENT Trial FL–8: Velocity Magnitudes (m/s)

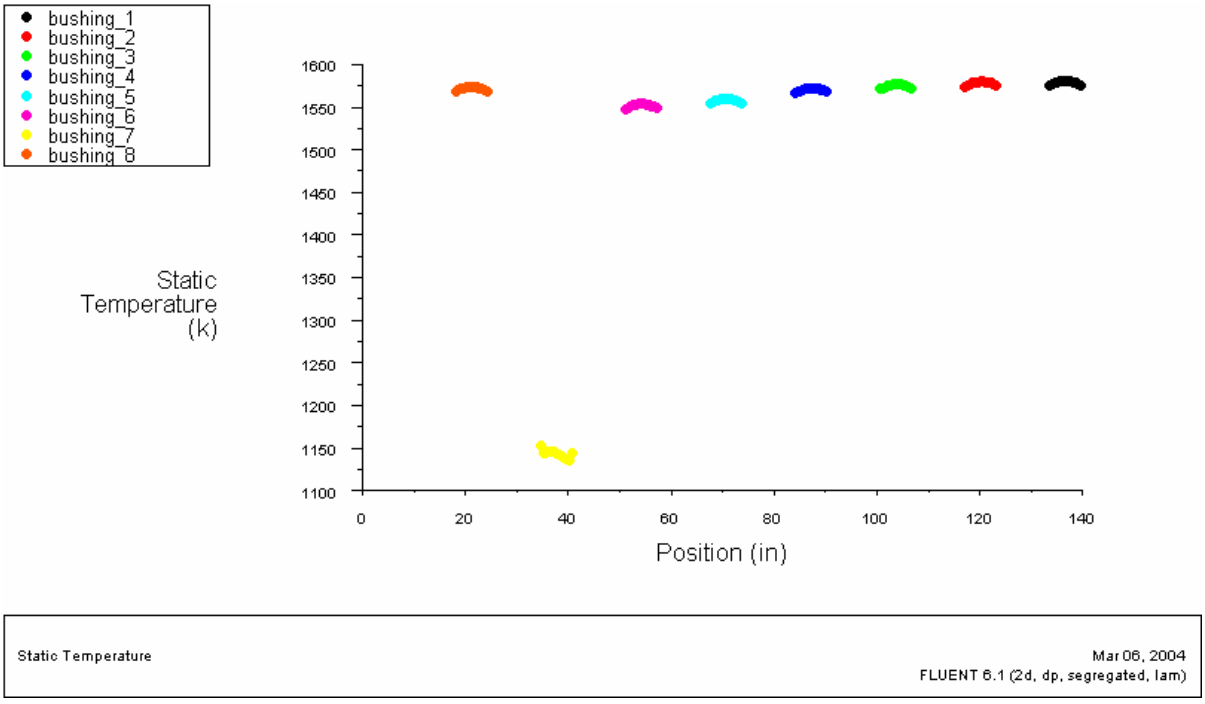

Figure 6.45 – FLUENT Trial FL–8: Bushing Outlet Temperatures 1 (°K)

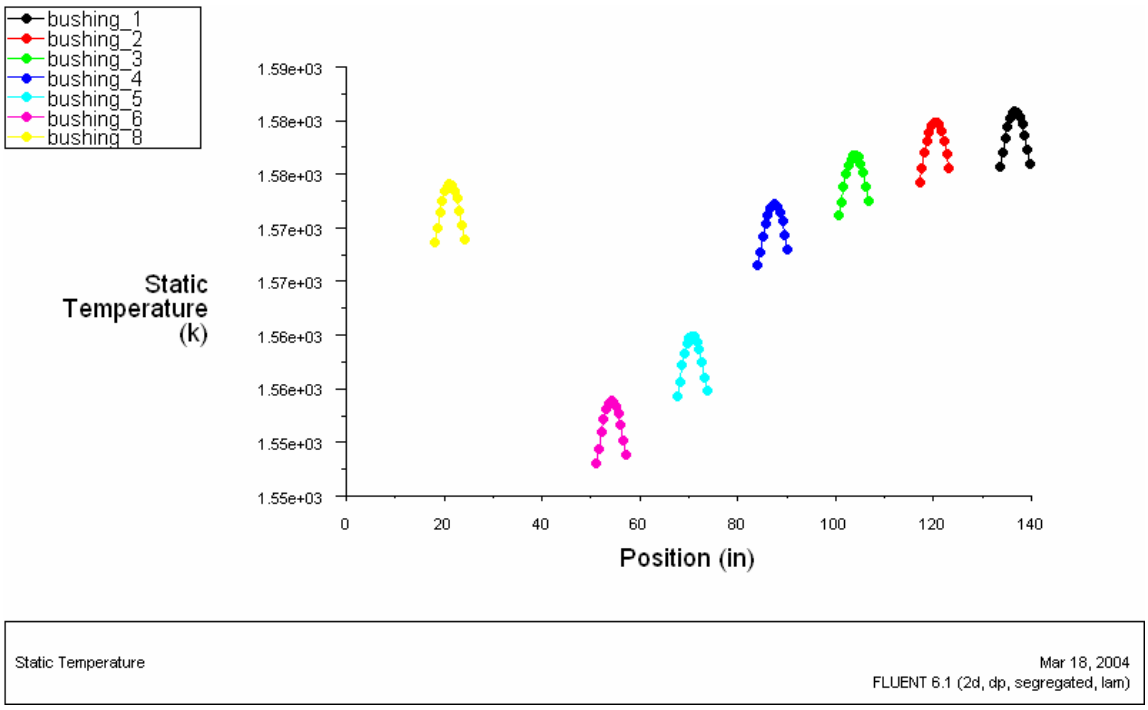

Figure 6.46 – FLUENT Trial FL–8: Bushing Outlet Temperatures 2 (°K)

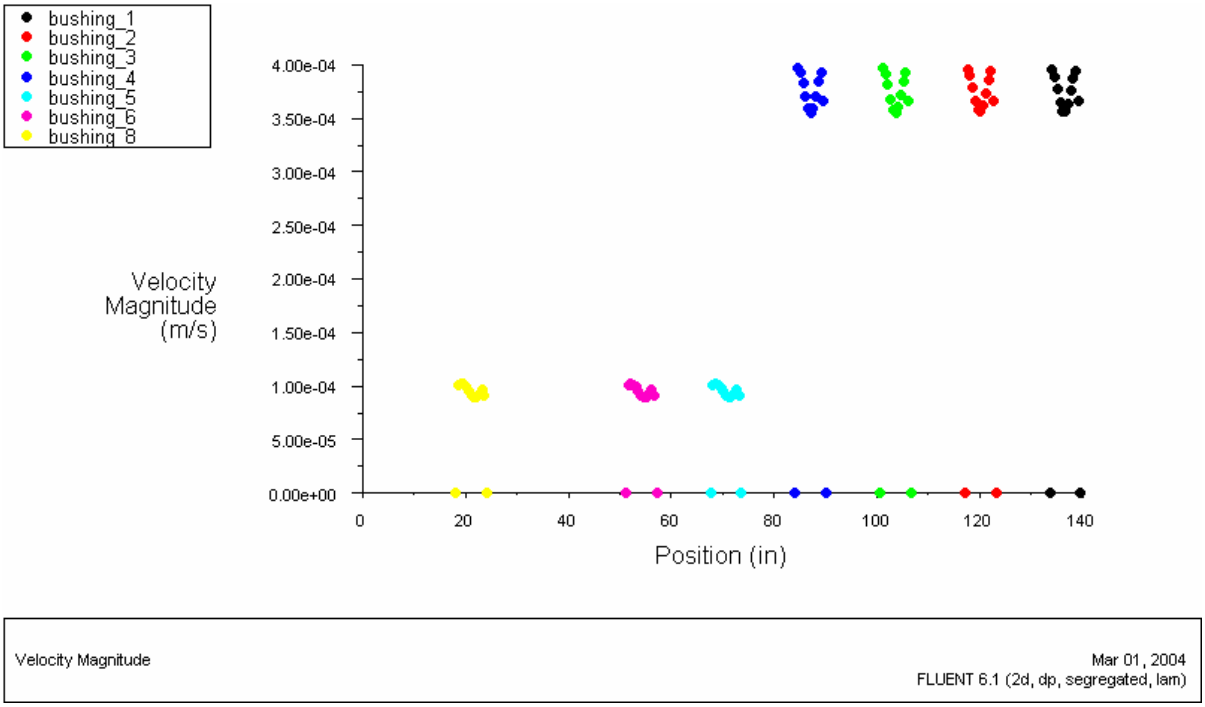

Figure 6.47 – FLUENT Trial FL–8: Bushing Outlet Velocity Magnitudes (m/s)

Trial FL–8a

Position	MFR (kg/s)
forehearth_inlet	0.6479
bushing_8	-0.0341
bushing_7	0.0000
bushing_6	-0.0341
bushing_5	-0.0341
bushing_4	-0.1364
bushing_3	-0.1364
bushing_2	-0.1364
bushing_1	-0.1364

ΔMFR =	0.0000

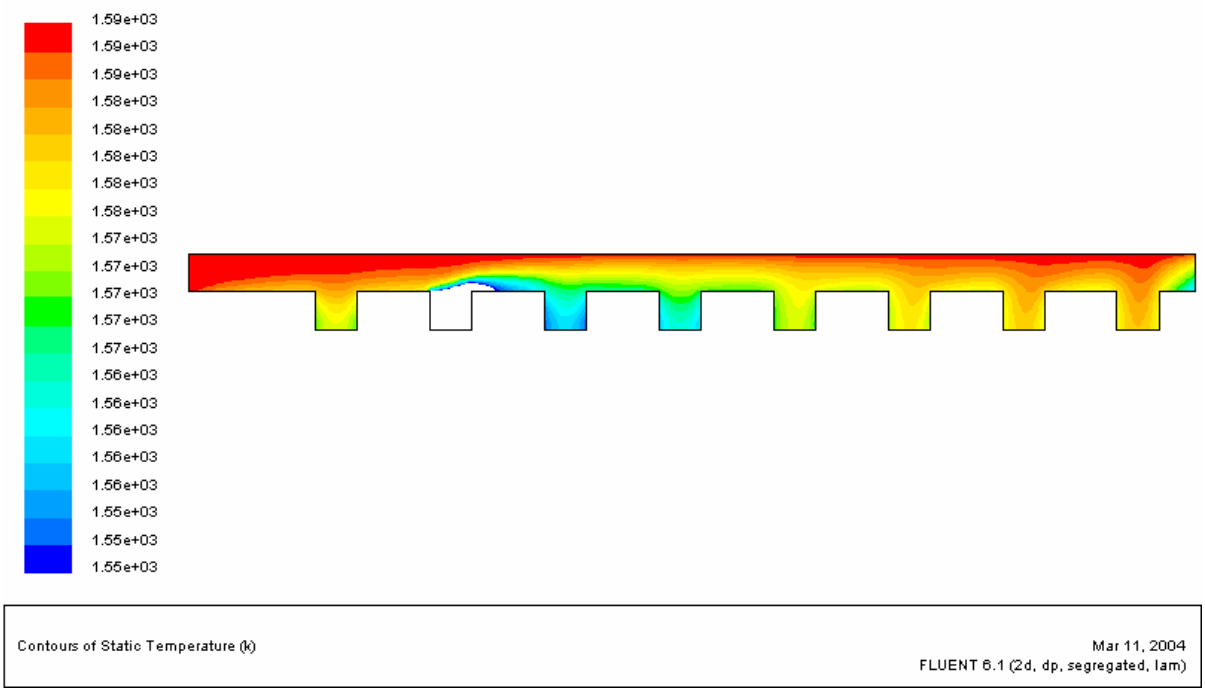

Figure 6.48 – FLUENT Trial FL–8a: Temperature Contours of Molten Glass (°K)

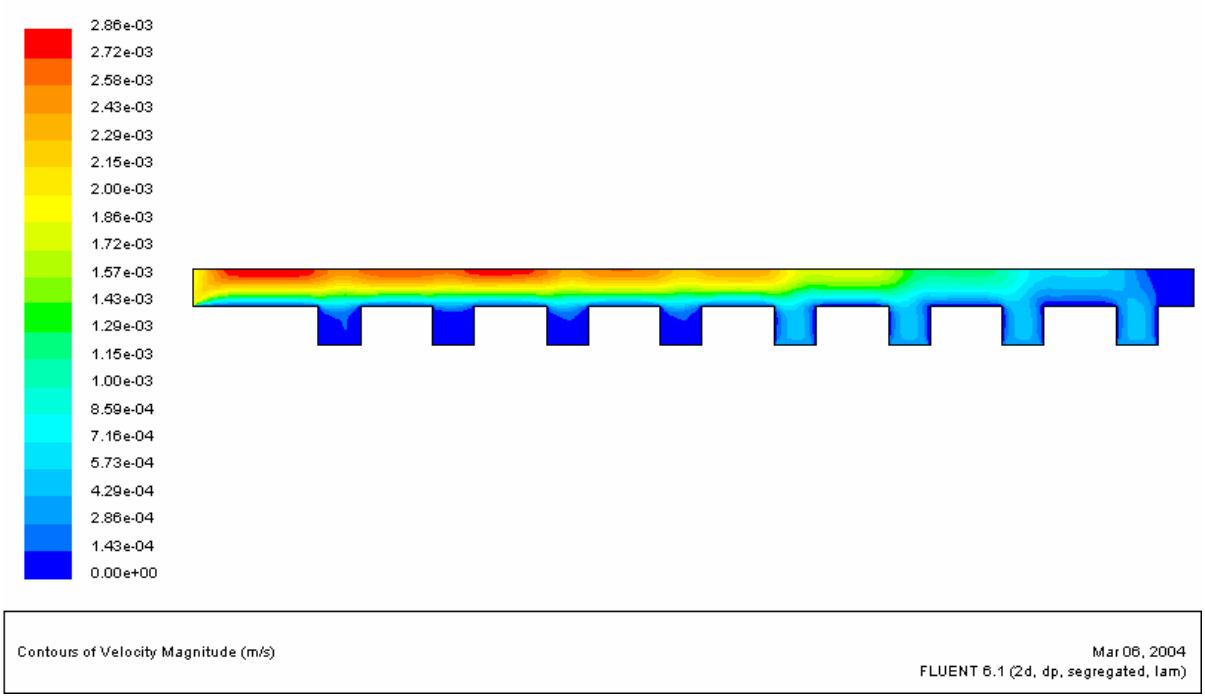

Figure 6.49 – FLUENT Trial FL–8a: Velocity Magnitudes (m/s)

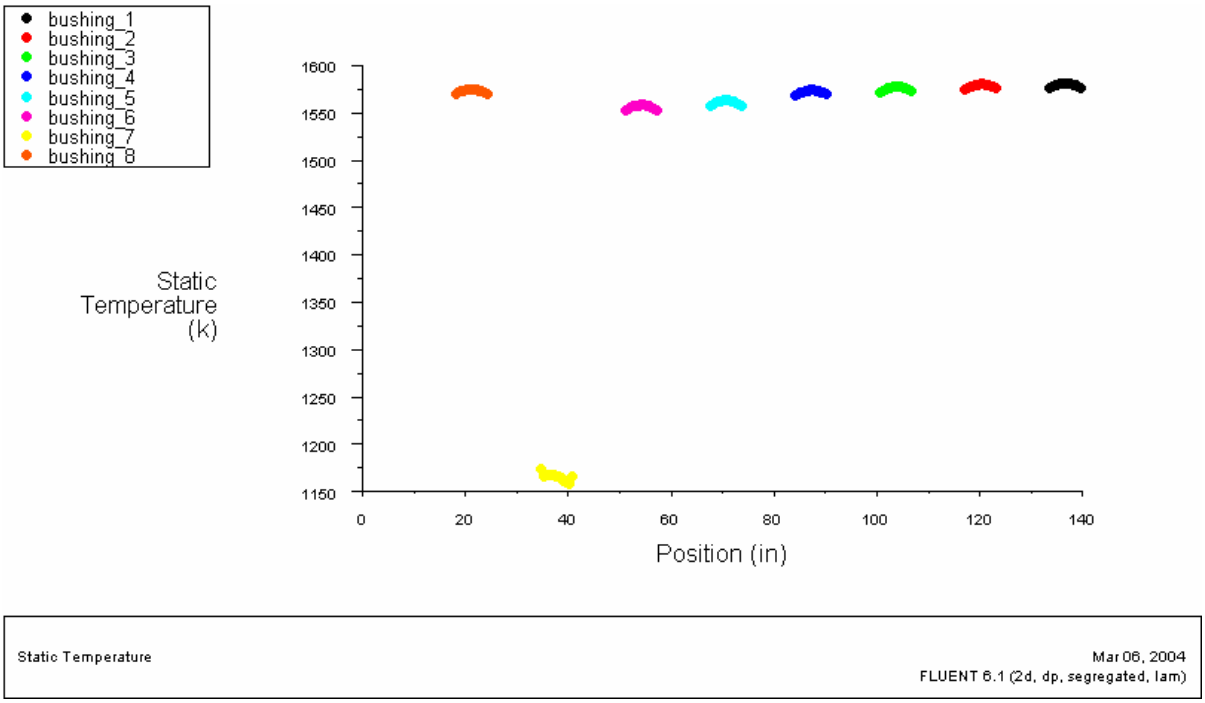

Figure 6.50 – FLUENT Trial FL–8a: Bushing Outlet Temperatures 1 (°K)

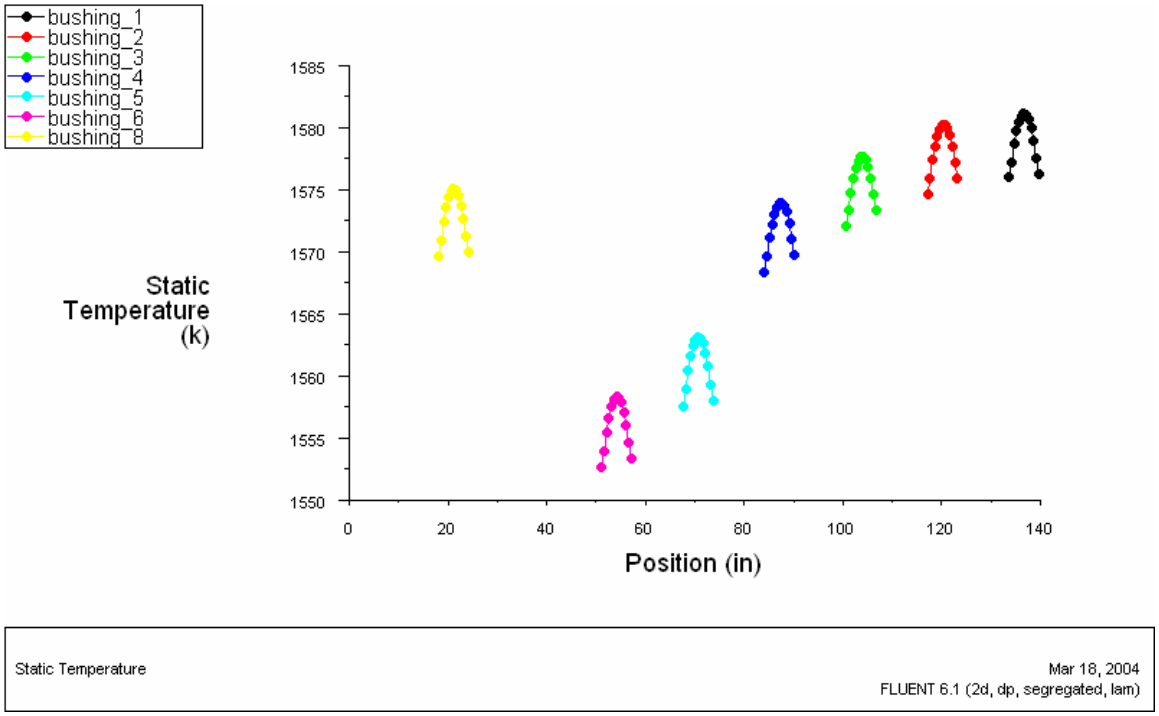

Figure 6.51 – FLUENT Trial FL– 8a: Bushing Outlet Temperatures 2 (°K)

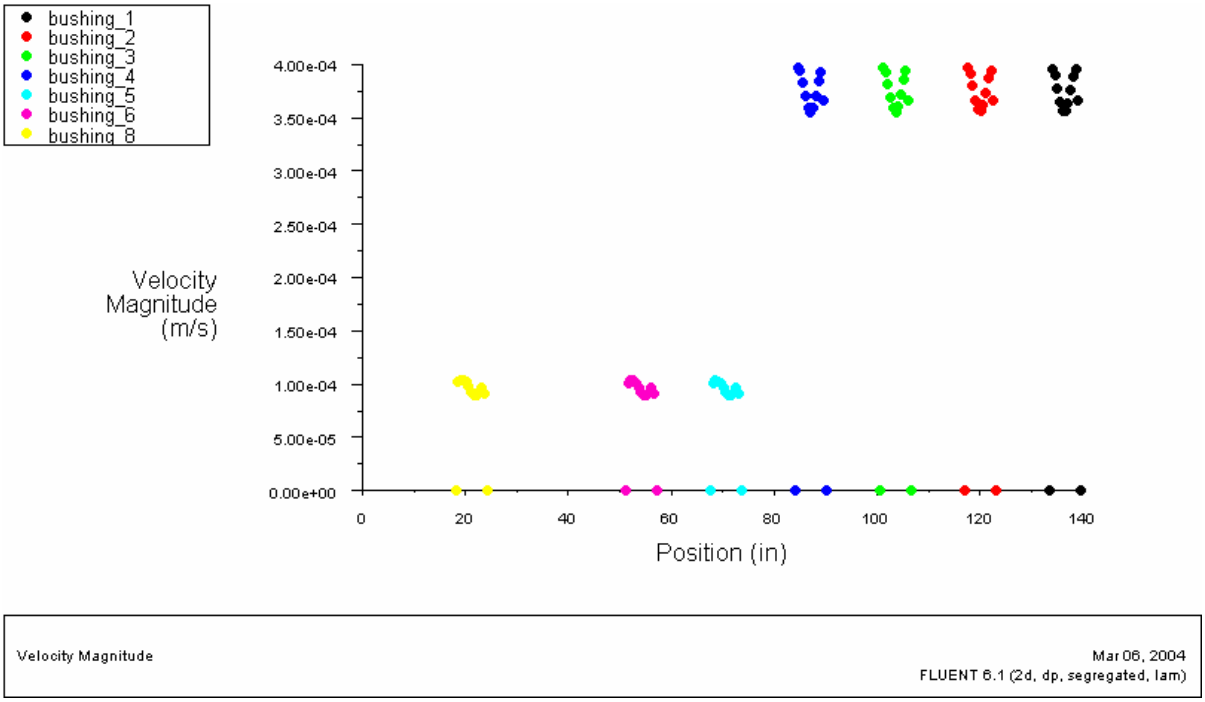

Figure 6.52 – FLUENT Trial FL–8a: Bushing Outlet Velocity Magnitudes (m/s)

Trial FL–9

Position	MFR (kg/s)
forehearth_inlet	0.5456
bushing_8	-0.0341
bushing_7	0.0000
bushing_6	-0.0341
bushing_5	-0.0682
bushing_4	-0.0682
bushing_3	-0.0682
bushing_2	-0.0682
bushing_1	-0.1364

ΔMFR =	0.0682

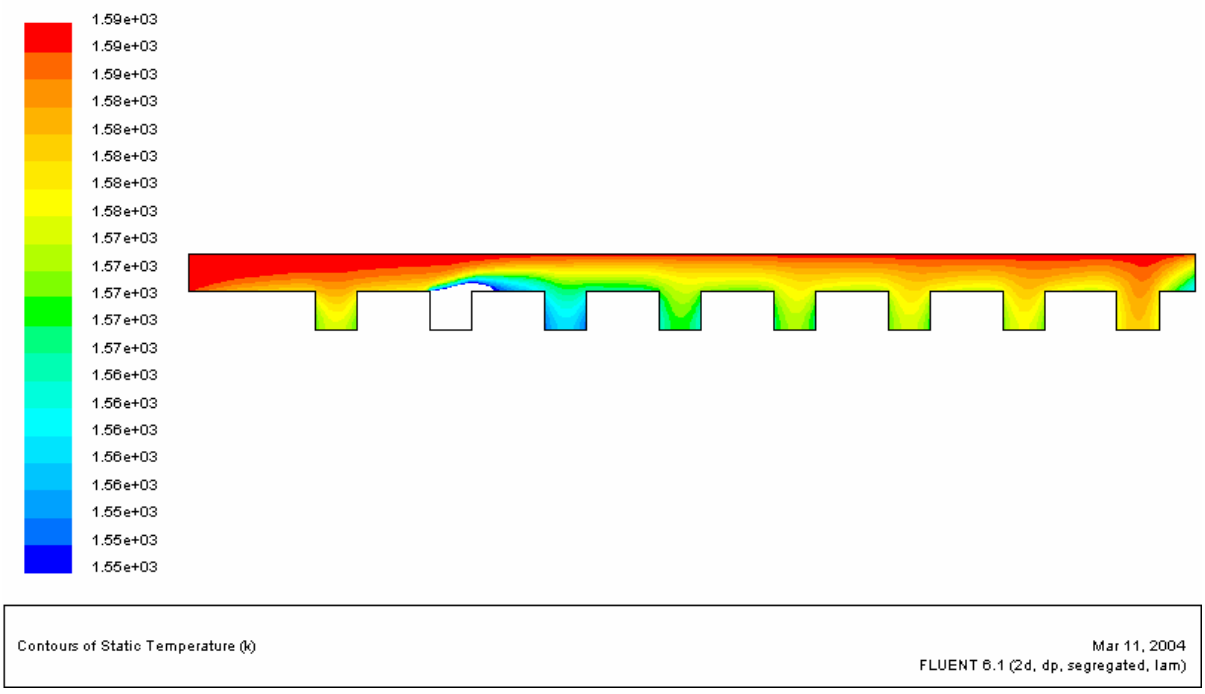

Figure 6.53 – FLUENT Trial FL–9: Temperature Contours of Molten Glass (°K)

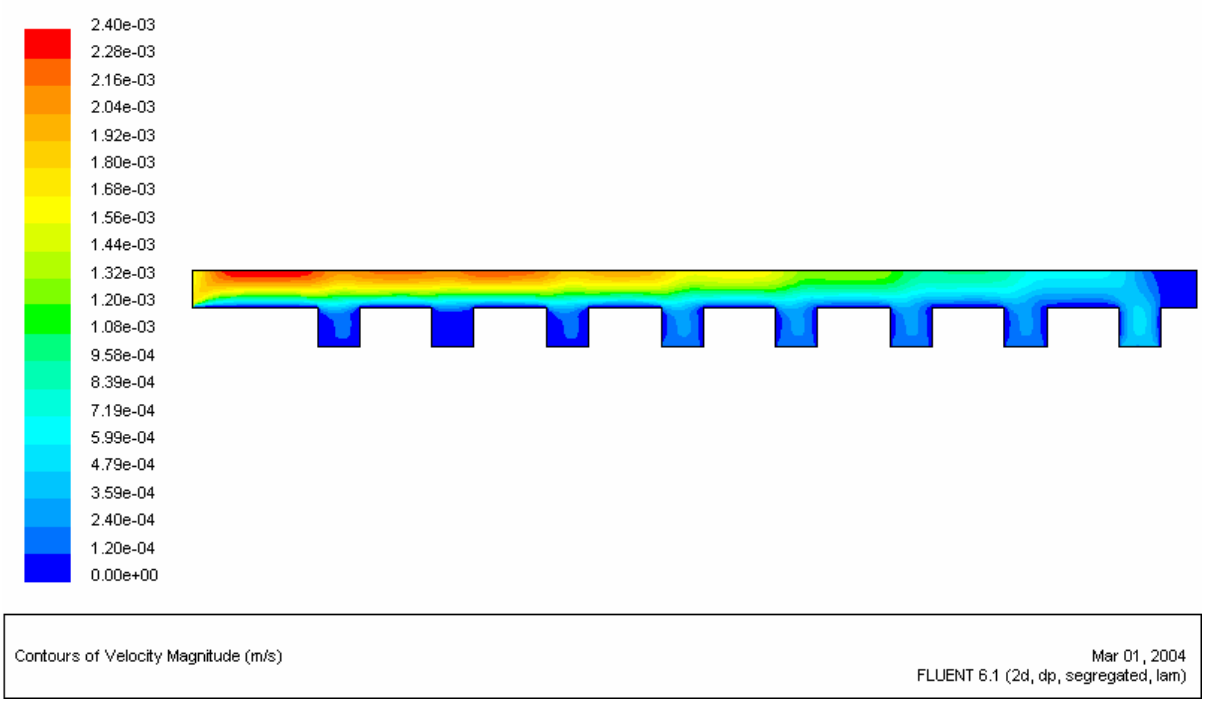

Figure 6.54 – FLUENT Trial FL–9: Velocity Magnitudes (m/s)

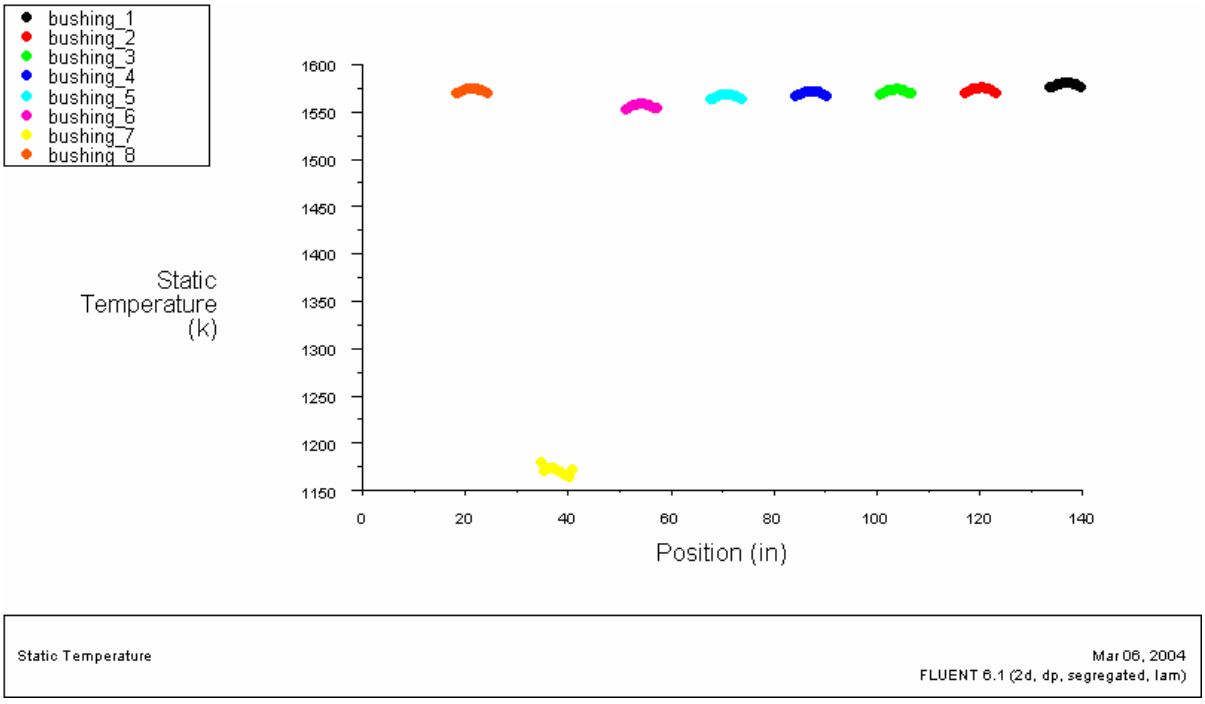

Figure 6.55 – FLUENT Trial FL–9: Bushing Outlet Temperatures 1 (°K)

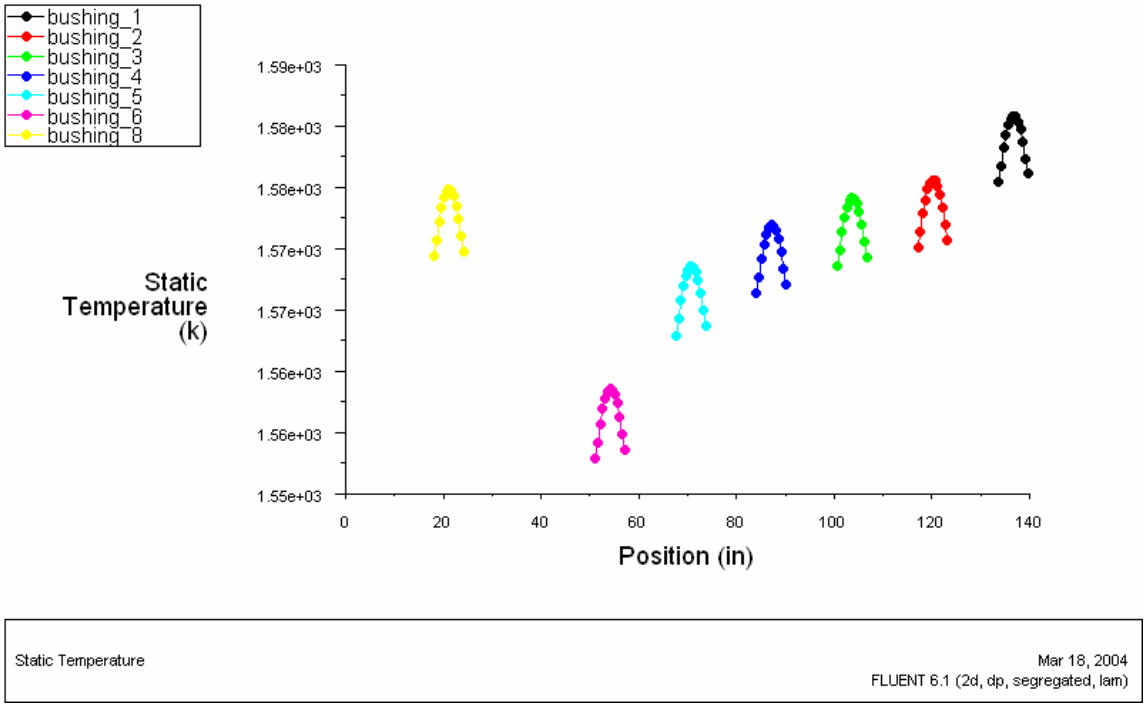

Figure 6.56 – FLUENT Trial FL–9: Bushing Outlet Temperatures 2 (°K)

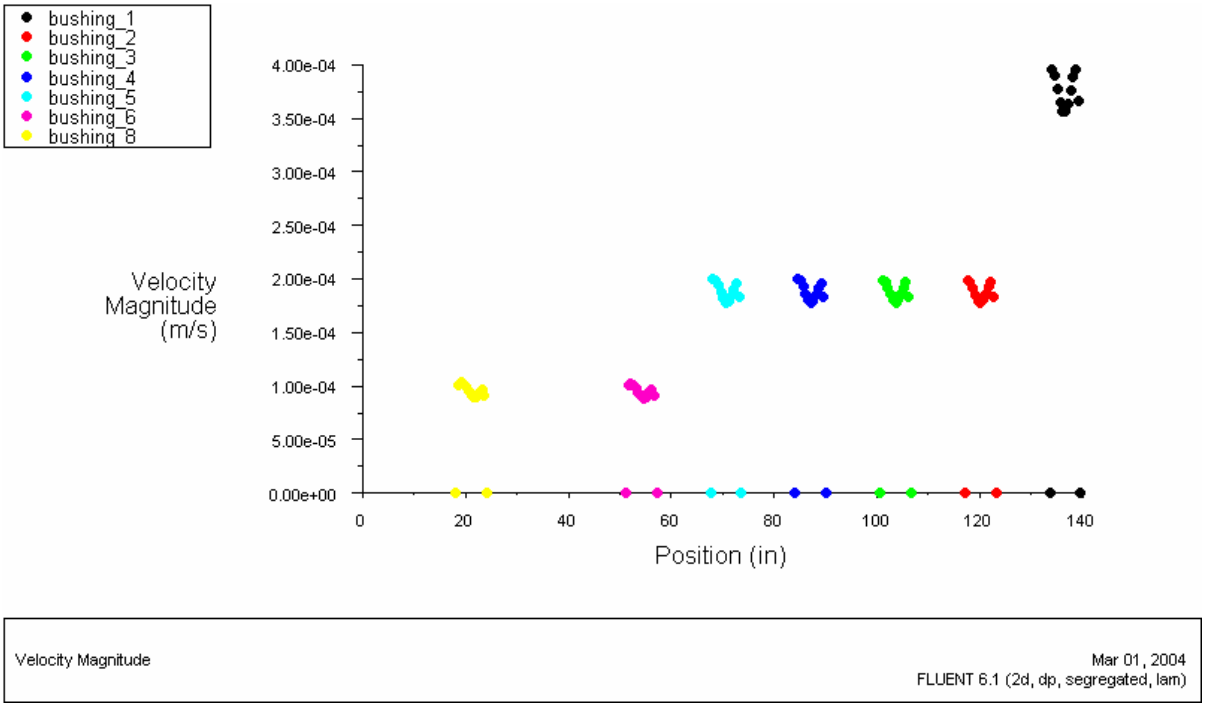

Figure 6.57 – FLUENT Trial FL– 9: Bushing Outlet Velocity Magnitudes (m/s)

Trial FL–10

Position	MFR (kg/s)
forehearth_inlet	0.5456
bushing_8	-0.0341
bushing_7	0.0000
bushing_6	-0.0341
bushing_5	-0.0682
bushing_4	-0.0682
bushing_3	-0.0682
bushing_2	-0.0682
bushing_1	-0.0341

ΔMFR =	0.1705

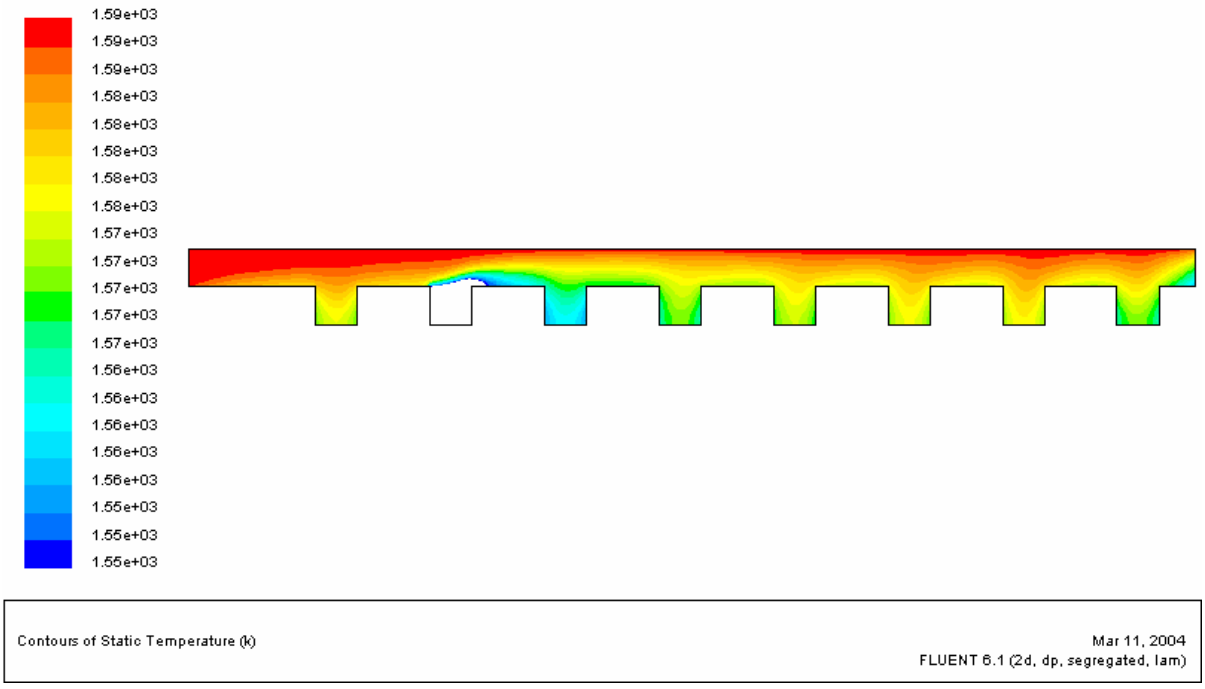

Figure 6.58 – FLUENT Trial FL–10: Temperature Contours of Molten Glass (°K)

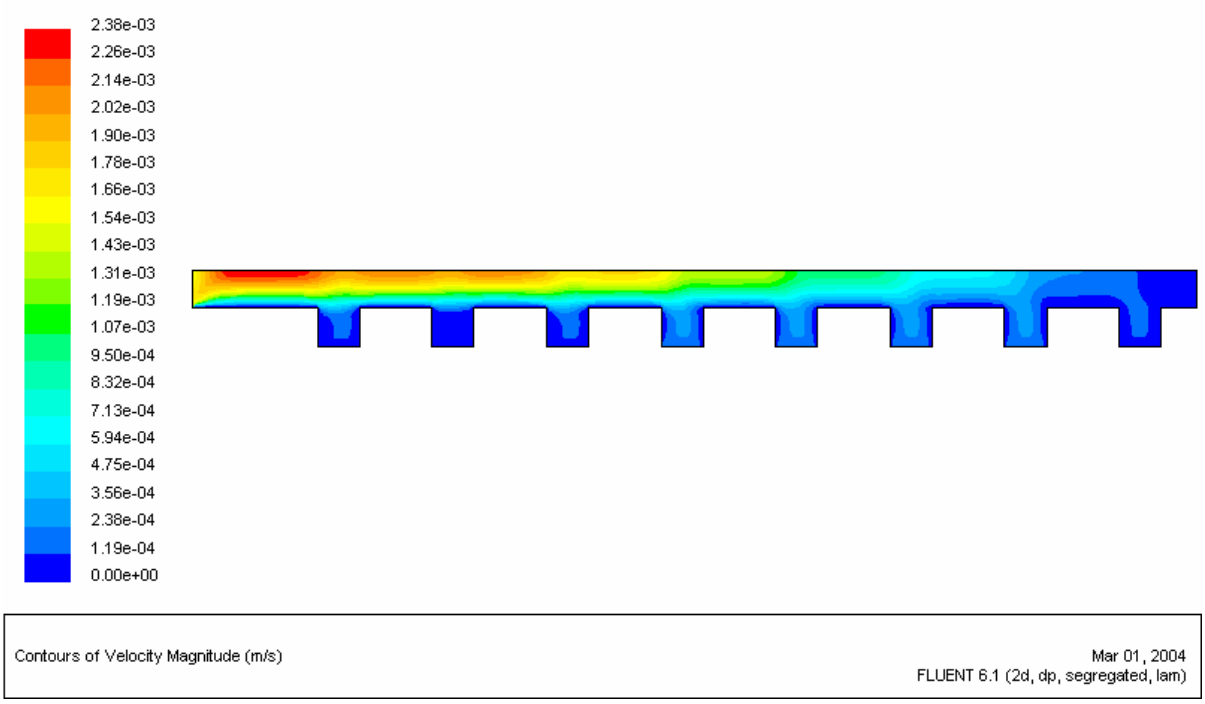

Figure 6.59 – FLUENT Trial FL–10: Velocity Magnitudes (m/s)

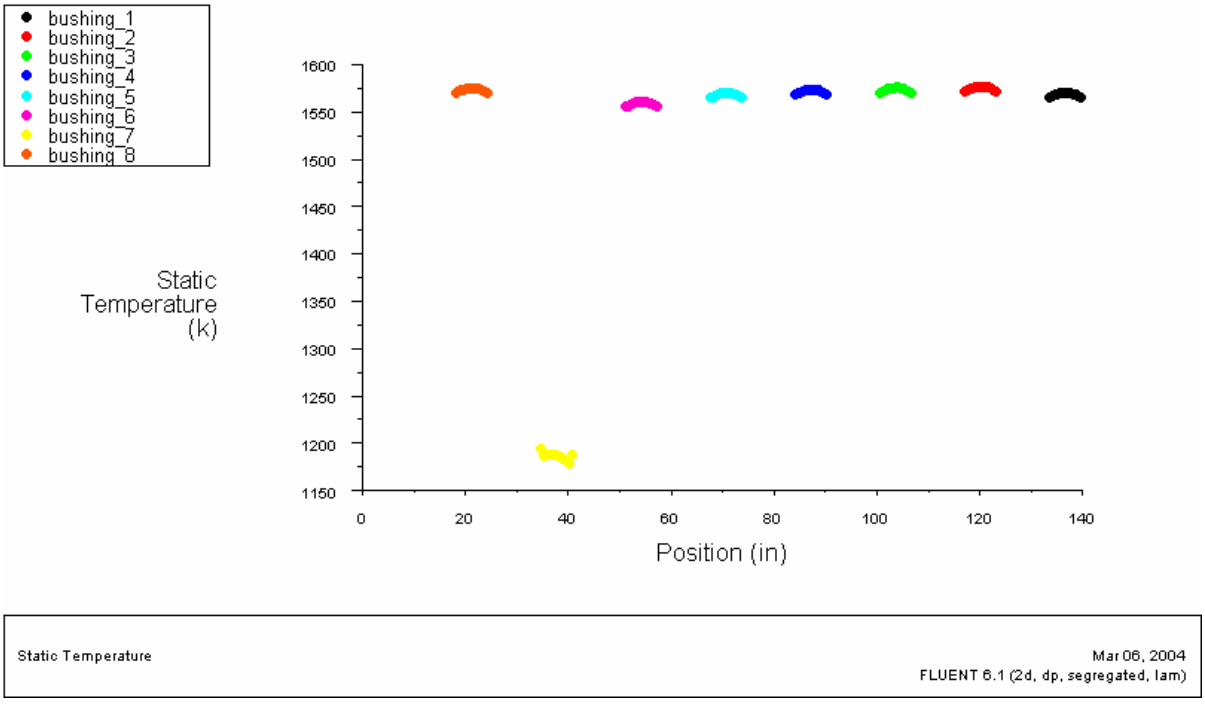

Figure 6.60 – FLUENT Trial FL–10: Bushing Outlet Temperatures 1 (°K)

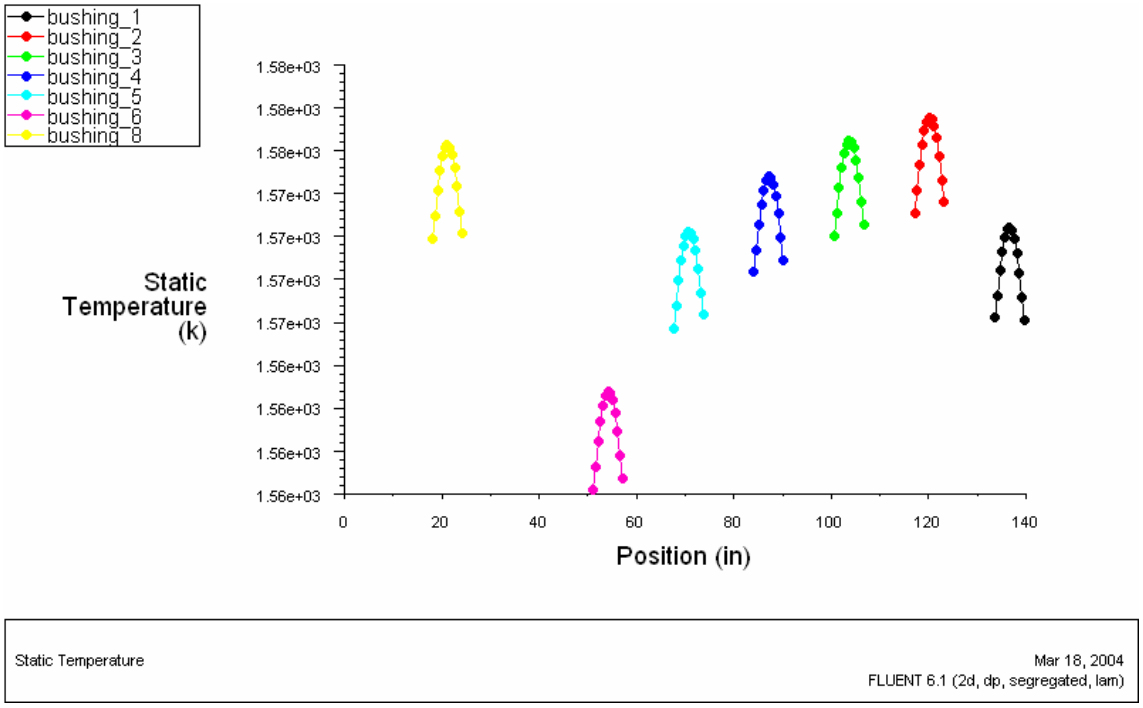

Figure 6.61 – FLUENT Trial FL–10: Bushing Outlet Temperatures 2 (°K)

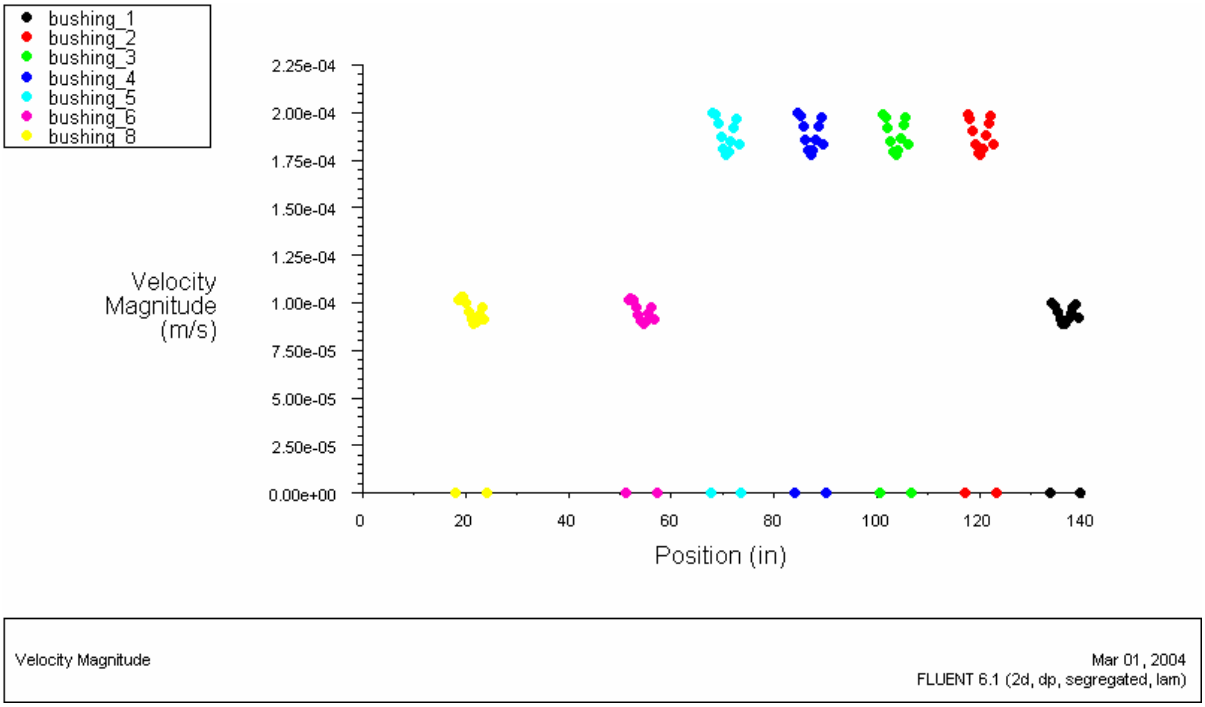

Figure 6.62 – FLUENT Trial FL–10: Bushing Outlet Velocity Magnitudes (m/s)

Trial FL–10a

Position	MFR (kg/s)
forehearth_inlet	0.3751
bushing_8	-0.0341
bushing_7	0.0000
bushing_6	-0.0341
bushing_5	-0.0682
bushing_4	-0.0682
bushing_3	-0.0682
bushing_2	-0.0682
bushing_1	-0.0341

ΔMFR =	0.0000

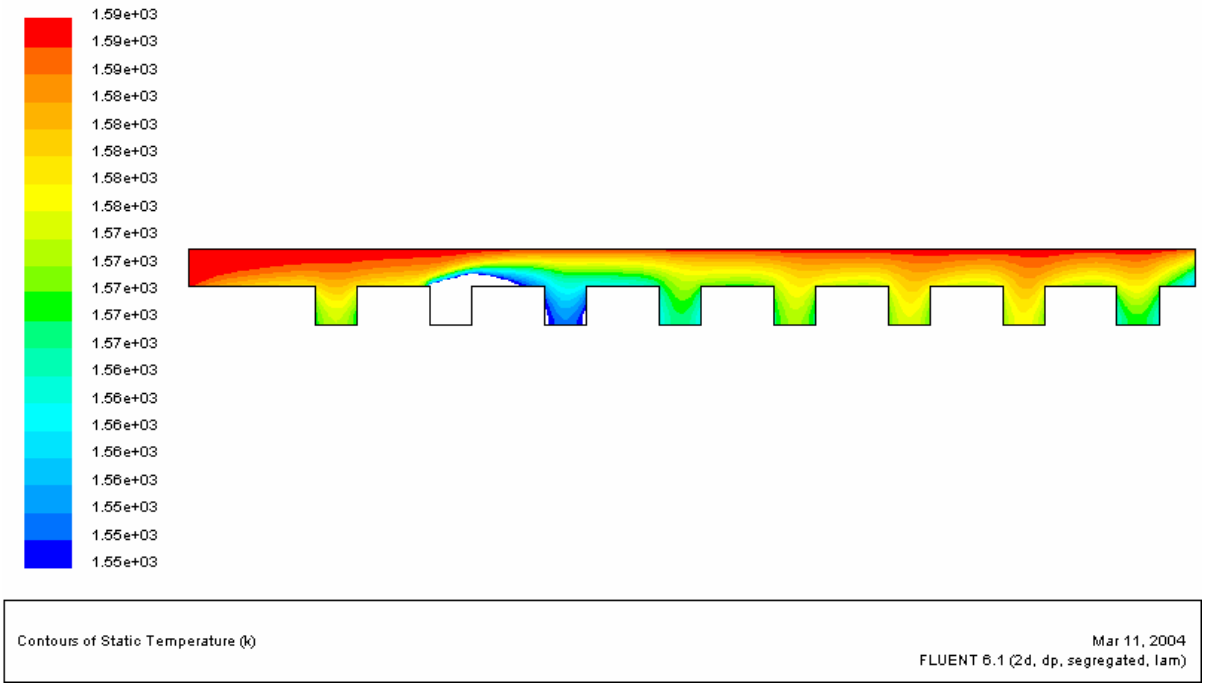

Figure 6.63 – FLUENT Trial FL–10a: Temperature Contours of Molten Glass (°K)

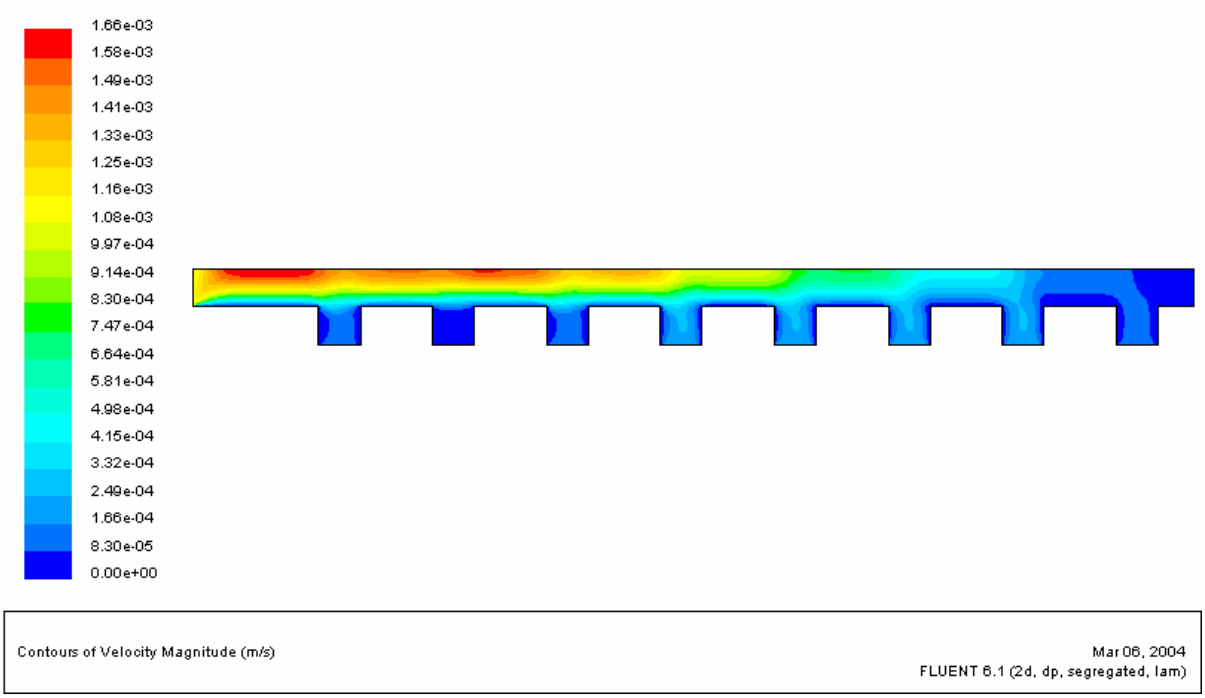

Figure 6.64 – FLUENT Trial FL–10a: Velocity Magnitudes (m/s)

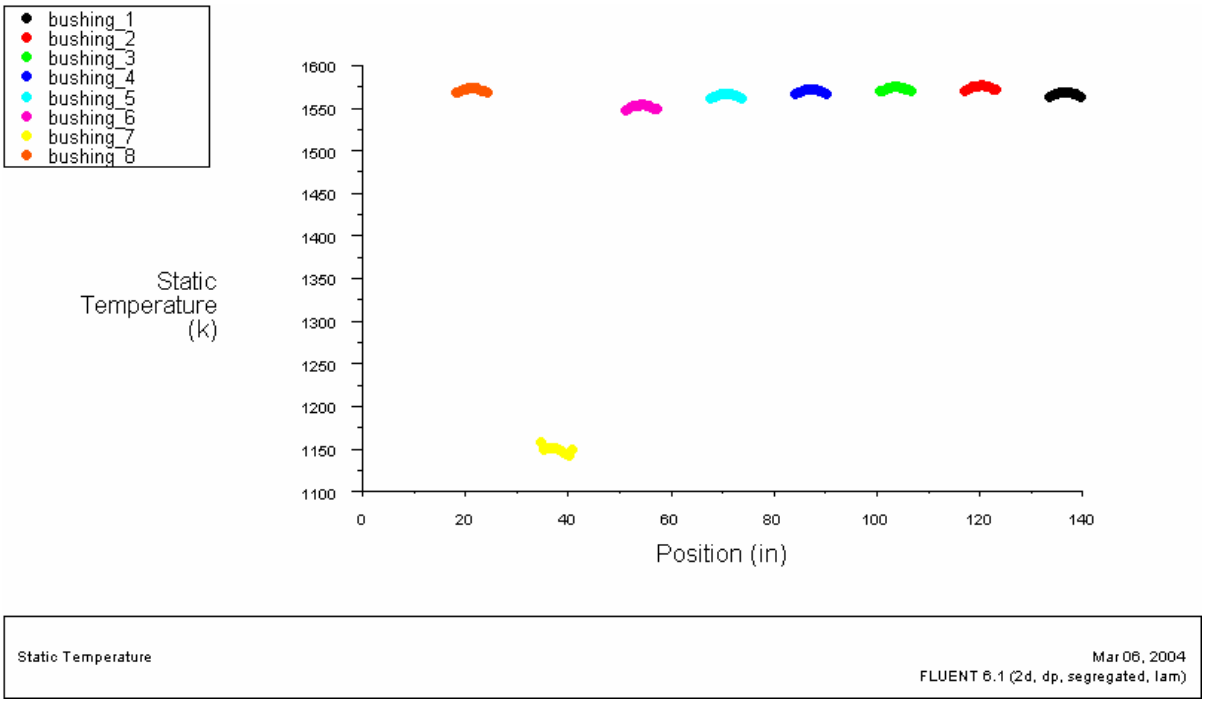

Figure 6.65 – FLUENT Trial FL–10a: Bushing Outlet Temperatures 1 (°K)

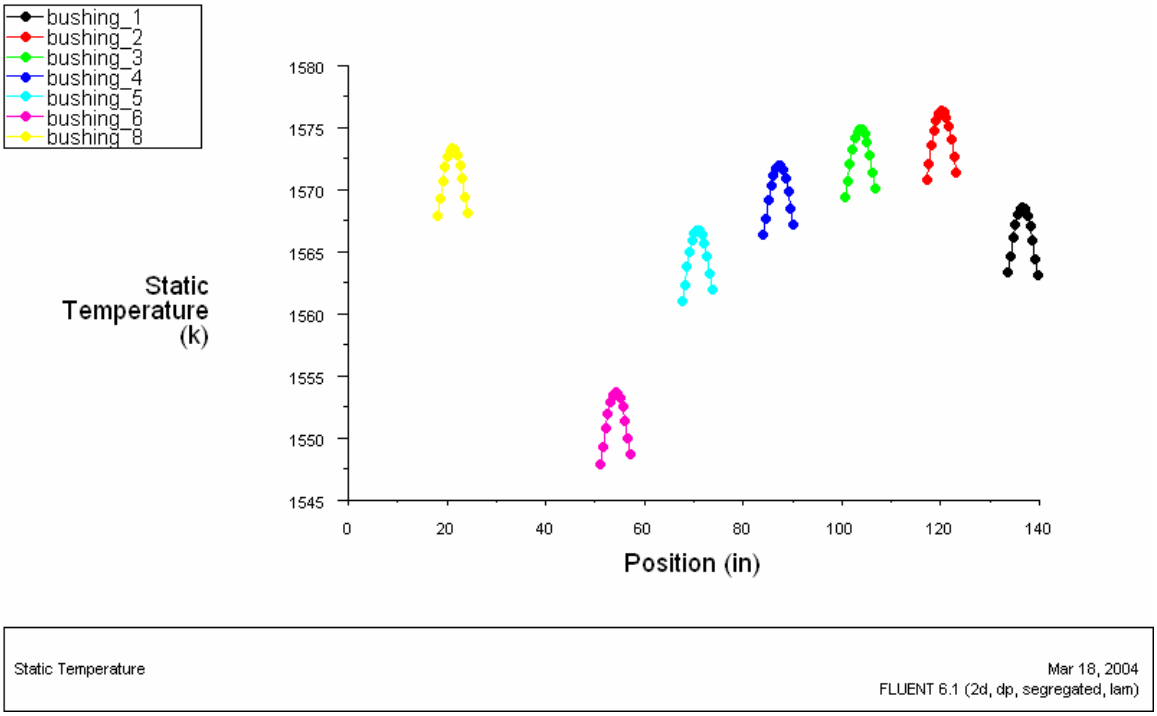

Figure 6.66 – FLUENT Trial FL–10a: Bushing Outlet Temperatures 2 (°K)

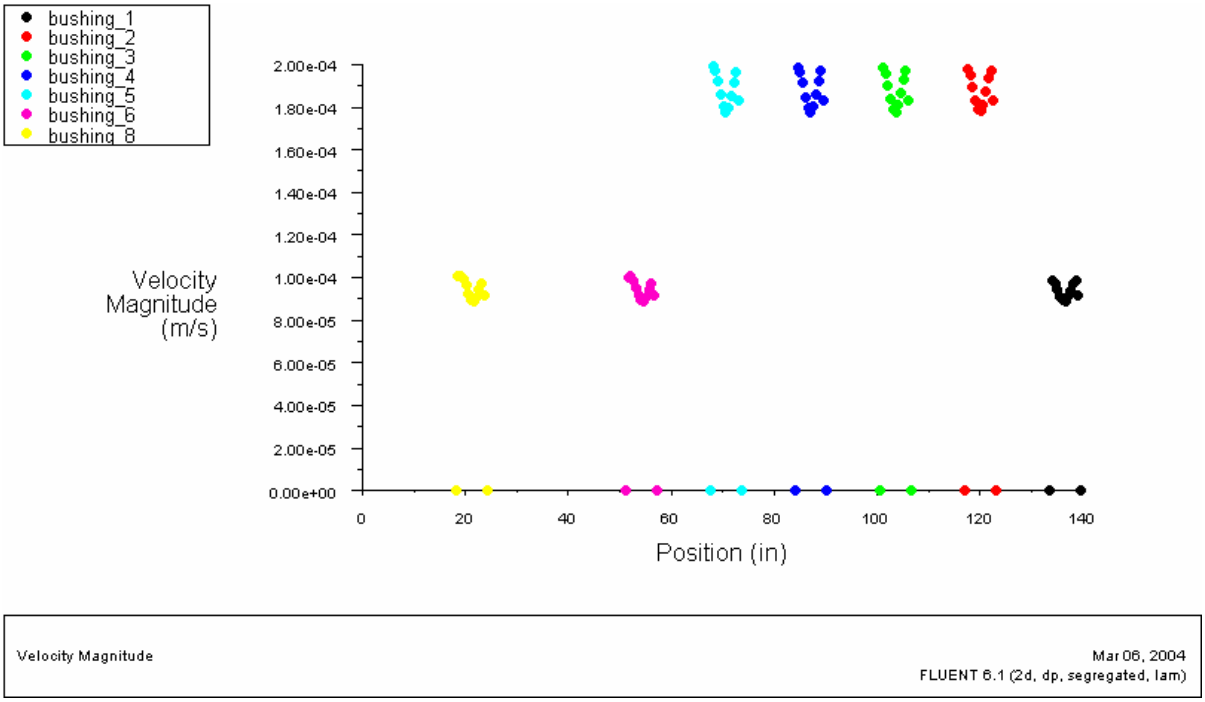

Figure 6.67 – FLUENT Trial FL–10a: Bushing Outlet Velocity Magnitudes (m/s)

6.6 Appendix F – FIDAP Simulation Results

Trial FD–1

Position	Property	Value	Units
glass height	H_2	0.20	m
forehearth_inlet	$\dot{m}$	0.55	kg/s

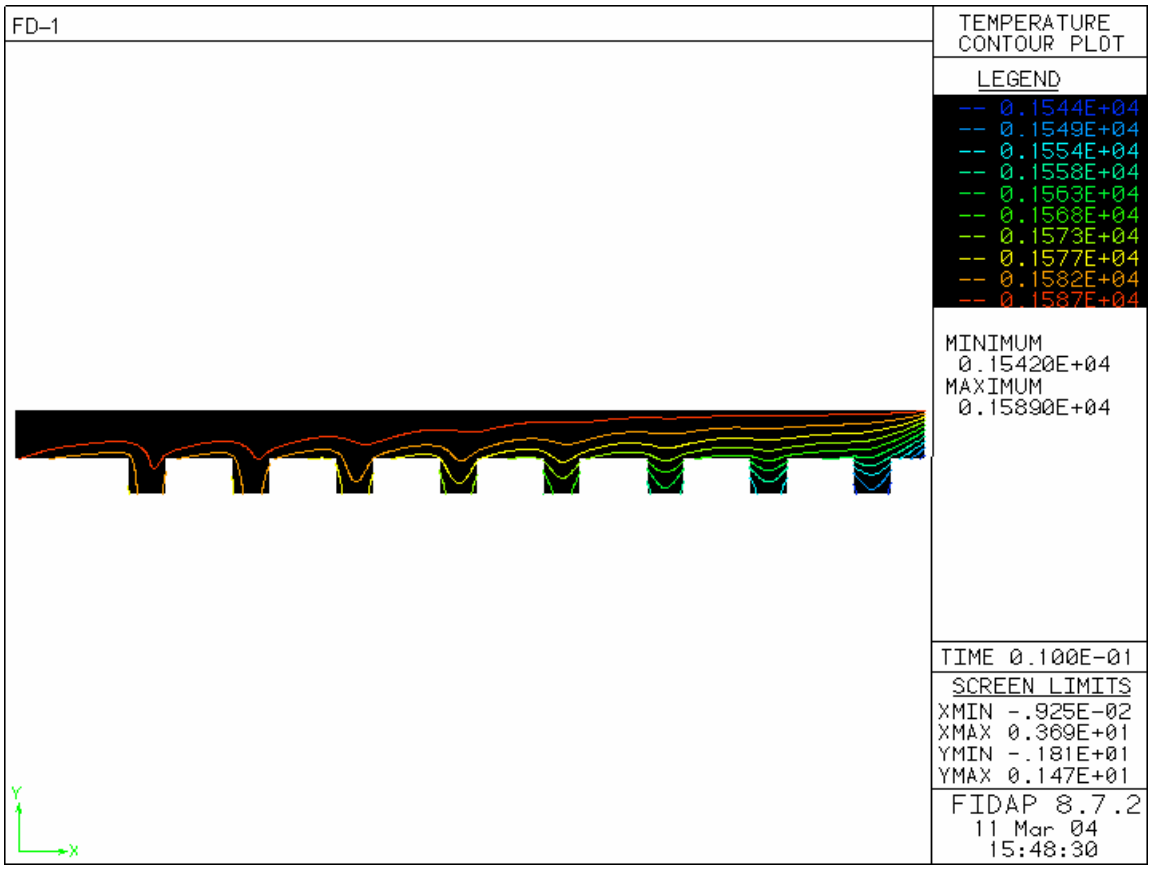

Figure 6.68 – FIDAP Trial FD–1: Molten Glass Isotherms (°K)

Trial FD–1a

Position	Property	Value	Units
glass height	H_2	0.14	m
forehearth_inlet	$\dot{m}$	0.55	kg/s

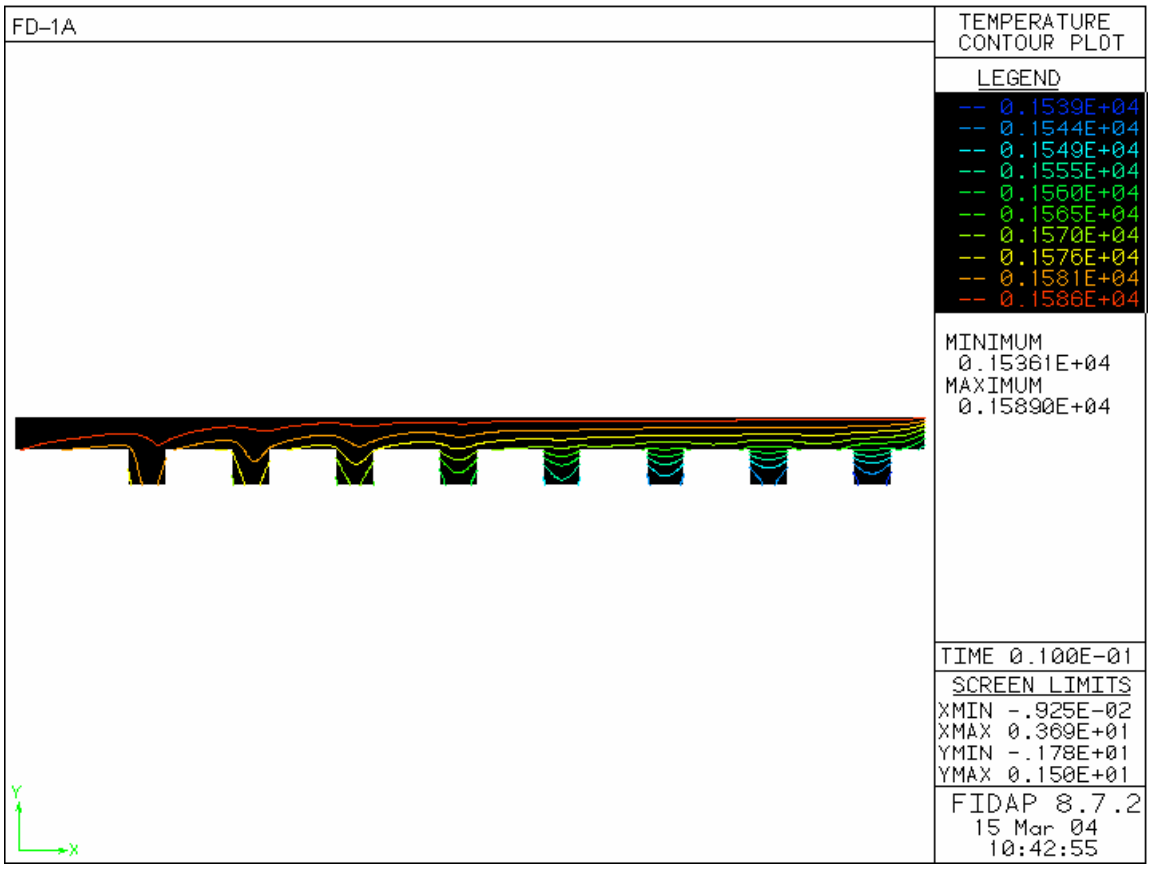

Figure 6.69 – FIDAP Trial FD–1a: Molten Glass Isotherms (°K)

Trial FD–2

Position	Property	Value	Units
glass height	H_2	0.14	m
forehearth_inlet	$\dot{m}$	0.55	kg/s
bushing_8	q"	-3.37E+05	W/m^2

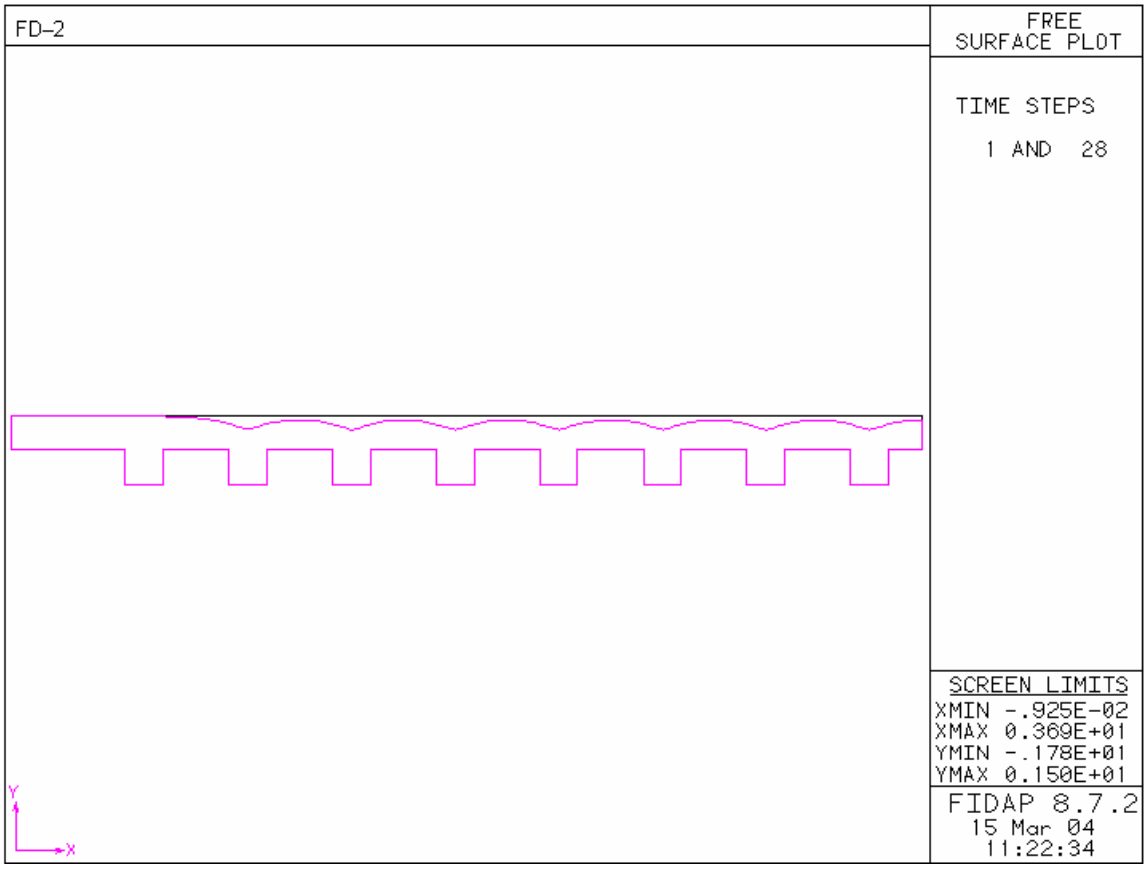

Figure 6.70 – FIDAP Trial FD–2: Free Surface Variations

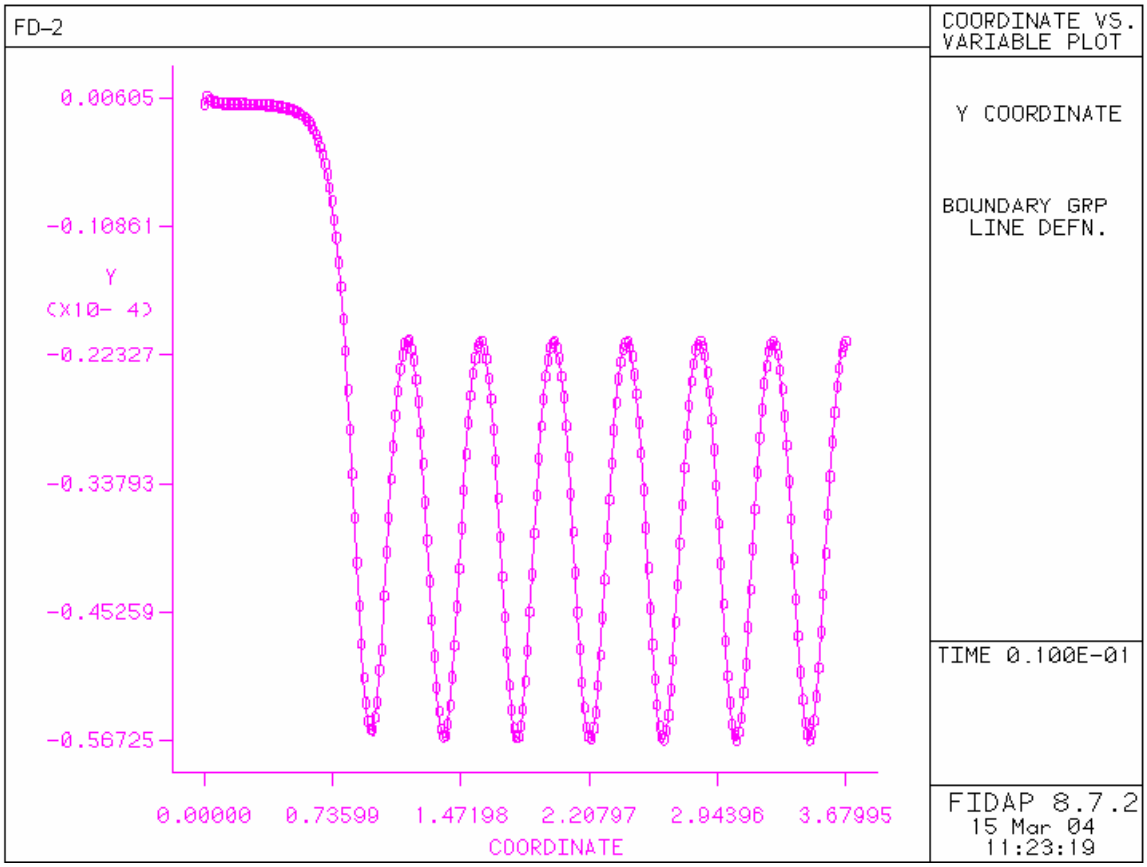

Figure 6.71 – FIDAP Trial FD–2: Glass Surface Deformation (m)

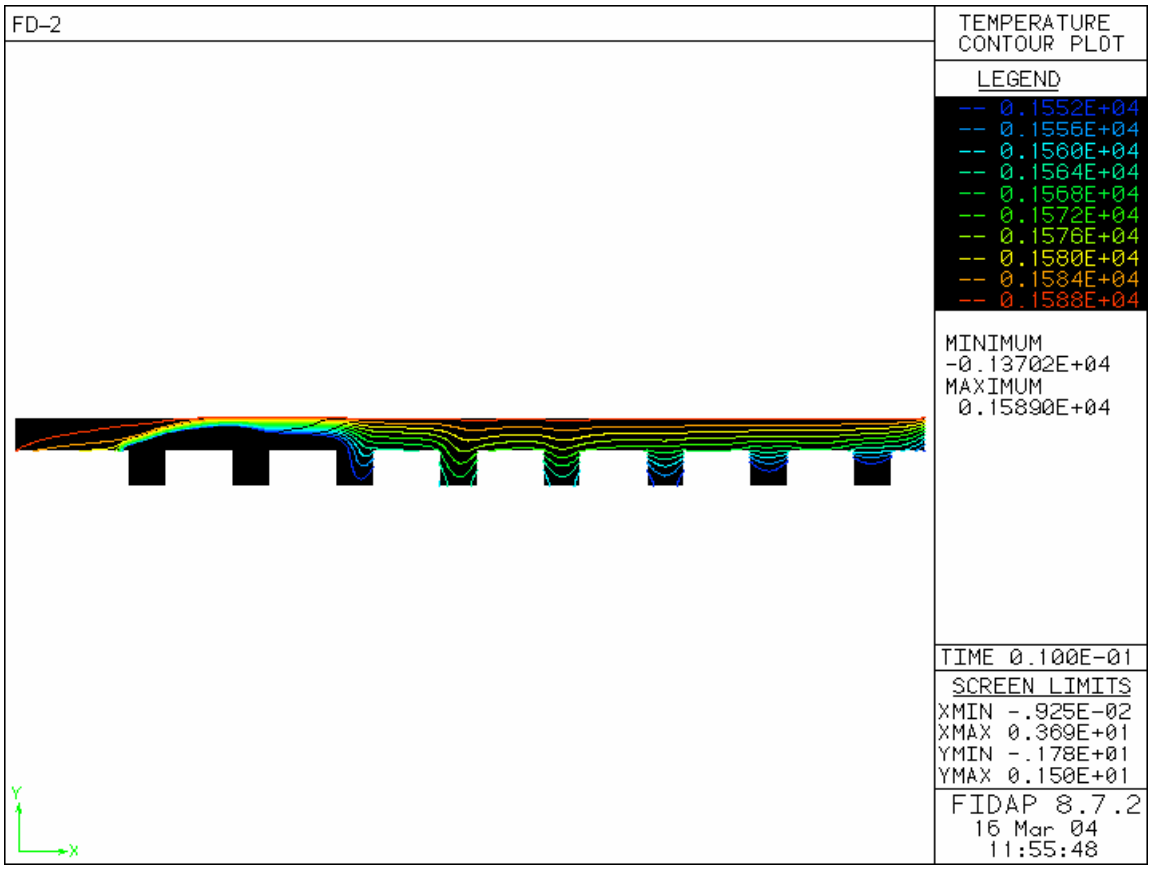

Figure 6.72 – FIDAP Trial FD–2: Molten Glass Isotherms (°K)

Trial FD–3

Position	Property	Value	Units
glass height	H_2	0.14	m
forehearth_inlet	$\dot{m}$	0.55	kg/s
bushing_5	q"	-3.37E+05	W/m^2

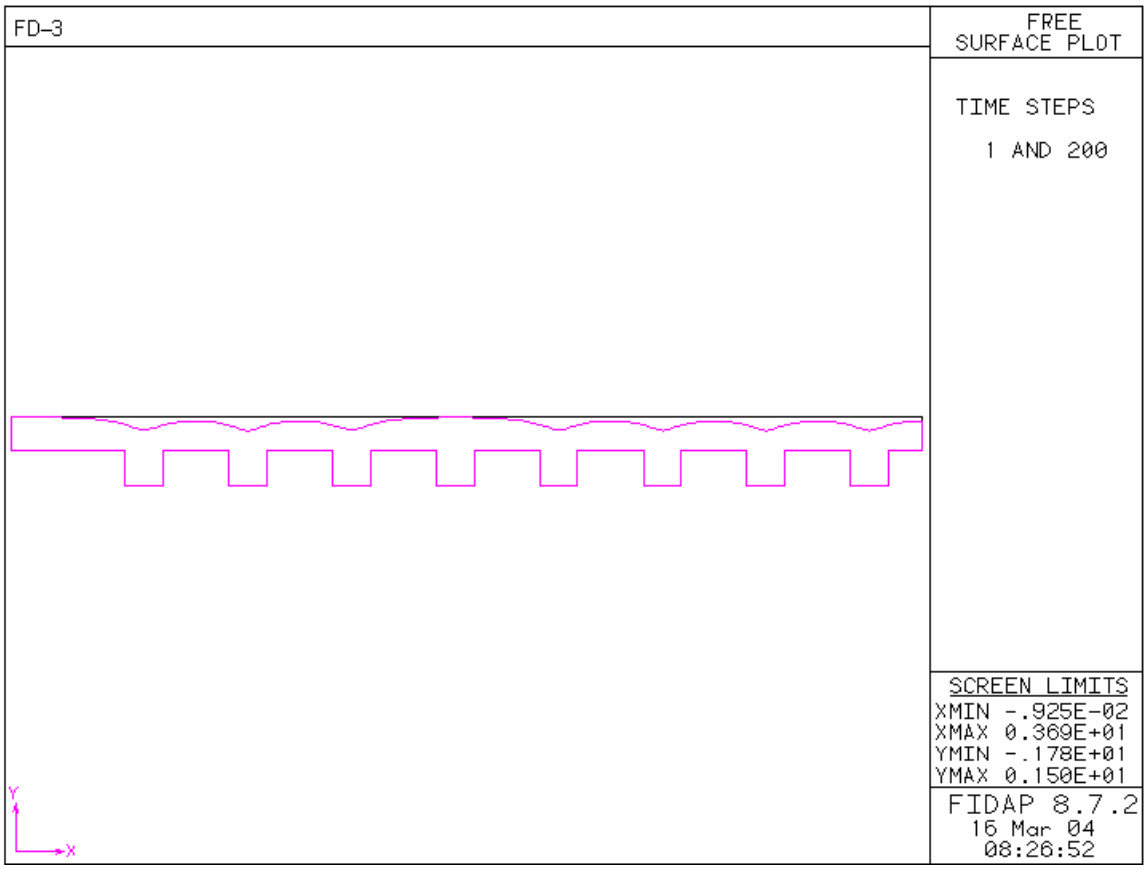

Figure 6.73 – FIDAP Trial FD–3: Free Surface Variations

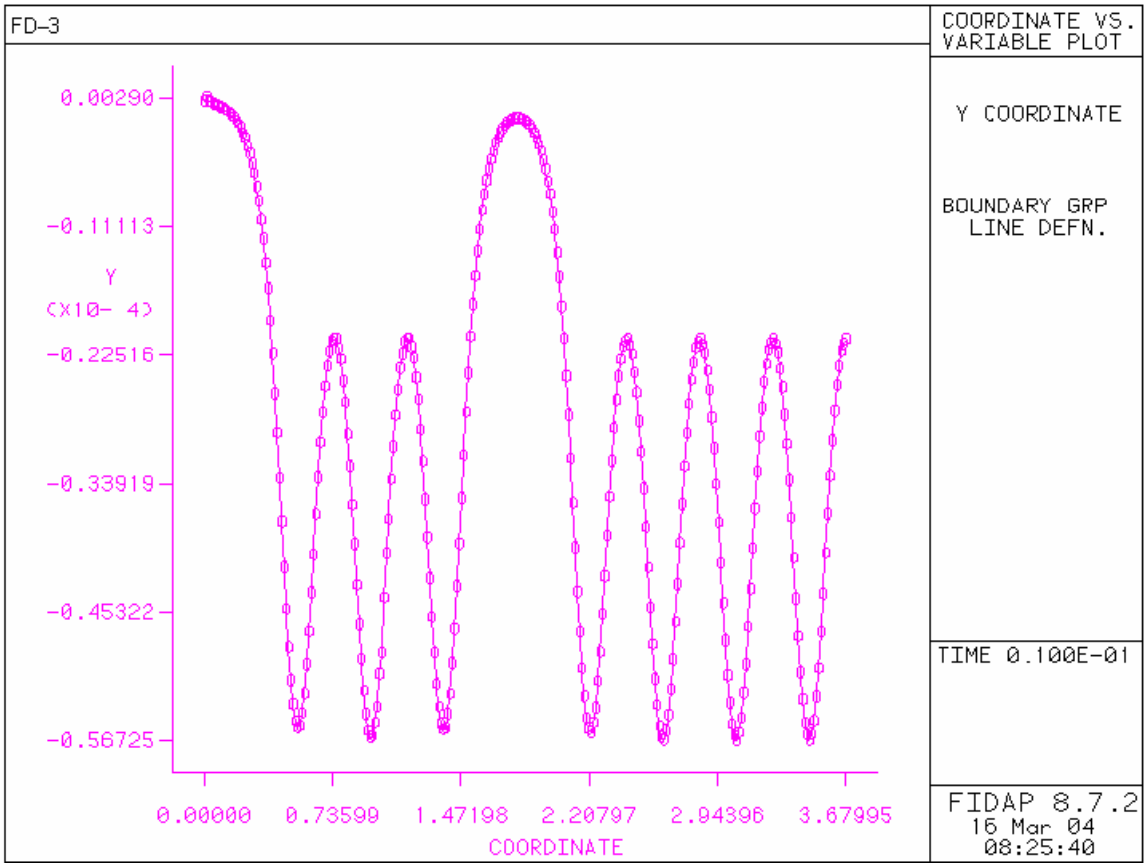

Figure 6.74 – FIDAP Trial FD–3: Glass Surface Deformation (m)

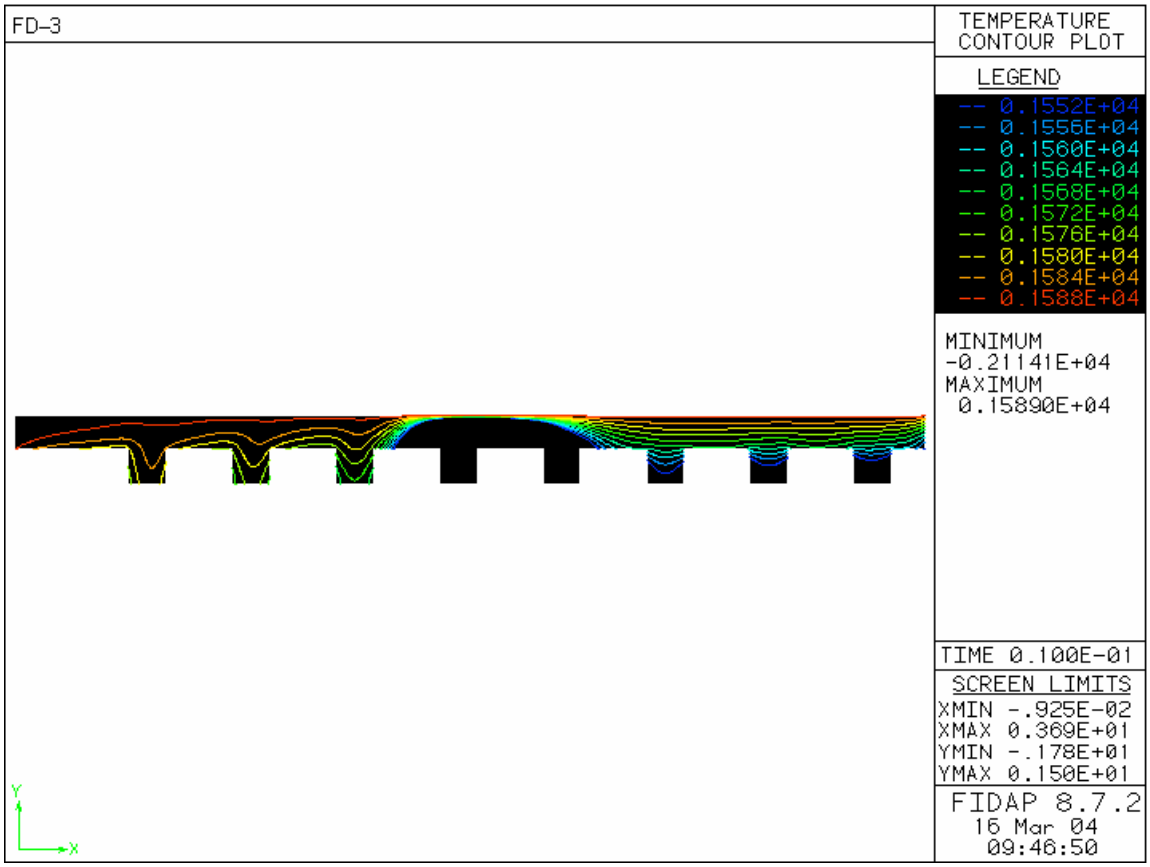

Figure 6.75 – FIDAP Trial FD–3: Molten Glass Isotherms (°K)

Trial FD–4

Position	Property	Value	Units
glass height	H_2	0.14	m
forehearth_inlet	$\dot{m}$	0.55	kg/s
bushing_2	q"	-3.37E+05	W/m^2

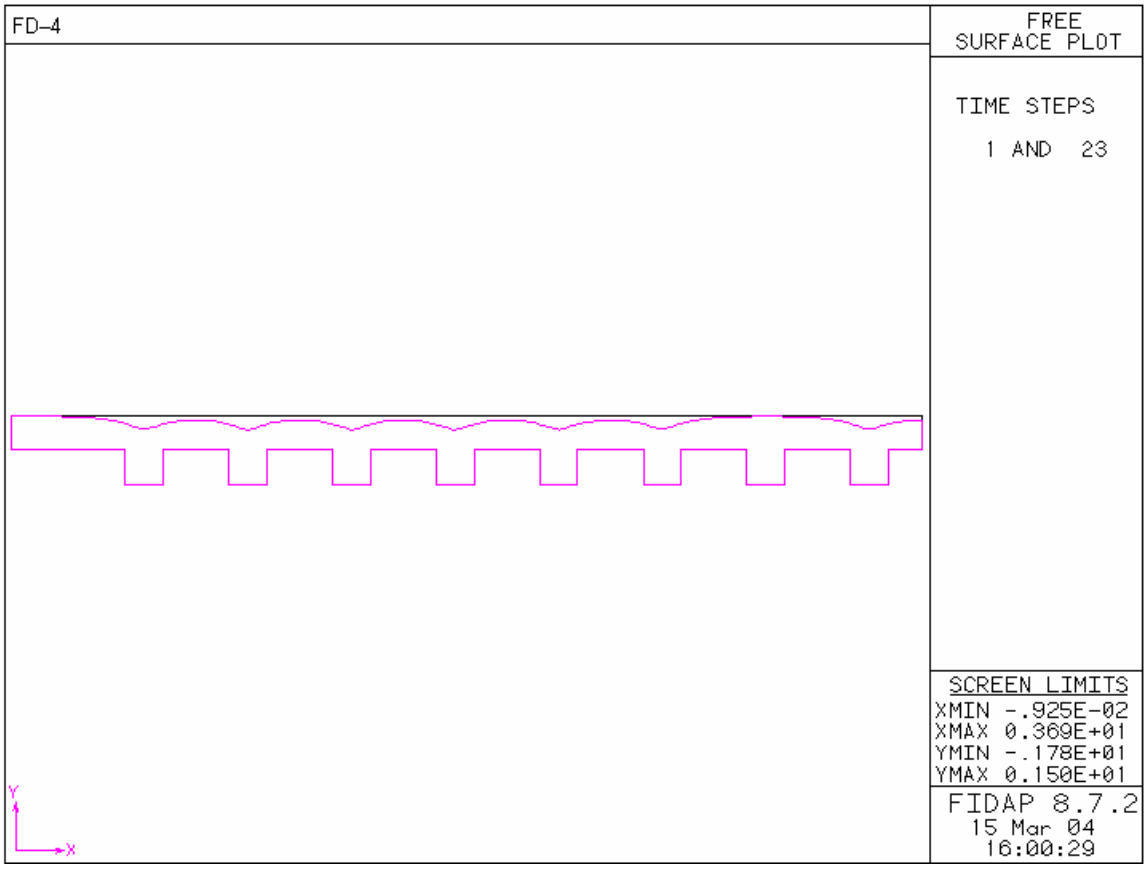

Figure 6.76 – FIDAP Trial FD–4: Free Surface Variations

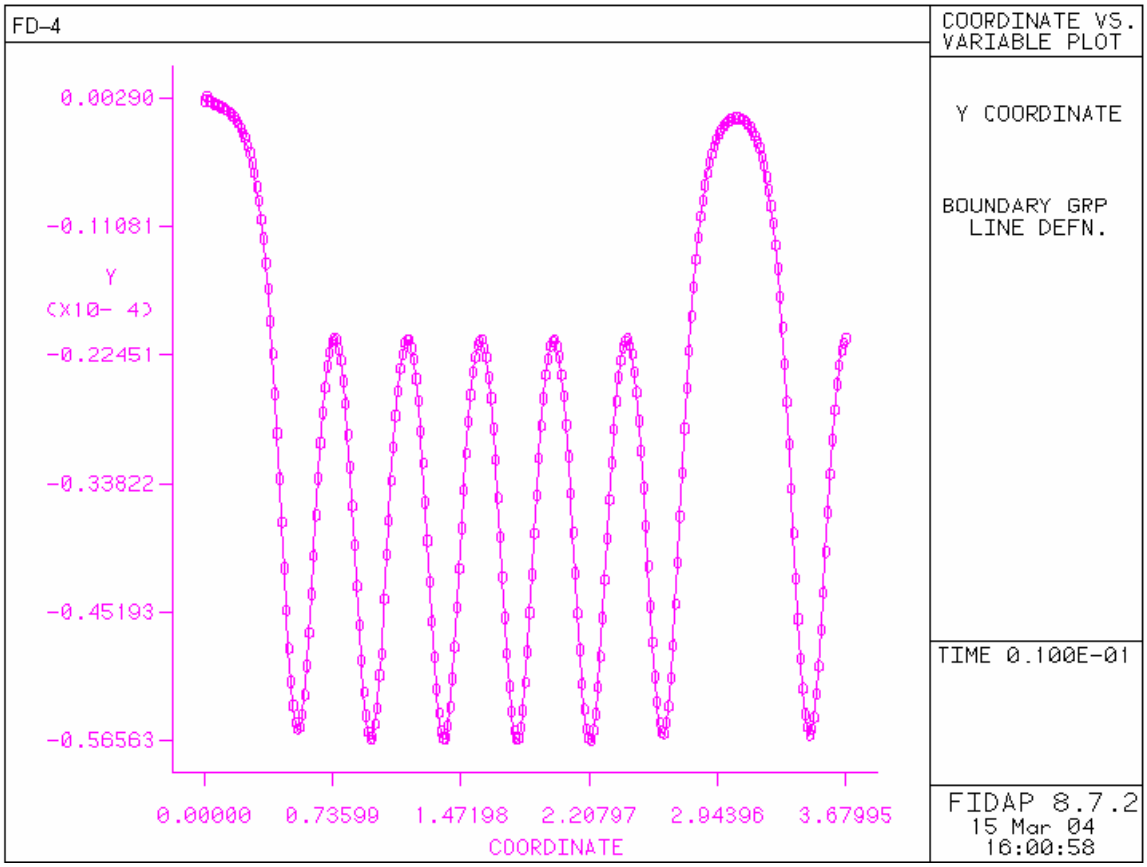

Figure 6.77 – FIDAP Trial FD–4: Glass Surface Deformation (m)

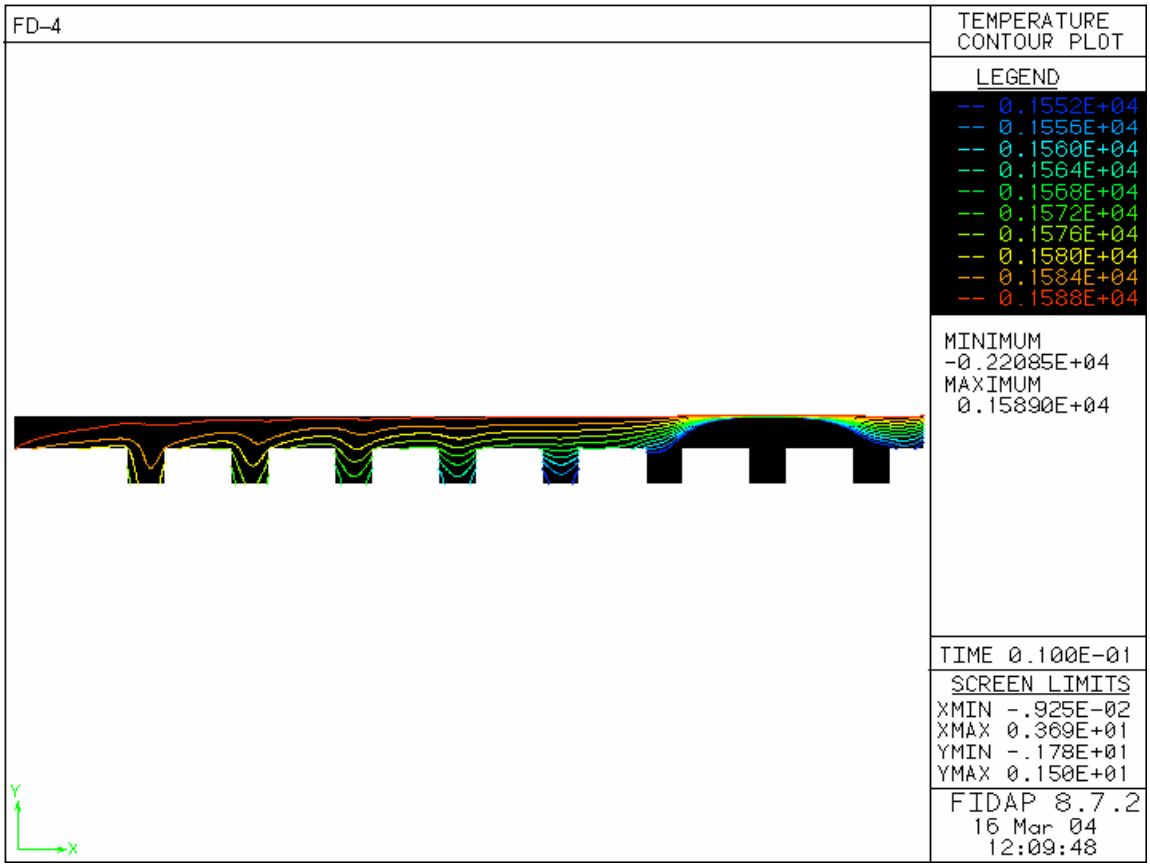

Figure 6.78 – FIDAP Trial FD–4: Molten Glass Isotherms (°K)